Clinching of AA7075 Aluminum Sheets

Clinching of AA7075 Aluminum Sheets

By

Mostafa Khalaf Sabra Atia, B.Sc., M.Sc.

A Thesis

Submitted to School of Graduate Studies in Partial Fulfillment of the Requirements for the Degree Doctor of Philosophy

McMaster University

Ph.D. Candidate (2017) McMaster University

Mechanical Engineering Hamilton, Ontario

TITLE: **Clinching of AA7075 Aluminum Sheets**

AUTHOR: Mostafa Khalaf Sabra Atia

B.Sc. (Military Technical College, Egypt)

M.Sc. (Military Technical College, Egypt)

SUPERVISOR: Professor Mukesh K. Jain

NUMBER OF PAGES: ix, 207

Abstract

Weight reduction, increased fuel economy, and increased safety of structures in transportation applications has led to much interest in lightweight higher strength structural aluminum alloys. Suitable joining techniques to create such structures with aluminum sheets are required. Generally, similar and dissimilar sheet metals can be joined by adhesive bonding, welding, and mechanical fastening. Difficulty of welding and long processing times for adhesive bonding make mechanical fastening a process of much interest for joining of high strength aluminum sheets.

Among the different mechanical fastening techniques available in manufacturing, clinching is a common method of joining by forming in which a punch and die are used to form a geometrical interlock. However, the process introduces surface steps on both sides of the joined sheets where one side consists of a protrusion and the other a pit. Also, clinch joining, a well-accepted and widely used process for joining ductile sheet metals, is more challenging for high strength lower ductility aluminum sheets such as AA7075.

The current work aims at studying clinch-ability of high strength lower ductility AA7075 aluminum sheets of different tempers by conventional as well as a new clinching technique called "die-less" clinching. A new tooling was designed in order to conduct die-less clinches. The results showed that room temperature clinching is possible for the softer tempers namely solution treated and annealed states. However, the peak aged sheets failed to form a successful joint. A novel electrical resistance heating technique (ERH) to provide ductility to the joined sheets was used to obtain die-less clinched joints in AA7075-T6. ERH technique provides a large range of heating temperatures from room temperature to 270°C for a current duration of 3 sec. The AA7075-T6 sheets showed a superior joining by using ERH. The joint showed a metallurgical locking mechanism in addition to the commonly available form locking mechanism.

Research Contributions

Due to reduced ductility of high strength AA7075 sheet metals and lack of studies of clinch-ability of this challenging sheet material, conventional clinching of this material has been studied experimentally as well as numerically. Also, a new tooling for die-less clinching process was designed and utilized for die-less clinching of AA7075 sheets. The following contributions have been made from conventional and die-less clinching studies of AA7075 sheets:

- Clinch joining involves very large plastic deformation that makes joining of high strength and lower ductility 7075 aluminum sheet a challenge. An investigation of the effect of the tool parameters on conventional clinch process as well as the associated joint strength was conducted. A new tooling for die-less clinch joining was designed. Also, the effect of parameters of new tooling on the formed joint was studied. Further, the material flow of the AA7075 sheet metal in different tempers (namely T6, W, and O) was studied. Lastly, a microstructure study of conventional as well as die-less clinching was carried out.
- 2D axisymmetric FE model of conventional clinching using extensible dies was developed, validated, and utilized to obtain a better understanding of the process. Material models based on Swift, Voce, and a mixed material hardening law incorporating both Swift and Voce laws with a weight function were utilized. The effect of the tool and forming process parameters on the final shape of the joint were also studied via FE simulation.
- A FE based parametric study of die-less clinching of AA7075 aluminum sheets was conducted. The effects of numerical model, boundary conditions, and material models parameters were studied. 3D FE models to assess the peel as well as shear strength of the die-less clinched joint were also developed and validated with experiments, and utilized to study the effect of forming process parameters on post-clinch joint strength.
- A novel hot die-less clinching technique was developed. Taking advantage of the simplicity of the new designed tool set, resistance heating was used to provide

ductility to the AA7075-T6 sheet materials. In the literature some recent heating techniques such as thermal and IR guns have been used to conventionally clinch high strength 6xxx aluminum sheets. In the present work, a considerably superior method of rapid electrical resistance heating was successfully developed and studied for die-less clinching of hard-to-clinch AA7075-T6 sheets. Modification of the pre-designed die-less tool set was carried to enable rapid application of current for resistance heating. Different current cycles were applied and the effects of applied current, current duration and forming force on the material flow, geometric parameter of the clinch, and post-clinch strength of the joint were studied.

Acknowledgements

It is my pleasure to acknowledge the roles of several individuals who were instrumental in the completion of my Ph.D. research. I am grateful to all people who contributed in some way to the work described in this thesis. I wish to express my most heartfelt thanks to them.

First and foremost, I thank my Ph.D. supervisor, Professor Mukesh K. Jain, for accepting me into the metal forming group. During my tenure, he contributed to a rewarding graduate school experience by giving me intellectual freedom in my work, engaging me in new ideas, and demanding a high quality of work in all my endeavors. Thank you for the advice, support, and willingness that allowed me to pursue research on topics for which I am truly passionate. Additionally, I would like to thank my committee members Professor Stephen Veldhuis, and Professor Phillip Koshy for their interest in my work, and, for the guidance, you have my ultimate gratitude. Also, I would like to thank Professor Tim Nye for his guidance during the first two years of my study.

I would like to express my great gratitude and thanks to the Egyptian Armed Force represented by The Egyptian Armament Authority who gave me the scholarship and the opportunity to join the PhD program at McMaster University.

Special thanks are also to Norlok Company and Mr. Byron Selorme for his assistance.

This acknowledgement would not be complete without mentioning the Department of Mechanical Engineering at McMaster University and McMaster Automotive Research Center (MARC). My sincere thanks also go to Ron Lodewyks, Michael Lee, Moisei Bruhis, Nicholas Andreae, and Doug Kelly.

I am very grateful for the friendship of all of my group colleagues, especially Mohamad Farid Mohamad Sharif, for their assistance and great help

My deepest appreciation belongs to my family for their patience and understanding.

Table of Contents

List of Abbreviations

T6	Artificial peak aged state which represents the hardest temper
O	Annealed temper state
W	Solution heat treated state
N	Neck thickness of the joint
U	Interlock depth of the joint
X	Joint bottom thickness
t	Blank holder groove depth
d	Blank holder groove diameter
R_{PC}	Punch corner radius
R_{DC}	Die corner radius
F	Forming force
OM	Optical microscopy
SEM	Scanning electron microscopy
σ_{eq}^{p}	Equivalent stress
ε_{eq}^{p}	Equivalent plastic strain
k_1	Stress coefficients for Voce hardening law
K_2	Stress coefficients for Swift hardening law
C	Material constant for Voce hardening law
m	Material constant for Voce hardening law
α	Weight function
δ	A continuous hardening parameter in Extended-Voce material model
σ_0	Initial yield stress
μ_{sh}	Sheet-to-sheet coefficient of friction
μ_t	Sheet-to-tool coefficient of friction
L^e	Smallest characteristic element length
C_d	Material dilatational wave speed
E	Modulus of elasticity
ρ_m	Density of the material
n	Strain hardening exponent
ERH	Electrical resistance heating
Q	Amount of heat generated
t_1	Beginning times of the resistance heating operation
t_2	Ending times of the resistance heating operation
T	Temperature
T_{max}	Peak temperature
I(t)	Heating current as function of time t
R(t)	Dynamic resistance of the sheet metals as function of time t
R_C	Constriction resistance
R_F	Film resistance
R_B	Bulk resistance

ρ	Resistivity
l	Length of current path
A	Area of current path
H	Hardness
F	Compressive force
ξ	Pressure factor
a	Contact spot number
ρ_t	Tunnel resistivity or the film resistance per unit area.
S	Joint shear strength.

Chapter 1

Introduction

1 Introduction

1.1 Overview

Aluminum and its alloys have a great demand in aerospace and automotive applications due to their low density, high strength to weight ratio, good corrosion properties and retention of strength at sub-zero temperatures. Aluminum structures are lightweight and recyclable and thus more fuel efficient and environmentally more sustainable. Among aluminum alloys, 7xxx series has the highest strength. However, its lower ductility makes it challenging to join by plastic forming processes at room temperature. The assembly of thin-walled aluminum structures often involves selection of an appropriate joining technique.

Clinching is a joining process by forming in which two or more sheet metals are locally deformed by using punch and die to form an interlock without the aid of consumable parts [1] as shown in Figure 1.1. The strength of the joint is entirely dependent on the amount of plastic work [2]. Simply, the punch exerts pressure on the sheet metals to plastically deform and fill the die cavity and create a geometric interlock [3]. The final shape of the joint as well as joint strength depends on the tool design, sheet material properties, and process parameters [4]. Joining by using clinching provides many advantages in manufacturing components from sheet materials. It provides joining of two or more sheet metals from similar or dissimilar materials in a large thickness range (individual sheet thickness can range from 0.4 to 4 mm) [5]. Clinching does not require the use of additional parts since joining depends on the formation of a geometric interlock

from the sheet materials themselves. Since no light is emitted and fumes from heating are not involved, the process is very clean, compared to other joining processes such as welding and brazing. It is a cheap technique and typically there is no need for expert technicians once the process is correctly set-up. High tool life compared with the other joining techniques is another advantage for clinching [6].

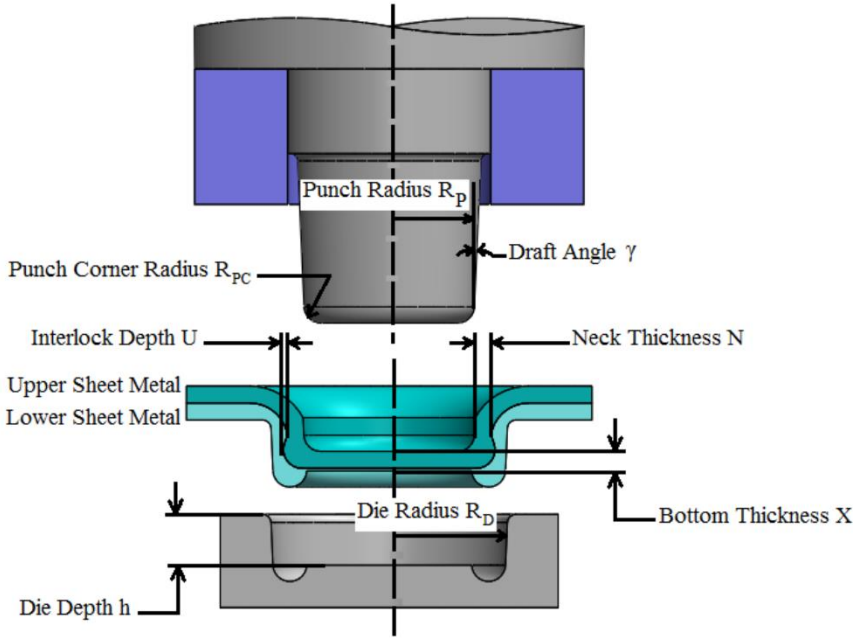

Figure 1.1. Cross section of a clinched joint showing the geometry of the joint and the different tool parameters.

There are also some disadvantages that may restrict the use of clinch joining in some applications. The formation of steps on both sides of the joined sheets represents the main disadvantage of the clinching process where a protrusion is formed on one side of clinched joint and an associated pit on the other side. Also, the large plastic strain associated with the joint formation makes clinch joining more suitable for relatively ductile sheet materials [7] and more challenging for high strength low ductility materials

such as AA7075 aluminum sheets. Many attempts have been made in the past to make clinching more aesthetically more appealing as described below.

1.2 Attempts to make clinches aesthetically appealing

1.2.1 Attempts to reduce protrusion height

In general, the main limitation of using clinching is the surface step on both sides of the clinched joint as mentioned earlier. Many attempts have been made to decrease the height of the protrusion of the clinched joint by subsequent reshaping [8-10]. In this regard, a countermeasure tooling was employed by Tong et. al. [11] to reduce the protrusion height by 50% of the conventionally clinched joint without affecting the strength of the joint. Francesco et al. [12] have conventionally clinched carbon fibre reinforced polymer (CFRP) to aluminum using extensible dies and followed the process by a second step of reshaping utilizing a punch and a flat die. Difficulty of aligning the pre-formed joint with the flattening punch represents the main disadvantage for this approach [13]. Borsellino et al. [14] suggested utilizing two flat anvils instead. The study showed a promising result in not only reducing the protrusion height but also increasing the joint strength compared to the conventional clinched joint without reshaping. Chen et al. used a pair of flat dies with (or without) the addition of a rivet to decrease the height of the protrusion of the conventional clinched joint [15, 16]. Chen et. al. [17] have utilized flat and bumped dies to reshape the conventionally clinched 5052 aluminum sheets with different thicknesses. All of the above reshaping techniques resulted in an increase in the processing time because of the extra step that utilizes a different tooling.

1.2.2 Die-less clinching

In order to make clinching more aesthetically appealing a new technique called die-less clinching has been developed [13]. Die-less clinch joining is a one-step joining process in which a punch, blank holder, and a flat anvil are used. In die-less clinching the surface steps occur only on one side of the formed joint, often on the punch side of the joint [18, 19]. The designed groove in the blank holder plays an important role in controlling the flow of the material to form the geometric interlock [2, 13]. The usage of flat anvil instead of die in die-less clinching not only improves the aesthetic appeal of the joined components but also reduces the joining time and die alignment issues. Neugebauer et al. [20] showed the possibility of forming a smaller protrusion in die-less clinching compared to the conventional clinch joining. The main disadvantage of die-less clinching is that the process requires a combined movement of blank holder and punch that makes the tool set more complex [11].

1.3 Attempt to make clinching suitable for low ductility sheets

The formation of permanent geometric interlock in clinch joining depends critically on the amount of plastic deformation that the sheet metals can undergo [21]. This makes clinching, in general, a well suited and widely used technique for joining ductile sheet metals. Recently, many researches aimed at extending clinch joining to join high strength and low ductility sheet metals. A heater gun was used by Lambiase et al. to locally heat AA6082-T6 aluminum sheets in order to provide some ductility for joining using conventional clinching [22-24]. Xiaocong et al. [25] have utilized oxyacetylene

flame gun to pre-heat the sheet metal to perform conventional clinches on TA1 titanium sheets. Abe et al. [26] have used another approach of tool adaptation to obtain conventional clinches in ultra-high strength steel sheets. In this work, rubber ring was used as a counter pressure tooling as shown in Figure 1.2. Neugebauer et al. [18] have utilized cartridge heaters underneath a flat anvil to obtain a die-less clinch. Hahn et al. [27] have used electromagnetic induction to heat AZ31 magnesium sheets to perform conventional clinches using a fixed die as shown in Figure 1.3. All of the above heating techniques suffer from significantly increased process times compared to room temperature conventional clinching.

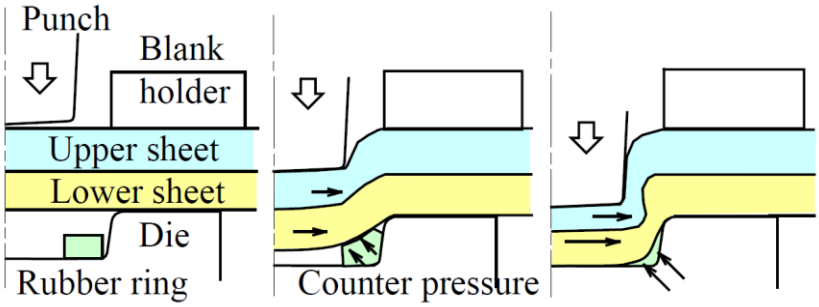

Figure 1.2. Scheme drawing showing the rubber counter pressure ring [26].

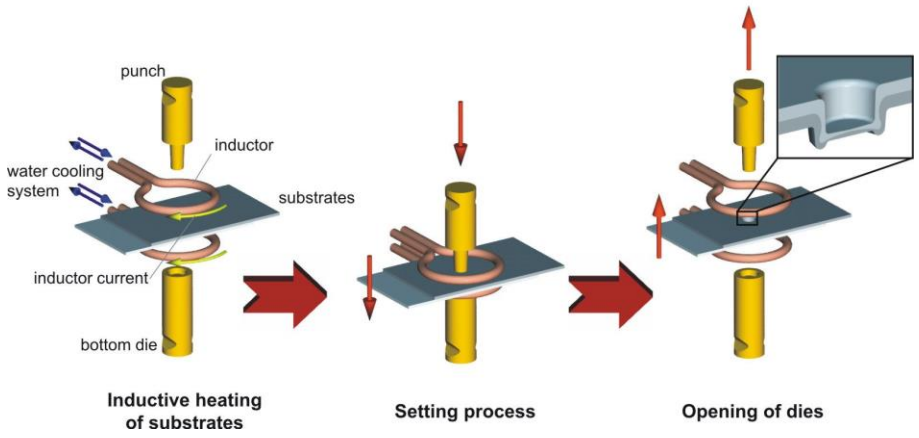

Figure 1.3. Scheme show clinch joining by using induction heating [27].

The present work is focused on joining of a high-strength, precipitation-hardenable aluminum alloy AA7075 in different temper states by clinch forming at room temperature as well as at higher temperatures. Two techniques were used for the room temperature joining study, conventional and die-less clinching. Each technique has its own advantages. The main advantage of conventional clinch is the relatively higher strength of resulting clinched joints. However, as stated earlier, the nature of the resulting interlock gives rise to unattractive surface steps on both surfaces of the joint. The die-less clinched joint, on the other hand, is characterized by one intact surface but a lower clinched strength. The die-less clinching study included a design of new tooling and a parametric study of the effect of the tool parameters on the formed joint. Also, the study involved development FE models to predict the final shape of the joint using different tool parameters. The elevated temperature die-less clinching operation is studied by locally heating the sheet materials using rapid electrical resistance heating.

1.4 Research Objectives

The general objective of the thesis is to join AA7075 aluminum sheets in different tempers by clinch joining for automotive as well as aerospace applications. The research objectives thus consist of the following specific objectives:

(i) Study of room temperature clinch-ability of AA7075 aluminum alloy under different temper states and assessment of joint strength:

Clinching is carried out by using two different processes, extensible conventional clinching and die-less clinching. Both of these processes are applied to study the clinch-ability of AA7075-O sheet materials to assess the effect of tool parameters on material flow and final shape of the formed joint. The die-less clinching study is extended to involve more tempers mainly T6 and W tempers to evaluate the effect of temper state on the flow of the material.

(ii) Numerical modeling of material flow during room temperature die-less clinching of AA7075 sheet materials and post-clinch performance of the joints:

With the aid of numerical methods such as finite element method (FEM), both the clinch joint formation as well as mechanical behavior of the clinched joint are studied. The numerical simulations are used to gain a better understanding of the relationship between geometrical parameter of the resulting clinched joint and the process parameters such as tool set configurations, numerical simulation parameters (element type and meshing), and sheet material properties (material model and friction behaviour). In order to accurately predict the flow of the material from the

models, the experimental results from Objective 1 are utilized for FE model validation.

(iii) High temperature die-less clinching of AA7075 aluminum alloy by rapid local electrical resistance heating:

This study deals with transient electrical resistance heating of the clinch region to increase its material flow, clinch-formability and post-clinch strength of low-formability AA7075-T6 sheets. Such a joint will help extend the range of structural applications of high strength AA7075-T6 sheet in automotive and aerospace body panels. Such studies are not available in the literature for high strength aluminum alloys including the AA7075 sheet material.

1.5 Thesis Organization

Subsequent chapters of the thesis are organized as follows:

Chapter 2. This chapter presents experimental as well as numerical results from conventional clinch joining process to understand the effect of tool parameters on the final shape of the joint and associated joint strength, Also flow of the material during the process is investigated. The post-clinching behaviour of the joint is studied by conducting single lap shear tests. A microstructure examination as well as micro-hardness mapping through a cross-section of the joint is carried out to gain further understanding of the material flow during joining was conducted. The experimental results are then used for validation of a FE model of clinching process. The content of this chapter is presented in

the journal paper format. The paper is currently under review in *Thin-Walled Structures* journal.

Chapter 3. This chapter deals with an experimental investigation of room temperature die-less clinch joining. The work includes a new tool design with different shapes of the blank holder which plays a key role in controlling the flow of the material during the process. Further, post-clinching behaviour of the formed joint was assessed using two types of tests, single lap shear and peel tests. This study is now published in *Thin-Walled Structures* [13] journal.

Chapter 4. This chapter deals with the effect of different parameters that affects the accuracy of FE simulation of die-less clinching process. The numerical parameters include mesh density, adaptive remeshing and the mass scaling factors. Also, the effect of the boundary conditions, which represent the tooling, on the formed joint are included. Further, the study includes various material models, the commonly used Swift, power and Voce laws in addition to a hybrid material model referred to as Extended-Voce model. The results from this study are written up as a journal publication that is currently under review in *International Journal of Material Forming*.

Chapter 5. In this chapter, background information and FE investigations are presented to study the material flow during the die-less clinch joining process. An axisymmetric 2D FE model is built and the die-less clinching is simulated based on a hybrid material model to predict the final shape of the formed joint. Furthermore, the predicted final shape of the joint is used to build 3D FE models to predict the strength of the joint. The results presented in this

chapter are written up as a journal publication that is currently under review for publication in *Thin-Walled Structures* Journal.

Chapter 6. In this chapter, background information and experimental investigations are presented to highlight a novel hot die-less clinching technique using a rapid electrical resistance heating system to enhance clinch-ability of AA7075 sheet in peak-aged condition. The study included a new tool design to enable passing current from the blank holder to the flat anvil through the joined sheets. The results presented in this chapter are written up as a journal publication and submitted to *Journal of Materials and Design*.

Chapter 7. In this chapter, common aspects of all results presented in Chapters 2-6 are discussed in the light of the research objectives of earlier Section 1.4

Chapter 8. In this chapter all conclusions from research on room temperature conventional clinching as well as room temperature and hot die-less clinching are presented, along with some suggestions for future work.

References

[1] P. Groche, S. Wohletz, M. Brenneis, C. Pabst, F. Resch, Joining by forming—a review on joint mechanisms, applications and future trends, Journal of Materials Processing Technology 214(10) (2014) 1972-1994.
[2] T. Gerstmann, B. Awiszus, Recent developments in flat-clinching, Computational Materials Science 81 (2014) 39-44.
[3] Y. Zhou, F. Lan, J. Chen, Influence of tooling geometric parameters on clinching joint properties for steel-aluminum hybrid car-body structures, Proceedings-2010 3rd IEEE International Conference on Computer Science and Information Technology, ICCSIT, 2010, pp. 441-445.
[4] M. Eshtayeh, M. Hrairi, A. Mohiuddin, Clinching process for joining dissimilar materials: state of the art, The International Journal of Advanced Manufacturing Technology 82(1-4) (2016) 179-195.
[5] J. Varis, Ensuring the integrity in clinching process, Journal of Materials Processing Technology 174(1) (2006) 277-285.

[6] K.-i. Mori, N. Bay, L. Fratini, F. Micari, A.E. Tekkaya, Joining by plastic deformation, CIRP Annals-Manufacturing Technology 62(2) (2013) 673-694.
[7] Y. Abe, K. Mori, T. Kato, Joining of high strength steel and aluminium alloy sheets by mechanical clinching with dies for control of metal flow, Journal of materials processing technology 212(4) (2012) 884-889.
[8] C. Chen, S. Zhao, X. Han, M. Cui, S. Fan, Investigation of the height-reducing method for clinched joint with AL5052 and AL6061, The International Journal of Advanced Manufacturing Technology (2016) 1-8.
[9] C. Chen, S. Zhao, M. Cui, X. Han, X. Zhao, T. Ishida, Effects of geometrical parameters on the strength and energy absorption of the height-reduced joint, The International Journal of Advanced Manufacturing Technology (2016) 1-9.
[10] C. Chen, S. Fan, X. Han, S. Zhao, M. Cui, T. Ishida, Experimental study on the height-reduced joints to increase the cross-tensile strength, The International Journal of Advanced Manufacturing Technology (2016) 1-8.
[11] T. Wen, H. Wang, C. Yang, L.T. Liu, On a reshaping method of clinched joints to reduce the protrusion height, The International Journal of Advanced Manufacturing Technology 71(9-12) (2014) 1709-1715.
[12] F. Lambiase, D.-C. Ko, Two-steps clinching of aluminum and Carbon Fiber Reinforced Polymer sheets, Composite Structures 164 (2017) 180-188.
[13] M.K.S. Atia, M.K. Jain, Die-less Clinching Process and Joint Strength of AA7075 Aluminum Joints, Thin-Walled Structures 120 (2017) 421-431.
[14] C. Borsellino, G. Di Bella, V. Ruisi, Study of new joining technique: flat clinching, Key Engineering Materials, Trans Tech Publ, 2007, pp. 685-692.
[15] C. Chen, S. Zhao, M. Cui, X. Han, N. Ben, Numerical and experimental investigations of the reshaped joints with and without a rivet, The International Journal of Advanced Manufacturing Technology (2016) 1-13.
[16] C. Chen, S. Zhao, M. Cui, X. Han, S. Fan, Mechanical properties of the two-steps clinched joint with a clinch-rivet, Journal of Materials Processing Technology 237 (2016) 361-370.
[17] C. Chen, S. Zhao, X. Han, M. Cui, X. Zhao, T. Ishida, Experimental investigation of the mechanical reshaping process for joining aluminum alloy sheets with different thicknesses, Journal of Manufacturing Processes 26 (2017) 105-112.
[18] R. Neugebauer, C. Kraus, S. Dietrich, Advances in mechanical joining of magnesium, CIRP Annals-Manufacturing Technology 57(1) (2008) 283-286.
[19] S. Lüder, S. Härtel, C. Binotsch, B. Awiszus, Influence of the moisture content on flat-clinch connection of wood materials and aluminium, Journal of Materials Processing Technology 214(10) (2014) 2069-2074.
[20] R. Neugebauer, R. Mauermann, S. Dietrich, C. Kraus, A new technology for the joining by forming of magnesium alloys, Production Engineering 1(1) (2007) 65-70.
[21] S. Coppieters, S. Cooreman, P. Lava, H. Sol, P. Van Houtte, D. Debruyne, Reproducing the experimental pull-out and shear strength of clinched sheet metal connections using FEA, International journal of material forming 4(4) (2011) 429-440.
[22] F. Lambiase, A. Di Ilio, A. Paoletti, Joining aluminium alloys with reduced ductility by mechanical clinching, The International Journal of Advanced Manufacturing Technology 77(5-8) (2015) 1295-1304.
[23] F. Lambiase, Clinch joining of heat-treatable aluminum AA6082-T6 alloy under warm conditions, Journal of Materials Processing Technology 225 (2015) 421-432.
[24] F. Lambiase, A. Di Ilio, Damage analysis in mechanical clinching: experimental and numerical study, Journal of Materials Processing Technology 230 (2016) 109-120.

[25] X. He, Y. Zhang, B. Xing, F. Gu, A. Ball, Mechanical properties of extensible die clinched joints in titanium sheet materials, Materials & Design 71 (2015) 26-35.
[26] Y. Abe, S. Nihsino, K.-i. Mori, T. Saito, Improvement of joinability in mechanical clinching of ultra-high strength steel sheets using counter pressure with ring rubber, Procedia Engineering 81 (2014) 2056-2061.
[27] O. Hahn, Y. Tan, M. Schroeder, M. Horstmann, Thermally supported mechanical joining of magnesium components, Materials Science Forum, Trans Tech Publ, 2005, pp. 365-370.

Chapter 2

Numerical modeling and experimental studies of extensible dies based clinching process for AA7075 aluminum sheet

---

Mostafa K. Sabra Atia, PhD student, is the first author and main contributor of the work who came up with the experimental design, analyzed the data, developed the model and composed the text as a paper describing the results. Mukesh K. Jain, Professor, is the supervisor who substantially contributed to the work by checking the experimental results and technical details of the model as well as improving the language of the paper. Byron Selorme provided technical support for the experimental work. This paper is under review in Thin-Walled Structures Journal.

Numerical modeling and experimental studies of extensible dies based clinching process for AA7075 aluminum sheet

MostafaK. Sabra Atia[a,b], Mukesh K. Jain[a], and Byron Selorme[c]

a Department of Mechanical Engineering, McMaster University, Hamilton, Ontario, Canada L8S 4L7.

b Corresponding author: Tel.: +1 905-920-0398. E-mail address: atiam@mcmaster.ca (M. Atia).

c Norlok Company, Brantford, ON, Canada N3S 7V2.

Abstract

Ability to mechanically clinch sheet materials depends on process and material parameters. An investigation of the effect of the tool parameters on material flow and the clinch quality of AA7075 high strength aluminum alloy was conducted experimentally and via numerical simulations. Various tool designs as well as different process parameters were used to obtain clinched joints using extensible dies. Further, micro-hardness measurements and microstructure examinations were carried out to gain a better understanding of material flow. Axisymmetric finite element (FE) model were also developed to simulate clinching experiments based on Swift, Voce, and a mixed material hardening law incorporating both Swift and Voce laws with a weight function. The results showed that using weight function of 0.5 gives good prediction of experimental clinching behavior. Experimentally validated FE model with a mixed hardening law was then used to systematically investigate the effect of tool parameters, namely punch and die corner radii, and die diameter, on geometry of the clinched joint. The results showed that punch-die clearance has a large effect on reduction in thickness of clinched sheets. Also, punch and die corner radii have a strong influence on ratio of thickness reduction of punch-sided and die-sided sheets respectively. The analysis was carried out in terms of forming load and geometrical parameter of the formed joint. Lastly, single shear test specimens were used to evaluate the joint strength.

Table 2.1. List of Abbreviations

T6	Artificial peak aged state which represents the hardest temper
O	Annealed temper state
N	Neck thickness of the joint
U	Interlock depth of the joint
X	Joint bottom thickness
R_{PC}	Punch corner radius
R_{DC}	Die corner radius
F	Forming force
σ_{eq}^{p}	Equivalent stress
ε_{eq}^{p}	Equivalent plastic strain
k_1	Stress coefficients for Voce hardening law
k_2	Stress coefficients for Swift hardening law
C	Material constant for Voce hardening law
m	Material constant for Voce hardening law
α	Weight function
$\sigma_{0.2}$	0.2 proof strength
n	Strain hardening exponent

Keywords: Clinching, extensible dies, experiments, numerical simulations, FE model

2.1 Introduction

Clinching is a forming process in which two or more sheet metals are locally deformed by using punch and die in order to form a geometrical interlock [1-4]. Unlike other traditional joining techniques such as riveting and bolting, joining by clinching does not need any auxiliary parts such as bolts, nuts, or rivets. Sheet clinching technology offers joining of similar or dissimilar sheets regardless of surface condition [5]. The thickness of the individual sheets can vary from 0.4 to 4 mm and thus the total thickness can range from 0.8 to 8 mm [2]. The main feature of the clinched joint is a protrusion on the die side and a pit on the punch side [2]. Generally, the required force for the clinching

lies between 10 and 100 kN based on the sheet material properties and the tool geometry [2]. Clinching requires an overlap between the two joined sheets and a die set-up where punch locally moves into the die pushing the sheets towards the die severely thinning the sheets and causing highly localized strains in the joint [6]. Tool dimensional parameters are the key to forming a strong joint [7-9]. Lee et al. [7, 8] have presented a tool design for clinching using fixed dies based on the volume of die-punch cavity. An optimum combination of tool parameters has been achieved using Taguchi's design of experiments [9]. Because of complexity of material flow during the clinching process, with equivalent plastic strain often exceeding unity, experimental approach alone is not sufficient [10]. FE modeling of the clinching process can provide an efficient method of optimizing the clinching process by analyzing the effects of individual process and material parameters on clinch characteristics [11-15]. In order to optimize the tool parameters, the effect of process parameters on the quality of the formed joint interlock depth and the neck thickness is essential [4, 16], see Figure 2.1. Also, the strength of the joint can be predicted analytically or by using a separate three-dimensional (3-D) FE model of the pull-out test [17].

The main difficulty for the use of clinching as a joining technique is the high stress concentration that often results in crack formation in the corners of punch and die-sided sheets or failure of interlock formation [18, 19]. In our view, this makes clinching more suitable for relatively softer and highly ductile sheet materials. Initially, most of research had focused on clinching of steel sheets [2, 20-23]. More recently, researchers have started to study clinching of light alloys including aluminum sheets. Clinching of

AA5xxx series aluminum sheets has been extensively studied [6, 24, 25] as well as some studies on clinching of AA6xxx series aluminum alloys [26, 27]. In a recent study, Lambiase et al. [15] have studied the clinch-ability of AA6111 aluminum alloy. A modified geometry of tooling set was developed in order to reduce the magnitude and localization of plastic strain. Also, Jiang et al. [28] have studied the effect of pre-straining aluminum on the static strength of the joint performed by clinching the aluminum sheet to steel. The results showed that the resulting work hardening from pre-straining causes a reduction in the ductility and damage in AA6111 sheet. A small pre-strain of 5% causes significant decrease in the joint strength (20%). It is to be noted that no investigation, to the authors' knowledge, has been reported on clinch joining of higher strength AA7xxx series aluminum sheets which are increasingly being considered for automotive applications. The present work is an attempt to address this shortcoming.

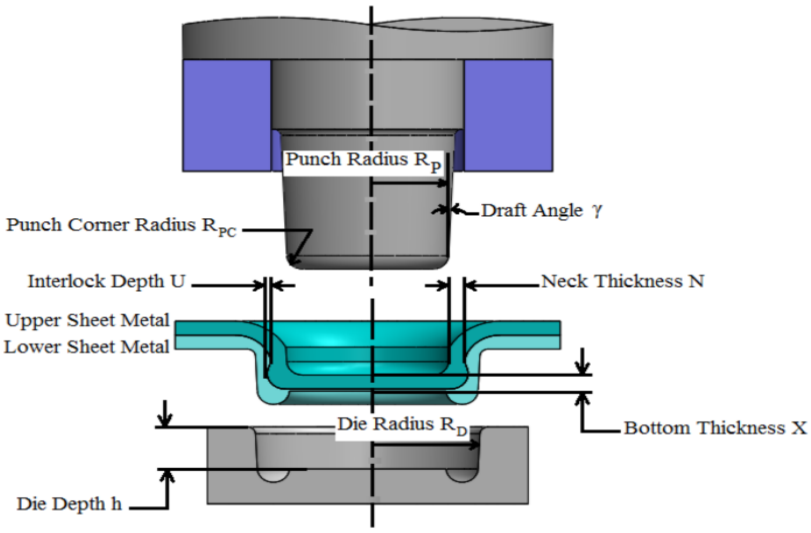

Figure 2.1. Cross section of a clinched joint showing the geometry of the joint and tool parameters.

The present study involves clinching of the high strength AA7075 aluminum sheet in the softer O-temper condition, referred to as AA7075-O sheet. A range of tool geometric parameters within the FE modeling approach are used to investigate the clinch-ability of this alloy. The FE method is used to improve clinch quality by studying the material flow and accompanying geometric changes in the formed joint.

2.2 Materials and Methods

2.2.1 Material

AA7075-T6 aluminum sheet of 1.27 mm nominal thickness was received in peak-aged T6- temper state. The sheet was partially annealed by heating at 413°C for 1 hour in a furnace, in ambient air, in order to enhance the ductility of the sheet (AA7075-O). The mechanical properties at each material state were obtained by conducting uniaxial tensile tests according to the ASTM-E8 standard for sheet materials. The tests were conducted using instrumented screw-driven Instron universal testing machine of load capacity of 100 kN at a cross-head speed of 1 mm/min. Sub-size sample dimensions of 120 mm length X 6 mm width, as per the ASTM standard E8M were utilized, as shown in Figure 2.2. The resulting mechanical properties in the as-received (T6) and annealed (O) temper states are presented in Table 2.2.

Table 2.2. Mechanical properties of 7075 aluminum alloy in T6 and O-temper states.

Mechanical properties from uniaxial tension tests				
Temper Designation	Description	$\sigma_{0.2}$ (MPa)	σ_{UTS} (MPa)	Total Elongation (%)
T6	As-received	580	695	12
O	Annealed	175	295	15

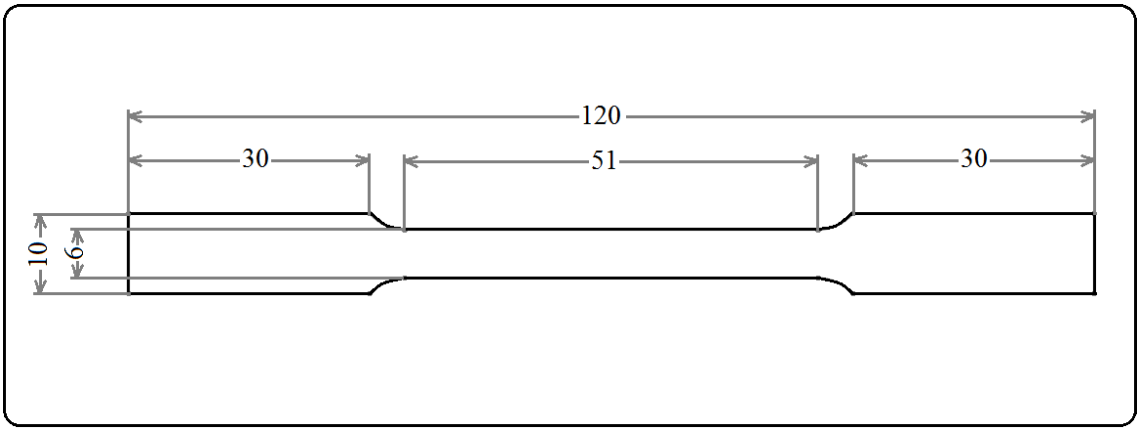

Figure 2.2. A drawing for the sub-size sheet tensile test specimen as per ASTM standard E8M (dimensions in mm).

2.2.2 Experimental Procedure

Clinching tests were carried out using LL4000 commercial press from Norlok Technology Inc., based in Brantford, Ontario, Canada, with a set of standard extensible dies. Dies of various depths were considered (with depth h values of 0.9 mm, 1 mm and 1.15mm, see Figure 2.3). A 4.6 mm diameter punch with a corner radius R_{PC} of 0.25 mm was used to perform the clinches. The joining process was controlled by either the forming force or the punch stroke (by controlling the X-parameter, see Figure 2.1). The X-parameter was introduced for the first time by Varis et al. [2] and has proved useful in characterizing the clinching process as it can be easily measured, without resorting to a destructive method. In the present work, various forming forces were selected, namely, 15 kN, 20 kN, 25 kN, and 30 kN, to control the joining process and the X-parameter was measured from the cut cross-sections through the joint. For an analysis of material flow and microstructure evolution during clinching, the joints formed at different punch strokes were cut and mounted using conventional optical metallographic methods of hot

and cold mounting in a polymeric resin. Various stages of specimen polishing were followed to obtain high quality, scratch-free, surfaces. For the microstructures of clinched, poorly clinched (or un-clinched) sheets, a caustic etchant consisting of a mixture of 10 gm NaOH and 90 ml of distilled water was used in a water bath at 60°C. The samples were then dipped in 50% Nitric acid to complete the etching process. A high magnification digital optical microscope (KEYENCE VHX-2000) was used to capture the microstructural images. Also, after etching, Vickers micro-hardness distribution maps were obtained in the clinched region as a measure of local strengthening of the joint from increased plastic flow.

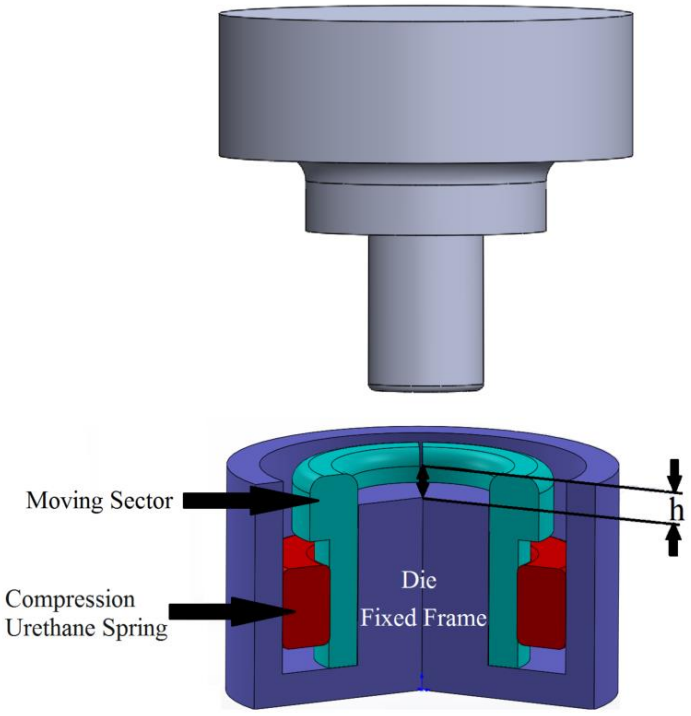

Figure 2.3. A schematic drawing of the tools utilized in the clinching process. The punch moves down from the top towards the lower, segmented, extensible die to create the clinched joint.

2.2.3 Mechanical characterization of clinched joints

In order to assess the mechanical strength of the clinched joints, single lap shear tests were conducted. Figure 2.4 shows the dimensions of the sample used as well as a schematic of a typical force versus displacement trace. An instrumented universal MTS testing machine of 100 kN load capacity was utilized for mechanical characterization. The tests were carried out at ambient temperature with a cross-head speed of 1 mm/min until the two sheets were completely separated. Five samples for each test condition were tested for repeatability of data. The resulting force-displacement curve were analyzed to obtain two main characteristics of the clinched joint: mechanical strength and toughness. The strength of the joint was expressed by the maximum force that the joint was able to withstand, while the joint toughness was expressed by total area under the force-displacement trace.

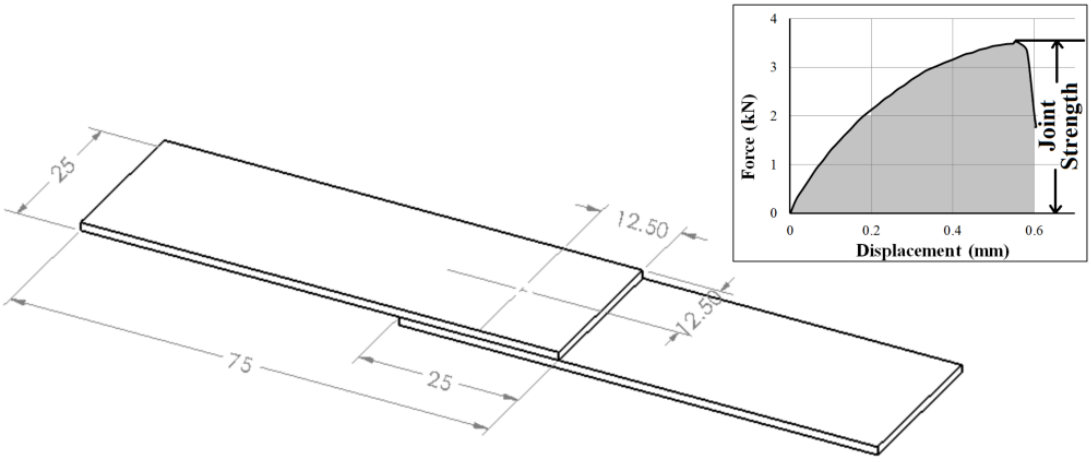

Figure 2.4. Drawing of the sample used for lap shear test sample and a typical force-displacement response from the test.

2.2.4 FE Modeling

Clinching is a rather complex forming process where very large plastic strains in the interlock region in the strain range of 2-3 exist. FE method offers a possibility of simulating this complex forming process by incorporating specific tool geometry, sheet thicknesses, sheet elastic and plastic properties, tool-sheet contact, and friction between all tool and sheet contacting surfaces. The simulation allows a systematic capture of the material flow and stress and strain evolution within the clinched members at different punch depths. Generally, such detailed flow behavior is experimentally unobtainable given the small geometry of the clinch, the test speeds of the process and the limitations of the experimental strain measurement equipment. The data in terms of sheet thickness variation in different regions of the clinch requires careful cutting, mounting of specimens in epoxy and careful measurements of thickness. These experimental process steps can be costly and time consuming. FE simulations offer an efficient and comprehensive means of understanding the clinching process.

The FE modeling was carried out using commercial FE code ABAQUS which has been extensively used for sheet metal forming simulations in the past. The explicit version of Abaqus is typically preferred when simulating complex sheet forming operation involving multiple tool-sheet interaction due to its more robust contact algorithm and solver for such problems. Also, as the model size increases, the explicit solver exhibits significant cost (or time) saving over implicit solver. As a result of axisymmetric nature of tooling and the clinch geometry as well as the loading conditions,

an axisymmetric 2D model was built by considering the tooling as rigid bodies to reduce number of elements. Tool motions and constraints were defined by boundary conditions in the simulation. Figure 2.5 illustrates the different tool parameters in the present study. The sheet materials were represented by 4-node bilinear axisymmetric quadrilateral element with reduced integration (CAX4R). Enhanced hourglass control option was used to avoid hour-glassing problem during very large deformation simulation. The sheet metals were initially divided into 35 elements through the thickness. The FE mesh size in the clinching region was kept small, of 0.03×0.02 mm, while outside the clinching region, it was kept larger, of 0.03×0.1 mm. Due to large deformation and highly localized nature of plastic strain in the clinch region, steps were necessary to prevent excessive mesh distortion. Adaptive re-meshing option within Abaqus was used to reduce computational run time using the arbitrary Lagrangian-Eulerian (ALE) method. Advanced algorithm based on evolving geometry with volumetric smoothing was implemented to attain stable numerical solution.

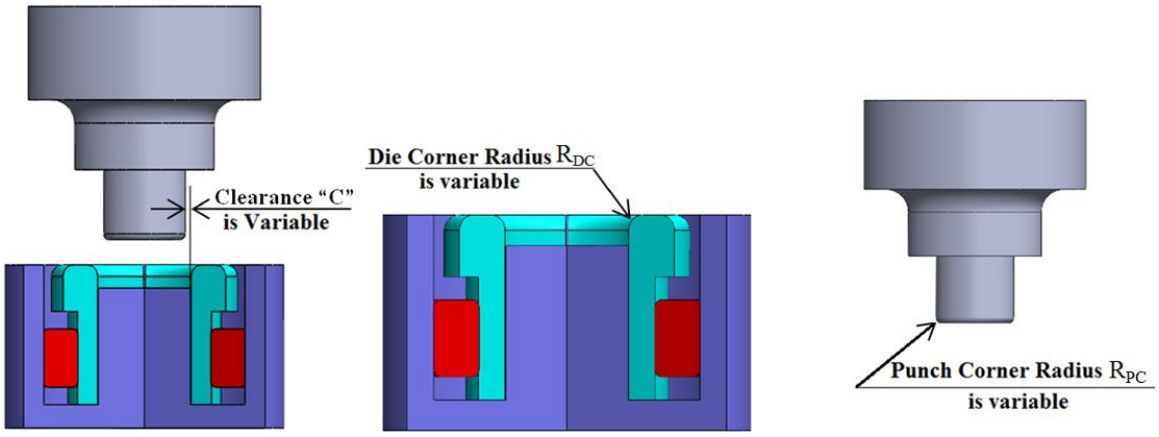

Figure 2.5. A schematic illustration of the different tool parameters in the modeling study.

The sheet materials were assumed to be isotropic elastic and work hardening plastic following Von Mises yield criterion. Two non-linear work hardening laws were used to represent the experimental plastic stress-plastic strain data from a uniaxial tensile test, and to extrapolate the data beyond the tensile stress-strain limit to large strains typical of highly strained regions of the clinch. The Voce and Swift (also referred as 'power') hardening laws utilized in the present work are expressed as:

$$\sigma_{eq}{}^{p} = C\left[1 - m\ exp\left(k_1 \varepsilon_{eq}{}^{p}\right)\right] \qquad (2.1)$$

$$\sigma_{eq}{}^{p} = k_2\left(\varepsilon_0 + \varepsilon_{eq}{}^{p}\right)^n \qquad (2.2)$$

where, σ_{eq}^{p} and ε_{eq}^{p} are the equivalent plastic stress and strain respectively, k_1 and k_2 are stress coefficients in eqns.(2.1) and (2.2) respectively, n is the strain hardening exponent, C and m are two other material constants. The values of hardening parameters of each model are shown below in Table 2.3.

Table 2.3. Material parameters from non-linear least square curve fitting to uniaxial true stress-true strain data for Swift and Voce hardening models.

Swift Parameters			Voce Parameters		
K_2 (MPa)	n	ε_0	C	K_1	m
485.9	0.2071	0.00124	319.4	24.19	0.4769

Voce hardening law assumes that plastic stress saturates at large plastic strains (equation 2.1). In contrast, the Swift hardening law assumes that the strain continues to increase with stress and no saturation is reached in stress. Both of these hardening laws are approximate for most aluminum alloys. Experimental true stress-true strain data beyond uniform elongation regime in a uniaxial tensile test typically lies between the two

curves. For this reason, the two hardening laws have been combined with a weight function approach to predict the plastic hardening behavior midway between the two hardening laws, as described by equation 3:

$$\sigma_{eq}{}^{p} = \alpha\ \sigma_{eq}{}^{p}\Big|_{Swift} + (1-\alpha)\ \sigma_{eq}{}^{p}\Big|_{Voce} \qquad (2.3)$$

where, a weight function $\alpha = 0.5$ was chosen after completing an assessment of the effect of different α values on clinch characteristics. Figure 2.6 demonstrates the extrapolation of true stress-true plastic strain curves using Voce, Swift and weight function ($\alpha = 0.5$) approaches.

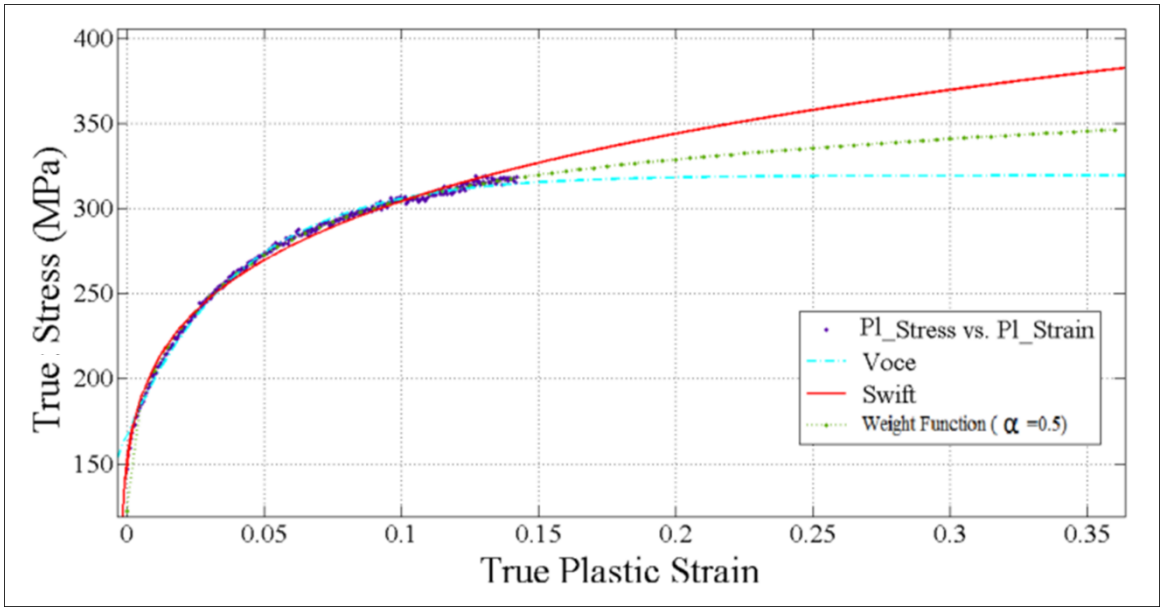

Figure 2.6. Experimental AA7075-O stress vs. plastic strain curve from uniaxial tension test and its extrapolation using different non-linear hardening laws.

The material model of the polymer spring was considered hyper-elastic with Mooney-Rivlin strain energy potential [25]. In order to simulate the interaction between each part, coulomb friction law was adopted. Different friction coefficient values were

utilized in a preliminary study. It was found that a coefficient of friction value of 0.15 and 0.4 for friction between sheet-tools and between the two sheets respectively provided the best match between the experimental and model results. These values were thus used in the present simulation work. The above values are comparable to those presented in reference [23].

2.3 Result and discussion

2.3.1 The effect of material constitutive model on FE results

Figure 2.7 illustrates the "S" shape interface between two sheets in the experimental and simulated joints by using different material models. The results show that the use of Voce model results in a larger interlock depth and a lower neck thickness when compared with Swift model. However, using weight function (α=0.5) gives a moderate interlock depth which is comparable to the experimental results (the deviation is of the order of 0.02 mm). The results reflect the significance of using a suitable hardening law for extrapolation of uniaxial stress-strain curves to large strains in predicting material flow in the clinched region.

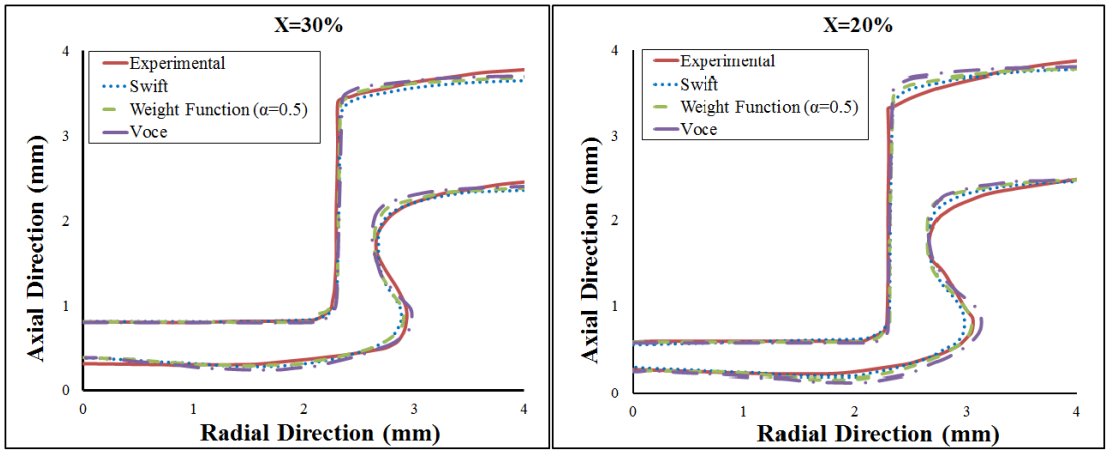

Figure 2.7. Effect of different material models on the clinch profile.(0.9 mm die depth, 0.25 punch corner radius, 0.5 die corner radius, and 0.25 % X-parameter)

Results similar to Figure 2.7 are shown in Figure 2.8 where experimental clinch profiles on the left from cut and mounted cross-sections are compared with those obtained from FE simulations by using weight function (α=0.5) at different punch depths. Figure 2.9 shows a plot of U versus X parameter and N versus X parameter values (see Figure 2.1 for nomenclature) as obtained from experiments and FE simulations. Again, an acceptable (the error in U and N values less than 3%) agreement is achieved in the two cases. Figure 2.10 represents a comparison between the equivalent plastic strain distribution obtained by FEM and measured micro-hardness contours in the clinched region from experiments. The punch-sided sheet exhibits high hardness in the neck-thickness as well as at the bottom corner. The higher hardness is attributed to high friction between the punch and the material of the upper sheet as well as the excessive tension in the neck region. In addition, the highest plastic strain was observed in the die-sided bottom sheet. This is because the bottom of the die-sided sheet is highly restrained by the

bottom die and subjected to a large compressive force that restricts the material flow in the axial direction.

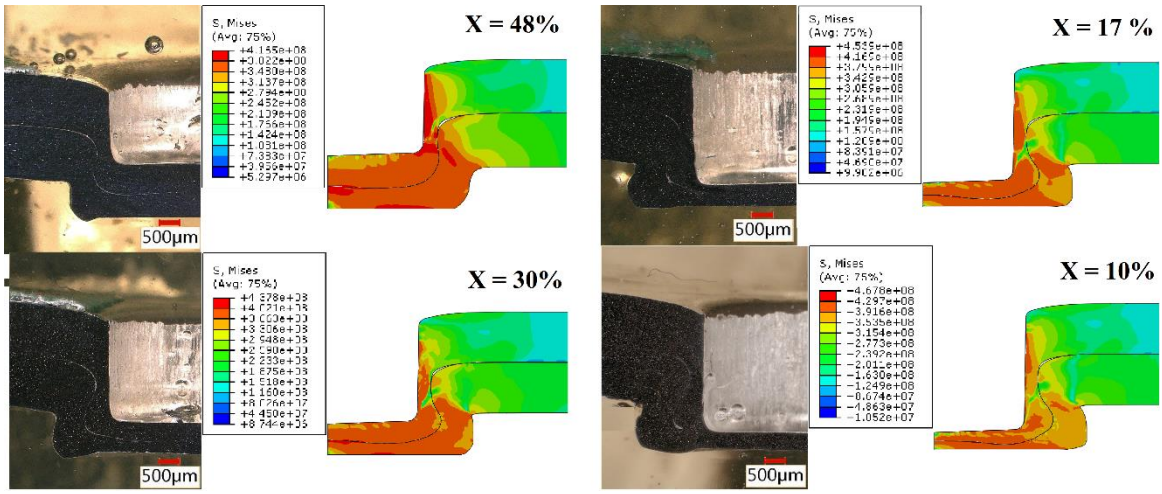

Figure 2.8. Experimentally obtained cut cross-sections through the clinched joint and corresponding FE predicted joint shapes (for weight function α = 0.5).

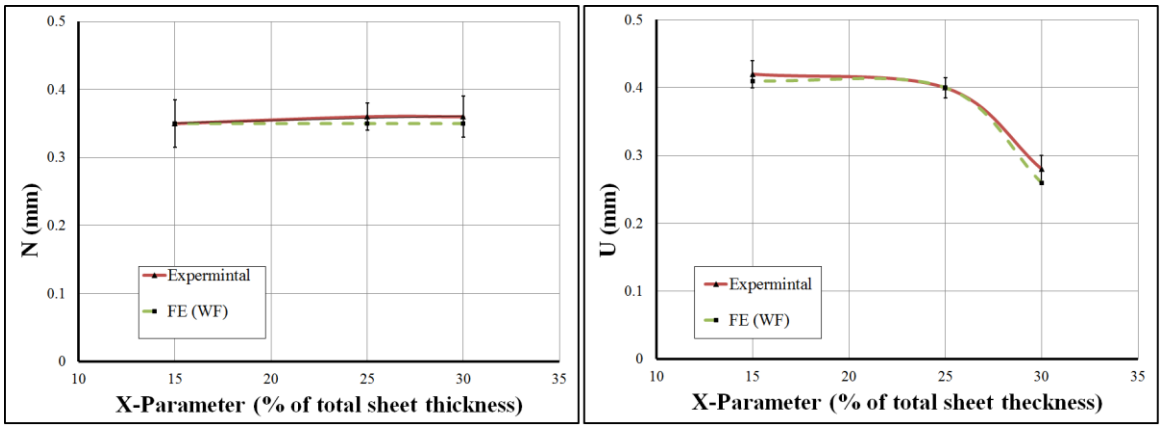

Figure 2.9. Comparison between experimental and FE-based U and N values as a function of X parameter (α=0.5) values (0.9 mm die depth, 0.25 punch corner radius, 0.5 die corner radius, and 0.25 % X-parameter).

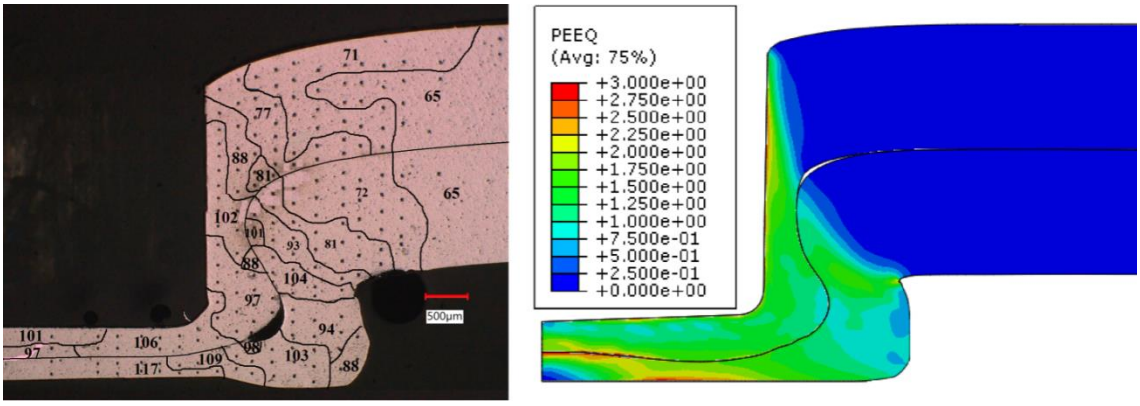

Figure 2.10. Comparison equivalent plastic strain distribution obtained by FE simulation and measured Vickers micro-hardness distributions (0.9 mm die depth, 0.25 punch corner radius, 0.5 die corner radius, and 0.25 % X-parameter).

2.3.2 Numerical analysis of material flow in the clinched region

Figure 2.11 shows a typical punch load-displacement trace for the clinching process obtained from the FE simulation. Four stages (I, II, III and IV) are identified on the trace based on the characteristic slopes associated with them. The clinched region corresponding to stages II, III and IV are presented with equivalent plastic strain contours in Figure 2.12. Plastic strain distribution points at the beginning of the stages II, III and IV as well as at points (a, b, and c) are selected for plotting the equivalent plastic strain distributions in Figure 2.12. For each of the 6 points, 3 plastic strain distributions correspond to 3 different cases of punch and die corner radii are included, as illustrated for point IIa in Figure 2.12. The plastic strains in the clinch region increase as one moves through stages II to IV, as shown in Figure 2.12. Also, the spread of plasticity depends up on the punch and die corner radii with increasing spread at large punch and die corner radii. In the first stage (stage I, Figure 2.11), the blank holder starts to apply a clamping force to the sheets. The second stage starts at point II (Figure 2.11), where the punch

starts to exert a load on the upper sheet (see Figure 2.12, stage II). It is also noted that at this stage, (points II and a in Figure 2.11 and Figure 2.12), there is no movement of the die sectors as indicated by a pair of vertical lines indicating the position of the bottom die at the bottom of each of the images in Figure 2.12. Decreasing the corner radius of the die or punch induces larger plastic strains at the die or punch-sided sheets respectively. Also, the punch corner radius affects the thickness reduction of the punch-sided sheet, whereas, the die corner radius affects the thickness reduction of die-sided sheet. In other words, a decrease in the punch and die corner radius means a smaller contact area and thus a higher thinning of the two sheets and the clinching process starts to resemble a metal cutting operation. The results with the smallest punch and die corner radii (the middle column) exhibits the highest plastic strain in both sheets when compared with the other cases. The third stage starts at point III, where the lower sheet begins to come in contact with the fixed frame of bottom die. This stage is accompanied by more significant increase in the forming force and is similar to the upsetting process for the two sheets. In this stage (points III and b on the curve), the material flow in the axial direction is highly restricted by the punch and bottom of the die. It results in large material flow in the radial direction that can be noted from the increased movement of the die sectors. The fourth stage starts at point IV at approximately 50% reduction in the sheet thickness (X=50%). The material starts to rotate around in the circumferential direction and lies on the intersection point between the die corner radius and the horizontal side of the die moving sector, shown as a point with a red dot. Stage IV results in the formation of a material interlock between the two sheets. The above interpretation of material flow and plastic

strain development is consistent with the microstructure study described later in subsection 2.3.4.

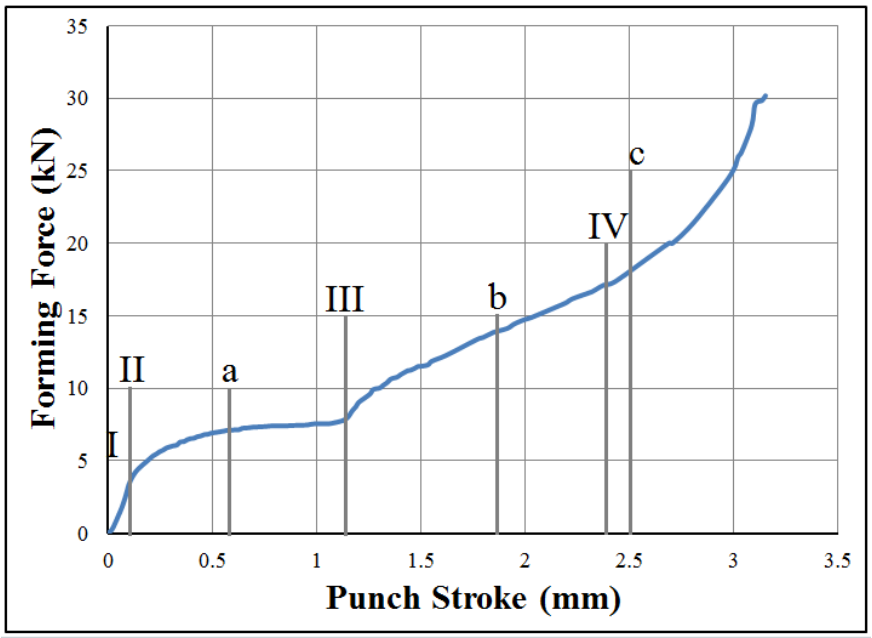

Figure 2.11. A typical punch stroke-displacement trace for the clinching process as obtained from FE simulations (0.9 mm die depth, 0.25 punch corner radius, 0.5 die corner radius, and 0.25 % X-parameter).

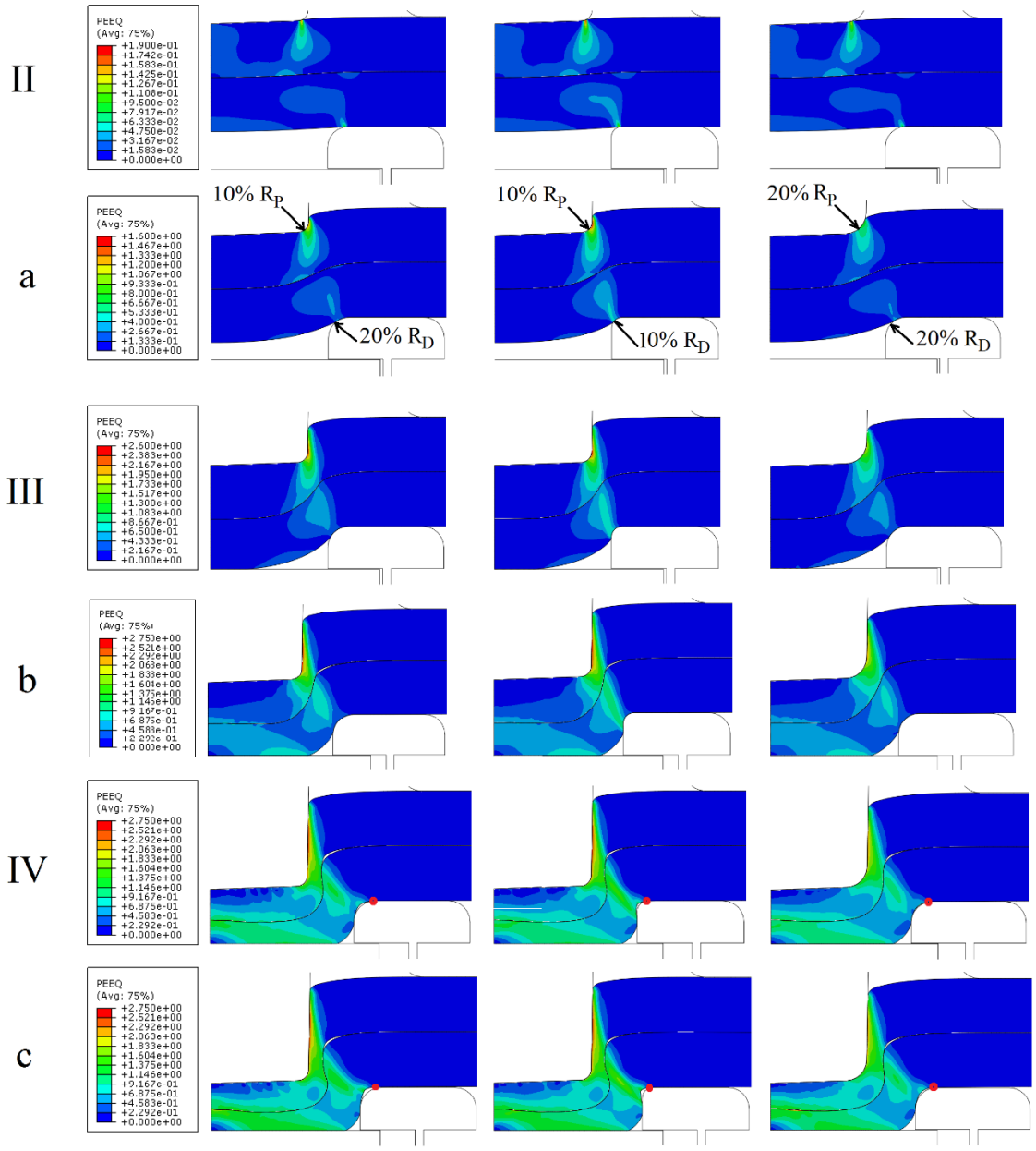

Figure 2.12. Equivalent plastic strain distributions in the clinched region for positions specified in Figure 2.11, for different tool configurations. The red dots in the last two rows demonstrate the rotation axis of the material in the last stage of clinching process resulting in an interlock formation (0.9 mm die depth, 0.25 punch corner radius, 0.5 die corner radius, and 0.25 % X-parameter).

2.3.3 The analysis of the geometry and forming force of the joint

2.3.3.1 Numerical analysis of effect of C-value

The effect of the C- value on the "S" shape of the joint is shown in Figure 2.13. In general, for different clearance values, an increase of the punch stroke results in an equivalent increase in the interlock as well as change in the shape from curvy “S” shapes to a flattened curve, as shown in Figure 2.14(b). Furthermore, Figure 2.15 presents neck thickness “N” and interlock depth “U” as a function of clearance C value and X parameter. A noticeable increase in the depth of the interlock can be observed compared with the reduction in the neck thickness. This is consistent with the result obtained by Mucha and Lambiase [16, 29]. The lower the C value, the higher the interlock depth and a moderate decrease in the neck thickness.

The reduction in the total sheet thickness is inversely proportional to the gap between punch and die (i.e., C) parameter. A smaller clearance results in larger flow in the radial direction (assuming the same amount of material trapped between punch and die for different C values). This increased radial flow can result in increased interlock. Moreover, decreasing the clearance between punch and die results in a reduction in the thickness of the punch-sided sheet in the neck region

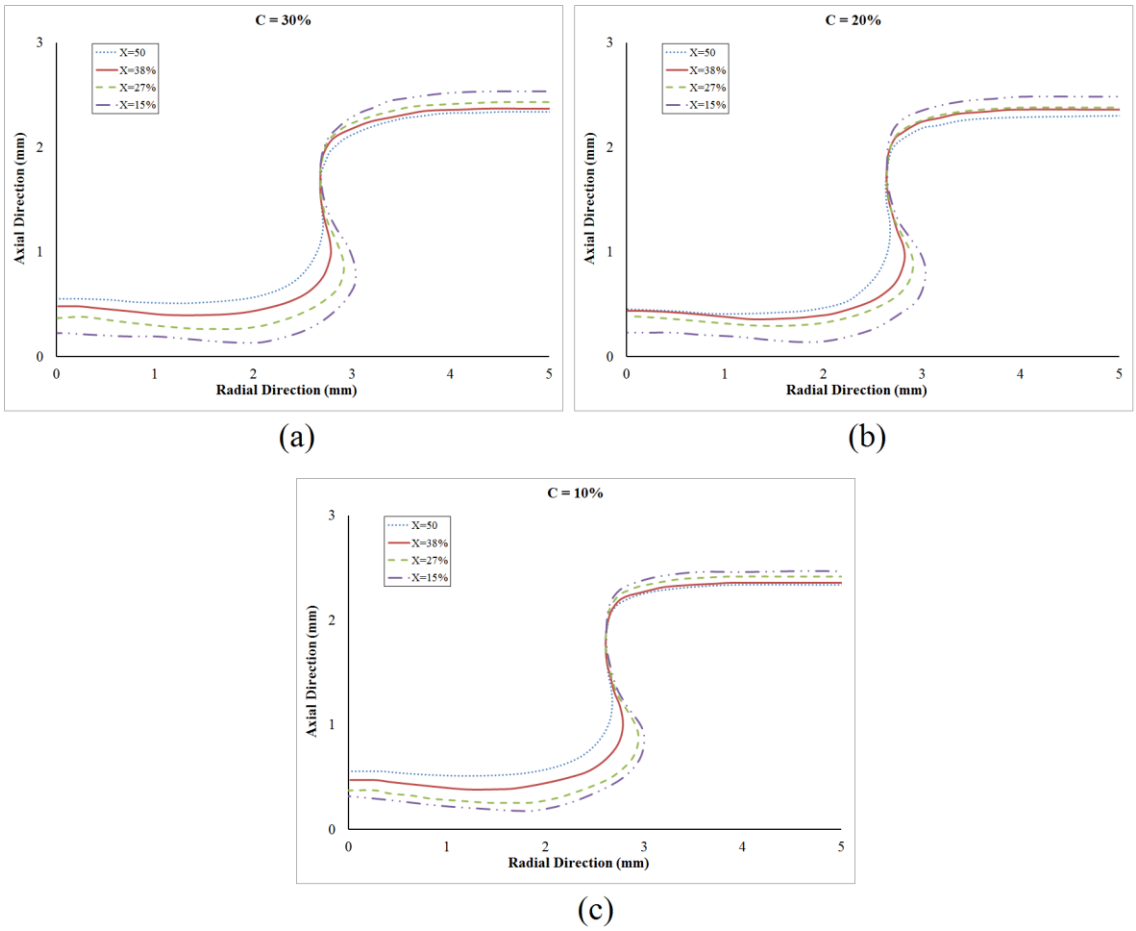

Figure 2.13. Effect of clearance C and X parameters on interlock characteristics (0.9 mm die depth, 0.25 punch corner radius, and 0.5 die corner radius).

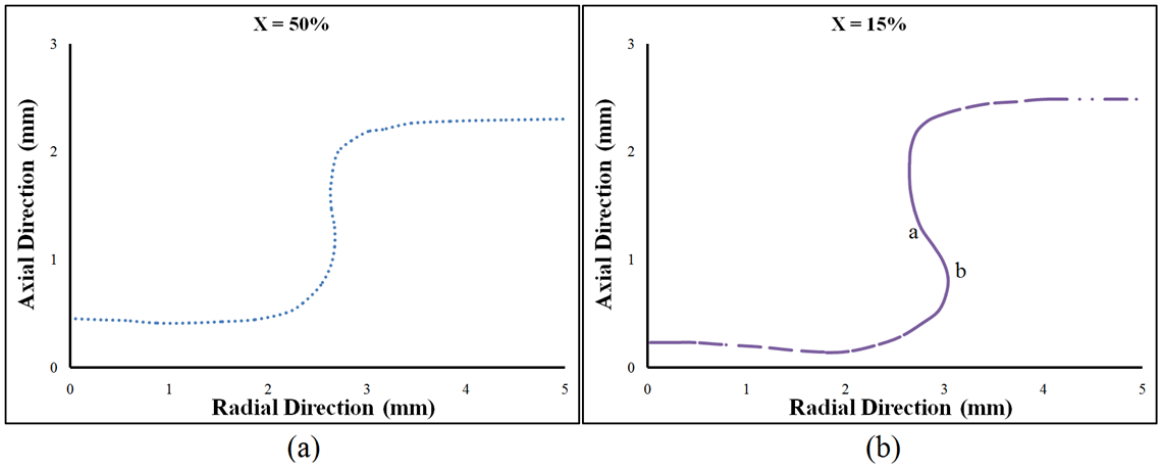

Figure 2.14. Effect of X parameters on interlock characteristics (20% C-value, 0.9 mm die depth, 0.25 punch corner radius, and 0.5 die corner radius).

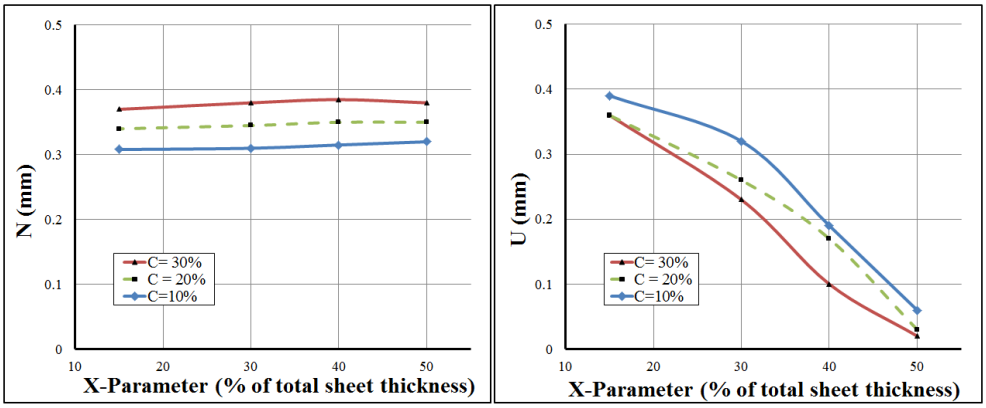

Figure 2.15. Effect of clearance C and X-parameter on N and U values (see Figure 2.1, 0.9 mm die depth, 0.25 punch corner radius, and 0.5 die corner radius).

A change in the clearance between the punch and die is accompanied by a change in the required forming force, and consequent change in the energy consumed during joining. The forming force is a useful signature of the clinching process as it can help with the selection of proper tooling. Figure 2.16 shows the required forming force as a function of change in clearance C for X-parameter value of 25% (an optimal value as per [29]). The figure shows almost linear increase in the force with a reduction in the

clearance. The increase in the force compensates for the higher reduction in the sheet thickness along the clinch wall.

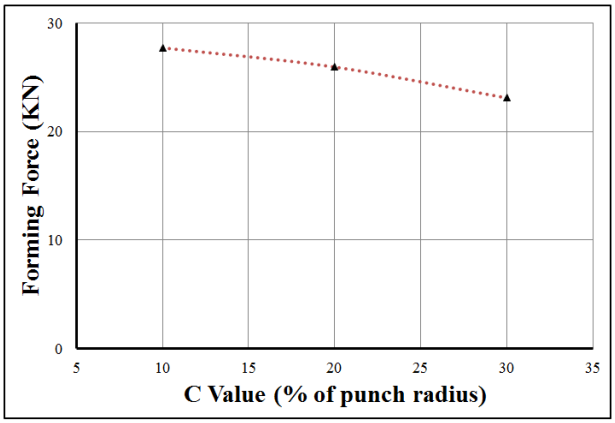

Figure 2.16. Forming force as a function of the clearance C for X=25% (0.9 mm die depth, 0.25 punch corner radius, and 0.5 die corner radius).

2.3.3.2 Numerical analysis of effect of R_{PC} and R_{DC} values

As shown in the previous sub-section 2.3.2, the punch and die corner radii have an effect on the strain distribution through cross-section as well as the amount of reduction in both sheets of the joint which in turn could affect the shape of the joint. This effect is further illustrated in Figure 2.17 and Figure 2.18 respectively. However, the effect of the punch corner radius is more dominant compared to die corner radius. An increase in the punch corner radius from 10% to 20% results in a decrease in interlock depth by 35% and an accompanying increase in neck thickness by 15% (Figure 2.17). This means that the reduction in the punch-sided sheet thickness in the neck region is more important to the clinching process. On one hand, it affects neck thickness, and, on the other hand, it greatly affects interlock formation. Clearance between punch and die fixed frame as well as punch and die corner radii, are critical to avoid blanking of the sheet. Collectively, the

above factors result in an increase in the plastic strain distribution with decreasing gap between the punch and die.

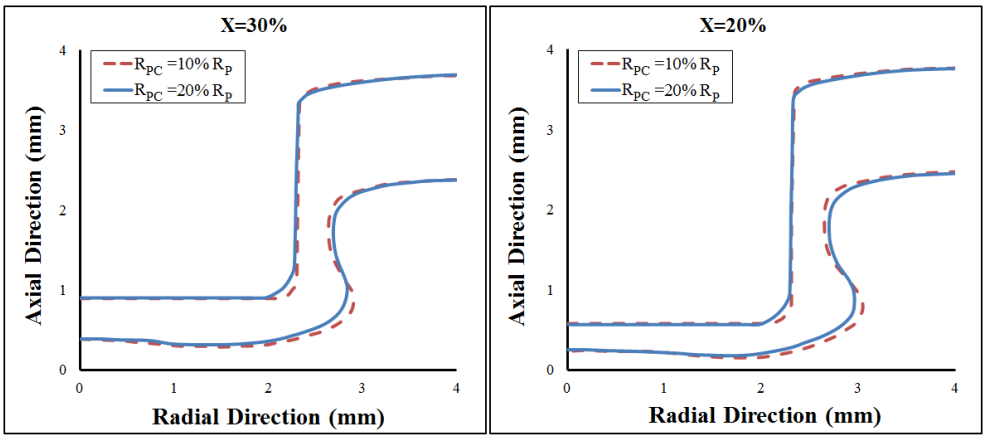

Figure 2.17. Effect of punch corner radius on clinch thickness profile for different X-parameters (0.9 mm die depth and 0.5 mm die corner radius).

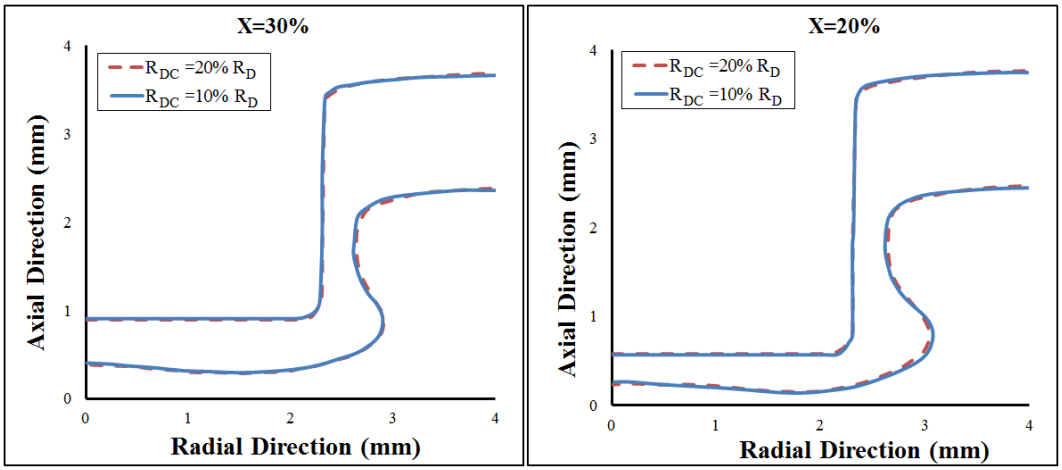

Figure 2.18. Effect of the die corner radius on clinch thickness profile for different X-parameters (0.9 mm die depth and 0.25 punch corner radius).

2.3.3.3 Experimental analysis of the effect of die depth

The effect of the die depth has been studied experimentally. The sheet materials were successfully joined by clinching using die depths h of 0.9 mm and 1 mm by

applying a range of forming forces. However, for forming forces below 25 kN, clinching could be achieved with 1.15 mm die depth only. Figure 2.19 shows cut and mounted joint cross-sections formed using different dies and by applying different punch forces. As shown, the higher forces cause greater material flow in the radial direction that result in larger interlock depths. However, the neck and bottom thicknesses (or X-parameter) decrease resulting in cracks and material separations.

Figure 2.20 illustrates the relation between the process variables, forming force and die depth, and resulting geometrical parameters of clinch. At higher forming forces, the X-parameter and the neck thickness (N) decreases whereas interlock depth (U) is increased. However, the forming force has a larger influence on interlock depth compared to the neck thickness. This experimental results is compatible with the simulation results as shown in the previous subsection 2.3.3.1. The X-parameter showed a rapid reduction from a large value at smaller die depth to a lower value at larger die depth. For the same die depth, the geometrical parameter changed more rapidly at first with increasing forming force and then more gradually at higher forming forces. The lowest die depth, with the smallest concentration of plastic deformation around the punch corner, results in retardation of sheet failure. However, the value of the interlock depth decreases. In other words, both the die depth and forming force exhibit the same trend in terms of the three geometrical parameters (X, N and U). Additionally, the effect of die depth on interlock depth and neck thickness is larger at lower forming forces.

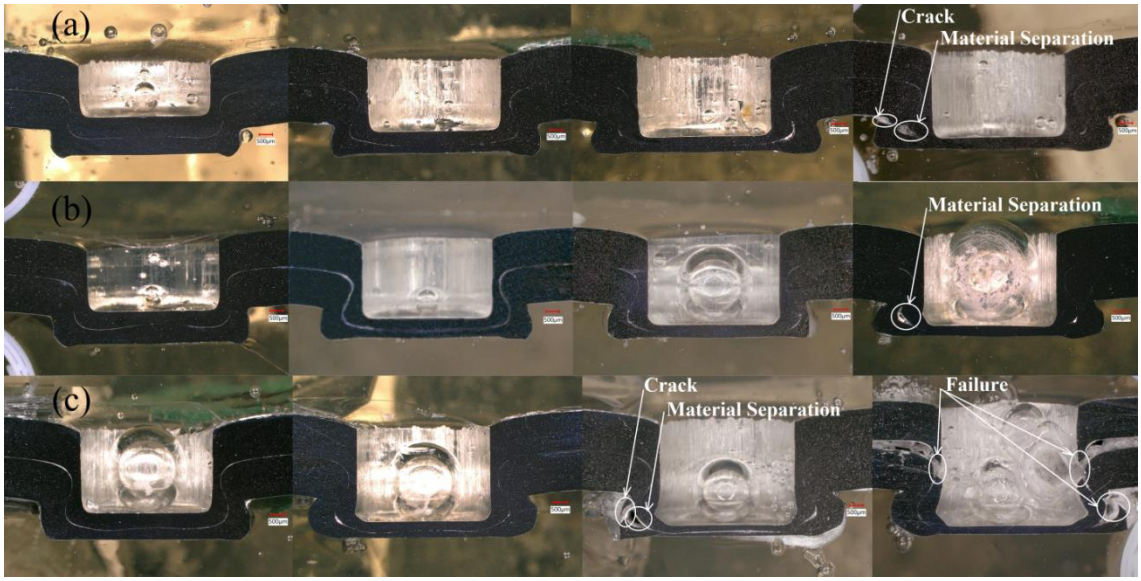

Figure 2.19. Cut and mounted cross-sections of clinched joints from different test conditions involving different dies and forming forces, 15 kN, 20kN, 25kN, and 30kN (from the left to the right), (a) die depth= 0.9mm, (b) die depth = 1mm, and (c) die depth= 1.15mm. A joint that failed in the neck is shown for die depth = 1.15mm at a forming force of 30 kN.

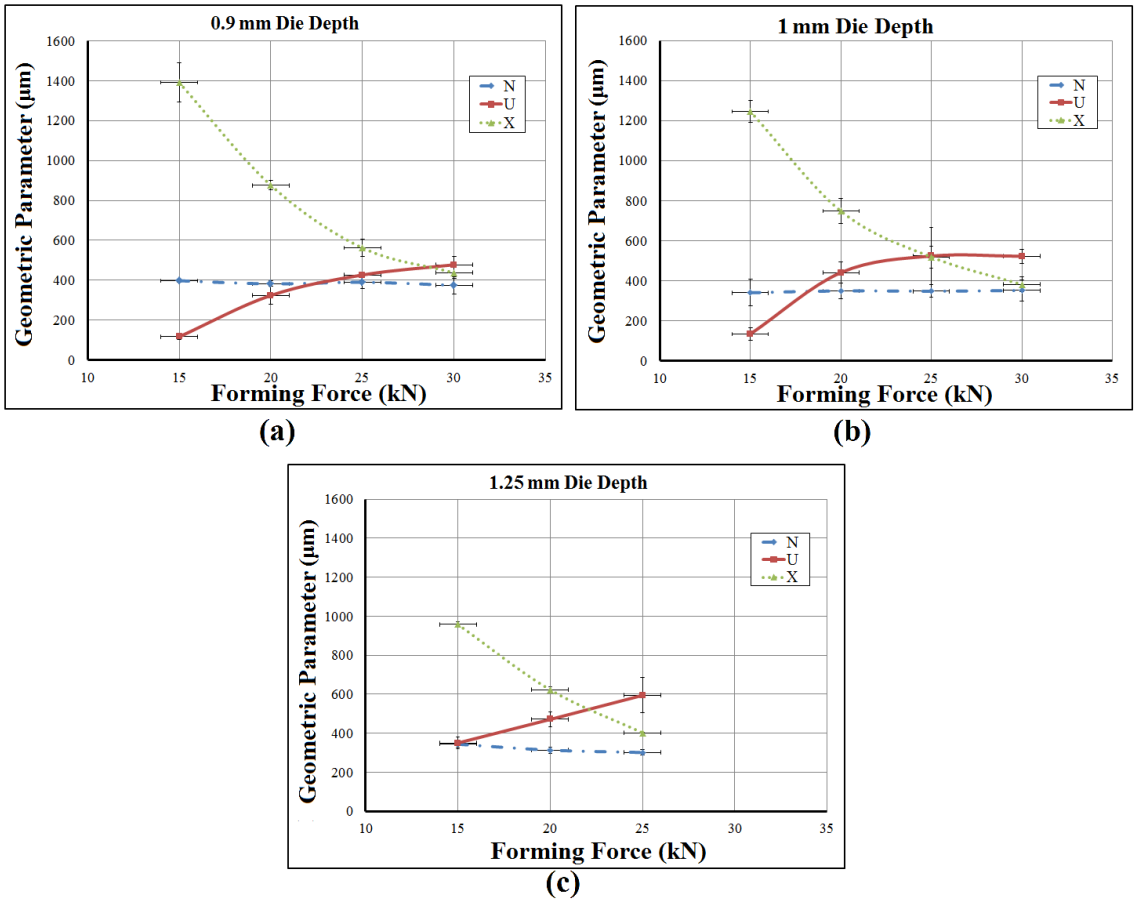

Figure 2.20. Relation between forming force and different geometrical parameters of the formed joints for three different die depths.

2.3.4 Analysis of the experimental post-clinch joint strength tests

Figure 2.21 shows typical photographs of the two tensile lap shear samples (both sides) with the clinched region in the middle of the test sample and the axis of loading in the horizontal direction corresponding to a die depth of 0.9 mm and forming forces of 15 kN and 30 kN. The shear behavior of the clinches in terms of applied load versus resulting displacement traces, under different forming conditions and using various die depths, are presented in Figure 2.22. An initial linear elastic increase in the force-

displacement curve can be recognized followed by a decrease in the slope of the curve which is attributed to the decrease in the joint stiffness. The decrease in the stiffness of the joint is due to the tendency of the punch-sided sheet of the joint to pull out of the die-sided sheet. Finally, crack is initiated on the outer surface of the punch-sided sheet. As a result a drop in the load occurs that further leads to a catastrophic drop in load as the crack propagates.

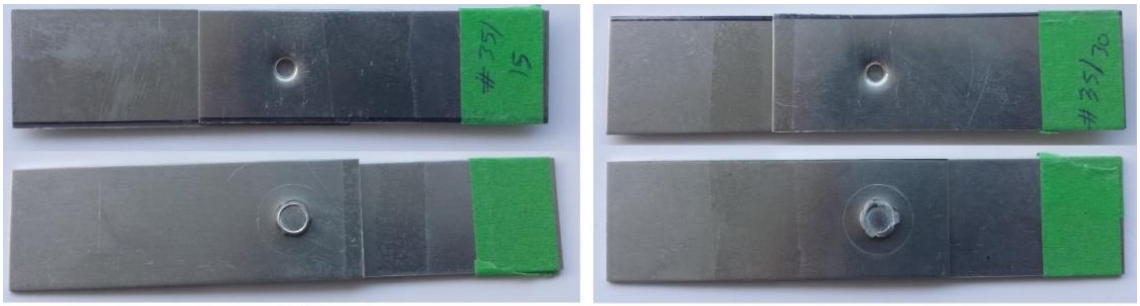

Figure 2.21. Photographs of tensile lap shear samples formed to 0.9 mm die depth with forming forces of 15kN (left) and 30kN (right).

Figure 2.23 demonstrates the joint strength as a function of the forming force for different die depths. The maximum force supported by the joint decreased with die depth. Also, the maximum force increased with increasing forming force at lower die depths but tended to be independent of the forming force at intermediate die depth. The joints were quite weak at larger die depths, and a higher forming force led to premature failure of the joint. A comparison of earlier Figure 2.20 and Figure 2.22 shows that shear strength of the joint is controlled by a combination of interlock depth and neck thickness, with the latter playing a more significant role. Figure 2.24 depicts the energy consumed by the clinched joint formed under different conditions as measured by area under the force-

displacement curve. This trend is similar to the earlier trend in joint strength (Figure 2.23).

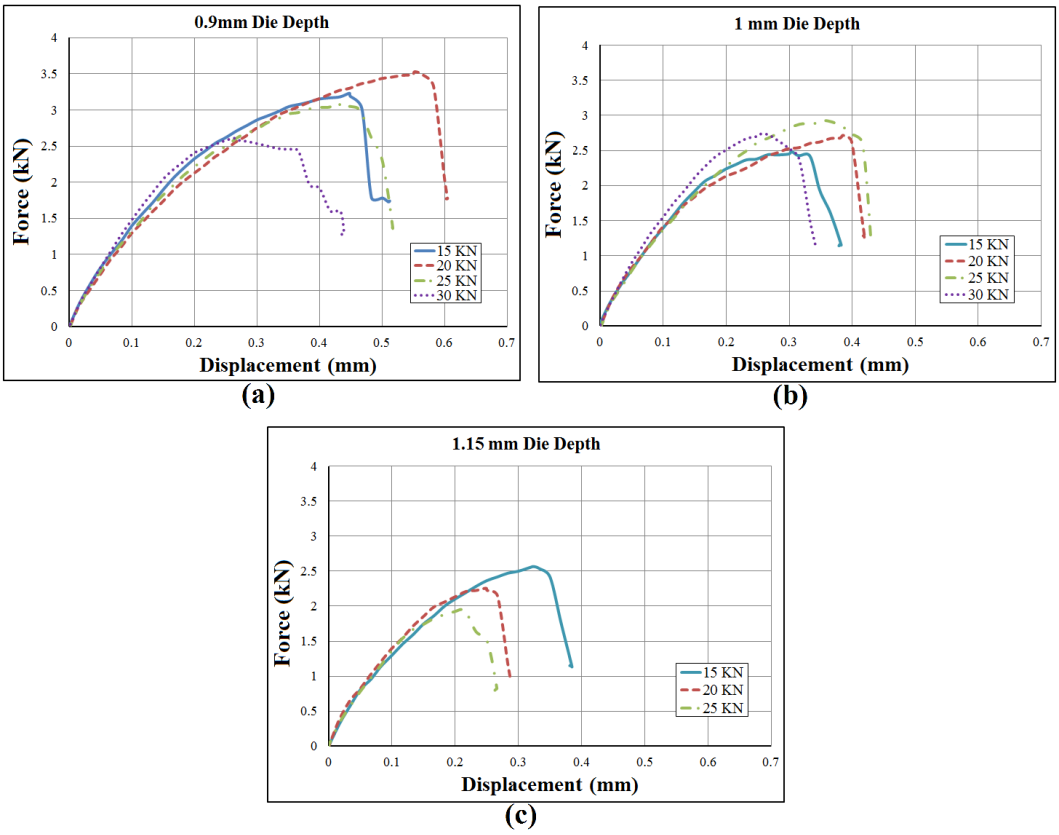

Figure 2.22. Applied force versus resulting displacement traces under the different forming conditions for annealed AA7075 sheets using various die depths.

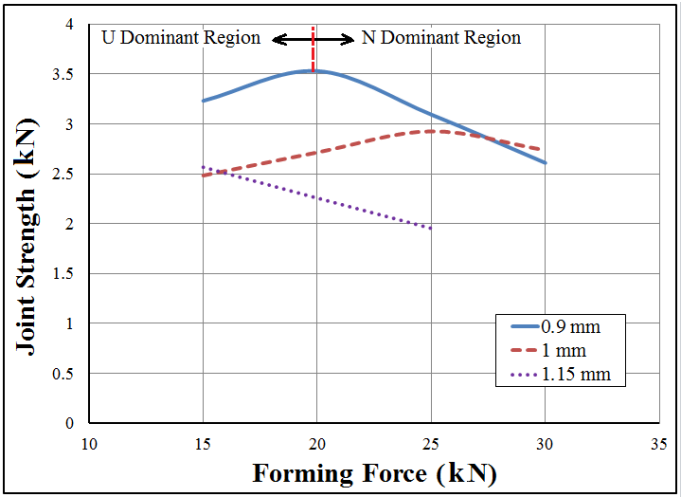

Figure 2.23. Joint strength as a function of the forming force for different die depths showing the two characteristic regions, for 0.9 mm, 1 mm, and 1.25 mm die depths.

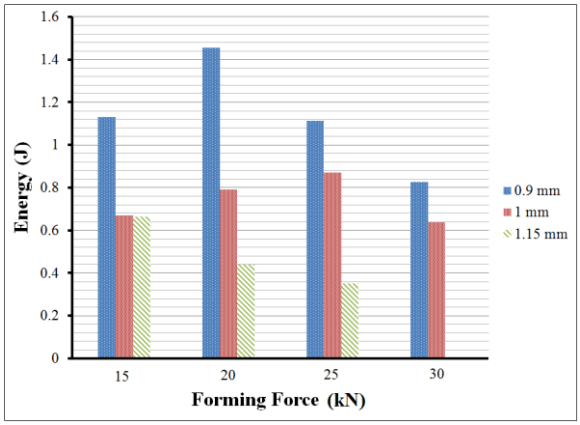

Figure 2.24. Energy consumed by the clinched joint formed using different die depths as a function of forming force.

Unbuttoning failure mainly occurred in joints that were formed with a relatively large force as shown in Figure 2.25. A change in tooling and forming conditions resulted in two opposite effects. At larger the forming force or die depth, the interlock depth U was increased but the neck thickness N was reduced. The joint stiffness and strength increased with an increase in the interlock depth. The failure mode for this case was unbuttoning accompanied by a large displacement at failure. The fracture was due to

reduced ductility of the sheet and large displacement was due to larger interlock. Displacement at failure decreased to the point when the effect of the neck reduction became more dominant. Maximum joint strength corresponded to an optimum combination on neck thickness and interlock depth as depicted in Figure 2.23.

Figure 2.26 shows microstructure of cut cross-sections in the terms of grain shape and size for un-deformed and highly plastically deformed neck and bottom regions. Highly rotated grains can be noted at the corner of the die-sided sheet which is consistent with the material flow analysis in sub-section 2.3.2. The average grain size in the un-deformed sheet was about 35μm. The grain size in the highly deformed region could not be determined reliably from the optical micrographs.

Figure 2.25. Unbuttoning failure mode of the clinched joint. The first two photos on the left show the upper surface of the punch-sided and die-sided sheets respectively. The photos on the right show the lower surface of the punch-sided and die-sided sheets respectively.

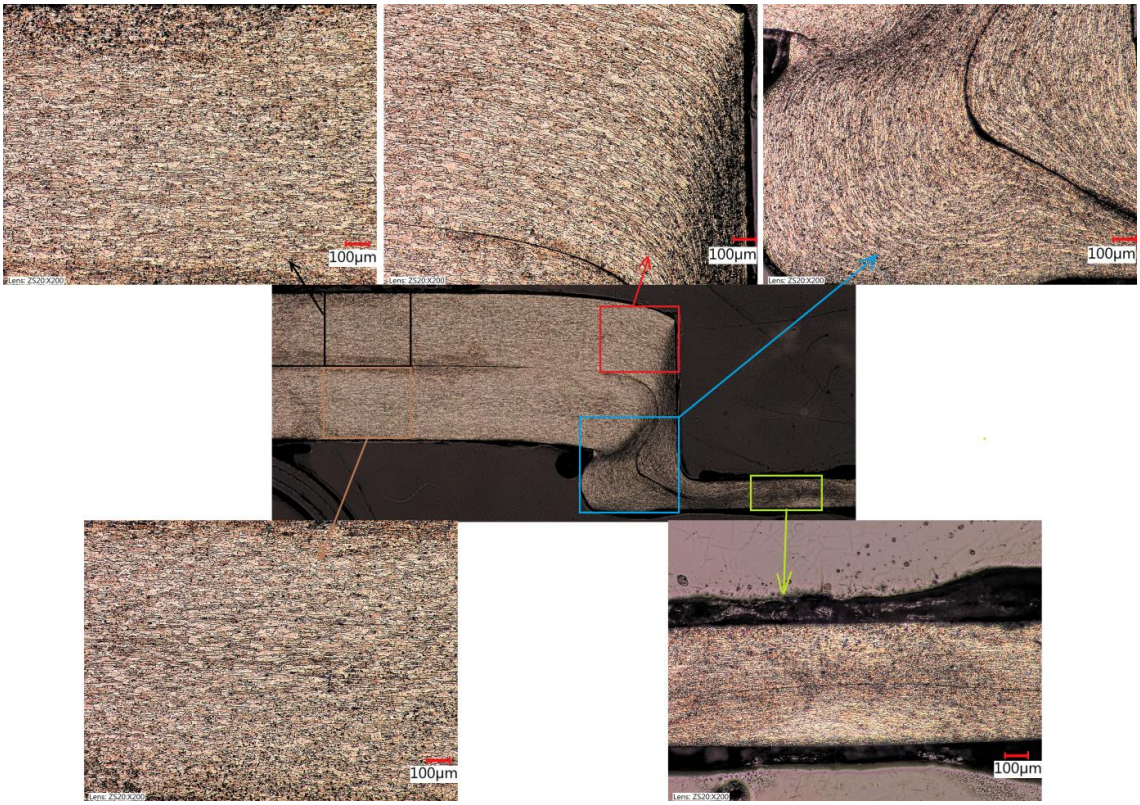

Figure 2.26. Optical micrographs of cut cross-section showing grain structure in the highly deformed clinch region (0.9 mm die depth, 0.25 punch corner radius, 0.5 die corner radius, and 25 kN Forming force).

2.4 Conclusions

The main aim of the present paper was to provide a better understanding of the influence of the tool design parameters on the shape of joint and material flow during the clinching process by using extensible dies. In this effort, experimental and numerical modeling approaches have been utilized in a complementary manner. The following points summarize the main conclusions:

1- Clinch joining is a complex process and its simulation is greatly dependent on the material model. Use of a weight function between Swift and Voice constitutive

models can provide a better material hardening law up to large strains to obtain better agreement between experimental and FE model results for AA7075 aluminum sheet.

2- Three forming stages, other than the initial stage of applying blank holding force, can be recognized during the clinching process by using extensible dies. During the first stage of forming, a great reduction in the thickness of the die-sided sheet occurs and it remains approximately constant with further punch movement.
3- Clearance between punch and die affects the reduction in the total thickness of the sheet metals. In contrast, punch and die corner radii affect the ratio of thickness reduction in punch and die-sided sheets respectively.
4- An increase in the punch corner radius from 10% to 20% of the punch radius, results in a decrease in interlock depth by 35% and an increase in neck thickness by 15 % during clinching of AA7075-O sheet.
5- The lowest die depth corresponds to the smallest concentration of plastic deformation around the punch corner that results in retardation of sheets failure by increasing the neck thickness. However, the value of the interlock depth decreases.
6- The joint strength decreases with die depth. Also, it increases with increasing forming force at lower die depths but tended to be independent of the forming force at intermediate die depth.

References

[1] C. Borsellino, G. Di Bella, V. Ruisi, Study of new joining technique: flat clinching, Key Engineering Materials, Trans Tech Publ, 2007, pp. 685-692.
[2] J.P. Varis, J. Lepistö, A simple testing-based procedure and simulation of the clinching process using finite element analysis for establishing clinching parameters, Thin-Walled Structures 41(8) (2003) 691-709.
[3] J. Varis, Ensuring the integrity in clinching process, Journal of Materials Processing Technology 174(1) (2006) 277-285.
[4] F. Lambiase, A. Di Ilio, Finite element analysis of material flow in mechanical clinching with extensible dies, Journal of materials engineering and performance 22(6) (2013) 1629-1636.
[5] M. Carboni, S. Beretta, M. Monno, Fatigue behaviour of tensile-shear loaded clinched joints, Engineering Fracture Mechanics 73(2) (2006) 178-190.
[6] V. Jayasekara, K.H. Min, J.H. Noh, M.T. Kim, J.M. Seo, H.Y. Lee, B.B. Hwang, Rigid-plastic and elastic-plastic finite element analysis on the clinching joint process of thin metal sheets, Metals and Materials International 16(2) (2010) 339-347.
[7] S.-H. Lee, C.-J. Lee, K.-H. Lee, J.-M. Lee, B.-M. Kim, D.-C. Ko, Influence of tool shape on hole clinching for carbon fiber-reinforced plastic and SPRC440, Advances in Mechanical Engineering (2014).
[8] C.-J. Lee, J.-M. Lee, H.-Y. Ryu, K.-H. Lee, B.-M. Kim, D.-C. Ko, Design of hole-clinching process for joining of dissimilar materials–Al6061-T4 alloy with DP780 steel, hot-pressed 22MnB5 steel, and carbon fiber reinforced plastic, Journal of Materials Processing Technology 214(10) (2014) 2169-2178.
[9] K.-i. Mori, N. Bay, L. Fratini, F. Micari, A.E. Tekkaya, Joining by plastic deformation, CIRP Annals-Manufacturing Technology 62(2) (2013) 673-694.
[10] X. He, L. Zhao, H. Yang, B. Xing, Y. Wang, C. Deng, F. Gu, A. Ball, Investigations of strength and energy absorption of clinched joints, Computational Materials Science 94 (2014) 58-65.
[11] S. Coppieters, S. Cooreman, H. Sol, D. Debruyne, Reproducing the experimental strength of clinched connections with finite element methods, Proceedings of the SEM Annual Conference and Exposition on Experimental and Applied Mechanics, 2007, pp. 572-579.
[12] X. He, Recent development in finite element analysis of clinched joints, The International Journal of Advanced Manufacturing Technology 48(5-8) (2010) 607-612.
[13] S. Coppieters, P. Lava, R. Van Hecke, S. Cooreman, H. Sol, P. Van Houtte, D. Debruyne, Numerical and experimental study of the multi-axial quasi-static strength of clinched connections, International journal of material forming 6(4) (2013) 437-451.
[14] K. Mori, Y. Abe, T. Kato, Mechanism of superiority of fatigue strength for aluminium alloy sheets joined by mechanical clinching and self-pierce riveting, Journal of Materials Processing Technology 212(9) (2012) 1900-1905.
[15] F. Lambiase, A. Di Ilio, A. Paoletti, Joining aluminium alloys with reduced ductility by mechanical clinching, The International Journal of Advanced Manufacturing Technology 77(5-8) (2015) 1295-1304.
[16] F. Lambiase, Influence of process parameters in mechanical clinching with extensible dies, The International Journal of Advanced Manufacturing Technology 66(9-12) (2013) 2123-2131.
[17] S. Coppieters, P. Lava, S. Baes, H. Sol, P. Van Houtte, D. Debruyne, Analytical method to predict the pull-out strength of clinched connections, Thin-Walled Structures 52 (2012) 42-52.
[18] Y. Abe, T. Kato, K.-i. Mori, S. Nishino, Mechanical clinching of ultra-high strength steel sheets and strength of joints, Journal of Materials Processing Technology 214(10) (2014) 2112-2118.

[19] Y. Abe, K. Mori, T. Kato, Joining of high strength steel and aluminium alloy sheets by mechanical clinching with dies for control of metal flow, Journal of materials processing technology 212(4) (2012) 884-889.
[20] R. Pedreschi, B. Sinha, An experimental study of cold formed steel trusses using mechanical clinching, Construction and Building Materials 22(5) (2008) 921-931.
[21] F. Lambiase, A. Di Ilio, An experimental study on clinched joints realized with different dies, Thin-Walled Structures 85 (2014) 71-80.
[22] W. Witkowski, Clinching joint forming speed impact on the joint strength, Zeszyty Naukowe Politechniki Rzeszowskiej. Mechanika (2014).
[23] B.J. Shi, Y.Q. Wang, S.L. Liu, H.Y. Tian, Design method of the parameters of tools for clinching technology, Advanced Materials Research, Trans Tech Publ, 2012, pp. 1491-1496.
[24] M. Oudjene, L. Ben-Ayed, On the parametrical study of clinch joining of metallic sheets using the Taguchi method, Engineering Structures 30(6) (2008) 1782-1788.
[25] X. He, F. Liu, B. Xing, H. Yang, Y. Wang, F. Gu, A. Ball, Numerical and experimental investigations of extensible die clinching, The International Journal of Advanced Manufacturing Technology 74(9-12) (2014) 1229-1236.
[26] T. Wen, H. Wang, C. Yang, L.T. Liu, On a reshaping method of clinched joints to reduce the protrusion height, The International Journal of Advanced Manufacturing Technology 71(9-12) (2014) 1709-1715.
[27] F. Lambiase, Joinability of different thermoplastic polymers with aluminium AA6082 sheets by mechanical clinching, The International Journal of Advanced Manufacturing Technology 80(9-12) (2015) 1995-2006.
[28] T. Jiang, Z.-X. Liu, P.-C. Wang, Effect of aluminum pre-straining on strength of clinched galvanized SAE1004 steel-to-AA6111-T4 aluminum, Journal of Materials Processing Technology 215 (2015) 193-204.
[29] J. Mucha, The analysis of lock forming mechanism in the clinching joint, Materials & design 32(10) (2011) 4943-4954.

Chapter 3

Die-less Clinching Process and Joint Strength of AA7075 Aluminum Joints

---

Mostafa K. Sabra Atia, PhD student, is the first author and main contributor of the work who came up with the experimental design, analyzed the data, and composed the text as a paper describing the results. Mukesh K. Jain, Professor, is the supervisor who substantially contributed to the work by checking the experimental results and technical details of the model as well as improving the language of the paper. This paper has been published in Thin-Walled Structures Journal.

Die-less Clinching Process and Joint Strength of AA7075 Aluminum Joints

Mostafa K. Sabra Atia[a,b] and Mukesh K. Jain[a]

a Department of Mechanical Engineering, McMaster University, Hamilton, Ontario, Canada L8S 4L7

b Corresponding author: Tel.: +1 905-920-0398. E-mail address: atiam@mcmaster.ca (M. Atia).

Abstract

AA7075 aluminum alloy sheets in different temper conditions (O, W and T6) were joined by die-less clinching. The material flow behavior, neck thickness and interlock characteristics during clinching were investigated by metallographic observations of clinched, cut and mounted samples. Blank holders of different shapes and dimensions were used to control the material flow. The effects of blank holder geometric parameters as well as forming forces on the shape of the formed interlock in clinching were studied. The highest strength temper state (T6) was shown to possess poor clinch-ability as it failed to clinch under most clinching conditions. This was attributed to its poor ductility and formability at room temperature compared to the other tempers. Lastly, mechanical performance of the formed joints was characterized by conducting single shear lap as well as peel tests. Various failure modes were observed for the different clinching conditions and material temper states.

Keywords: Die-less clinching, AA7075 aluminum, temper, material flow.

Table 3.1. List of Abbreviations

T6	Artificial peak aged state which represents the hardest temper
O	Annealed temper state
W	Solution heat treated state
N	Neck thickness of the joint
U	Interlock depth of the joint
X	Joint bottom thickness
R_{PC}	Punch corner radius
R_{DC}	Die corner radius
F	Forming force
σ_{eq}^{p}	Equivalent stress
ε_{eq}^{p}	Equivalent plastic strain
k_1	Stress coefficients for Voce hardening law
k_2	Stress coefficients for Swift hardening law
C	Material constant for Voce hardening law
m	Material constant for Voce hardening law
α	Weight function
$\sigma_{0.2}$	0.2 proof strength
n	Strain hardening exponent

3.1 Introduction

Vehicle weight reduction, increased fuel economy, and increased safety of the structures in transportation applications has led to much interest in lightweight higher strength structural aluminum alloys [1, 2]. Suitable joining techniques to create such structures with aluminum sheets are required [1]. Generally, similar and dissimilar sheet metals can be joined by adhesive bonding, welding, and mechanical fastening [3, 4]. Difficulty of welding high strength aluminum sheets and long times for adhesive bonding make mechanical fastening a process of much interest for joining of high strength aluminum sheets [5].

Among the different mechanical fastening techniques available in manufacturing, clinching is a common method of joining by forming in which two or more sheet metals are locally deformed using punch and die to form a geometrical interlock [6-8] as shown in Figure 3.1. Clinching enables joining of two or more similar or dissimilar sheet materials where individual thickness can vary from 0.4 to 4 mm [9]. A clinched joint is formed entirely by the geometric interlock alone and without adding any additional physical component to the joint. A high throughput, low cost, clean and environmentally friendly manufacturing environment of the clinching process arises from no harmful light, heat or smoke emissions. Lastly, clinching offers a high tool life compared with the other joining techniques [4]. The main geometric parameters that affect joint strength are neck thickness “N” and interlock depth “U”[10],as shown in Figure 3.1. Clinched structures can withstand loads in shear and axial modes [11]. The shear strength of a clinched joint is comparatively higher than its axial strength[11]. In general, clinching results in lower joint strength compared to riveting which can limit its use in certain high strength applications [12].

The main limitation of using the conventional clinching technique is that the process introduces surface steps on both surfaces of the joined sheets where one side consists of a protrusion and the other a pit. Effort has been made to reduce the protrusion height by reshaping the conventional clinched joint [13-15]. Countermeasure tooling has been used in this regard by Tong et al. [16]. The study showed a reduction of 50% in protrusion height without affecting the joint strength. Francesco et al. [17] utilized two steps clinching to join aluminum and a carbon fiber reinforced polymer (CFRP) where the

first step included conventional clinching by using extensible dies while the second was a reshaping step using punch and flat die as shown in Figure 3.2. The main disadvantage for this approach is the difficulty of aligning the flattening punch with the pre-formed joint. Borsellino et al. [6] proposed a solution consisting of flattening of the pre-formed joint using two flat anvils. In addition to eliminating the protrusion height, the flattened clinched joint was also found to withstand higher loads than the conventional clinched joints. Chen et al. used a pair of flat dies with (or without)a rivet to reduce the protrusion height of conventional clinched joint produced by extensible dies [18, 19]. All of the above reshaping techniques suffer from increased cycle time due to the additional step that involves a different tool set.

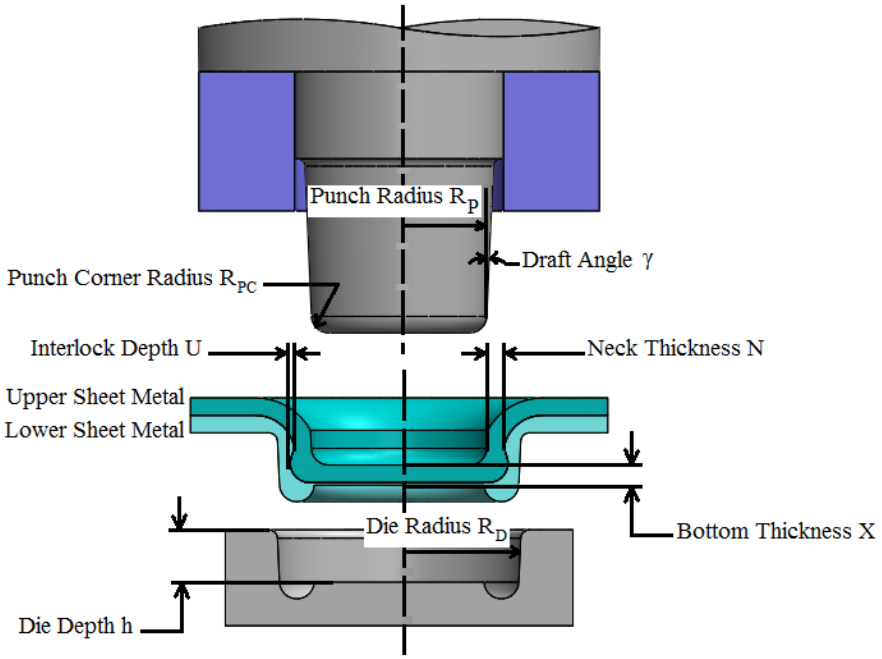

Figure 3.1. Cross-section of a conventional clinched joint showing the geometry of the joint and different geometric parameters.

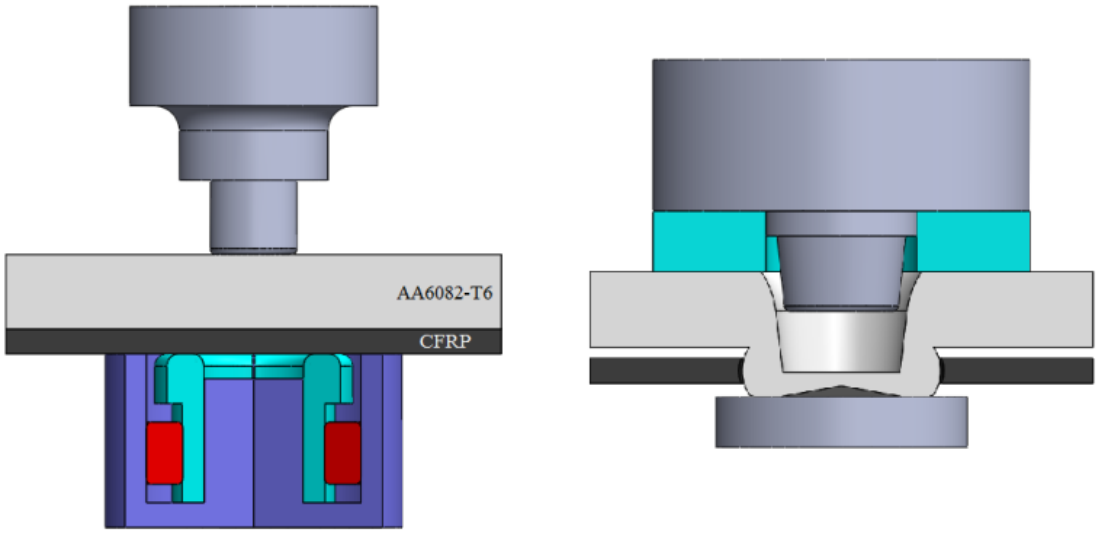

Figure 3.2. Drawing shows two steps clinching process. The first step (on the left side) is a conventional clinching process by using extensible die. The second step (on the right side) is a reshaping process by using punch and flat die. Adjustable ring was used to adopt the height of reshaping.

To make clinching more aesthetically appealing a new approach called die-less clinching has been developed in which surface step exist only on one side, often on the unexposed side of the joint [20, 21]. Die-less clinching is a one-step process using a punch and a flat anvil, as shown below in Figure 3.3. The design groove in the blank holder is a key factor in controlling the material flow in order to form the geometric interlock. The use of flat anvil in one-step die-less clinching eliminates the need for good alignment between the punch and the anvil as well as keeping joining time as short time as possible. Neugebauer et al. [22] showed that a very small protrusion is formed in die-less clinching compared to the conventional clinching. The combined movement of blank holder and punch makes the tooling for die-less clinching more complex [16].

In general clinch joining is a well-accepted and widely used process for joining ductile sheet metals. The joining greatly depends on formation of a permanent interlock by application of plastic work [23]. In recent years, much effort has been made to extend clinching process to join higher strength (and lower ductility) sheet materials. F. Lambiase et al. have utilized a heater gun to locally increase ductility of AA6082-T6 sheets for joining using conventional clinching [24-26]. Xiaocong et al. [27] have preheated the sheet metal by using oxyacetylene flame gun in order to perform conventional clinches on TA1 titanium sheets. Abe et al. [28] have used a counter pressure of a rubber ring to conventionally clinch ultra-high strength steel sheets. Neugebauer et al. [20] have taken the advantage of using flat anvil in the die-less clinching process to heat the reduced ductile magnesium sheet metal from underneath the anvil using cartridge heating.

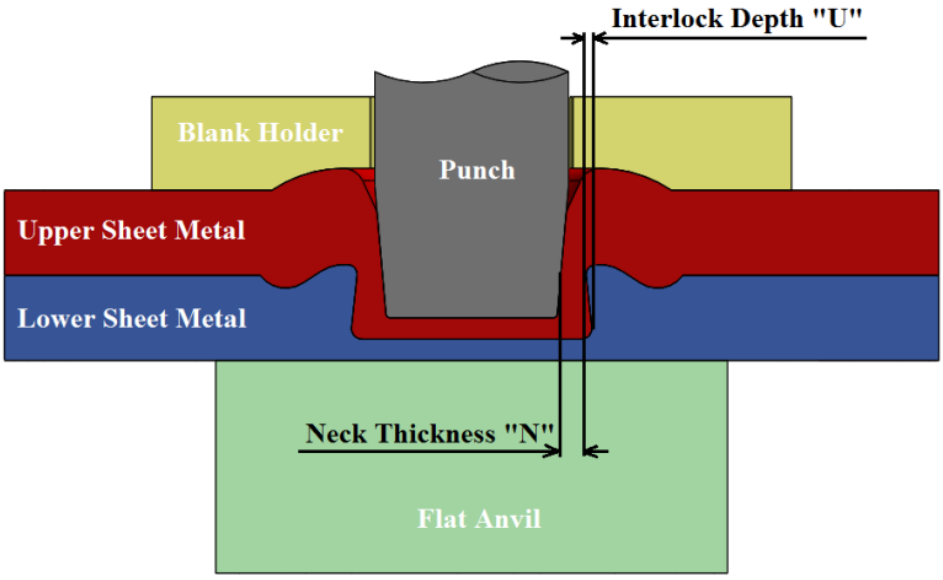

Figure 3.3. A schematic of cross-section across a single-step die-less clinched joint showing the main geometric parameters of the joint.

Three failure modes are generally encountered in performance testing of clinched joints [29]. These include (i) button failure due to plastic deformation on the formed interlock, (ii) unbuttoning failure due to neck fracture, and (iii) combined failure due to combination of plastic deformation and neck fracture.

Present work presents a new simple tool design for die-less clinching process for joining two similar sheet metals as well as a parametric study of the new tool in terms of load versus displacement characteristics during the clinching process. The material flow and joint interlock characteristics in different temper states have been investigated by observing the cut cross-sections of the joints with optical microscope. In addition, shear and axial strengths and failures modes of the joint have been assessed by using single shear and peel tests.

3.2 Material and experimental procedure

3.2.1 Material

One-step die-less clinch joints were performed on 1.27 mm thickness sheets made of 7075 aluminum alloy. The sheets were initially in T6- temper, a peak aged condition that yields the hardest state (or the largest ultimate tensile strength). Two more tempers were subsequently obtained by annealing, a partially annealed state at 413°C for 1hr (O1 temper) and a fully annealed state at 413°C for 3 hrs (O2 temper). Lastly, another heat-treatment was carried out at 480°C for 3 hrs followed by water quenching to obtain the solution heat treated metastable state (W-temper). Also, mechanical properties at each temper state were obtained by conducting tensile test according ASTM standard

(E8/E8M) using an Instron universal testing machine at a cross-head speed of 1 mm/min (see Table 3.2). In order to save used material, sub-size sample of dimension 120 mm length X 6 mm width was used according to ASTM standard (E8/E8M) as shown in Figure 3.4.

Table 3.2. Mechanical properties of AA7075 aluminum alloy at different temper states.

No.	Temper		Mechanical Properties				
	Designation Symbol	Description	$\sigma_{0.2}$ (MPa)	σ_{Ult} (MPa)	Max % Elongation	K (MPa)	n
1	T6	As-received	620	695	12	976.9	0.1102
2	W	Solution Treated	230	434	25	823.4	0.2852
3	O	O1-Partially Annealed	175	295	15	485.9	0.2071
4	O	O2-Fully Annealed	135	245	17	428.7	0.2141

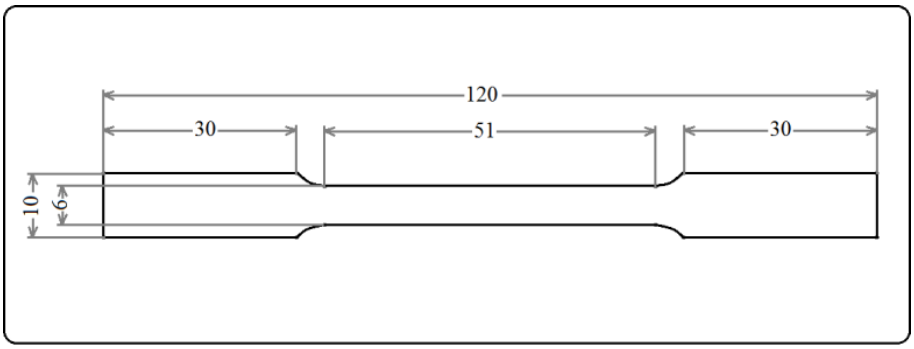

Figure 3.4. A drawing for the sub-size sheet tensile test specimen as per ASTM standard E8M.

3.2.2 Die-less clinching process

Die-less clinches were performed by using a tool-set mounted on a 100 kN servo-hydraulic, computer-controlled, Instron tensile test machine at a punch speed of 30 mm/sec. The tool set consisting of various adaptable components was designed to study

the material flow and join-ability of the sheet metals under various punch and die-set configurations. The tool set consisted of punch, flat anvil, blank holders as well as compression polymeric spring in order to apply a blank holding force as shown in Figure 3.5. Various blank holder shapes utilized in die-less clinching have been reviewed in reference [1]. The blank holders differed in shape and dimensions as illustrated in Figure 3.6. The material flow was expected to be affected by the diameter d of the blank-holder groove. Additionally, the groove depth t was considered important in interlock formation especially at the later stage of joint formation which requires restriction of material flow in the axial direction to increase interlock depth. A summary of the main blank-holder design parameters studied in the present work is provided in Table 3.3. The blank holder groove diameter and depth was taken as a percentage of punch diameter and sheet thickness respectively. The punch with diameter of 4.6 mm and 2.5° draft angle was made of tungsten carbide to withstand the high forming force. The material flow was greatly affected by the diameter *d* of the blank-holder groove. Forming forces used were in the range 30 kN - 45 kN.

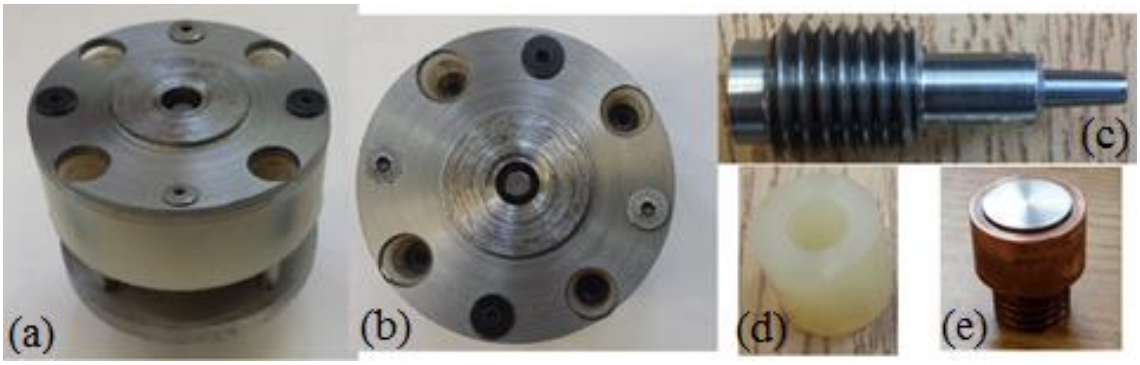

Figure 3.5. Photographs of die-less clinching tools in the present study; (a) and (b) tooling assembly, (c) punch, (d) polymeric spring, and (e) flat anvil.

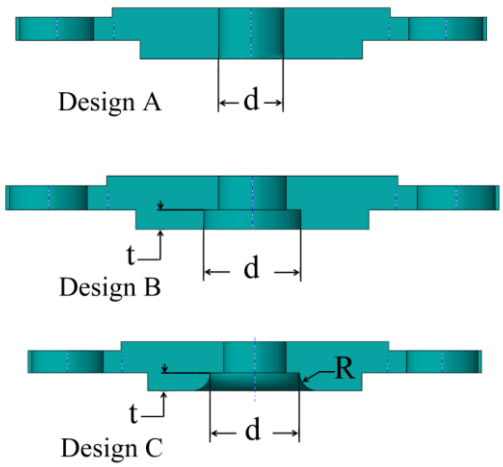

Figure 3.6. Blank holder designs utilized in die-less clinching experiments.

Table 3.3.Blank-holder design parameters.

Design	Tool Parameters	
	Parameters range as percentage	Parameter range in (mm)
A	d = 150% of punch diameter	d = 7 mm
B	d = 170:220% of punch diameter t = 15:80% of sheet thickness	d = 7.5:10.5 mm t = 0.2:1 mm
C	d = 170:220% of punch diameter t = 15:80% of sheet thickness R = t	d = 7.5:10.5 mm t = 0.2:1 mm R = 0.2:1 mm

3.2.3 Geometrical measurements and mechanical characterization of joints

The geometry of the joints produced had a large influence on the joint strength and failure mode as presented in this section. Therefore, a geometrical analysis was carried out in order to make a correlation among the different geometrical parameters and strength of the joint. Also, to study the material flow during the joining process, various punch strokes were applied to the two sheet layers. The clinched test samples were cut

and mounted using conventional optical metallographic methods of hot and cold mounting in a polymeric resin. The mounts were then polished to clearly reveal the clinched geometry using a high magnification digital optical microscope (KEYENCE VHX-2000).

In order to study the microstructure of the clinched, poorly clinched (or un-clinched) sheets, the test samples were cut using a precision saw. They were then mounted in polymeric resin, polished and etched. A caustic etchant consisting of a mixture of 10gm NaOH and 90 ml of distilled water was used in a water bath at 60°C. The samples were then dipped in 50% Nitric acid to complete the etching process. Also, after etching, Vickers micro-hardness data was obtained as a measure of local strengthening of the joint from increased plastic flow.

3.2.4 Joint testing

Single shear lap tests as well as peel tests were carried out to assess the mechanical behavior of the produced joint. Five sample were test under each condition to ensure test repeatability. The sheet samples of size 25 mm width and 75 mm length were cut from AA7075 sheet. The sheets were die-less clinched with an overlap between two sheets of 25 mm and 50 mm for single shear and peel tests respectively, as shown in Figure 3.7, where the location of the joint was marked by two perpendicular centerlines in the figure. A universal MTS 100 kN servo-hydraulic testing system was utilized for mechanical characterization. The tests were carried out at ambient temperature with a cross-head speed of 1mm/min until the two sheets were completely separated. The load versus displacement data was continuously recorded during the test.

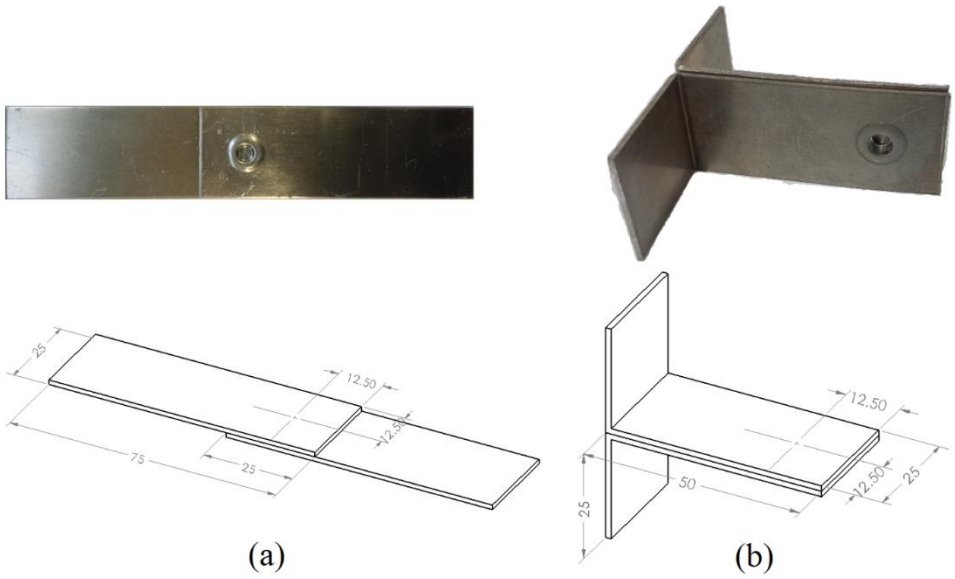

Figure 3.7. Drawings of the samples used for, (a) single shear test and (b) peel test. The joint location corresponds to the intersection of the two centerlines.

3.3 Results and discussion

3.3.1 Material flow during joining

Figure 3.8 shows forming curve (forming force versus punch stroke) measured during the joining process for O2-temper sheet. Generally, several stages can be distinguished from such graphs based on changes in the characteristic slopes of the curves and corresponding geometry of the joint as presented in Figure 3.9. During stage one which ends at point I on the curve, the blank holder exerts a pressure (i.e., a compressive force) in the clamped region on the pair of sheet materials. Stage II is initiated by the punch coming in contact with upper sheet. The forming force is an indication of the initial insertion of the punch into the upper sheet. Stage II ends with penetration of the punch in the upper sheet only. The upper sheet material flows in the axial direction only, while the lower sheet flows in both the axial and radial directions. During the third stage (between

points II and III on the curve) the material flow in the radial direction increases significantly. The fourth stage starts when the upper sheet material contacts the top of the blank holder groove. During this stage the flow of the upper sheet in the radial direction is increased significantly and geometrical interlock begins to form. In the fifth, the material flow in the axial direction is limited by the blank holder that results in much increase in geometric interlock. Finally, the force drops due to punch retraction and the change in the slope is likely an indication of the end of elastic recovery as the punch moves under the action of the urethane compression spring. Figure 3.9 presents a schematic of the five stages of die-less clinching.

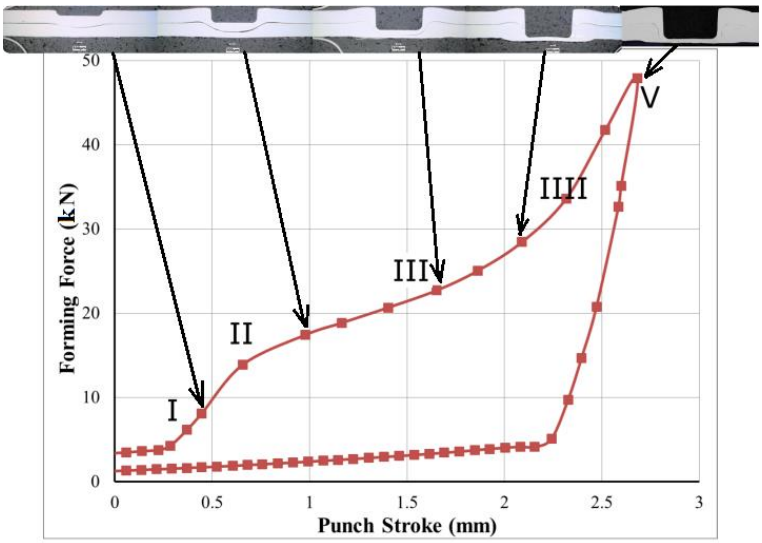

Figure 3.8. A typical forming force versus punch displacement curves for die-less clinching.

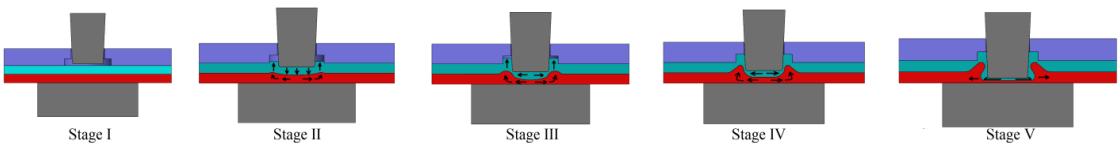

Figure 3.9. Schema illustrations of the progression of die-less clinching from left to right.

Figure 3.10 shows a set of photographs from optically mounted cross-sections of the die-less joints at different punch strokes, for different temper states. The photographs have been arranged in 4 separate columns, one for each temper state. As shown beneath each of the photographs, a higher force was required to apply the same punch stroke as the sheet temper was changed to a higher strength temper. The mounted samples also helped assess the spring-back effect (as measured by indentation depth) under different clinching conditions. For example, in the early stage of forming, a higher spring-back effect (i.e., a smallest punch depth) for the T6-temper and a lowest spring-back (or the largest punch depth) for the W-temper (compare columns 1 and 2 of Figure 3.10) was obtained. The higher spring-back in T6 results from a higher yield strength and larger elastic strain value for this temper state compared to the other tempers. Noticeably, in the last stage, the material flow in the radial direction increases significantly for the softer temper states leading to increased material flow and in turn a larger amount of interlock. Figure 3.11 shows final geometrical parameters (interlock depth "U" and neck thickness "N" as in Figure 3.3) as a function of forming force for partially and fully annealed sheets. Sheets in T6-temper state failed to perform interlocking due to limited flow-ability in the reverse axial direction, opposite to punch movement. On the other hand, the other temper states successfully formed die-less joints. Thus, the flow of the upper sheet material in the direction opposite to punch movement from the earlier stages is a decisive parameter in the formation of a good interlock in the die-less clinched joint. At approximately 2.8 mm punch stroke, interlocking starts to form in the softer-temper due to increase in the material flow in the radial direction. Additionally, by comparing the

optical images in the last row in Figure 3.10, a small protrusion can be noticed on the anvil-sided sheet. The depth of the protrusion shows an increase as the temper changes from a lower strength to a higher strength.

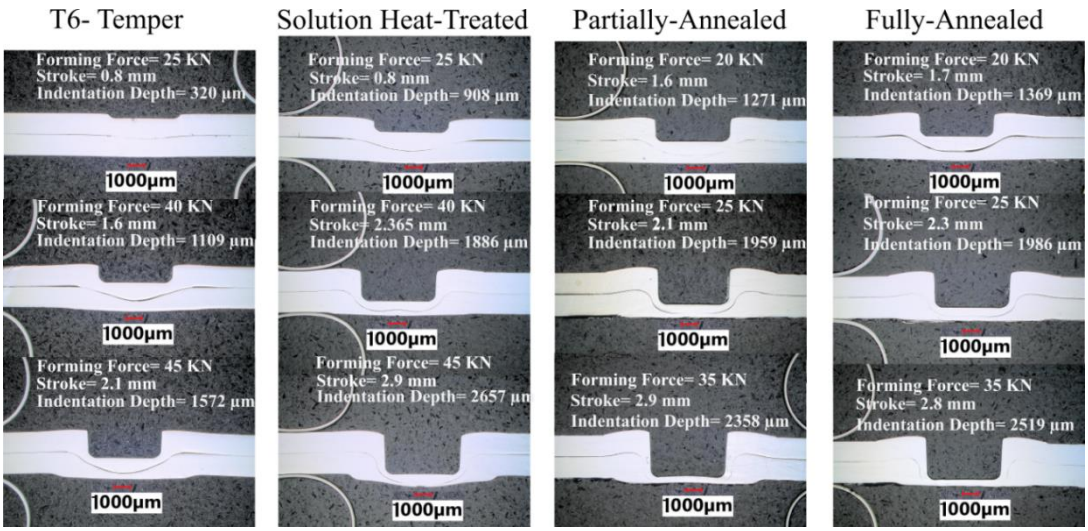

Figure 3.10. Optical images of through-thickness mounted cross-section of die-less joints formed at different punch strokes for various temper states (blank holder B, d=175%, and t=75%).

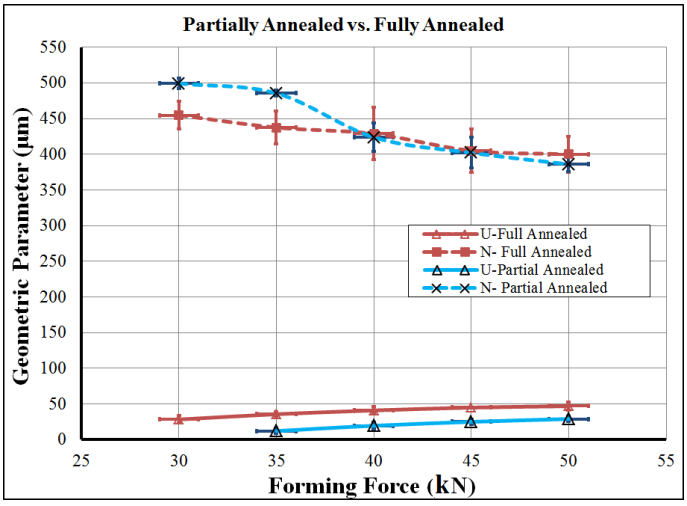

Figure 3.11. Geometrical parameters (U and N) of clinched joints as function of forming force for partially (O1) and fully annealed (O2) sheets.

Die-less clinching tests were also conducted in T6 temper to compare with the other fully annealed sheets. A minimal interlock was achieved by placing the softer (fully annealed) sheet on the punch-side and the T6 sheet on anvil-side. For this sheet combination, the most material flow in the axial direction occurred in the soft sheets. Left column of photographs in Figure 3.12 demonstrates the flow of the material during these experiments. However, when the sheets in T6 temper state was placed on the punch side, as shown in the right column, no clinching could be achieved. This is because the flow of the material in the vicinity of the punch was limited in the direction opposite to the motion of the punch. In fact, in the early stages, the material flow occurred in the same direction as the punch movement. Therefore, it is inferred that the ability of the punch-sided sheet metal to flow in opposite of the punch movement is critical to the formation of the interlock. This was not the case for T6 temper sheet.

Figure 3.13 shows the optical micrographs of cut cross-sections of several different regions of die-less clinched joints. The grain shape and grain size characteristics for undeformed and highly plastically deformed neck and bottom regions are clearly revealed. The average grain size in the undeformed sheet was about 35μm. The grain size in the highly deformed region could not be determined reliably from optical micrographs.

Figure 3.14 shows a map of Vickers hardness distributions through cross-section of a clinch specimen tested at a forming force of 40kN. The material before forming was partially annealed and had a relatively low micro-hardness of 65 VH. As expected, the micro-hardness in a given region increased with increasing plastic deformation (or plastic

work). The sample exhibited the highest micro-hardness values in the neck region as well as at the bottom corner region in both of the sheets.

Figure 3.12. A set of optical images of the cross-sections through die-less clinch joints formed in O and T6 tempers. The left and right columns present the case of T6 temper sheet on the punch-side and anvil-side respectively.

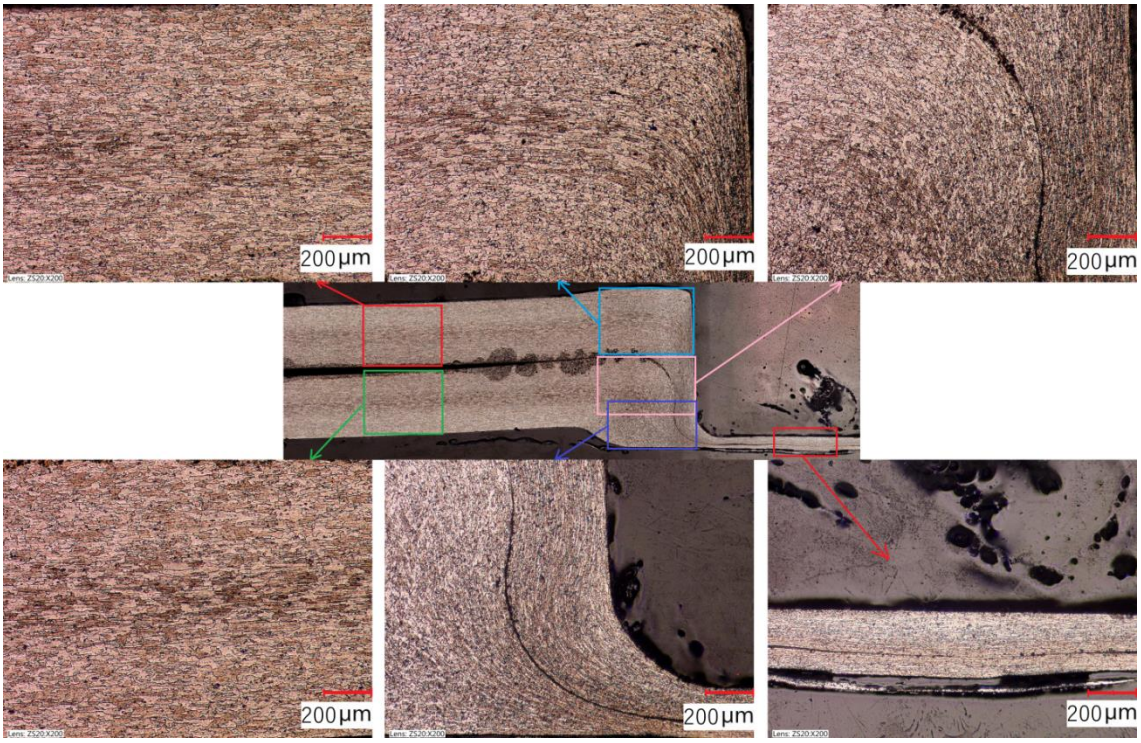

Figure 3.13. Optical micrographs of cut cross-section of die-less clinched joint performed on partially annealed sheets.

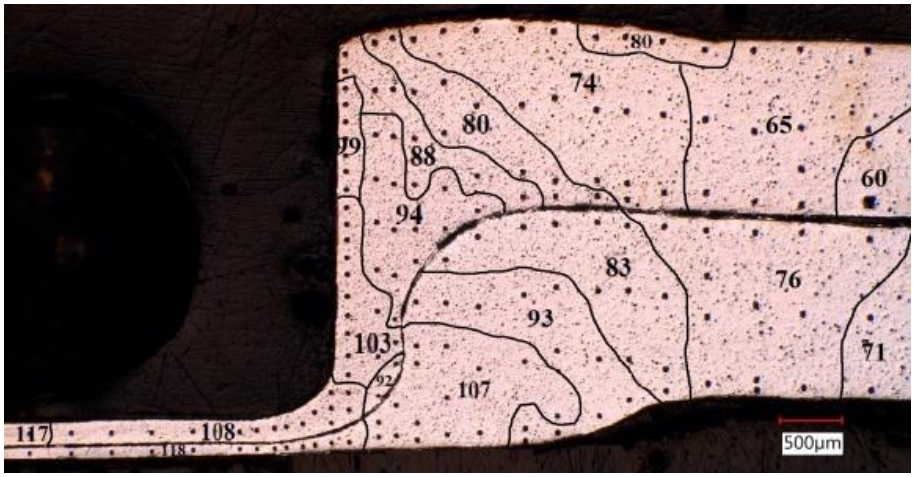

Figure 3.14. An optical image of a die-less clinch joint showing superimposed Vickers micro-hardness contours. Clinched joints were produced using blank holder type B with groove depth of 25% of sheet thickness and groove diameter of 220% of punch diameter.

3.3.2 Post-clinch strength of joint

3.3.2.1 Single-Shear Test

Figure 3.15(a, b) shows the force – displacement traces from single lap shear tests on clinched joints formed by using blank holder type B with groove diameter 175% of punch diameter and 40% of sheet thickness groove depth. The samples tested in lap-shear were obtained at different forming forces using fully annealed AA7075 sheets. Force-displacement traces typically exhibited an initial linear elastic region, followed by a slower rise of the curve due to a decrease in the joint stiffness from gradual pull-out of the punch-sided sheet. The load drop in the last stage corresponded to crack initiation from the inner surface of the punch sided sheet. The curves become less smooth and start to exhibit catastrophic drops as crack propagation occurs. It can be noted that the displacement at failure decreases with increasing forming force. However, the joint strength increases by increasing the forming load up to 40 kN. Beyond this value, the joint strength starts to decrease with an increase in the forming force (see Figure 3.15(b)). The decrease in the displacement is due to increases in the amount the plastic work within the joint. The increase in the forming force enhances the interlock and decreases the neck thickness, and consequently an increase in the joint strength until a critical interlock depth is reached. Further punch movement results in decreased joint strength due to the neck thickness becoming more dominant compared to the interlock depth.

Figure 3.16 shows the force-displacement behavior from lap shear test conducted with blank holder type B of groove diameter 220% of punch diameter and groove depth

of 25% of sheet thickness. A comparison of Figure 3.15(a) with Figure 3.16 shows the effect of the change in groove diameter. The increase in the diameter of the groove from d=175% to 220% results in an increase of the joint strength by 30 and 45 % by using 35 and 40 kN forming force respectively. The increase in the joint strength is due to increase in the neck thickness as shown later in Figure 3.27.

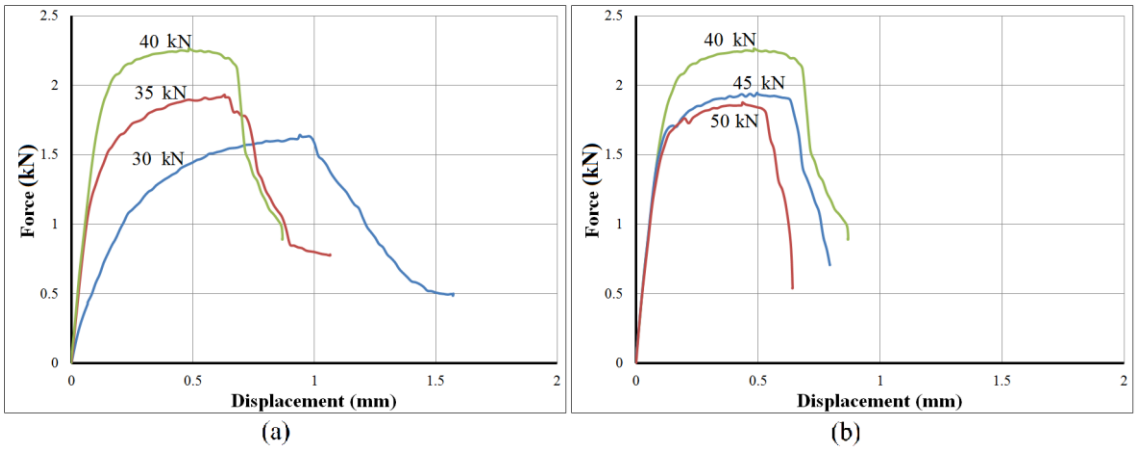

Figure 3.15. Force-displacement behavior from lap shear tests on clinched joints formed at different forming forces, (a) for 30, 35, and 40 kN, and (b) for 40, 45, and 50 kN for fully annealed (O2) sheets.

Figure 3.17 shows a comparison of force-displacement traces of lap shear joints formed on sheets in W-temper and after natural aging of 30 days using a forming force of 40 kN. The same blank holder dimensions were utilized as in the previous case of Figure 3.15. The result show a comparatively low joint strength in W temper when the joint was tested immediately after clinching process while the joint strength increased significantly when the clinched sample was left to naturally age. The increased force and displacement from aging is attributed to significant precipitation hardening that occurs in AA7075 sheet.

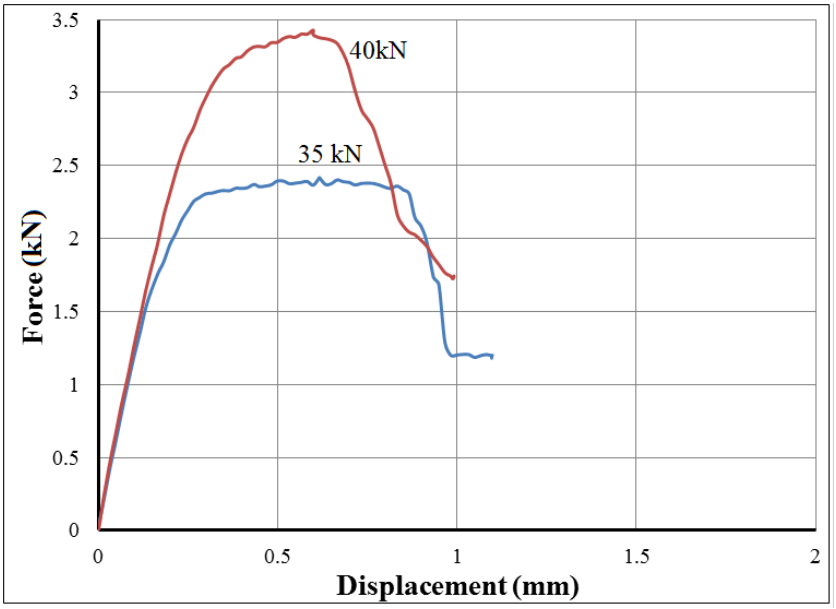

Figure 3.16. Force-displacement responses from lap-shear test on clinched joints at two different forming forces for fully annealed (O2) sheets.

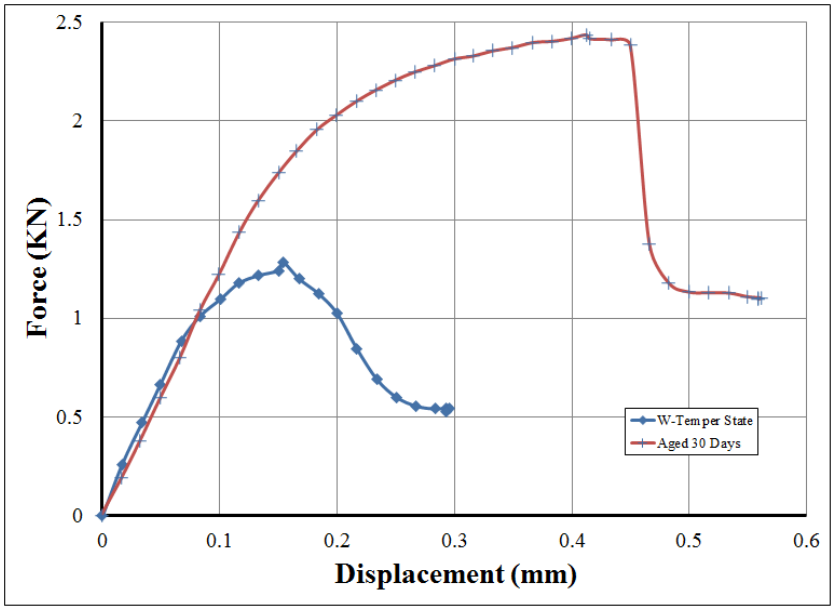

Figure 3.17. Force-displacement traces from lap-shear test for joints formed on sheets in W-temper using blank holder type B with a groove diameter of 175% of punch diameter and groove depth of 25% of sheet thickness.

Various failure modes were observed in failed lap-shear test specimens as shown in Figure 3.18. These included unbuttoning, button failure and a combination of the two. Unbuttoning failure mainly occurred on joints that were formed with a relatively smaller punch force and lower interlock depth so the interface of the upper sheet could easily slip over the surface of the lower sheet under the applied force. The button (or neck) failure typically occurred on joints that were formed with a large punch force, and likely involved competing events. While a larger forming force led to a larger interlock depth and an increased joint stiffness, a larger forming force also caused a large reduction in the neck thickness which reduced the load carrying capacity of the joint. Good forming condition can lead to an optimum interlock depth and neck thickness, and therefore a higher joint strength. An example of a combined failure mode characterized by a mixture of buttoning and unbuttoning failures, for blank holder B and forming force 40kN, is shown in Figure 3.18(c).

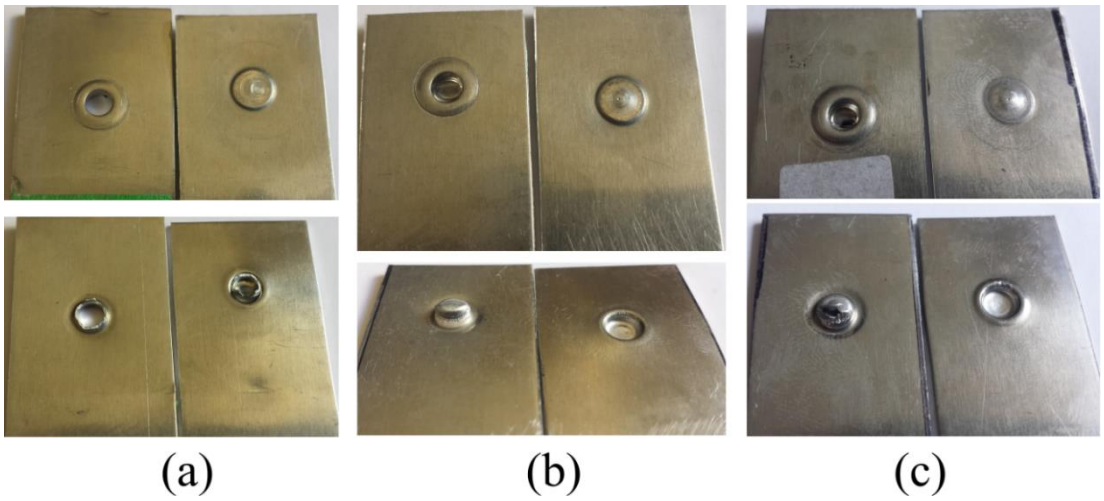

Figure 3.18. Various failure modes in lap shear testing of clinched joints, (a) unbuttoning failure, (b) button (or neck) failure, and (c) combined unbuttoning and neck failure.

Figure 3.19 shows the force-displacement traces from peel tests for clinched joints formed at different forming forces under fully annealed condition. In contrast to lap shear strength, the curves show an increase in peel strength with increasing forming force suggesting that peel strength is largely affected by the interlock depth. In other words, the neck thickness has little effect on the peel strength.

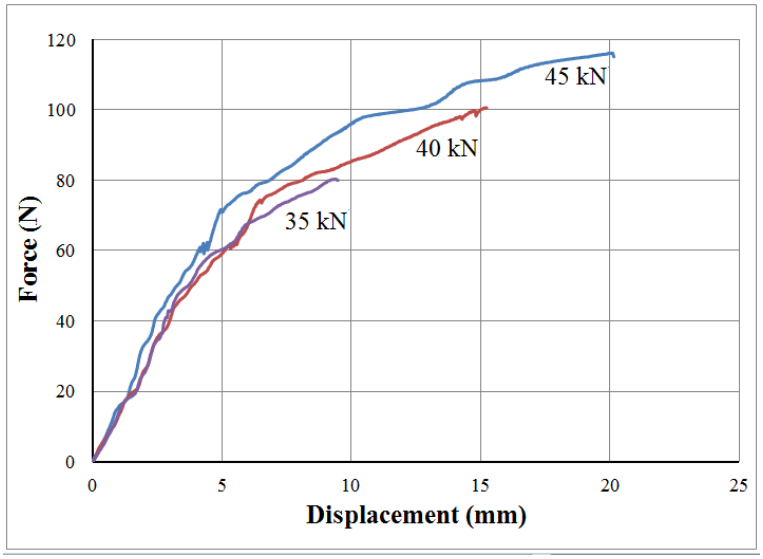

Figure 3.19. Force-displacement traces from peel tests on clinched joints. The joints were formed by using blank holder type B with groove diameter 175% of punch diameter and 40% of sheet thickness groove depth.

3.3.3 Correlations between other die-less clinch characteristics and post-clinch joint strength

3.3.3.1 Effect of blank holder shape

In order to study the effect of blank holder shape on the formed joint, three different blank holder shapes (A, B, and C shown in Figure 3.6) were considered. Blank

holder A failed to clinch whereas the other two blank holders (B and C) resulted in successful clinches. Figure 3.20 demonstrates the results from post-clinch tensile lap-shear tests for the different forming conditions in the form of maximum load at failure versus forming force for blank holders B and C. As shown, a maximum strength of about 2 kN for both blank holders (B and C) was obtained at approximately 40 kN forming force. However, blank holder C performed better than blank holder B at all other forming forces. The results were consistent with a higher interlock formation (at low forming force) as well as lower neck thickness reduction (at high forming force) for blank holder C compared to blank holder B, as shown in Figure 3.21.

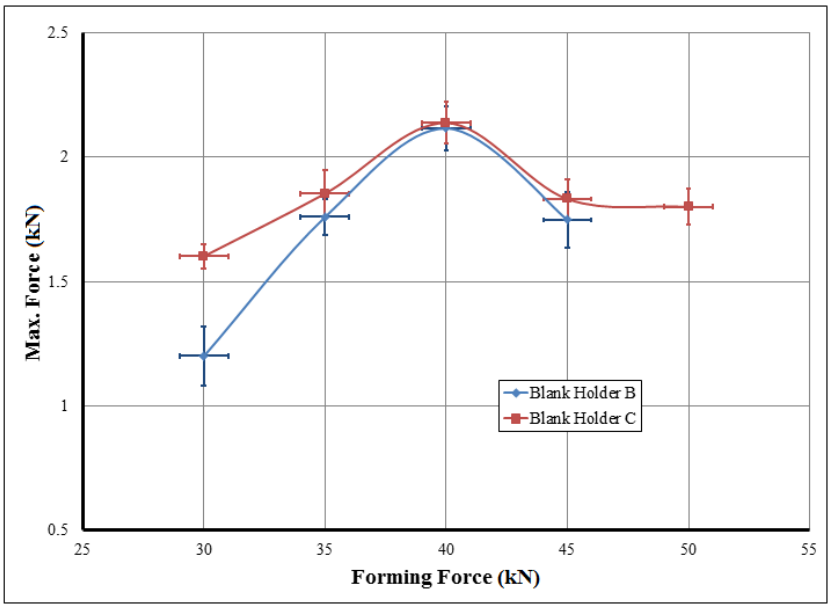

Figure 3.20. Maximum shear force from tensile lap shear tests versus forming force for die-less clinched joints produced by using blank holder types B and C with groove depth 80%, for fully annealed AA7075 sheet.

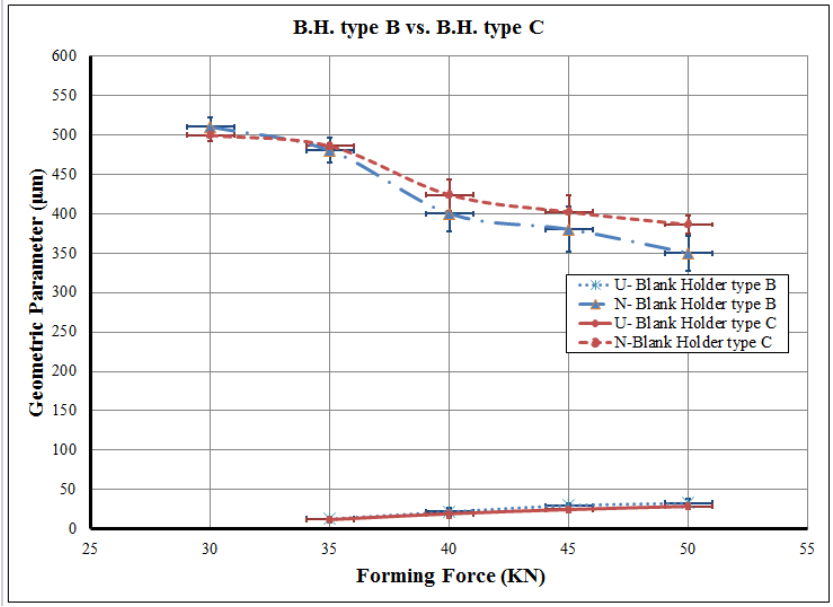

Figure 3.21. Geometrical parameters of the joint versus forming force for die-less clinch joints produced by blank holders B and C, each with a groove depth of 80%. Sheet material was fully annealed.

3.3.3.2 Effect of blank holder groove depth

Figure 3.22 shows the effect of reduction in groove depth as a function of sheet thickness. A reduction in groove depth to 30% of sheet thickness resulted in increase of joint strength by approximately 27% and 24% for blank holders B and C respectively, compared to a reduction in groove depth of 75%, as shown in Figure 3.22. In fact, a decrease in groove depth improved interlock formation, as shown in Figure 3.23, due to influence of material flow restriction in the axial direction which in turn increased the flow of material in the radial direction [1]. The curves show that the smaller groove depth enhances the reduction in neck thickness as a result of increasing forming force. However, the anvil-sided protrusion increased by approximately 15% of sheet thickness at groove depth of 30% sheet thickness as a result of decrease in the groove depth as

shown in Figure 3.24. Extreme reduction of groove depth results in failure of interlock formation as shown on right side of Figure 3.25. The reduction in the groove depth to 20% of sheet thickness results in high protrusion depth and failure of interlock formation.

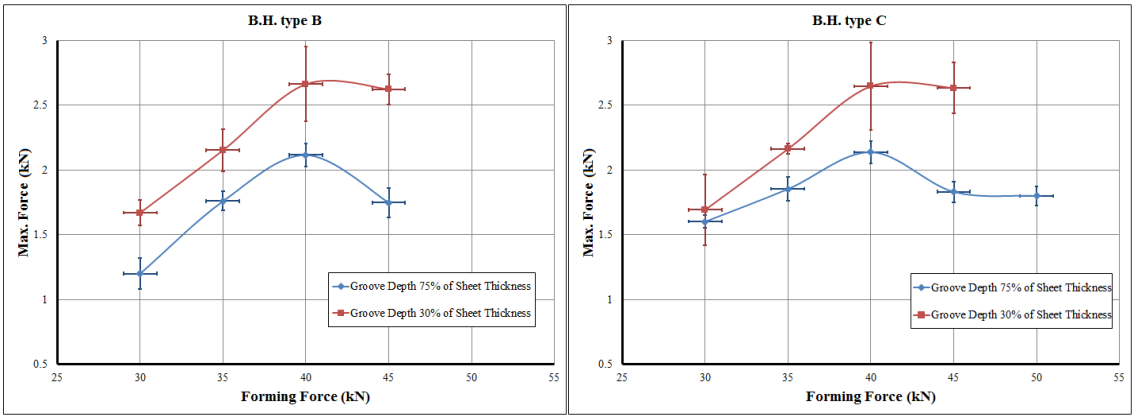

Figure 3.22. Effect of depth of blank holder groove on maximum shear force in tensile lap-shear tests. The joints were produced by different blank holders as well as different forming forces. The sheets were fully annealed.

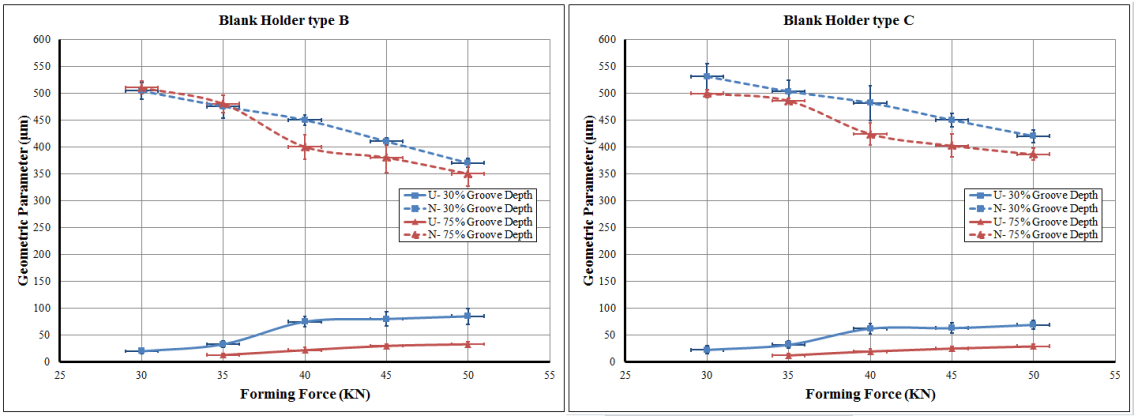

Figure 3.23. Effect of depth of blank holder groove on geometrical parameters of clinched joint produced using different blank holders and forming forces. The sheets were fully annealed.

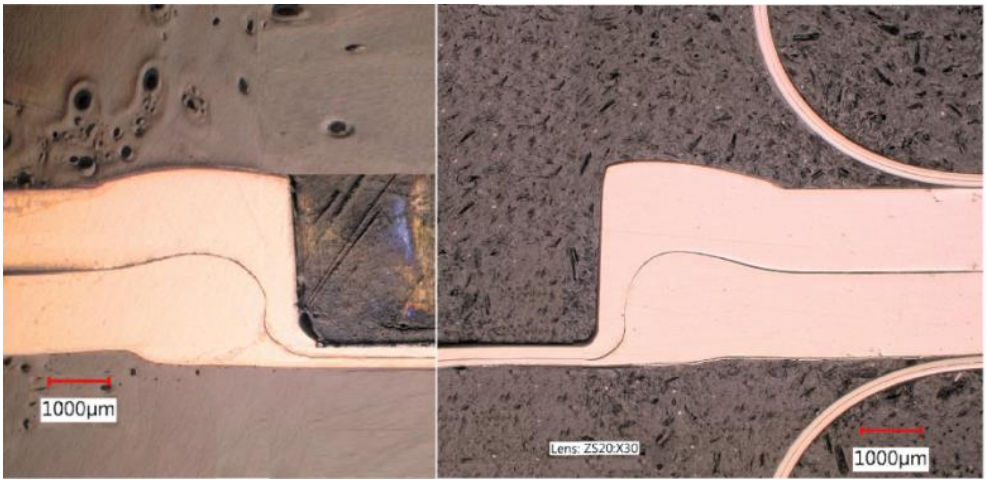

Figure 3.24. Optical images of mounted cross-sections through the clinched joint from fully-annealed sheets for forming force of 40 kN and blank holder type B with groove depths of30% (left) and 75% (right) of sheet thickness.

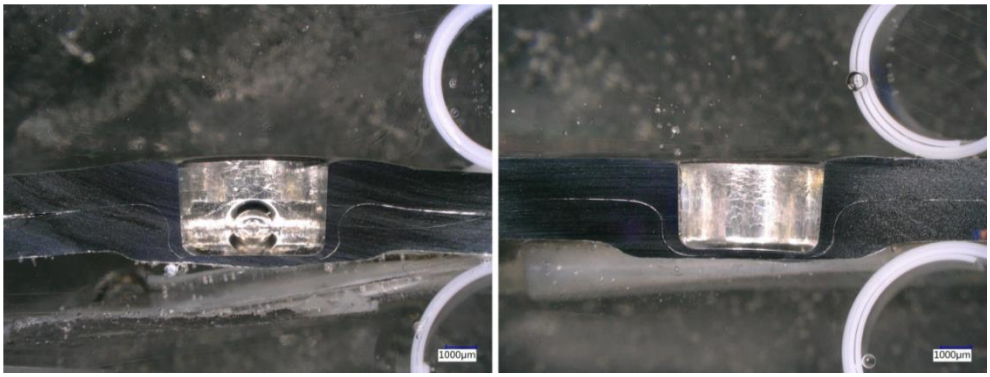

Figure 3.25. Optical images of mounted cross-sections through joints made by using blank holder B with groove depth 25 % (on the right) and 20 % (on the left) of the sheet thickness. The sheet metal was in full annealed conditions. Using groove 15 % depth, results in higher protrusion and failure of interlock formation.

3.3.3.3 Effect of blank holder groove diameter

The effect of the groove diameter was also studied as a function of the punch diameter by considering two different grove diameters of 175% and 215% of punch

diameter. The tests were carried out using blank holder type B with different groove depths. The joint strength increased by 20% for the 215% groove diameter case as shown in Figure 3.26. Similarly, the geometrical interlock was higher for the 215% groove diameter as shown in Figure 3.27. Due to the increase in groove diameter, there is a clear enhancement in neck thickness reduction with increasing forming force. The material flow is increased towards the clinched region from the outer regions of blank holder rather than from the nearby regions. There was no noticeable change in the interlock depth which depends significantly on depth of the blank holder groove. Figure 3.28 summarizes the effect of the different tool parameters on the strength of the die-less clinched joint. Blank holder with small groove diameter (≤150% of punch diameter) led to failure of interlock formation regardless the groove thickness. Similarly, blank holder with small groove depth (≤15% of sheet thickness) resulted in failure of interlock formation regardless the groove diameter. It is to be noted that the bars in Figure 3.28 with zero value indicate that no interlocking was achieved and therefore joint did not exhibit any joint strength.

Optical image of a clinch in the solution heat-treated (W temper) corresponding to the forming force of 40 kN is shown in Figure 3.29. A geometric interlock started to form with a rather small interlock of approximately 17 μm. A large protrusion on the anvil-side of the sheet indicates that sheets in this temper state required a higher clamping force in order to decrease the protrusion as well as increase the interlock depth (see earlier Figure 3.16, where force-displacement traces for W temper, and W temper and aged, conditions are compared from lap-shear tests).

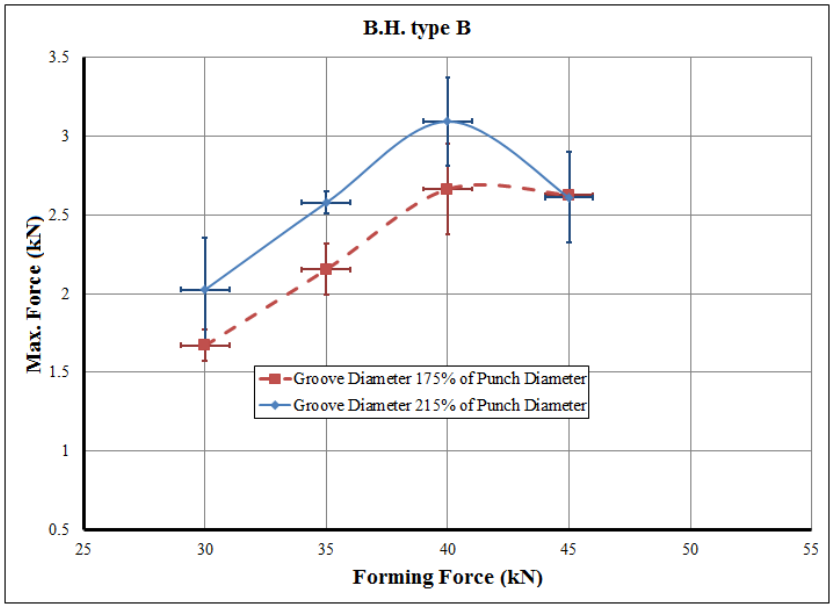

Figure 3.26. Maximum shear force that the joint can withstand as a function of forming force of the joints created by using blank holder types B with different groove diameters, fully annealed sheet (groove depth 30%).

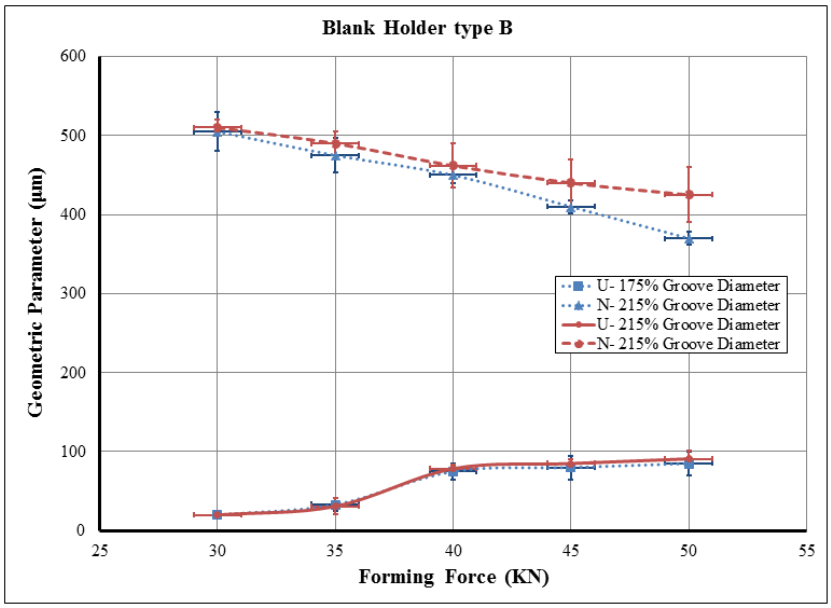

Figure 3.27.Effect of diameter of blank holder groove on the final geometry of clinched joint produced by blank holder type B at different forming forces, fully annealed sheet (groove depth 30%).

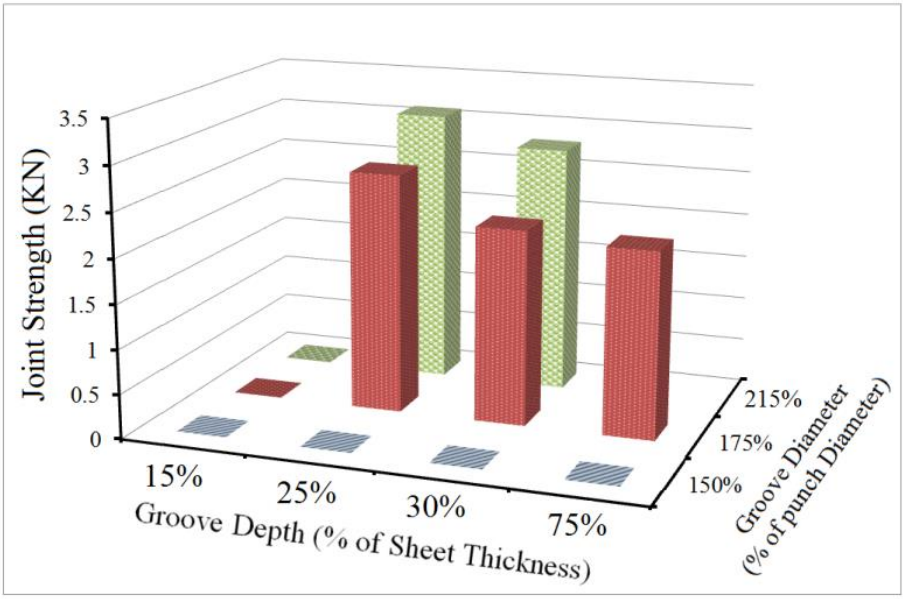

Figure 3.28. Effect of the different tool parameters on the strength of the die-less clinched joint.

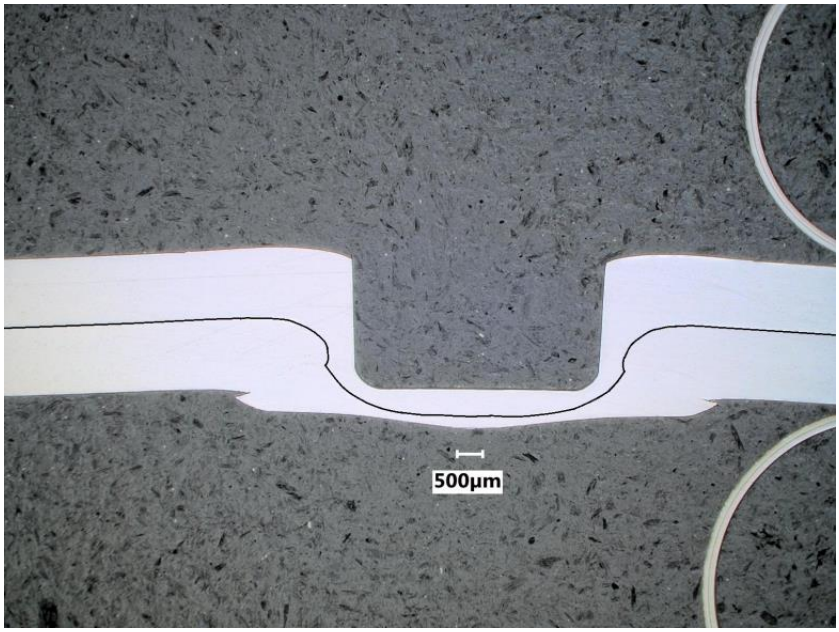

Figure 3.29. Cross-section through the clinched joint from solution heat-treated sheet, forming force of 40 kN, blank holder type C.

3.4 Conclusions

Studies involving die-less clinched joints using two layers of AA7075 aluminum sheets in different temper states were carried out. The effects of tool parameters such as blank holder shapes, process parameters such as forming force as well as different material temper states (T6, O, and W) on material flow behavior, neck thickness, and interlock depth were investigated. Subsequently, effects of clinched geometrical and process parameters on lap shear joint and peel strengths were also investigated. The following specific conclusions were made from this study.

1- Clinch-ability is strongly affected by the temper state where the ability of the material to flow in the direction opposite to the punch movement is critical to the clinching process. In general, annealed temper states resulted in better quality clinches in terms of interlock depth. Conversely, clinching of the 7075-T6 was considerably more difficult due to its higher strength and reduced ductility.

2- Clinching of AA7075 in W temper produced a much smaller interlock depth compared to the other tempers and resulted in poor joint strength. However, natural aging of this temper state (leaving the sheets at room temperature for 30 days) resulted in increased interlock depth and improved joint strength due to precipitation hardening.

3- Tool parameters, and especially the design of groove in the blank holder, was effective in enhancing the joint strength. The depth of the groove had considerable influence on the interlock formation, while its diameter had a stronger influence on the reduction in the neck thickness.

4- A blank holder of groove diameter greater than 150% of the punch diameter and groove depth greater than 20% of sheet thickness is recommended for interlock formation with reasonable joint strength of 3.2 kN.

5- Shear strength of the die-less clinched joints depended largely on neck thickness and the interlock depth. In contrast the joint peel strength depended largely on the neck thickness.

References

[1] T. Gerstmann, B. Awiszus, Recent developments in flat-clinching, Computational Materials Science 81 (2014) 39-44.
[2] C.-J. Lee, J.-M. Lee, H.-Y. Ryu, K.-H. Lee, B.-M. Kim, D.-C. Ko, Design of hole-clinching process for joining of dissimilar materials–Al6061-T4 alloy with DP780 steel, hot-pressed 22MnB5 steel, and carbon fiber reinforced plastic, Journal of Materials Processing Technology 214(10) (2014) 2169-2178.
[3] T. Barnes, I. Pashby, Joining techniques for aluminium spaceframes used in automobiles: Part I—solid and liquid phase welding, Journal of materials processing technology 99(1) (2000) 62-71.
[4] I.R.P. T.A. Barnes, Joining techniques for aluminium spaceframes used in automobiles Part II -adhesive bonding and mechanical fasteners, Journal of Materials Processing Technology 99 (2000) 72-79.
[5] K.-i. Mori, N. Bay, L. Fratini, F. Micari, A.E. Tekkaya, Joining by plastic deformation, CIRP Annals-Manufacturing Technology 62(2) (2013) 673-694.
[6] C. Borsellino, G. Di Bella, V. Ruisi, Study of new joining technique: flat clinching, Key Engineering Materials, Trans Tech Publ, 2007, pp. 685-692.
[7] J. Varis, Ensuring the integrity in clinching process, Journal of Materials Processing Technology 174(1) (2006) 277-285.
[8] F. Lambiase, A. Di Ilio, Finite element analysis of material flow in mechanical clinching with extensible dies, Journal of materials engineering and performance 22(6) (2013) 1629-1636.
[9] J.P. Varis, J. Lepistö, A simple testing-based procedure and simulation of the clinching process using finite element analysis for establishing clinching parameters, Thin-Walled Structures 41(8) (2003) 691-709.
[10] J. Mucha, W. Witkowski, The clinching joints strength analysis in the aspects of changes in the forming technology and load conditions, Thin-Walled Structures 82 (2014) 55-66.
[11] S. Coppieters, P. Lava, S. Baes, H. Sol, P. Van Houtte, D. Debruyne, Analytical method to predict the pull-out strength of clinched connections, Thin-Walled Structures 52 (2012) 42-52.
[12] K. Mori, Y. Abe, T. Kato, Mechanism of superiority of fatigue strength for aluminium alloy sheets joined by mechanical clinching and self-pierce riveting, Journal of Materials Processing Technology 212(9) (2012) 1900-1905.

[13] C. Chen, S. Zhao, X. Han, M. Cui, S. Fan, Investigation of the height-reducing method for clinched joint with AL5052 and AL6061, The International Journal of Advanced Manufacturing Technology (2016) 1-8.
[14] C. Chen, S. Zhao, M. Cui, X. Han, X. Zhao, T. Ishida, Effects of geometrical parameters on the strength and energy absorption of the height-reduced joint, The International Journal of Advanced Manufacturing Technology (2016) 1-9.
[15] C. Chen, S. Fan, X. Han, S. Zhao, M. Cui, T. Ishida, Experimental study on the height-reduced joints to increase the cross-tensile strength, The International Journal of Advanced Manufacturing Technology (2016) 1-8.
[16] T. Wen, H. Wang, C. Yang, L.T. Liu, On a reshaping method of clinched joints to reduce the protrusion height, The International Journal of Advanced Manufacturing Technology 71(9-12) (2014) 1709-1715.
[17] F. Lambiase, D.-C. Ko, Two-steps clinching of aluminum and Carbon Fiber Reinforced Polymer sheets, Composite Structures 164 (2017) 180-188.
[18] C. Chen, S. Zhao, M. Cui, X. Han, N. Ben, Numerical and experimental investigations of the reshaped joints with and without a rivet, The International Journal of Advanced Manufacturing Technology (2016) 1-13.
[19] C. Chen, S. Zhao, M. Cui, X. Han, S. Fan, Mechanical properties of the two-steps clinched joint with a clinch-rivet, Journal of Materials Processing Technology 237 (2016) 361-370.
[20] R. Neugebauer, C. Kraus, S. Dietrich, Advances in mechanical joining of magnesium, CIRP Annals-Manufacturing Technology 57(1) (2008) 283-286.
[21] S. Lüder, S. Härtel, C. Binotsch, B. Awiszus, Influence of the moisture content on flat-clinch connection of wood materials and aluminium, Journal of Materials Processing Technology 214(10) (2014) 2069-2074.
[22] R. Neugebauer, R. Mauermann, S. Dietrich, C. Kraus, A new technology for the joining by forming of magnesium alloys, Production Engineering 1(1) (2007) 65-70.
[23] S. Coppieters, S. Cooreman, P. Lava, H. Sol, P. Van Houtte, D. Debruyne, Reproducing the experimental pull-out and shear strength of clinched sheet metal connections using FEA, International journal of material forming 4(4) (2011) 429-440.
[24] F. Lambiase, A. Di Ilio, A. Paoletti, Joining aluminium alloys with reduced ductility by mechanical clinching, The International Journal of Advanced Manufacturing Technology 77(5-8) (2015) 1295-1304.
[25] F. Lambiase, Clinch joining of heat-treatable aluminum AA6082-T6 alloy under warm conditions, Journal of Materials Processing Technology 225 (2015) 421-432.
[26] F. Lambiase, A. Di Ilio, Damage analysis in mechanical clinching: experimental and numerical study, Journal of Materials Processing Technology 230 (2016) 109-120.
[27] X. He, Y. Zhang, B. Xing, F. Gu, A. Ball, Mechanical properties of extensible die clinched joints in titanium sheet materials, Materials & Design 71 (2015) 26-35.
[28] Y. Abe, S. Nihsino, K.-i. Mori, T. Saito, Improvement of joinability in mechanical clinching of ultra-high strength steel sheets using counter pressure with ring rubber, Procedia Engineering 81 (2014) 2056-2061.
[29] X. He, L. Zhao, H. Yang, B. Xing, Y. Wang, C. Deng, F. Gu, A. Ball, Investigations of strength and energy absorption of clinched joints, Computational Materials Science 94 (2014) 58-65.

Chapter 4

A Parametric Study of FE Modeling of Die-less Clinching of AA7075 Aluminum Sheets

---

Mostafa K. Sabra Atia, PhD student, is the first author and main contributor of the work who conceptualized the topic, built FE model, interpreted the results and drafted the paper. Mukesh K. Jain, Professor, is the supervisor who substantially contributed to the work by checking the experimental results and technical details of the model as well as polishing the language of the paper. This paper is under review in International Journal of Material Forming.

A Parametric Study of FE Modeling of Die-less Clinching of AA7075 Aluminum Sheets

Mostafa K. Sabra Atia[a,b] and Mukesh K. Jain[a]

a Department of Mechanical Engineering, McMaster University, Hamilton, Ontario, Canada L8S 4L7

b Corresponding author: Tel.: +1 (905) 920-0398. Fax: +1(905) 572-7944. E-mail address: atiam@mcmaster.ca (Mostafa K. Sabra Atia).

Abstract

Die-less clinching process is a relatively new process for joining two sheet materials and aspects of this process are being optimized for many sheet materials. Die-less clinching tool optimization by conducting many experimental trials with different tool design parameters can be quite expensive and time consuming. Tool optimization via numerical simulations can be an effective and economical alternative provided material and other characteristics during clinching are adequately captured by the models. Also, there are several material, process and simulation parameters that can affect the simulation accuracy. In the present work a finite element (FE) modeling investigation of the influence of different numerical, material and process parameters on die-less clinch characteristics is carried out with a goal towards clarifying and optimizing die-less clinching simulations for improved and efficient predictions. The numerical parameters include element size and aspect ratio, adaptive re-meshing criterion, model boundary conditions (dependent on the tool configuration) and material and process parameters (such as non-linear work hardening behavior and friction between mating tool-sheet surfaces respectively). Adaptive re-meshing technique is required to avoid excessive element distortion as the strain is very large in die-less clinching. A mass scaling factor of less than 150 is suggested for acceptable accuracy from the model. Extended-Voce constitutive material model has been shown to accurately capture the large strain behaviour of AA7075-O sheet for die-less clinching simulations. Inter-sheet as well as punch-sheet friction are shown to primarily influence geometric interlock.

Keywords: Die-less clinching, numerical simulation, finite element modeling.

Table 4.1. List of Abbreviations

N	Neck thickness of the joint
U	Interlock depth of the joint
X	Joint bottom thickness
t	Blank holder groove depth
d	Blank holder groove diameter
σ_{eq}^{p}	Equivalent stress
ε_{eq}^{p}	Equivalent plastic strain
k_1	Stress coefficients for Voce hardening law
K_2	Stress coefficients for Swift hardening law
C	Material constant for Voce hardening law
m	Material constant for Voce hardening law
K	Material constant for Power hardening law
δ	A continuous hardening parameter in Extended-Voce material model
y_0	Initial yield stress
μ_{sh}	Sheet-to-sheet coefficient of friction
μ_t	Sheet-to-tool coefficient of friction
n	Strain hardening exponent
L^e	Smallest characteristic element length
C_d	Material dilatational wave speed
E	Modulus of elasticity
ρ_m	Density of the material

4.1 Introduction

Conventional clinching is a room temperature mechanical fastening technique that uses punch and die to locally deform the sheet metal to produce a geometric interlock [1]. Unlike welding and brazing, it is an environmentally cleaner process with no heat effects or emissions and energy efficiency [2]. However, conventional clinching results in undesirable surface features in the form of a pit on one side of the joint and a protrusion on the other. The advantages and limitations of using conventional clinch joining have

been extensively reported in the literature [3-6]. A new joining technique called die-less clinching has been developed in order to make clinching more aesthetically appealing in which surface step exist only on one side. In this process, a flat anvil is used instead of the die and the material flow is controlled through a designed groove in the blank holder as in Figure 4.1 . Very few experimental and numerical studies of die-less clinching of high strength aluminum alloys have been reported in the literature. A parametric study based on finite element (FE) simulations offers a systematic and cost-effective method towards process optimization of die-less clinching for high strength aluminum alloys.

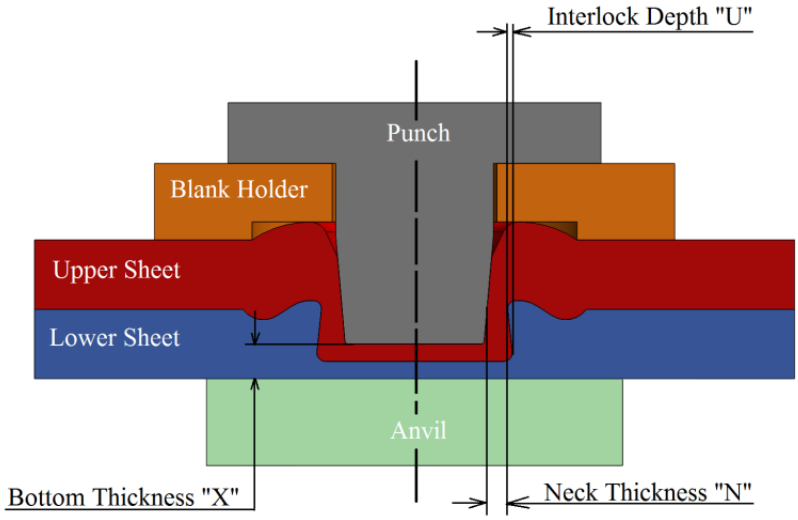

Figure 4.1. Schematic drawings of die-less clinching process showing the tool set as well as the main geometric parameters of the joint.

In order to obtain optimum joint parameters that maximize shear and peel strengths, many experiments involving a range of tool geometric, material, and process parameters are required to attain proper geometrical interlocking [7]. In addition, separate experiments are required to assess the joint strength such as shear and peel tests [8].

Parametric studies via FE modeling, as an alternative to experiment based trials, can be a cost-effective and efficient means of tool design for the die-less clinching process [9]. FE methodology can aid in the assessment and selection of suitable constitutive material law as well process parameters for die-less clinching. FE allows virtual experiments to be carried out to not only form the joint but also conduct post-forming joint strength assessment via simulations [8-11]. While there are many useful studies on simulation of conventional clinching [9, 10, 12-14], as briefly discuss below, the work reported in the literature on simulation of newer and more complex die-less clinching process is limited. Substantial differences persist in the two forming processes. For example, the equivalent plastic strain for die-less clinch can be substantially larger, exceeding a value of 5 in some cases, whereas in conventional clinching it is typically much less [4].

In the present work, a FE study of die-less clinching is carried out for joining high strength 7075-O aluminum sheet materials. Different FE simulation parameters that influence simulation of the die-less clinch joining such as element size and mass scaling, boundary condition which represents by tool configuration and material parameters such hardening law are studied for their influence on clinch geometry and other characteristics.

4.2 Brief review of numerical modeling of clinching process

Die-less clinching is a joining process by sheet forming using a simpler tool configuration in which the strength of the joint is entirely determined by how far the two sheets can be plastically deformed to create a geometrical interlock while the bottom surface of the bottom sheet remains planar as shown in Figure 4.1. The process to create

the geometric interlock, also called S-shape, employs a flat circular punch, a flat anvil, and a blank holder. The main geometric parameters of the clinched joint include neck thickness N, interlock depth U, and bottom thickness X [15], as depicted in Figure 4.1. The specific tool shapes to control material flow are critical to the creation of the geometrical interlock. In addition to the tool shape parameters, there are other parameters that influence the accuracy of process simulation; (i) numerical parameters such as element size, mass scaling, and adaptive re-meshing procedure, (ii) model boundary conditions that try to capture the actual die-less clinching process, and (iii) material parameters which involve hardening law, anisotropy, friction model, and spring-back. Generally, accurate and reliable FE modeling of the clinch joining process is a complex problem since the joint strengths are influenced not only by the final shape of the joint but also by the forming parameters [9].

There have been a number of studies on simulation of conventional clinching [9, 10, 12-14]. Coppieters et al. [8] have utilized ABAQUS software to build an axisymmetric 2D model as well as a 3D model to simulate conventional clinching of DC05-aluminum sheets of thickness 1.12 mm and 1.5. In these analyses, CAX4R and C3D8R elements were used with reduced integration and hourglass control were used in 2D axisymmetric and 3D models respectively. Coulomb friction law was used with coefficients 0.15 and 0.4 for sheet-tool and sheet-sheet interactions. The result showed the ability of the FE model to predict the forming force and post-formed joint strength despite some inconsistency between the experimental and simulation results. Gerstmann et al. [4] have published the most comprehensive study on FE simulation of die-less clinching.

They have used Simufact forming software to simulate flat clinching process to join 99.5 % pure aluminum sheet of 1 mm thickness to 2 mm thick polystyrene sheet. An axisymmetric model was built representing clinching tools as rigid bodies and deformable sheet materials as 4-node quadrilateral shell elements. The non-linear work hardening material model parameters were obtained from plain strain upsetting test as shown in Figure 4.2. The FE results showed good general agreement with the experiments in terms of final shape of the joint with an error of about 7%. However, the deviation in forming force between the FE and experimental results was relatively large in the range of 10%. The model was limited to clinching of two very ductile aluminum-polystyrene sheets. The proposed plane strain test to obtain material properties is problematic as it requires very accurate alignment of two long and narrow punches that are used to achieve plane strain compression. Another study by Neugebauer et al. [16] utilized DEFORM-2D FE software to simulate die-less clinching of magnesium sheets. This study employed automatic re-meshing and rigid tool assumption. This paper is a brief experimental study of die-less clinching of magnesium sheet that includes a section on FE modeling. While there are some interesting results on the effect of punch profile radius on geometric interlock, the details of the modeling work are not covered. The result showed that the punch geometry had the greatest effect on the shape of the clinched joint.

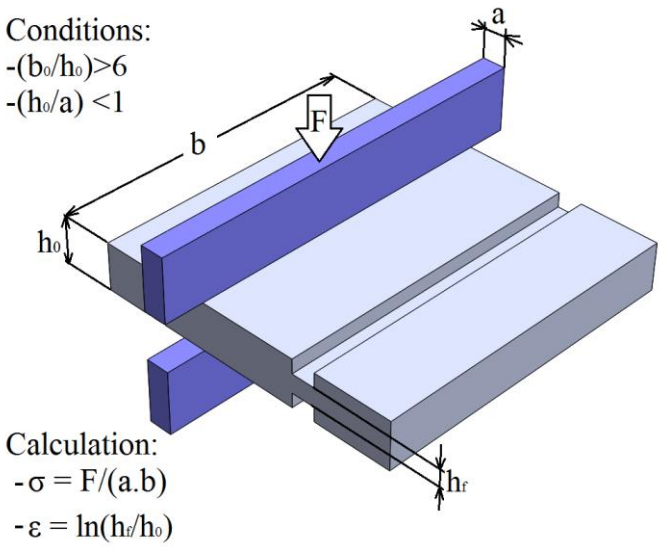

Figure 4.2. Drawing shows the plan strain upsetting test [8].

4.3 FE Simulation Details

4.3.1 Brief review of recent experimental and FE simulation work of the present authors

The present authors have recently published a largely experimental study of die-less clinching process (see reference [15]). Figure 4.3(a) shows a schematic of the tool set utilized in this work, and consisting of an anvil, punch and blank-holder made from tungsten, tungsten carbide and tool steel respectively. The groove in the blank holder had a diameter and depth of 10 mm and 0.3 mm respectively. The tooling also included a compression urethane spring to apply a clamping force. The total clamping force was determined by the stiffness of the urethane spring and its interaction with the casing. Abaqus-Explicit was used to simulate the die-less cinching process for a high strength AA7075 aluminum sheet. Explicit module was considered more suitable for complex

sheet forming processes with multiple sheet-tool interactions. The die-less clinching was modeled as an axisymmetric 2D process in terms of geometry of the joint, loading and boundary conditions as shown in Figure 4.4. The present study focuses on a parametric study of the above tooling to study the influence of numerical parameters such as meshing, mass scaling, adaptive re-meshing, boundary conditions, AA7075 sheet material parameters including the selection of the material constitutive model, friction between all sliding surfaces during clinching and spring-back of the part after clinching.

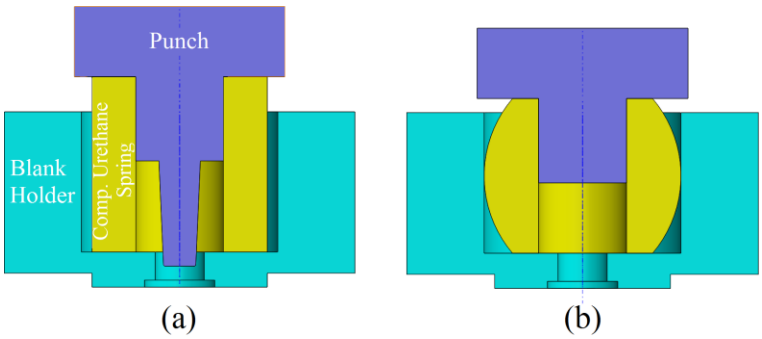

Figure 4.3. Schematic drawings illustrating; (a) configuration of die-less tooling and (b) the interaction between the compression urethane spring and outer casing as well as the half punch used in the measurement of the clamping force.

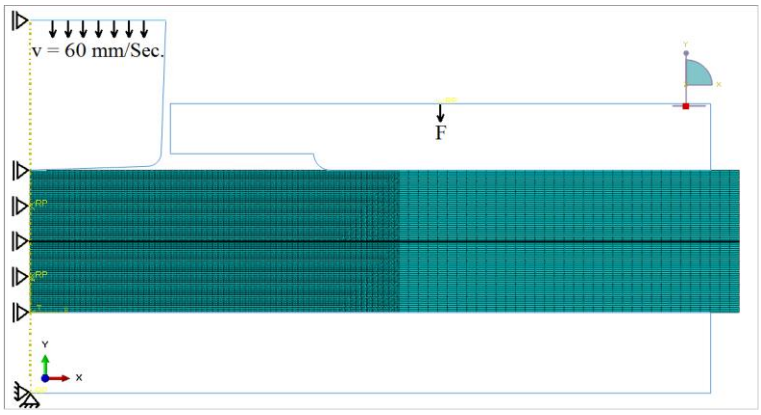

Figure 4.4. Axisymmetric 2Dmodel of the die-less clinching process.

4.3.2 Influence of the numerical parameters

4.3.2.1 Meshing

Meshing is a critical step in the FE model development that directly influences the accuracy and the simulation time of the clinching process. A four node bilinear axisymmetric quadrilateral element with reduced integration (CAX4R) element was used to represent the sheet materials. In order to address the hour glass problem of the first order element with reduced integration, the enhanced hourglass option in Abaqus was used. Because the sheet materials were subjected to highly localized plastic deformation, a very fine mesh was used in the region of the clinching zone whereas coarse mesh was utilized elsewhere to reduce the computation time (see Figure 4.4). Initially, the tools (flat anvil, blank holder and punch) were assumed to be rigid. Figure 4.5 shows the results of a parametric study for different element sizes and element aspect ratios. The element aspect ratio was defined as the ratio of the vertical length to the horizontal length of the element. Meshing with relatively large element size, up to $1/15^{th}$ of the sheet thickness, failed to predict interlocking and resulted in the lifting of the upper sheet, a behavior not observed in the experiments. However, element sizes lower than $1/15^{th}$ of the sheet thickness produced interlocking. The interlock depth increases with decreasing element size until the result starts to converge at element size of $1/40^{th}$ of the sheet thickness with a convergence error of less than 3%. Further mesh refinement did not yield a significant change in the result. The element size had less effect on the neck thickness compared with its effect on interlock depth as shown in Figure 4.6. The decrease in the element size led to an exponential increase in the computational time as shown in Figure 4.7 where

computation time has been normalized using the computational time for the case of 10 elements through the sheet thickness. The computational time could be reduced by 40 % by increasing the aspect ratio of the element to 1.3 without a significant effect on the results. It is to be noted that the number of elements in the radial direction had the biggest effect on the stress state and interlock formation due to the direct effect of friction on material flow behavior. Based on this parametric study, an element size of 1/40th of the sheet thickness with an aspect ratio 1.3 was utilized in all subsequent simulations.

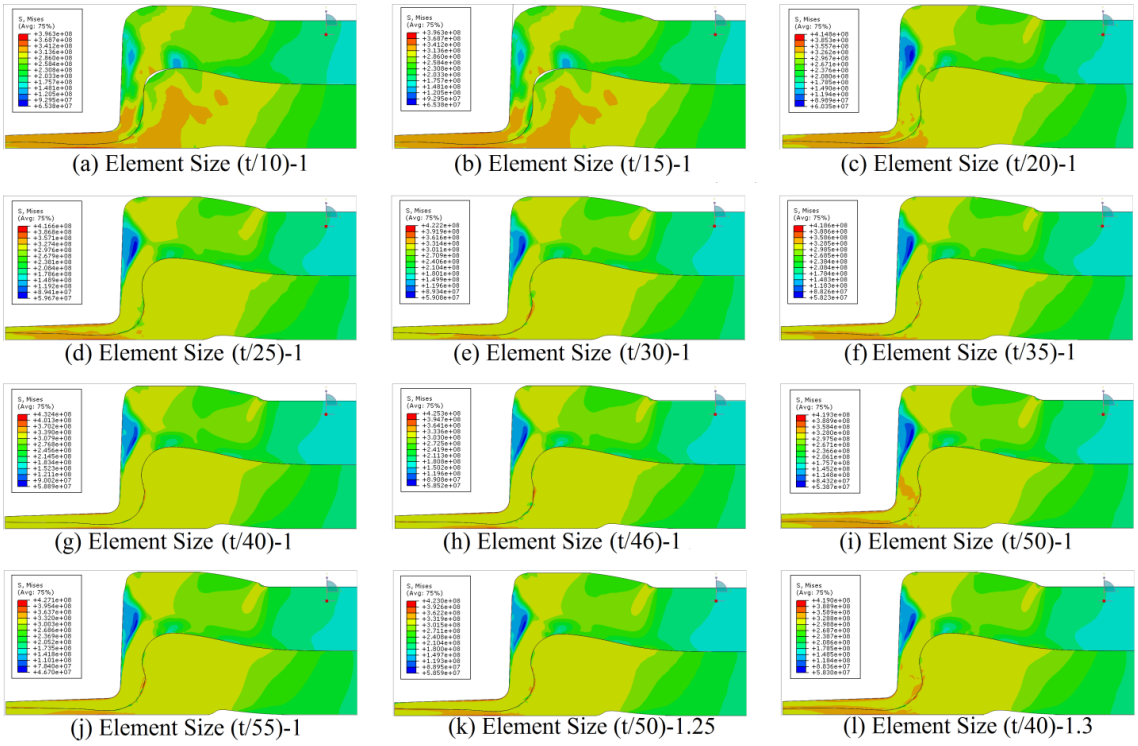

Figure 4.5. Mises stress contours after die-less clinching from different element sizes as well as different element aspect ratio corresponding to a punch displacement of 2.3 mm. The first number in the brackets below each result refers to the element size in terms of sheet thickness "t" while the second number refers to the element aspect ratio. The simulation utilized the extended-Voce material model (to be discussed later).

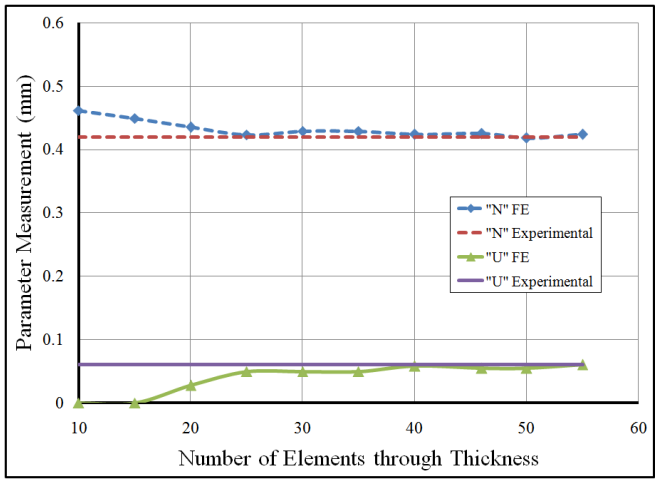

Figure 4.6. Effect of element size on neck thickness N and interlock depth U (see Figure 4.1).The simulation utilized the extended-Voce material model (to be discussed later).

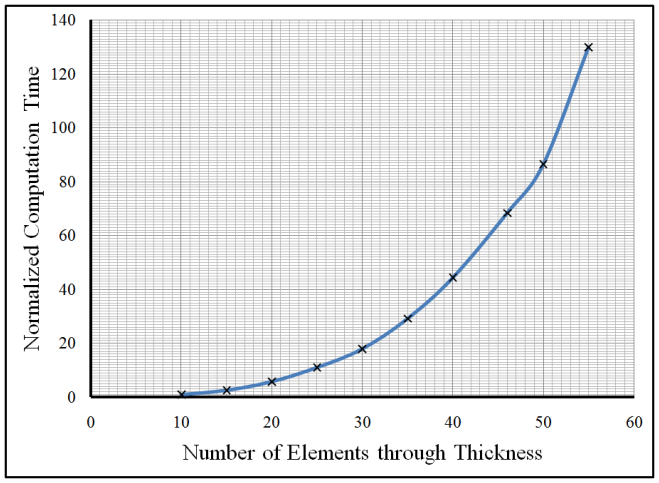

Figure 4.7. Effect of the element size on normalized computation time using extended-Voce material model (to be discussed later).

4.3.2.2 Mass scaling factor

Mass scaling, by adding mass to the model or part of the model, is typically used in dynamic explicit FE codes as an effective technique to decrease simulation time. The

stability limit, a measure of calculation efficiency, is expressed in terms of the maximum time increment as [17]:

$$\Delta t = \left(\frac{L^e}{C_d} \right) \tag{4.1}$$

where L^e is the smallest characteristic element length and C_d is the material dilatational wave speed for linear elastic material, expressed as [17]:

$$C_d = \sqrt{\frac{E}{\rho_m}} \tag{4.2}$$

where E and ρ_m are the modulus of elasticity and density of the material. From equations (4.1) and (4.2), the stability time is proportional to element size as well as the material density. Therefore, by squaring material mass (factor f^2) results in an increase in the stability time by f. In other words, mass scaling can be used to compensate for the negative effect of small element size on the computational efficiency. However, too much mass scaling could deteriorate the computational accuracy since mass scaling does not reflect the true material inertia and can induce an inertial (or dynamic) effect on the results [13]. Typically, dynamic effect are neglected if the mass scaling keeps the total kinetic energy to total internal energy ratio in the simulations to less than 10% [18, 19].

Figure 4.8 shows the simulation profiles of clinched joints using various mass scaling factors of 100, 150, 300, 500, 900, and 1600. As shown, the profiles obtained by using different mass scaling factors are almost the same. However, the associated geometric parameters of the resulting clinched joints varied depending on the value of the

mass scaling factor. From the quantitative analysis shown in Figure 4.9. The geometric parameters of the joint predicted using mass scaling factors up to 150 agreed well with the experimental results within a rather small error band. This is consistent with the ratio of total kinetic energy and total internal energy of the various simulations (see Figure 4.10). It is to be noted that, for mass scaling up to 150, some oscillations in the ratio of total kinetic energy to total internal energy resulted from initial insertion of the punch into the upper sheet arising from sudden contact between the punch and sheet and making the system somewhat unstable. As the contact was established and the system became stable, the ratio of total kinetic energy to total internal energy fell below the acceptable 10% and the simulations results were deemed acceptable. A mass scaling factor of 100 was chosen for simulation of the clinching process to improve the computational efficiency.

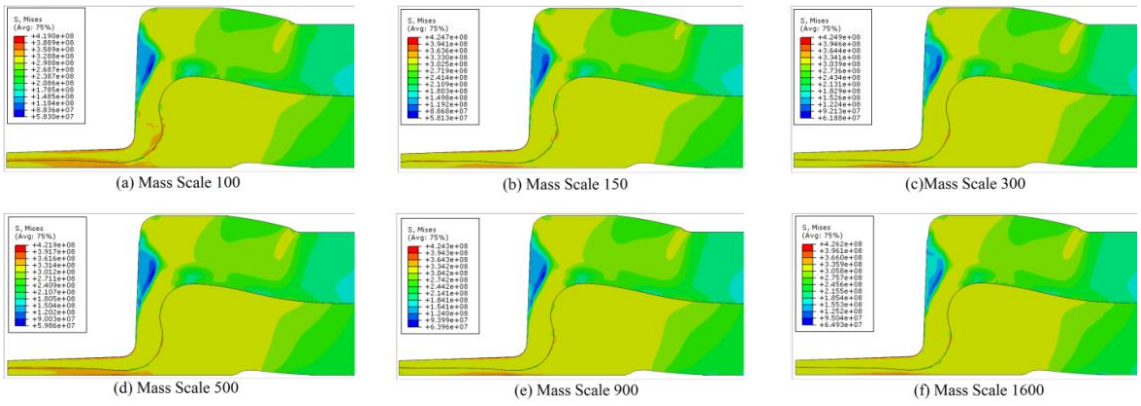

Figure 4.8. Profiles of clinched joint obtained using different mass scaling factors and extended-Voce material model.

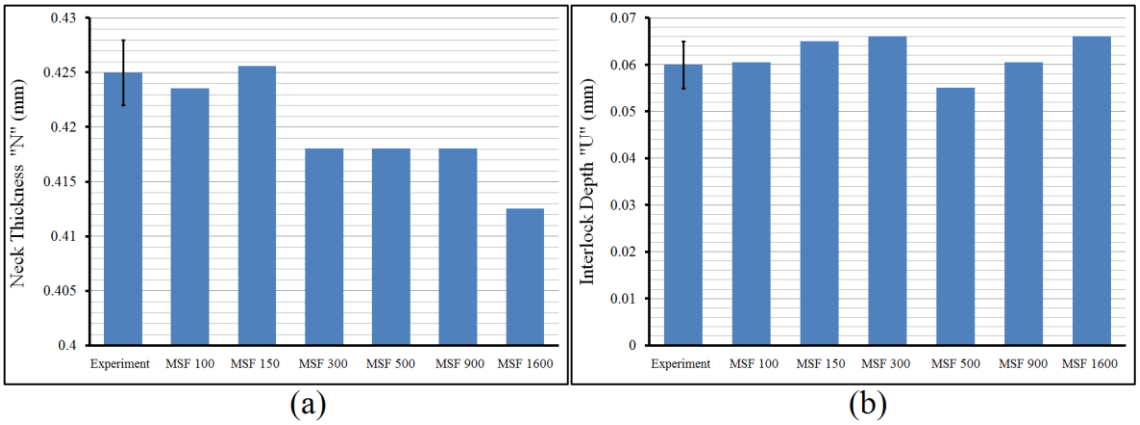

Figure 4.9. Plots show the effect of the mass scaling factor (MSF) on the geometric parameters; (a) neck thickness "N" and (b) interlock depth "U".

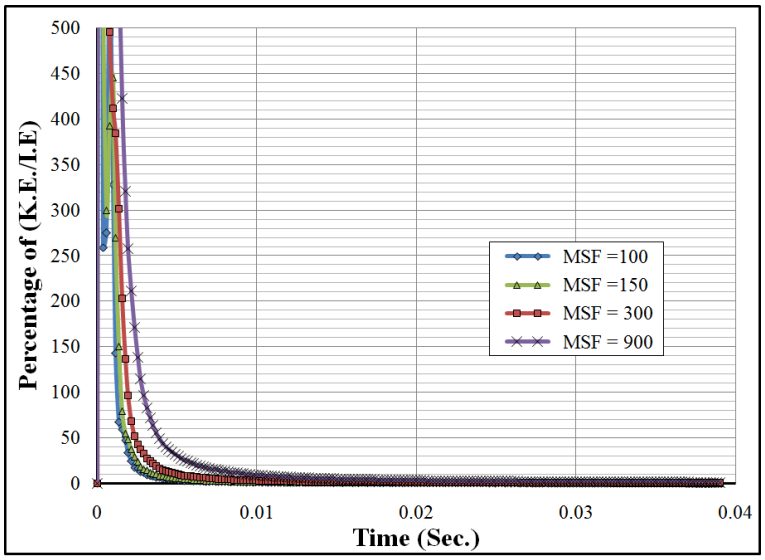

Figure 4.10. A plot of ratio of the total kinetic energy to the total internal energy versus time of punch movement (punch speed of 60 mm/sec).

4.3.2.3 Adaptive re-meshing

Adaptive re-meshing technique is an effective tool to avoid element distortion from large deformation that accompanies die-less clinching. Generally, re-meshing

process requires a criterion, and algorithms to convey the nodes, map the solution variables, and transmit them from an old nodes to new ones [10]. In fact, Abaqus software uses Arbitrary Lagrangian-Eulerian (ALE) method of adaptive meshing. Within Abaqus-Explicit there are three available smoothing algorithms to determine the new location of each node: volumetric smoothing (default), Laplacian smoothing, and equipotential smoothing [20]. In volumetric smoothing, the nodes are relocated based on calculation of average volume weight of element center. In Laplacian Smoothing, the nodes are relocated based on average position of each adjacent node. In equipotential smoothing, the node transfer is based on solving Laplace-equation [20]. The effect of all three types of smoothing on die-less clinching using their full weight were studied in the present work. Figure 4.11 shows the distribution of the equivalent plastic strain (PEEQ) of the punch-sided sheet along the upper, mid plane, and the lower set of elements using the three smoothing algorithms. In order to gradually smooth the meshing during the analysis, certain re-meshing frequency is also required. The default frequency of 10 which has been widely used in the literature [10] was selected in the present work as well as a base frequency of 1 for comparison. The meshing priority selected was to set the element aspect ratio. The results shown in Figure 4.11 did not show any noticeable change in the PEEQ distribution between the three studied smoothing algorithms. Based on this study, volumetric smoothing algorithm was utilized in all of the simulations.

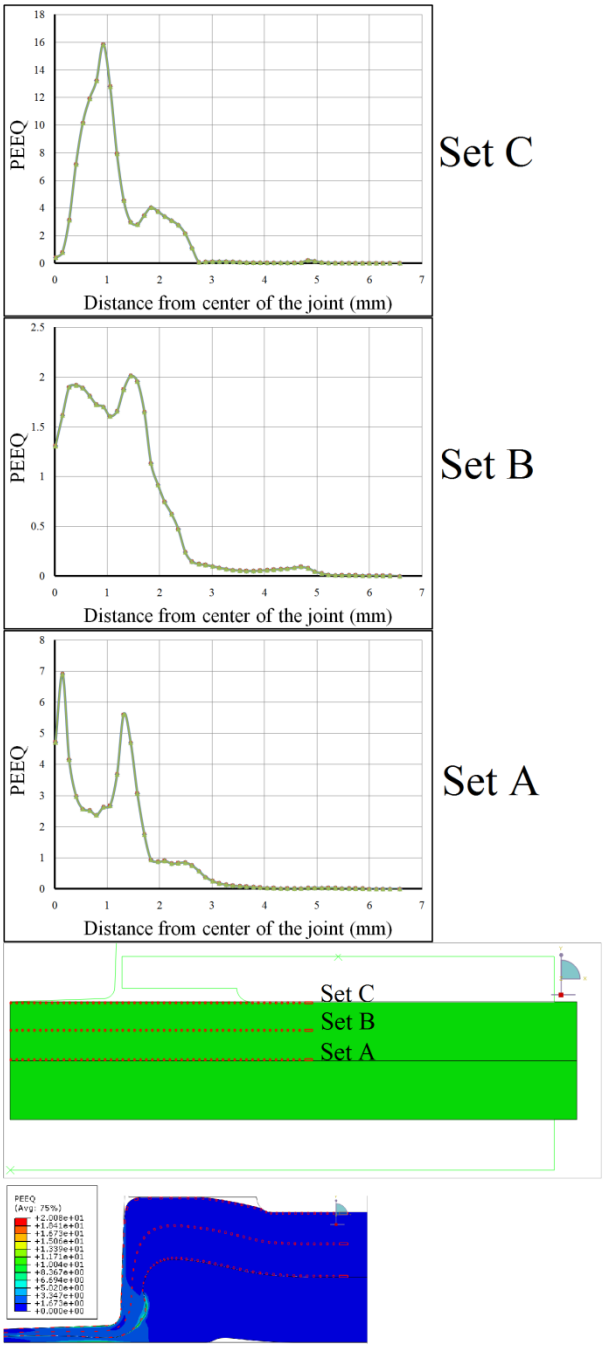

Figure 4.11. PEEQ results from re-meshing study showing undeformed mesh (in green) and deformed configuration of the die-less clinch for three different rows of elements in the upper sheet (referred to as sets A, B and C for the bottom, middle and top rows respectively) using three smoothing algorithms. An extended-Voce material model was used (to be discussed).

4.3.3 Influence of model boundary conditions

In die-less clinching, the blank holder exerts a relatively large force over a small area in order to form the geometrical interlock. The total forming force, that includes the blank-holder and punch forces, is even larger in the range of 50 kN. Such a large force can induce elastic deflection in the tooling as well as in the C shaped loading frame that can affect the actual punch motion and joint formation. The shape of the tool set, its material model (i.e., rigid or elastic), blank-holding force, and consequently punch movement (and the nature of loading) determine the boundary condition of the process simulation. In order to simplify the numerical model, some assumption are often made that affect the physical reality of the die-less clinching process. For example, the assumption of infinitely rigid tooling is quite common in automotive sheet forming simulations that involve large tools [10].

In the present work, effect of stiffness (or rigidity) was studied in the die-less clinching simulations. The blank-holder force, represented by the stiffness of the compression urethane spring and its interaction with the outer casing of the blank holder, was measured using a half punch as shown earlier in Figure 4.3(b). For modeling purposes, eight different tool configurations were considered as noted in Table 4.2. The first configuration (top row) assumed that all the tool components were rigid. In the other extreme, reflected by the bottom row configuration, all components were treated as elastic (and referred to as the compliance model). The rest of the configurations were intermediate involving a combination of the two extremes (rigid and compliant) configurations where some component(s) were rigid while the others were compliant. The

simulation results from the different tool configurations of Table 4.2 are presented in Figure 4.12 and Figure 4.13 where completely rigid configuration is used for comparison purposes. Figure 4.12(a) shows the final geometry of the joint based on the assumption of elastic tooling. The elastic punch is shown to decrease the bottom thickness and the lifting of the bottom surface resulting from a change in the punch height due to elastic deformation. However, an opposite effect was observed from the blank holder due to a change in the blank holder shape and an increase in the blank holder groove depth due to elastic deformation. Figure 4.12(b) shows the combined effect of the different components. A more compliant elastic system resulted in an increase in the bottom thickness and a decrease in the lifting of the bottom surface. Figure 4.13 is a magnified view of the S-shape region of Figure 4.12 for the different model systems. Results from Figure 4.13(a) - predominantly rigid case indicate that simulating punch or anvil as an elastic part causes a shift in the "S" shape of the geometric interlock toward the joint axis as well as an increase in the interlock depth at the expense of the neck thickness. Also, the effect of punch is more pronounced than that of the anvil. There is only a slight effect when the blank holder is modelled as an elastic part. The combined effect of modeling different parts in the predominantly elastic case is shown in Figure 4.13(b). An effect similar to the predominantly rigid case can be noted, where model 6 treating punch and anvil as elastic parts results in a larger “S” shape shift. However, the effect of a rigid blank holder is more dominant in the predominantly elastic case. Lastly, the fully compliant model shows the largest reduction in neck thickness. Table 4.3 summarizes the effect of the different models on S-shape formation.

Table 4.2. A summary of the different tool stiffness combinations in various models utilized in die-less clinch simulations.

Models	Component of tool Set		
	Punch	Blank Holder	Anvil
Rigid Model	-	-	-
Model 1	√	-	-
Model 2	-	√	-
Model 3	-	-	√
Model 4	-	√	√
Model 5	√	√	-
Model 6	√	-	√
Compliance Model	√	√	√

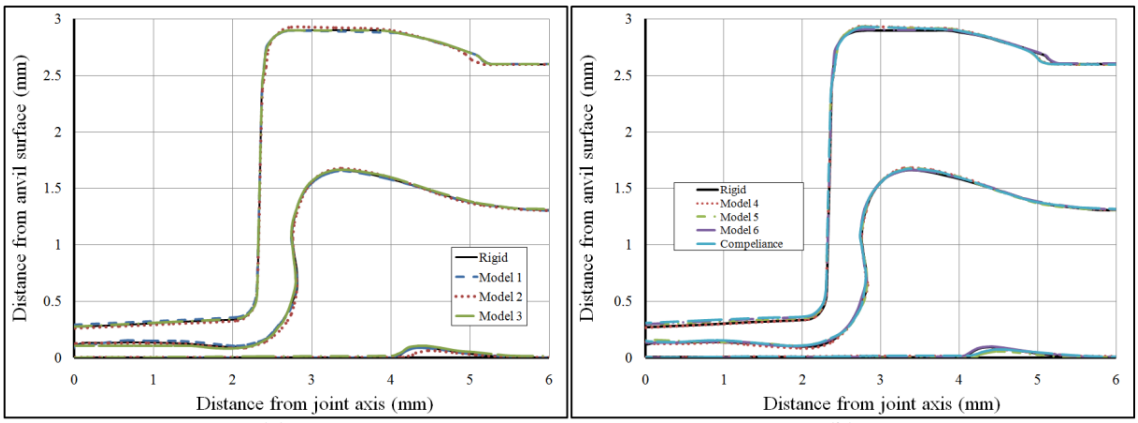

Figure 4.12. Geometry of the die-less clinched joints from different tool stiffness combinations as per Table 4.2 (an extended-Voce material model is used in the simulations).

Figure 4.14 shows a comparison of experimental and simulation forming force-punch stroke curves. These are often referred to as process graphs [10]. It is to be noted that the FE simulations started from a punch position just above the upper sheet while the experiment started at a higher, and somewhat variable (from test-to-test), punch position,

a geometrical correction to the raw experimental data of Figure 4.14 was required to allow comparison of model and experimental results. Also, since the different models did not exhibit any significant effect on the process graph, only the curve for rigid FE model is presented in Figure 4.14. In general, the simulation punch force versus displacement results showed good agreement with the experimental results.

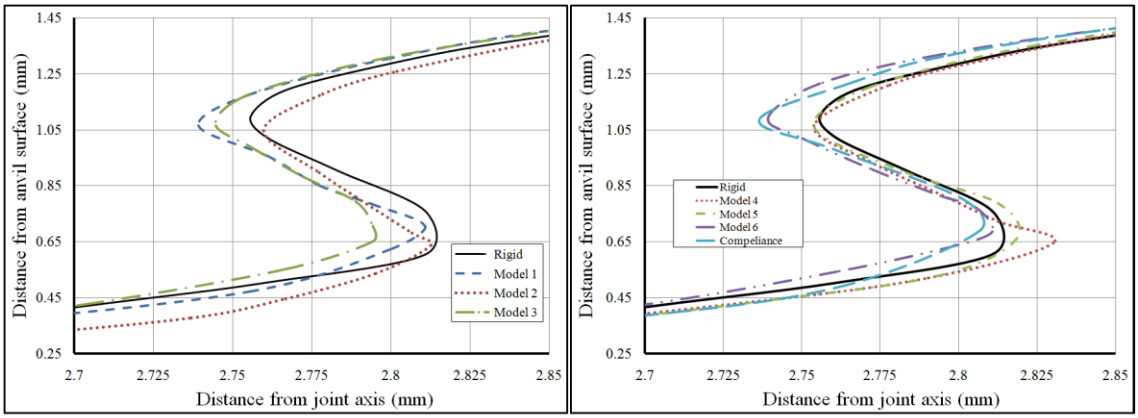

Figure 4.13. The interface shape of the die-less clinch resulting from different tool stiffness models(an extended-Voce material model is used in these simulations).

Table 4.3. A summary of the effect of the different models on S-shape formation.

Model number	Changes in S-shape compared to the rigid model
Model 1	Large shift in S-shape towards punch (i.e., a decrease in neck thickness)
Model 2	Almost no change
Model-3	Moderate shift in S-shape towards punch (i.e., a decrease in neck thickness)
Model-4	Slight shift in S-shape towards punch as well as a large increase in interlock depth
Model-5	Slight shift in S-shape towards punch as well as a moderate increase in interlock depth
Model-6	Large shift in S-shape towards punch.
Compliance Model	Largest shift in S-shape towards punch

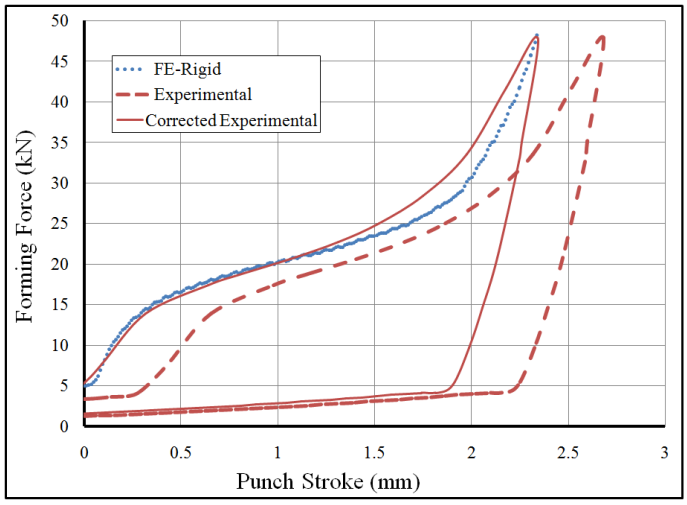

Figure 4.14. Typical forming force versus punch stroke curves from experiments and corresponding simulation based on rigid tooling.

4.3.4 Influence of material parameters

4.3.4.1 Material model

As mentioned earlier, the die-less clinching is a complex process involving very large plastic strain that can exceed 5 [4]. Such strains cannot be easily achieved from typical uniaxial tension test or hydraulic bulge tests in the laboratory. Therefore, to capture large strain behavior in the FE models of die-less clinching, the stress-strain curve must be extrapolated beyond the range of experimental measurements. A suitable constitutive law that represents the experimental data accurately is needed. Also, the extrapolation using such a constitutive law must yield physically realistic stress-strain curves up to very large strains typical of die-less clinching. An elastic-plastic material model with Von-Mises yield criterion was used to define the yield locus of AA7075-O

sheet. The plastic stress-plastic strain data obtained from uniaxial tensile test on AA7075 sheet was extrapolated using three different empirical hardening laws; power, Swift and Voce laws which are expressed as:

Power law: $\sigma_{eq}{}^{p} = y_0 + K(\varepsilon_{eq}{}^{p})^n$ (4.3)

Swift Law: $\sigma_{eq}{}^{p} = k_1\left(\varepsilon_0 + \varepsilon_{eq}{}^{p}\right)^n$ (4.4)

Voce Law: $\sigma_{eq}{}^{p} = C\left[1 - m\ exp\left(k_2\varepsilon_{eq}{}^{p}\right)\right]$ (4.5)

where $\sigma_{eq}{}^{p}$ and $\varepsilon_{eq}{}^{p}$ are the equivalent stress and plastic strain respectively. All other parameters, k_1, k_2 (stress coefficients), n (strain hardening exponent), C and m are material constants typically obtained from non-linear least square curve fitting to the above empirical equations the true stress versus true strain uniaxial tensile experimental data. The values of these constant are presented in

Table 4.4. Voce hardening law (equation 4.5) assumes that the plastic stress saturates at plastic strains higher than defused neck. In contrast, the power and Swift hardening laws (equations 4.3 and 4.4 respectively) consider the material to be perpetually strain hardening. Additionally, a hybrid hardening law involving power and Voce laws, referred to as the extended-Voce law in this paper, has been used to predict the plastic die-less clinching characteristics. The extended Voce law is expressed as:

Extended-Voce Law: $\sigma_{eq}{}^{p} = \sigma_0 + C_1\left[1 - m_1\ exp\left(k_3\varepsilon_{eq}{}^{p}\right)\right] + \alpha\varepsilon_{eq}{}^{p}$ (4.6)

Table 4.4. Parameter values of AA7075-Oaluminum sheet for the different material models

Power Law			Swift Parameters			Voce Parameters			Extended-Voce Parameters				
y_0 (MPa)	K (MPa)	n	ε_0	K (MPa)	n	C	K_1 (MPa)	m	σ_0 (MPa)	C_1	m_1	K_3 (MPa)	α (MPa)
145	376.9	0.375	0.002	485.9	0.2071	319.4	24.19	0.4769	147	171.6	0.8834	24.34	5

Figure 4.15 presents the results of “S” shape from the interlock region of the interface from the different hardening models. Power and Swift laws yielded significant deviation from the experimental “S” shape for the lower side. The Voce model showed a smaller deviation compared to the experimental results from both the upper and lower sheets. Overall, the extended-Voce model provided the closest “S” shape response compared to all other hardening laws. The results were also consistent with the quality of fit to the uniaxial tensile data and the extrapolated shape of the stress-strain curve. Figure 4.15 also suggests that the formation of the interlock "U" is inversely correlated to work hardening capacity of the material model. Based on the results of Figure 4.15, Extended - Voce material model was selected for future simulations.

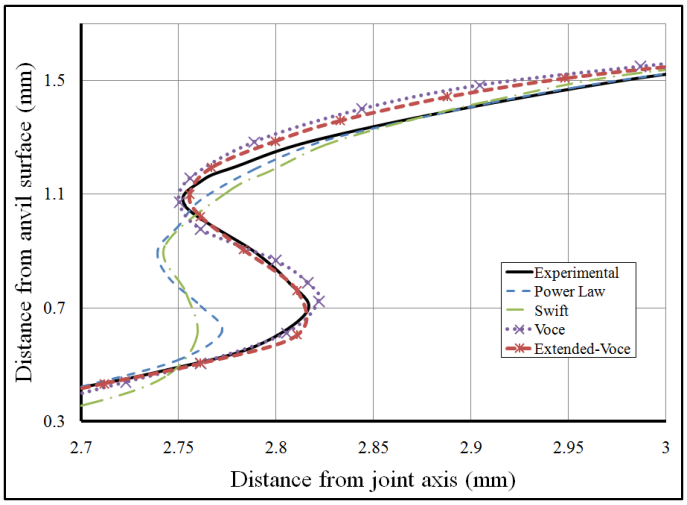

Figure 4.15. A comparison of the simulated and experimental interlock shapes in die-clinching for the different hardening laws.

4.3.4.2 Friction

The die-less clinching process involves multiple tool-sheet and sheet-sheet contact and sliding events. Therefore, contact and friction play a critical role in governing material flow and the joint formation in die-less clinching. Also, process conditions such as large interface pressure, small sliding force, large plastic deformation, and enlargement of the contact area as the process continues make it quite difficult to identify the actual friction behavior by common friction tests and to comprehensively assess the relevance of classical Coulomb friction law for die-less clinching. It is likely that the Coulomb friction coefficient will change with normal pressure and from the enlargement of contact area. The present simulation assume coefficient of friction to be an average value over the entire contact region and over the entire duration of clinching. However, considering the differences in the surface topographies of tool and sheets, two separate friction coefficient

values were considered; sheet-to-sheet coefficient μ_{sh} and sheet-to-tool coefficient μ_t. The sensitivity of the geometric parameters "N" and "U" to μ_{sh} and μ_t is shown in Figure 4.16. The trend of the results showed the tendency of neck thickness to decrease with an increase of the friction of the interface while the interlock depth showed an opposite behavior. In general, the friction of the tool-sheet affected the neck thickness whereas the interlock depth was independent of friction coefficient.

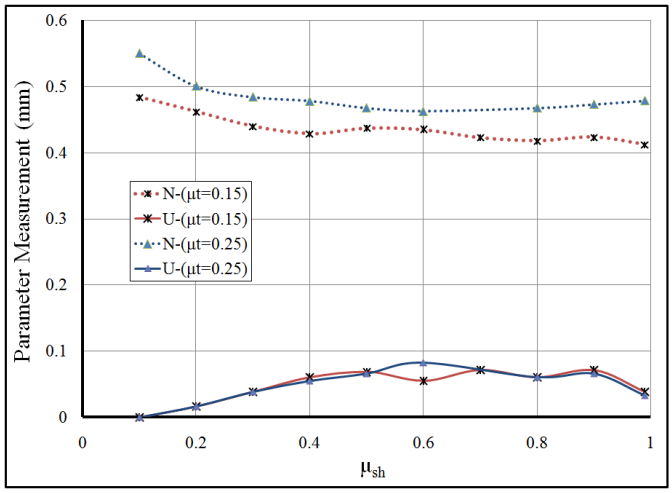

Figure 4.16. Geometric parameter of die-less clinched joint from simulations using different friction sheet-sheet and tool-sheet friction coefficients.

An attempt was made to track the relative motion of the sheet during the clinching process. The top image in Figure 4.17 depicts a schematic layout of 8 locations at the sheet-sheet and tool-sheet contact regions in the initial FE model geometry. The subsequent images of these locations at various punch displacements are shown directly beneath the top image. Also, the nomenclature for assessing the relative displacement of the marked locations is presented in the schematic in Figure 4.18. The location that moved towards left of its current position was termed negative and *vice versa.*

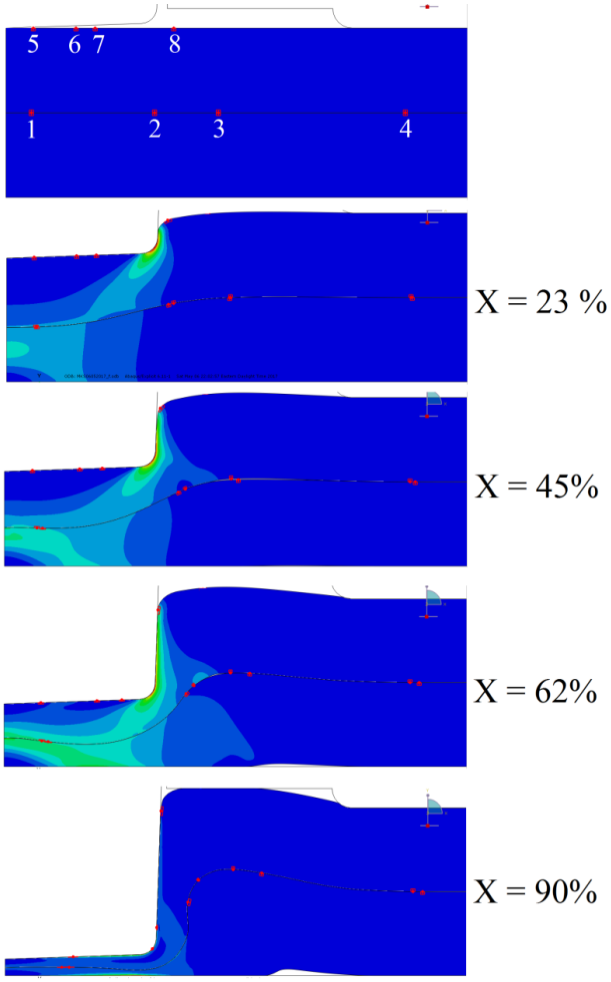

Figure 4.17. A schematic layout of 8 different positions, 4 on the sheet-sheet and 4 on the tool-sheet contact surfaces with the undeformed layout at the top and subsequent layout at different punch displacements. The punch and blank-holder outlines are marked in grey.

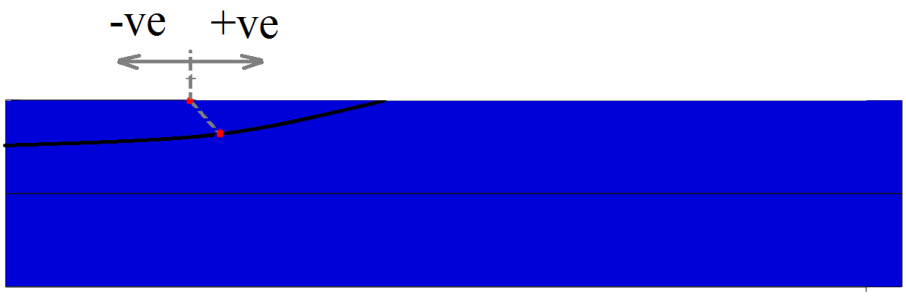

Figure 4.18. Nomenclature for assessing relative displacement at the marked positions in Figure 4.17.

The results of relative displacements with increasing punch stroke are shown as a family of graphs in Figure 4.19. The results were obtained for 3 different friction coefficient combinations. Results for the different positions 1 to 8 are plotted separately and in sequential order for clarity. Position 1 lies at the sheet-sheet interface directly below the center of the punch. The relative sliding is reduced at the largest values of sheet-sheet and sheet-tool friction coefficient values (blue curve) in the early stages compared to the other 2 values. The displacements, however, converge towards larger punch strokes. Position 2 in the inter-sheet region located directly below the punch profile radius, on the other hand, showed an opposite trend where higher friction coefficients lead to rather similar relative displacements in the early stages but quite divergent behavior at larger punch displacements. Position 3 to the right of position 2 in the inter-sheet region continues to move inward into the punch region where relative movement was largely independent of the friction coefficient. Position 4 located well to the right of position 3 moved to the right of its original position and exhibited larger movement with lower friction coefficient values. Results for tool-sheet displacements at positions 5-8 show a rather different characteristics compared to the sheet-sheet displacement. Firstly, the sensitivity to friction coefficient combination was found to be weak at all 4 positions 5-8. Also, the maximum relative displacement was much larger compared to the sheet-sheet interface. Lastly, the trends in relative displacement were mostly linear with respect to the punch stroke and exhibited a sharp discontinuity in the relative displacement was observed in the punch stroke range of 0 to 1 mm. This discontinuity moved to the left as the positions changed to the right from 5 to 8. Overall, the results suggest a significant

role of friction and relative sliding that results from it at the sheet-sheet and sheet-tool interfaces in controlling the material flow and formation of geometric interlock. The tool-sheet interface appears to be more critical than the sheet-sheet interface in the formation of the geometric interlock. However, this preliminary result should be supported by more detailed experimental studies of the interface behavior in die-less clinching with more advanced friction models to further clarify the role of friction in die-less clinching. Table 4.5 shows a quantitative analysis of the total relative movement of each point in Figure 4.19. It can be noted that the points on the top free surface have a rather large total relative movement compared to the points at the sheet-sheet interface.

Table 4.5. Data from Figure 4.20 is presented in the form of total relative movement of each point as a function of the friction coefficients.

Interface			Top Surface		
Position	Friction Values	Total Rel. Mov.(mm)	Position	Friction Values	Total Rel. Mov.(mm)
1	$\mu_t = 0.15, \mu_{sh} = 0.2$	0.087	5	$\mu_t = 0.15, \mu_{sh} = 0.2$	3.42
	$\mu_t = 0.15, \mu_{sh} = 0.4$	0.071		$\mu_t = 0.15, \mu_{sh} = 0.4$	3.42
	$\mu_t = 0.25, \mu_{sh} = 0.4$	0.066		$\mu_t = 0.25, \mu_{sh} = 0.4$	3.31
2	$\mu_t = 0.15, \mu_{sh} = 0.2$	0.16	6	$\mu_t = 0.15, \mu_{sh} = 0.2$	3.22
	$\mu_t = 0.15, \mu_{sh} = 0.4$	0.16		$\mu_t = 0.15, \mu_{sh} = 0.4$	3.266
	$\mu_t = 0.25, \mu_{sh} = 0.4$	0.11		$\mu_t = 0.25, \mu_{sh} = 0.4$	3.215
3	$\mu_t = 0.15, \mu_{sh} = 0.2$	0.35	7	$\mu_t = 0.15, \mu_{sh} = 0.2$	2.67
	$\mu_t = 0.15, \mu_{sh} = 0.4$	0.28		$\mu_t = 0.15, \mu_{sh} = 0.4$	2.768
	$\mu_t = 0.25, \mu_{sh} = 0.4$	0.326		$\mu_t = 0.25, \mu_{sh} = 0.4$	2.704
4	$\mu_t = 0.15, \mu_{sh} = 0.2$	0.115	8	$\mu_t = 0.15, \mu_{sh} = 0.2$	0.377
	$\mu_t = 0.15, \mu_{sh} = 0.4$	0.127		$\mu_t = 0.15, \mu_{sh} = 0.4$	0.368
	$\mu_t = 0.25, \mu_{sh} = 0.4$	0.09		$\mu_t = 0.25, \mu_{sh} = 0.4$	0.396

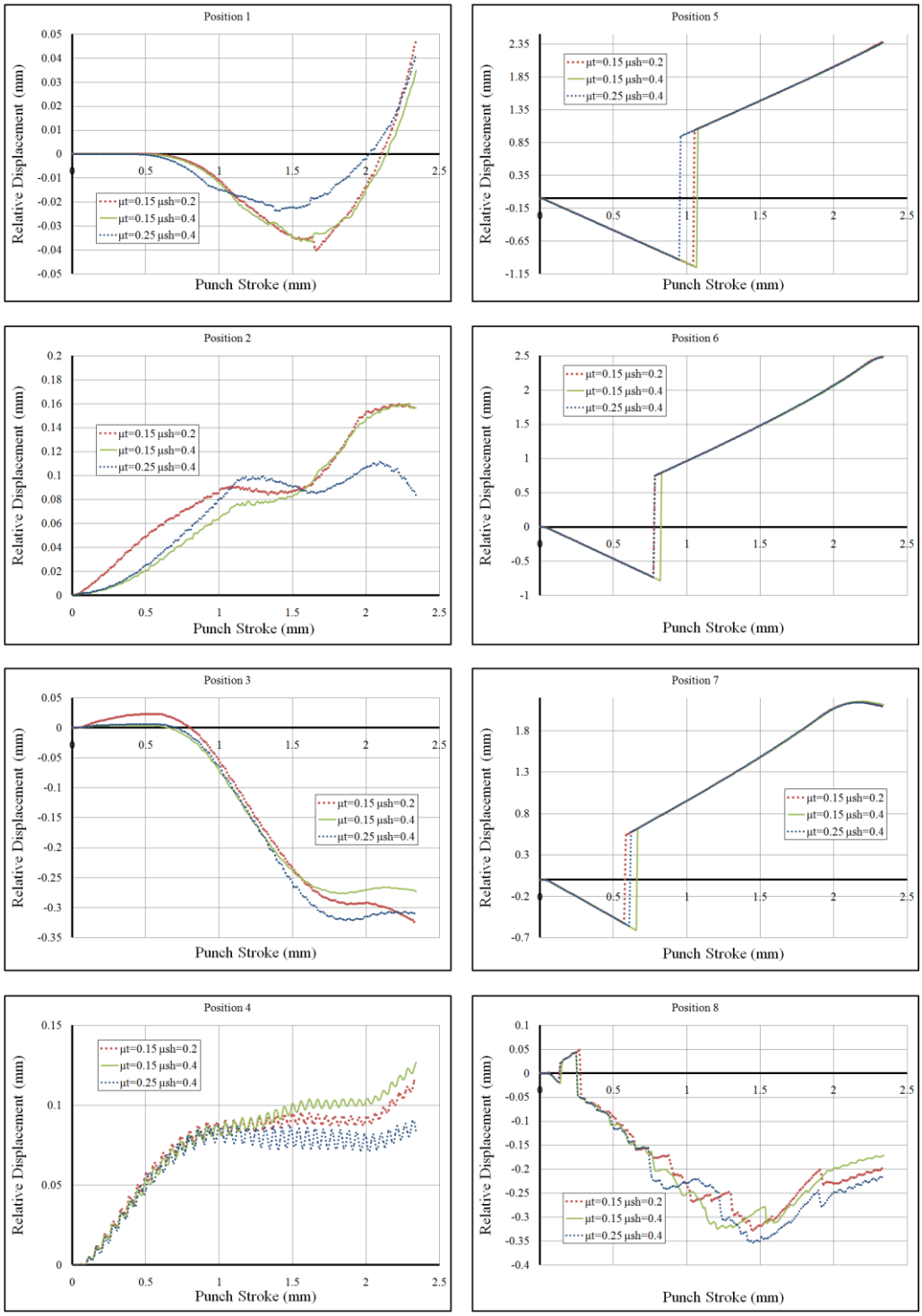

Figure 4.19. A set of plots of relative maximum displacement of marked 8 positions as a function of punch stroke for 3 different sheet-sheet and sheet-tool friction coefficient combinations from clinching simulations.

4.3.4.3 Spring-back

The spring-back is caused by the recovery of the elastic strain after forming release of the forming and clamping loads. Spring-back can make changes to the dimensions of the final geometry and is undesirable artifact of the forming process. Spring-back depends not only on the modulus of elasticity and yield strength of the material but also on the geometric constraint of the part and the clinching process. In the present work, a parametric study of the effect of elastic modulus (E) and friction coefficients at the sheet-tool and sheet-sheet interfaces (μ_{sh} and μ_t) on spring-back was carried out. Table 4.6 presents 6 sets of parameter combinations in the spring-back study of die-less clinching simulations. The results in the form of geometric interlock (or "S") shapes before and after spring-back from the 6 sets of model parameters are presented in Figure 4.20. In general, only a marginal change in the final shape of the joint on spring-back simulation was observed from a change in the elastic modulus. The effect of friction coefficient on spring-back was more pronounced.

Table 4.6. Values of parameter combinations in the springback study of die-less clinching.

Model	E(GPa)	μ_t	μ_{sh}
SB1	71	0.15	0.4
SB 2	68	0.15	0.4
SB 3	65	0.15	0.4
SB 4	71	0.25	0.4
SB 5	68	0.25	0.4
SB 6	65	0.25	0.4

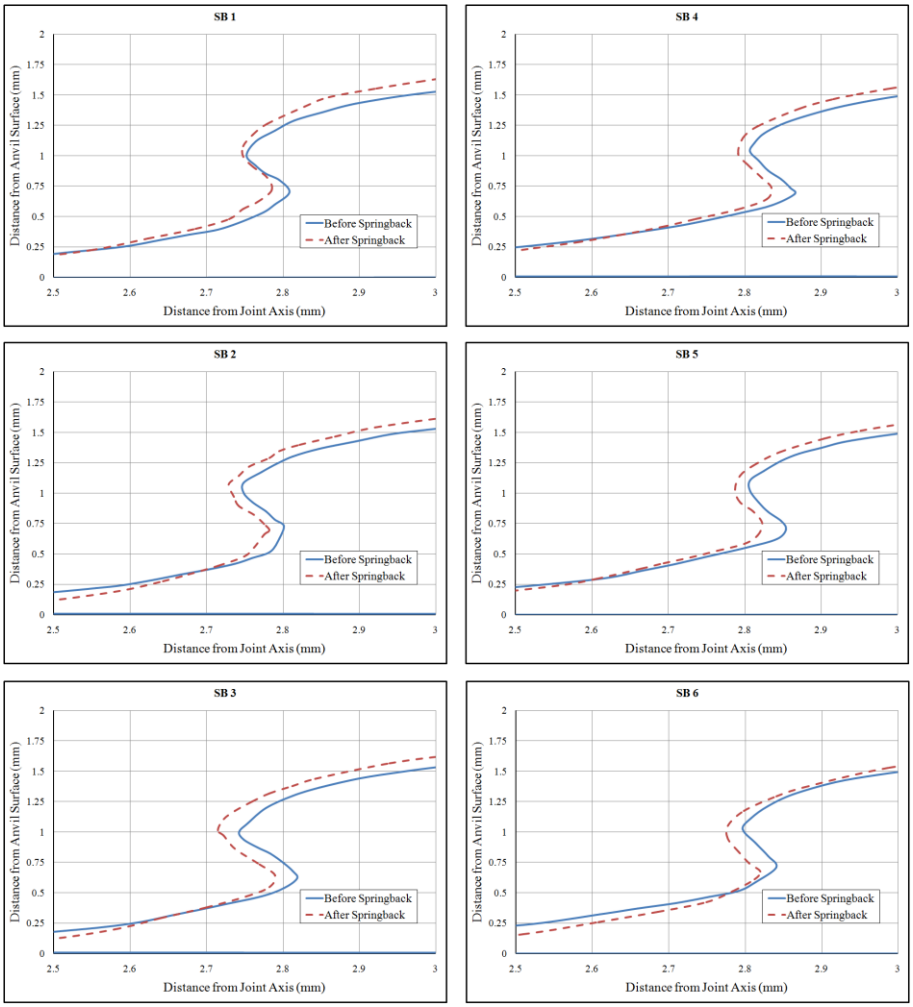

Figure 4.20. Effect of various parameter combinations of Table 4.6 on "S" shape before and after the spring back.

4.4 Summary and Conclusions

Effect of a number of FE simulation parameters consisting of element size, mass scaling factor, adaptive re-meshing strategies, and model boundary conditions on die-less clinch characteristics were studied. Additionally, choice of material model and extrapolation of material data to large strains typical of die-less clinching on clinched

shape were analyzed. Lastly, the effect of elastic modulus and friction coefficient variation on spring back after clinching was assessed. Previous experimental work on die-less clinching of AA7075 aluminum sheet of the present authors was used to analyze and optimize the FE simulation results.

In summary, this paper presents a comprehensive study of the parameters that affect the simulation of die-less clinching process. The model validation was based on a recently published experimental work of the present authors [15]. The validation has been carried out in terms of final geometry of the clinched joint as well as the punch force versus stroke curves. The error shown in the paper are individual errors for each type of measurement. However, cumulative errors can be reduced by proper selection of tool design, material and process parameters. It is shown that accuracy of simulation depends critically on the numerical parameters. However, computation time is another important factor which should be taken into consideration. The size of the element is a critical parameter for prediction of geometrical interlock shape as well as the computation time. Adaptive re-meshing technique is required to avoid excessive element distortion. However, the relocating algorithm as well as the frequency of re-meshing has almost no effect on the results. Mass scaling factor is a key parameter to decrease the computational time. However, large values can induce an inertial effect that can reduce the accuracy. A mass scaling factor of less than 150 is suggested for acceptable accuracy from the model. Also, the material model is a critical factor of the simulation and should be selected carefully because the die-less clinching process involves very large plastic strains. Further, assuming the tool set as a rigid body is a common assumption and can be used in

the simulation. Lastly, proper choice of friction coefficient is important factor for accurate prediction of geometrical interlock as well as spring-back. A study of the effect of material anisotropy on die-less clinching should be a useful study in the future. The following specific conclusions can be drawn from this study:

1- Using a small element size of less than $1/40^{th}$ of total sheet thickness is required to reach reasonable result with a low error of about 3% in the both of the interlock depth and neck thickness. However, this results in an exponential increase in the computational time. The time can be reduced by about 40% by increasing element aspect ratio by 33%.
2- Mass scaling factor up to 150 is an effective tool in compensating the effect of using very small element size. However, larger mass scaling beyond 150 introduces dynamic effects which deteriorate the prediction of joint formation.
3- Adaptive re-meshing is a useful method to simulate die-less clinching and the smoothing algorithm has no effect on the results.
4- Simulating punch or anvil as an elastic part results in shift of the geometric interlock shape toward the joint axis as well as an increase in the interlock depth at the expense of the neck thickness. However, punch elasticity has a stronger effect than that of the anvil.
5- The rigidity (or elasticity) of tooling did not show a significant effect on the process graph.
6- The material model is the most important parameter in the simulation of the die-less clinching process. Extended-Voce material model is effective in predicting the

post- necking behaviour of the high strength AA7075 aluminum sheets in clinching. Other common hardening laws such as power and Swift laws cannot accurately predict the formation of geometrical interlock in die-less clinching due to their poor extrapolation behavior.

7- Material sliding and friction behavior is critical to obtaining a good die-less clinch. The sliding behavior at the tool-sheet surface can be quite different from the inter-sheet sliding behavior and affect the geometric interlock characteristics. More comprehensive studies with advanced friction models and suitable experimental friction coefficient data is needed for even better die-less clinching simulations.

References

[1] A. Pramanik, A. Basak, Y. Dong, P. Sarker, M. Uddin, G. Littlefair, A. Dixit, S. Chattopadhyaya, Joining of carbon fibre reinforced polymer (CFRP) composites and aluminium alloys–A review, Composites Part A: Applied Science and Manufacturing 101 (2017) 1-29.
[2] X. He, Clinching for sheet materials, Science and Technology of Advanced Materials 18(1) (2017) 381-405.
[3] F. Lambiase, A. Di Ilio, An experimental study on clinched joints realized with different dies, Thin-Walled Structures 85 (2014) 71-80.
[4] T. Gerstmann, B. Awiszus, Recent developments in flat-clinching, Computational Materials Science 81 (2014) 39-44.
[5] S. Coppieters, H. Zhang, F. Xu, N. Vandermeiren, A. Breda, D. Debruyne, Process-induced bottom defects in clinch forming: simulation and effect on the structural integrity of single shear lap specimens, Materials & Design (2017).
[6] C.-J. Lee, B.-M. Kim, B.-S. Kang, W.-J. Song, D.-C. Ko, Improvement of joinability in a hole clinching process with aluminum alloy and carbon fiber reinforced plastic using a spring die, Composite Structures 173 (2017) 58-69.
[7] P. Groche, S. Wohletz, M. Brenneis, C. Pabst, F. Resch, Joining by forming—a review on joint mechanisms, applications and future trends, Journal of Materials Processing Technology 214(10) (2014) 1972-1994.
[8] S. Coppieters, P. Lava, R. Van Hecke, S. Cooreman, H. Sol, P. Van Houtte, D. Debruyne, Numerical and experimental study of the multi-axial quasi-static strength of clinched connections, International journal of material forming 6(4) (2013) 437-451.
[9] M. Eshtayeh, M. Hrairi, Recent and future development of the application of finite element analysis in clinching process, The International Journal of Advanced Manufacturing Technology 84(9-12) (2016) 2589-2608.

[10] S. Coppieters, S. Cooreman, P. Lava, H. Sol, P. Van Houtte, D. Debruyne, Reproducing the experimental pull-out and shear strength of clinched sheet metal connections using FEA, International journal of material forming 4(4) (2011) 429-440.
[11] X. He, L. Zhao, H. Yang, B. Xing, Y. Wang, C. Deng, F. Gu, A. Ball, Investigations of strength and energy absorption of clinched joints, Computational Materials Science 94 (2014) 58-65.
[12] X. He, F. Liu, B. Xing, H. Yang, Y. Wang, F. Gu, A. Ball, Numerical and experimental investigations of extensible die clinching, The International Journal of Advanced Manufacturing Technology 74(9-12) (2014) 1229-1236.
[13] F. Lambiase, Influence of process parameters in mechanical clinching with extensible dies, The International Journal of Advanced Manufacturing Technology 66(9-12) (2013) 2123-2131.
[14] B.J. Shi, Y.Q. Wang, S.L. Liu, H.Y. Tian, Design method of the parameters of tools for clinching technology, Advanced Materials Research, Trans Tech Publ, 2012, pp. 1491-1496.
[15] M.K.S. Atia, M.K. Jain, Die-less Clinching Process and Joint Strength of AA7075 Aluminum Joints, Thin-Walled Structures 120 (2017) 421-431.
[16] R. Neugebauer, C. Kraus, S. Dietrich, Advances in mechanical joining of magnesium, CIRP Annals-Manufacturing Technology 57(1) (2008) 283-286.
[17] D.S. Simulia, Abaqus/CAE user's manual, Providence, RI (2007).
[18] A. Prior, Applications of implicit and explicit finite element techniques to metal forming, Journal of Materials Processing Technology 45(1-4) (1994) 649-656.
[19] T. Huo, E. Nakamachi, Evaluation of the dynamic explicit/elastoviscoplastic finite-element method in sheet-forming simulation, Journal of materials processing technology 50(1-4) (1995) 180-196.
[20] D. Systémes, Abaqus Theory Guide, Abaqus, 2013.

Chapter 5

Finite Element Analysis of Material Flow in Die-less Clinching Process and Joint Strength Assessment

---

Mostafa K. Sabra Atia, PhD student, is the first author and main contributor of the work who conceptualized the topic, built FE model, interpreted the results and drafted the paper. Mukesh K. Jain, Professor, is the supervisor who substantially contributed to the work by checking the experimental results and technical details of the model as well as polishing the language of the paper. This paper is under review in Thin-Walled Structures Journal.

Finite Element Analysis of Material Flow in Die-less Clinching Process and Joint Strength Assessment

Mostafa K. Sabra Atia[a,b] and Mukesh K. Jain[a]

[a] Department of Mechanical Engineering, McMaster University, Hamilton, Ontario, Canada L8S 4L7

[b] Corresponding author: Tel.: +1 (905) 920-0398 Fax: +1(905) 572-7944. E-mail address: atiam@mcmaster.ca(M. Atia).

Abstract

Die-less clinching is a joining process in which punch, flat anvil, and blank holder of a certain specified shape are used to form a geometric interlock. The blank holder design is especially important for die-less clinching because of its influence on flow of the material. In the present work, a numerical investigation of the effect of the blank holder parameters on material flow and the final geometry of the die-less clinched joint is conducted. Various blank holder designs as well as different process parameters are used to obtain clinched joints. Axisymmetric finite element (FE) model was developed to simulate die-less clinching experiments. A hybrid material model with a weight function between the two common used hardening laws, Swift and Voce, was utilized to better represent the material behavior in the FE model. Another hybrid material model, referred to as extended-Voce model, was also utilized in the FE simulation and the results compared with the weight function approach. The weight function material model resulted in smaller geometric interlock compared with the experiment, whereas, the extended-Voce model led to better prediction of experimental geometric interlock with an error of less than 5%. The results showed that the interlock forms due to a large material flow in the axial and radial directions. The interlock can be maximized by controlling the material to flow in radial direction instead of axial direction, by decreasing blank holder depth. Also, distortion of the bottom of the die-less clinched joint can be avoided by achieving a bottom thickness of at least 10 % of the total sheet thickness. Lastly, finite element models were also developed to predict the joint strength of the shear and peel failure modes.

Table 5.1. List of Abbreviations

T6	Artificial peak aged state which represents the hardest temper
O	Annealed temper state
N	Neck thickness of the joint
U	Interlock depth of the joint
X	Joint bottom thickness
t	Blank holder groove depth
d	Blank holder groove diameter
F	Forming force
σ_{eq}^{p}	Equivalent stress
ε_{eq}^{p}	Equivalent plastic strain
k_1	Stress coefficients for Voce hardening law
K_2	Stress coefficients for Swift hardening law
C	Material constant for Voce hardening law
m	Material constant for Voce hardening law
α	Weight function
δ	A continuous hardening parameter in Extended-Voce material model
σ_0	Initial yield stress
μ_{sh}	Sheet-to-sheet coefficient of friction
μ_t	Sheet-to-tool coefficient of friction
n	Strain hardening exponent

Keywords: Clinching, Die-less clinching, FE simulation.

5.1 Introduction

Adhesive bonding, welding, and mechanical fastening are the main techniques for joining of sheet materials [1, 2]. Mechanical fastening provides some advantages over the other two techniques in terms of efficiency, cost, quality and appearance of the joints [3]. Mechanical joining can be further divided into two categories, (i) joining by using consumable parts such as rivets, and (ii) joining by forming such as hemming and clinching. Clinching is a rapid and clean process where two or more sheets are locally deformed by using punch and die to form a geometrical interlock [4-6]. Clinching can be carried out with or without metal cutting [7]. In fact, the recent clinching operations

involve no metal cutting and only redistribution of the material by plastic flow in the vicinity of the clinched region during geometrical interlocking. Clinching can be carried out using a die (conventional clinching) or without a die (referred to as die-less clinching) [8], as shown in Figure 5.1.

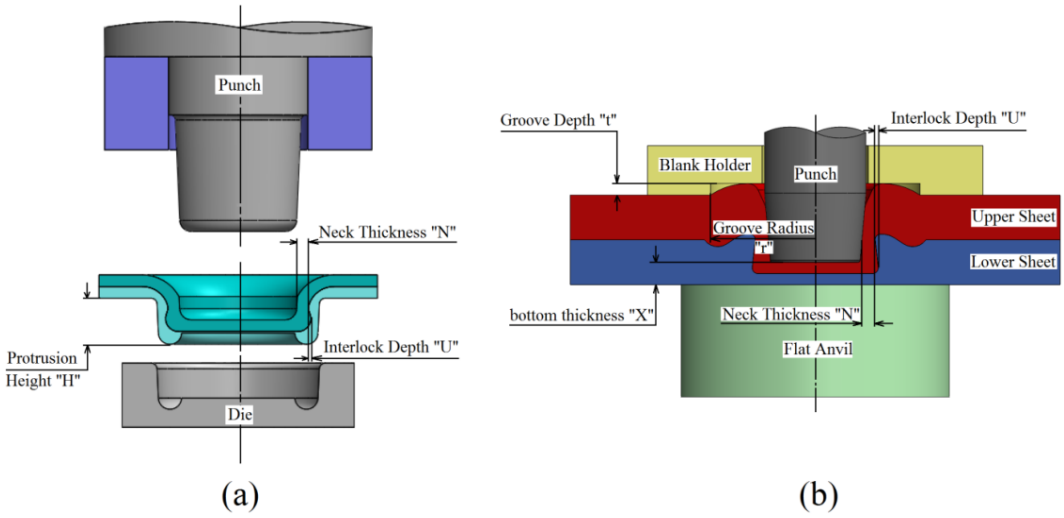

Figure 5.1. Scheme drawings showing the various geometric parameters in; (a) conventional clinching and (b) die-less clinching [9].

In the second category of die-less clinching, a flat anvil is used instead of a die. Consequently, the resulting joint does not lead to a protrusion on the anvil side [10]. A blank holder of a certain specified shape is used to control the material flow in the direction opposite to the punch movement [9]. As shown in Figure 5.1, the neck thickness N, interlock depth U and bottom thickness X are the main geometric parameters of the clinched joint [11]. The X-parameter, first introduced by Varies [7, 12], is a useful parameter for inspection of the joint.

Shear and peel tests are commonly used in the characterization of strength of clinched joints [13]. The experiments required to optimize joint parameters that yield

higher strength joints can be costly and time consuming. Numerical simulation via finite element (FE) method offers an cost-effective, efficient and systematic method of analyzing the effect of tool design and material parameters on die-less clinching process [14]. Also, a 3-D FE model of the conventional clinched joint can be used in characterizing the joint strength [13, 15-17]. Many papers have been published to describe the FE simulation of conventional clinches [12, 14, 15, 18-24]. The die-less clinching process is recent and a more complex process compared to conventional clinching. Therefore, very few studies have been carried out to simulate the die-less clinching process. The maximum equivalent plastic strain in die-less clinching are very large, of the order of 5, whereas, in conventional clinching, the plastic strains are only of the order of unity [10]. Special procedures are often utilized with the FE simulation to deal with solution convergence problems at large plastic strains in die-less clinching.

In the present study, the focus is on effect of clinch tool design and forming force on the material flow and final geometry of the die-less clinched joint as well as post-clinch joint strength. A better material model to capture the large strain work hardening behavior of AA7075 sheet is proposed. This material model is then used within the FE model to simulate and assess the die-less clinch joining and post-strength characteristics.

5.2 Material and Methods

The jointed sheets were made of AA7075-O aluminum sheet of 1.27 mm nominal thickness. The sheet metal was initially received in the peak-aged T6- temper state. In order to enhance its low ductility in the peak T6 condition, the sheet was partially annealed by heating to 413°C for 1 hour in a furnace. Uniaxial tensile tests were

conducted to assess the mechanical properties of the material using instrumented screw-driven Instron universal testing machine of 100 kN load capacity at a cross-head speed of 1 mm/min. Sub-size sample dimensions of 120 mm length × 6 mm width, as per the ASTM standard E8M, were utilized for the uniaxial tension tests. The resulting mechanical properties in the as-received (T6) and annealed (O) temper states are presented in Table 5.22.

Clinching primarily results from formation of geometric interlock, or S-shape, which mainly depends on the tool configuration. The tool set in the present work involved an anvil, punch and blank holder made of tungsten, tungsten carbide, and tool steel respectively, designed to control the flow of material. In addition, a urethane spring was incorporated to apply the blanking force. The tool set is presented in Figure 5.2. The total blanking force was determined by the stiffness of the urethane spring and its interaction with the case. The clamping force was measured experimentally as a function of punch stroke by using a punch without tip to avoid interaction between punch tip and sheets. Figure 5.3 shows the experimentally measured blanking force profile as well as two other clamping force profiles used for the simulation purpose as will be shown later in Section 5.4.3.

Table 5.2. Mechanical properties of AA7075 aluminum sheet in T6 and O-temper states.

Mechanical properties from uniaxial tension tests				
Temper Designation	Material state	0.2% Yield strength (MPa)	σ_{UTS} (MPa)	Total Elongation (%)
T6	As-received	580	695	9
O	Annealed	175	295	15

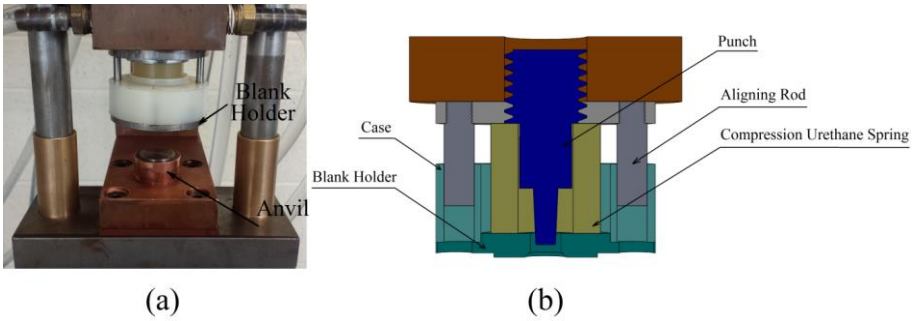

Figure 5.2. Die-less clinching tool set-up; (a) photograph for the installation of the tooling and (b) schematic drawing showing the punch, blank holder shape and compression urethane spring.

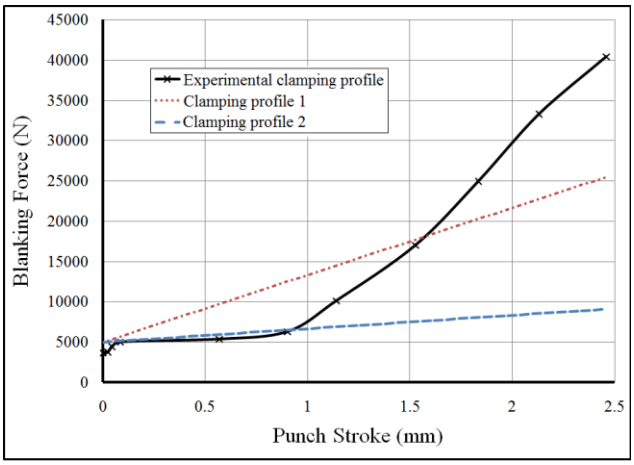

Figure 5.3. Experimental and two different FE model blank holder force profiles utilized in the present study.

5.3 FE Modeling Methodology

Die-less clinching process was simulated by incorporating the geometry of tooling, sheet thickness, sheet elastic and plastic properties, sheet-sheet contact, and friction between all tool and sheet contacting surfaces. The above geometric, material and process parameters could be studied by systematically varying their values and observing the material flow and the evolution of the stress state of the sheet with the punch movement. Generally, such details are quite difficult to study experimentally due to very

small clinching area, not amenable to camera viewing, and the high speed of the process. The commercial FE code Abaqus was used to carry out the FE model. The FE model was set-up in commercially available FE package, Abaqus-Explicit. This code was preferred over other available codes due to its ability to simulate multiple tool-sheet and sheet-sheet interactions that occur in clinching problem and its more robust contact algorithm and solver. Also, the explicit solver exhibits significant time saving over implicit solver as the model size increases. An axisymmetric 2D model was developed due to the axisymmetric nature of tooling, the clinch geometry, and the loading conditions. The tooling was considered as rigid and the boundary conditions were defined by tool motions and constraints. Two different blank holder types were included, defined as stepped edge and rounded edge blank holders as shown in Figure 5.4, where groove radius r and depth t, as first and second numbers respectively, were used to represent various stepped edge blank holders. Similarly, for the round edge blank holder, radius R and fillet radius S were used as first and second numbers respectively in Table 5.3. The parameters that affect the FE simulation such as numerical parameters, material parameters and boundary condition have been studied in a previous work of the present authors [25]. The sheet materials were modeled using 4-nodebilinear axisymmetric quadrilateral elements with reduced integration (CAX4R element in Abaqus) and enhanced hourglass control option was utilized to avoid hour-glassing problems at large plastic strains. A large number of elements through the sheet thickness totaling 40 were used to mesh the sheet metals in the clinched area to account for large through-thickness strain gradient in the die-less clinching process. Also, an aspect ratio of 1.3 was utilized to minimize element distortion

where aspect ratio was defined by the ratio of the element size in axial and radial directions. The FE mesh size in the area outside the clinching region was kept relatively large, totaling 30 elements through the thickness with an aspect ratio of 0.25. Due to large deformation and highly localized plastic strain in the clinch region, adaptive re-meshing option with volumetric smoothing was used to prevent excessive mesh distortion, and an advanced algorithm based on evolving geometry was implemented to attain stable numerical solution. A mass scaling factor of 100 was used to reduce the computational run time.

Figure 5.4. Two different blank holder designs utilized in the FE simulation of die-less clinching, (a) stepped edge blank holder and (b) round edge blank holder.

Table 5.3. Blank holder design parameters in the present study.

Blank holder type	Stepped edge		Rounded edge	
Parameter	r (mm)	t (mm)	R (mm)	S (mm)
Range of values	4-7.5	0.2-1	2.5 and 3.5	1-5

The sheet material was assumed to be isotropic elastic-plastic following von Mises yield criterion. An extended-Voce hardening law was used to extrapolate the experimental plastic stress-plastic strain data obtained from the uniaxial tensile test beyond the tensile stress-strain limit to large strains.

$$\sigma_{eq} = \sigma_0 + C\left[1 - m\, exp\left(k\varepsilon_{eq}{}^{p}\right)\right] + \delta\varepsilon_{eq}{}^{p} \qquad (5.1)$$

where, σ_{eq}, σ_0 and ε_{eq}^{p} are the equivalent stress in equation (1), the initial yield stress and equivalent plastic strain respectively, *k* is stress coefficient, and *C* and *m* are two other material constants. The third term on the right side of equation (5.1), $\delta\varepsilon_{eq}{}^{p}$, was added to describe continued hardening behaviour at larger strains [26].

In previous studies [25, 27], the authors have shown that commonly used swift and Voce hardening laws cannot reliably predict the final shape of the conventional as well as die-less clinched joints because of large strains associated with the clinching process. However, a weight function between the two laws successfully predicted the geometric interlock shape in conventionally clinched joint [27]. Therefore, the weight function based mixed hardening law was also used in this study as shown below:

$$\sigma_{eq} = \alpha\ \sigma_{eq}\big|_{Swift} + \left(1-\alpha\right)\ \sigma_{eq}\big|_{Voce} \qquad (5.2)$$

where *Voce*: $\sigma_{eq} = C_1\left[1 - m_1\ exp\left(k_1\varepsilon_{eq}{}^{p}\right)\right]$ (5.3)

and *Swift*: $\sigma_{eq} = k_2\left(\varepsilon_0 + \varepsilon_{eq}{}^{p}\right)^{n}$ (5.4)

In the above equations, k_1 and k_2 are strength coefficients in eqns. (5.3) and (5.4) respectively, *n* is the strain hardening exponent, *C* and *m* are two other material constants, α is a weight of the function with values in the range 0.25 - 0.9. It is to be noted that, for α values of 0 and 1, the mixed hardening law of equation (5.2) reverts simply to Voce and Swift laws respectively. Table 5.44 presents the values of hardening parameters for AA7075-O sheet. Figure 5.5 shows the extrapolation of stress – strain curves to large plastic strains by using different weight functions in equation as well as another extended-Voce law.

The experimentally measured clamping force versus punch displacement profile as well as two other theoretical clamping forces were employed in the FE study. The interaction between tool and sheet and between the two sheet materials was described by Coulomb friction law. Based on a previous study by the present authors [25], different friction coefficient values were utilized and the friction value that gave interlock shape as well as force-displacement curve comparable to experimental study was chosen in the present FE study. It was found that 0.15 and 0.4 friction coefficients between sheet-tools and between the two sheets respectively provided the best match between experimentally obtained final geometry of the joint and that obtained numerically. Figure 5.6 illustrates the axisymmetric model of the die-less clinching simulation showing that the blank holder clamping force is a function of time.

Table 5.4. Material model parameters.

Voce				
C_1		k_1 (MPa)		m_1
319.4		24.19		0.4769
Swift				
ε_0		k_2 (MPa)		n
0.002		485.9		0.2071
Extended-Voce				
σ_0 (MPa)	C	m	k (MPa)	δ (MPa)
147	171.6	0.8834	24.34	5

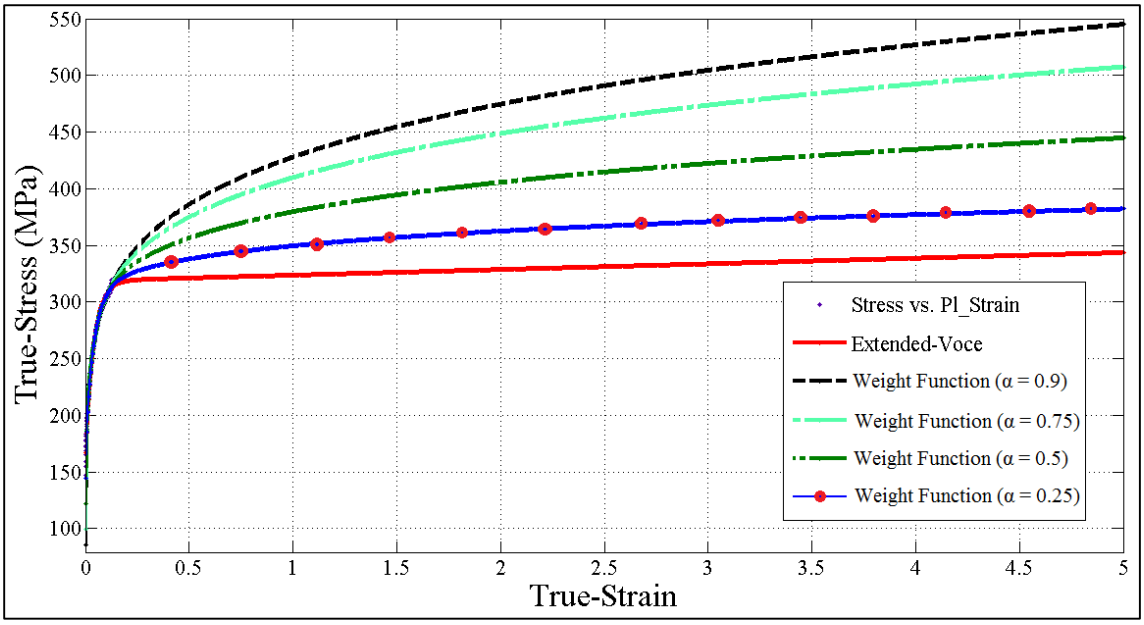

Figure 5.5. Extrapolation of the true-stress-true plastic strain data by using extended-Voce as well as different weight functions.

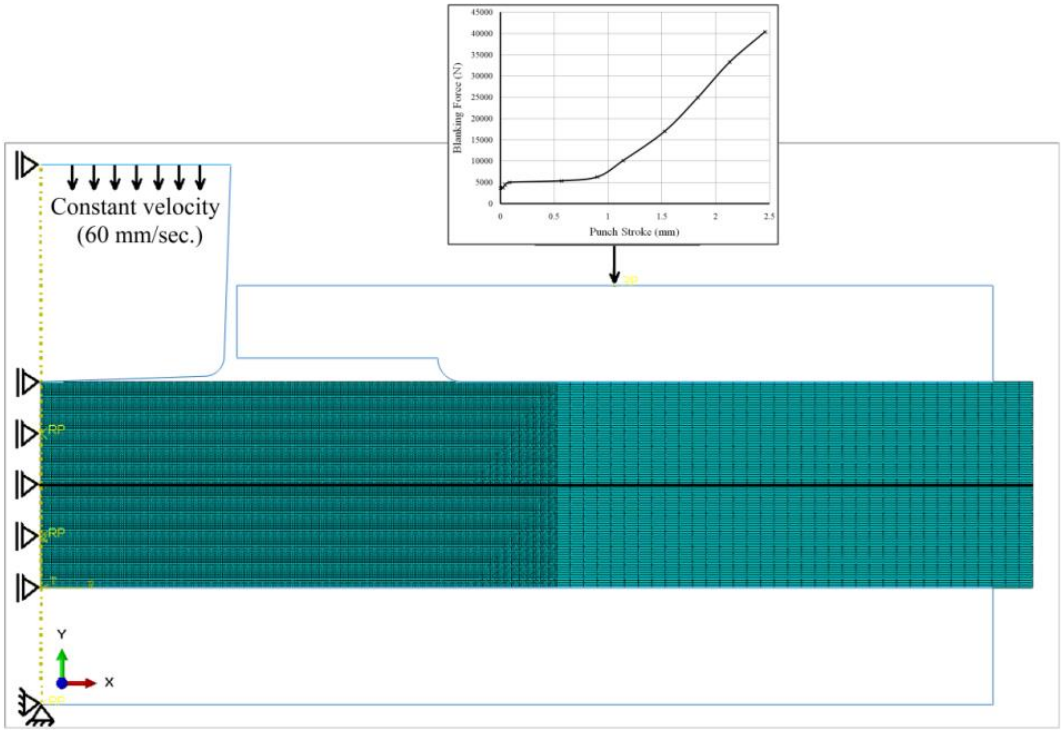

Figure 5.6. Axisymmetric 2-D FE model set-up for die-less clinching simulation with blank holder clamping force versus time profile shown above, as model input data.

5.4 Result and discussion

5.4.1 FE Model Validation

Figure 5.7 demonstrates a comparison between the final interlock shape of the die-less clinched joint obtained experimentally and from the FE model using different weight functions in the mixed hardening law 2 (Equation 5.2). It can be noted a lower value of the weight function α (i.e., a hardening behaviour closer to the Voce-model) results in increases in both the predicted neck thickness "N" and the interlock depth "U" and closer to the experimental values, with an error of about 35%. It is to be noted that in our previous work on predicted final shape of a conventionally clinched joint by using extensible dies [27], a weight function value of 0.5 was found to yield good prediction of interlock depth. This difference in the weight function value for interlock depth prediction for conventional and die-less clinching can be attributed to the very large plastic strains associated with die-less clinching process that exceed 5 compared with plastic strain of the range of unity in case of conventional clinching. From Figure 5.5 it can be noted that at a plastic strain of 1 the difference in post-necking behaviour between the weight function of 0.25 and extended-Voce material models is small. However, at higher strains the difference in the mechanical behaviour becomes significant.

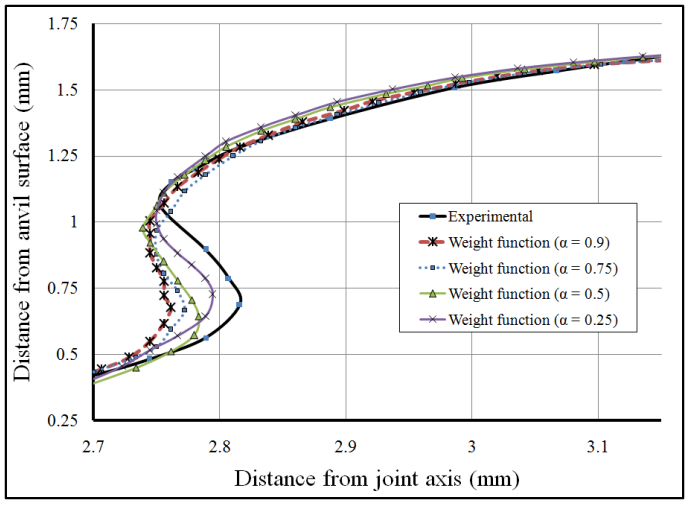

Figure 5.7. A comparison of experimental and FE predicted interlock shapes from different weight functions. (X-parameter = 90%).

Figure 5.8 shows a comparison of the final geometry of the die-less clinched joint between FE modeling using extended-Voce material model and the experimentally obtained joints by using two different stepped edge blank holders. Also, Figure 5.9 shows an expanded view of the critical interlock region from experiments and simulations. The two figures show a good prediction in the final shape of the die-less clinched joint from the extended-Voce based FE model with an error of less than 5%. Specifically, the experiment using 5/0.4 and 5/0.2 stepped-edge blank holders resulted in interlock depths of 0.065 mm and 0.05 mm respectively compared to 0.062 mm and 0.047 mm from FE prediction. Figure 5.10 also presents rather good agreement in through-thickness profiles from extended-Voce law based FE model and experiment. Lastly, punch load versus displacement traces comparing overall process behavior from experimental and simulation clinches are presented in Figure 5.11. Figures 5.7-11 collectively indicate good overall agreement between experimental and numerical results with an error less than 5%.

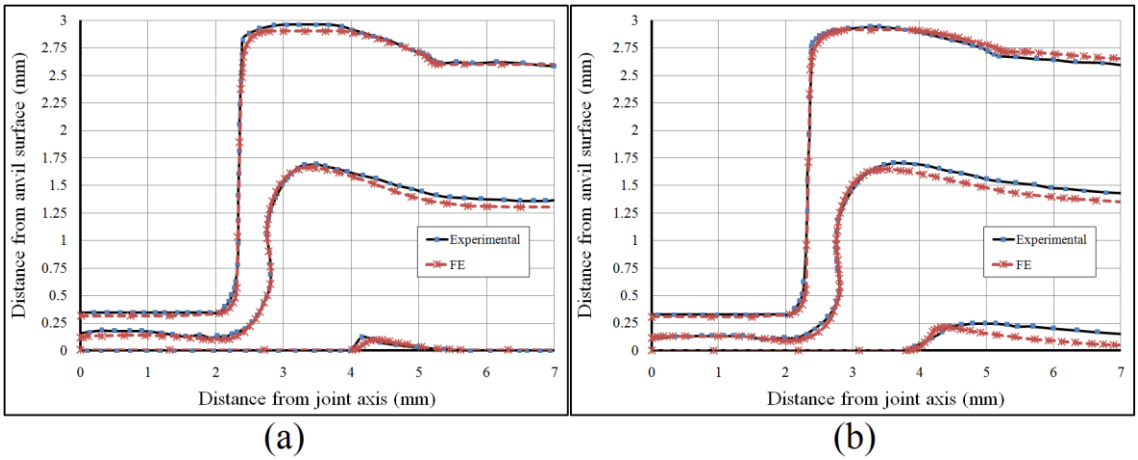

Figure 5.8. A comparison of experimental and FE predicted shape profiles for; (a) stepped edge blank holder 5/0.4 and (b) stepped edge blank holder 5/0.2. (X-parameter = 90%).

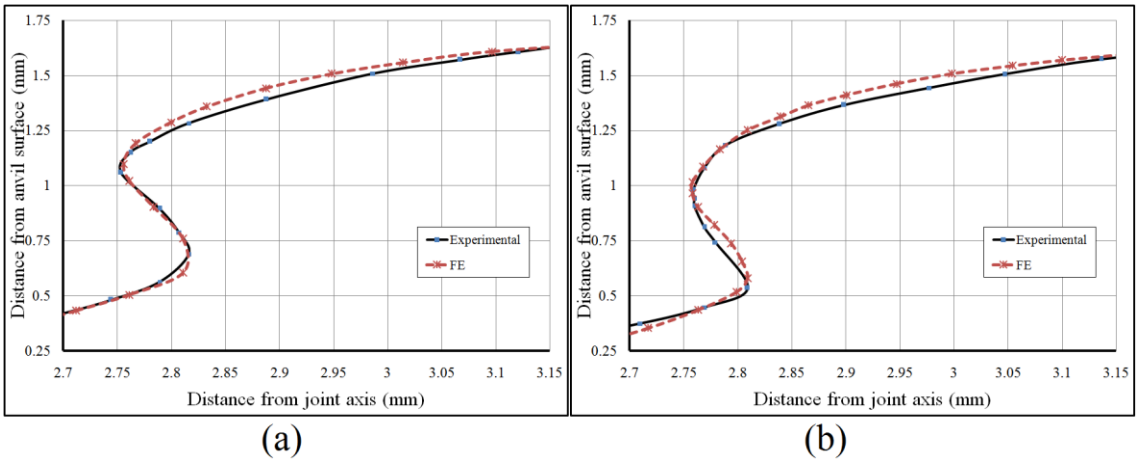

Figure 5.9. A comparison of experimental and FE predicted interlock region for; (a) stepped edge blank holder 5/0.4 and (b) stepped edge blank holder 5/0.2.

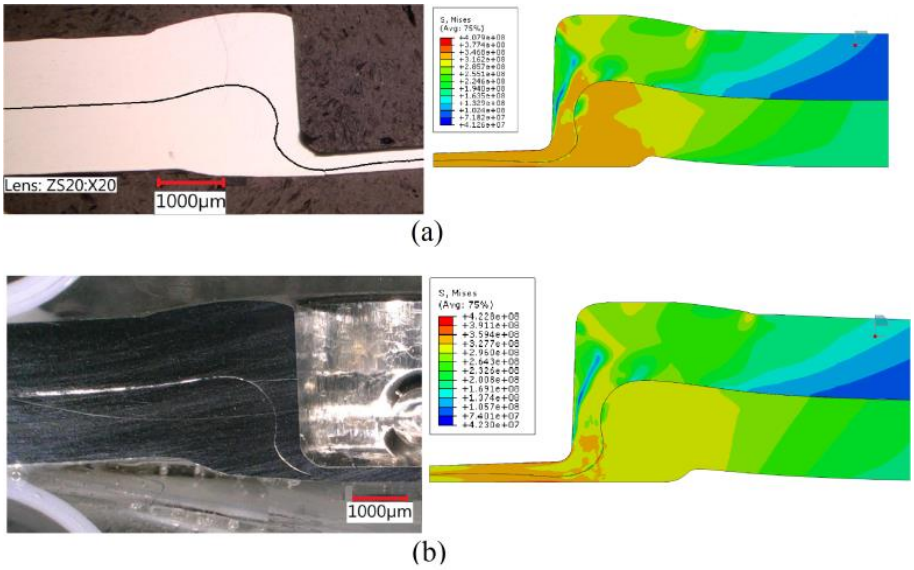

Figure 5.10.Experimental and corresponding FE predicted through-thickness clinched shapes for; (a) stepped edge blank holder 5/0.4 and (b) stepped edge blank holder 5/0.2.

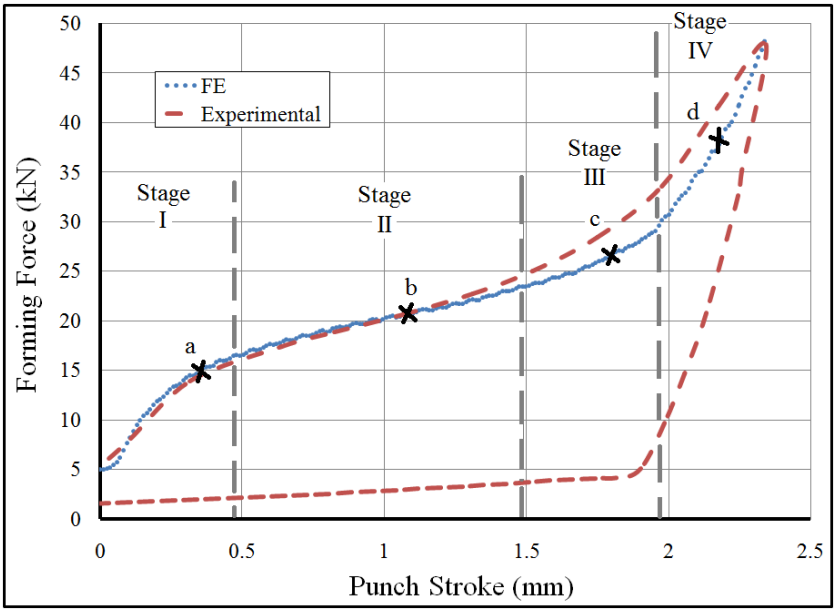

Figure 5.11. A comparison of punch forming force versus displacement traces from experiment and FE simulation for stepped edge blank holder 5/0.4.

5.4.2 Material Flow

The die-less clinching process can be divided into four stages (I, II, III, and IV) from the instance of punch contact with the upper sheet, as shown in Figure 5.11. For the explanation purposes, four different points (a, b, c, and d) within each stage on the curve are chosen. The radial (ε_{11}^{pl}) and axial (ε_{22}^{pl}) plastic strain components of each of the 4 chosen points are presented as left and right columns respectively in Figure 5.12. For point a (within stage I), the sheet material under the punch flows axially along the direction of the punch movement while the material outside of the punch region flows predominantly in the radial direction by sliding with only a limited flow in axial direction. Large tensile and compressive strain regions along the y-direction begin to develop at the upper and lower points of the punch corners respectively. With increased forming force and further punch movement, stage II (and point b in Figure 5.11) is reached where the material flow in the radial direction becomes more difficult due to increased blanking force and curvature of the punch sheet contact interface. Consequently, the axial material flow under blank holder groove occurs opposite to the direction of the punch movement. The upper sheet material in contact with the side of the punch is subjected to a tensile force causing it to stretch and form the wall of the joint. This wall region has a compressive radial strains and tensile axial strains. Stage III, corresponding to point c, is then reached with further punch movement when the sliding motion becomes more restricted and a lifting force is induced in the area under blank holder groove due to the free surface on the top of the punch-sided sheet thereby causing the lower surface of the anvil-sided sheet to rise. It is to be noted that, in a previous work [9], the present authors

have referred to the rise of the anvil-sided sheet as a protrusion. The punch-sided sheet thus comes under increased compression in the radial direction and increased tension in the axial direction. This stage continues until the top surface of the punch-sided sheet comes in contact with the top of the blank holder groove. With increased lifting of the anvil-sided sheet, the interface of the lower sheet exerts higher pressure on the upper sheet that results in the formation of the S-shape. With further punch movement and due to high resistance of the blank holder, the stage IV (and point d) is reached, and the material in the groove volume starts to flow radially to fill the upper groove and in turn increase the interlock.

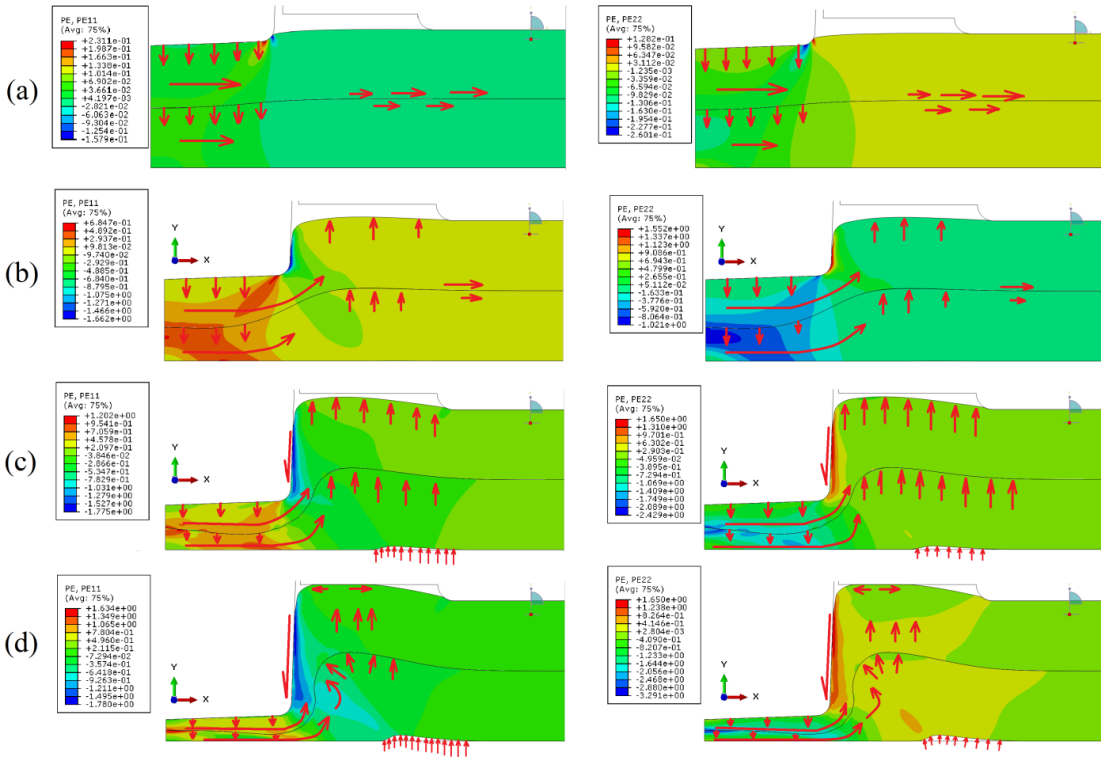

Figure 5.12. Plastic strain ε_{11}^{pl} (left column) and ε_{22}^{pl} (right column) in the clinched region at points corresponding to positions (a-d) in Figure 5.11, for a stepped edge blank holder.

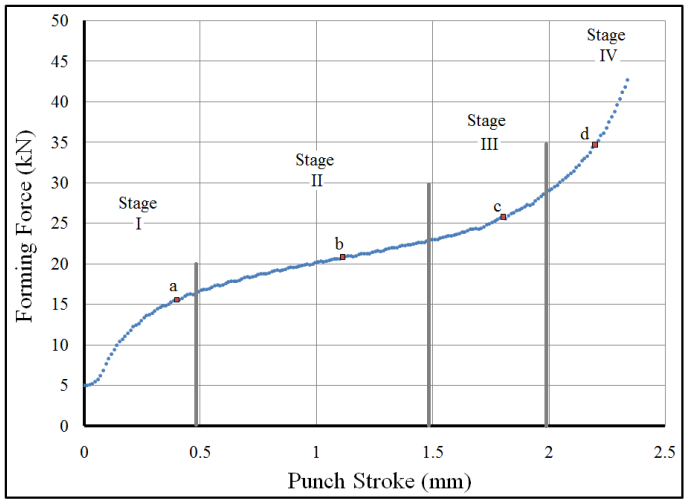

Figure 5.13. Forming force versus displacement trace for FE simulation by using rounded edge blank holder 4/2.5.

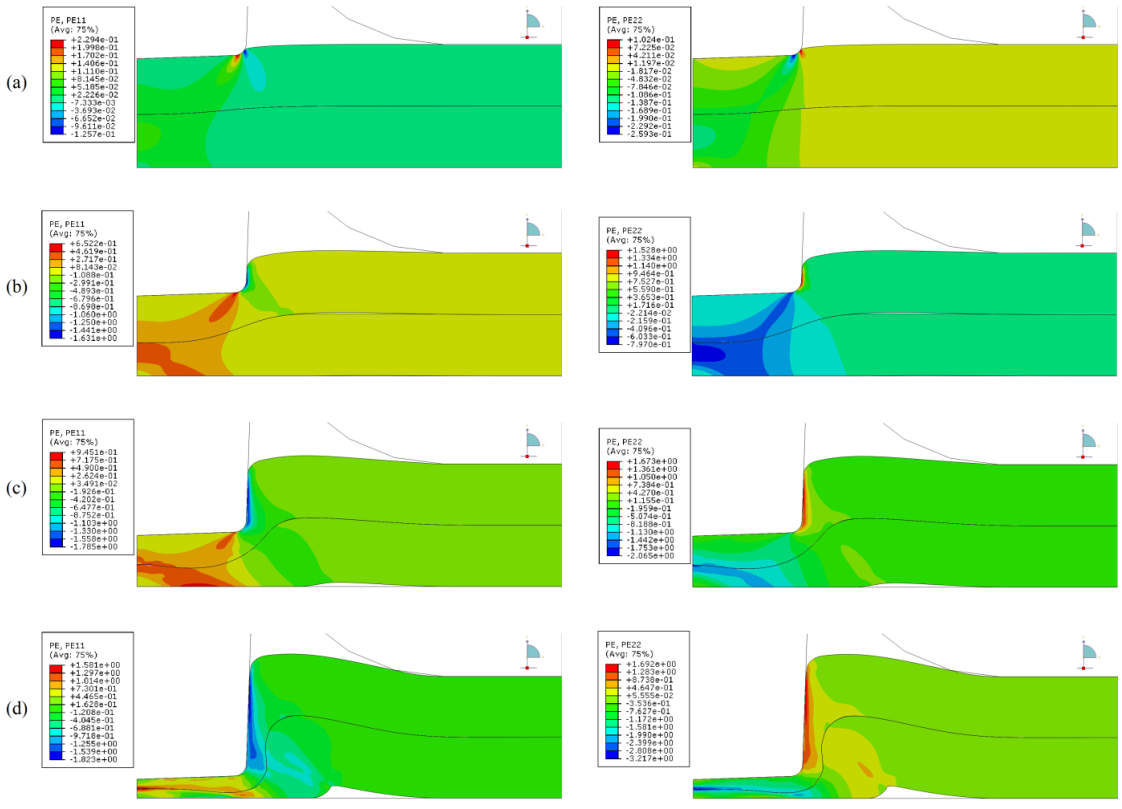

Figure 5.14. Plastic strains ε_{11}^{pl} (left column) and ε_{22}^{pl} (right column) in the clinched region at points corresponding to positions (a-d) in Figure 5.13, for a 4/2.5 rounded edge blank holder.

The same four stages (I to IV) can be recognized for a rounded edge blank holder as shown in Figure 5.13 and 5.Figure 5.14. However, the limit between stage II and stage III is not quite as distinct, and the lifting of the anvil-sided sheet occurs earlier and increases more significantly in stages III and IV. Also, the lifting is higher compared to the case of stepped edge blank holder due to increased material flow in radial direction and towards the punch.

5.4.3 Effect of blank holder and forming forces

Figure 5.15 shows the effect of the stepped edge blank holder design parameters, groove depth "t" and radius "r", on the geometric interlock characteristics. Note that the bars in Figure 5.15 with zero value indicate that no interlocking was achieved. As shown in Figure 5.15(a), a reduction in groove depth from 1 mm to 0.4 mm resulted in an increase in the interlock depth U by approximately 210 %, 190 % and 170 % for groove diameters of 7.5 mm, 6 mm and 5 mm respectively. This is due to increased material flow in the radial direction arising from restricted material to flow in the axial direction. Further reduction in groove depth, however, blocks the axial flow of the material at an earlier stage thus reducing the interlocking formation. It is to be noted that restriction in material flow in the axial direction is more vital to interlock formation when the groove diameter is small, such as in case of 4 mm blank holder diameter, as shown in Figure 5.15(a). In contrast, a smaller groove depth results in an increase in the neck thickness N due to the limited flow of the material which in turn decreases the thinning of the sheet material.

The interlock depth was increased by 210% and 160 % for groove radius r of 7.5 mm and 6 mm compared with 5 mm radius at a groove depth 0.4 mm (see Figure 5.15(a)). Also, due to the increase in groove radius, there was less neck thickness reduction especially at smaller groove depth due to the flow of the material from regions away from the punch (see Figure 5.15(b)). Generally, the neck thickness increased with increasing groove radius. There was a tendency for the material from the outer regions, rather than from the adjacent regions, to flow towards the clinched region. Lastly, an increase in blank holder groove radius resulted in an increase in the lifting of the lower sheet due to the larger groove volume, as shown in Figure 5.16.

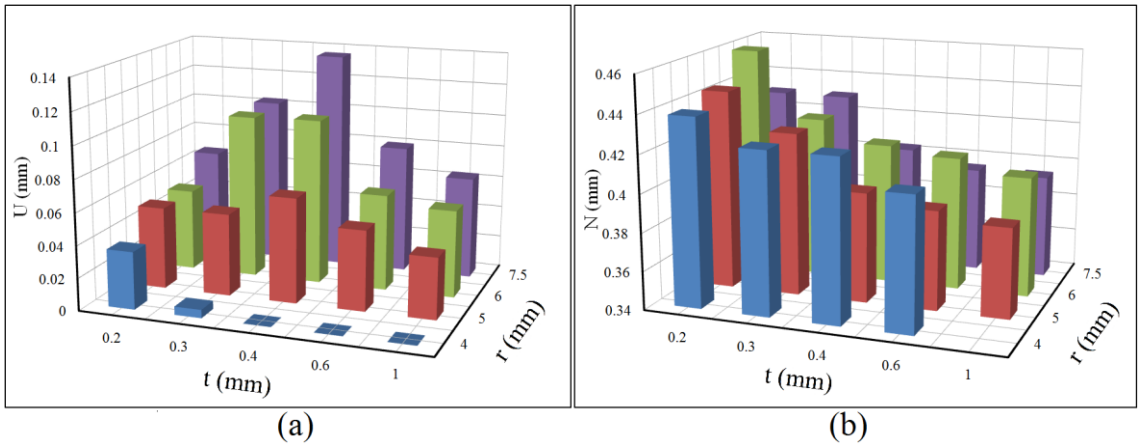

Figure 5.15. 3D bar charts showing the effect of stepped edge blank holder design parameters, groove depth t and radius r, on interlock depth U and neck thickness N.

Figure 5.17 shows the effect of rounded edge blank holder design parameters on final clinch shape (i.e., parameters U and N). The higher the blank holder radius (R) and fillet radius (S) the higher was the interlock depth (U). This effect was similar to increase in stepped edge blank holder radius where it increased the flow of the material from outer

regions towards clinched area. However, increasing blank holder radius (R) or fillet radius (S) resulted in significant increase in the lifting of the lower sheet h as shown in Figure 5.18.

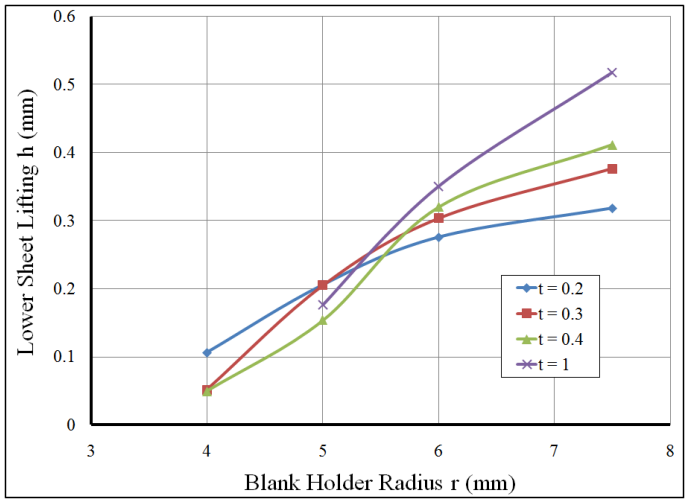

Figure 5.16. Effect of the stepped edge blank holder radius on the lifting of the lower sheet h for different blank holder groove diameter values.

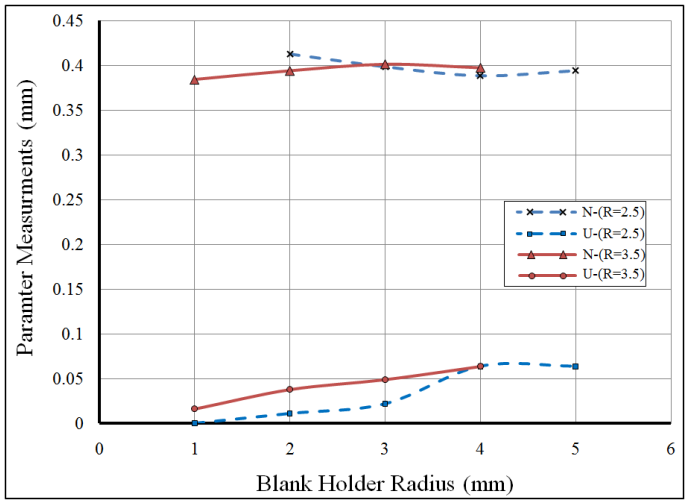

Figure 5.17. Effect of rounded edge blank holder radius R on measured parameters U and N.

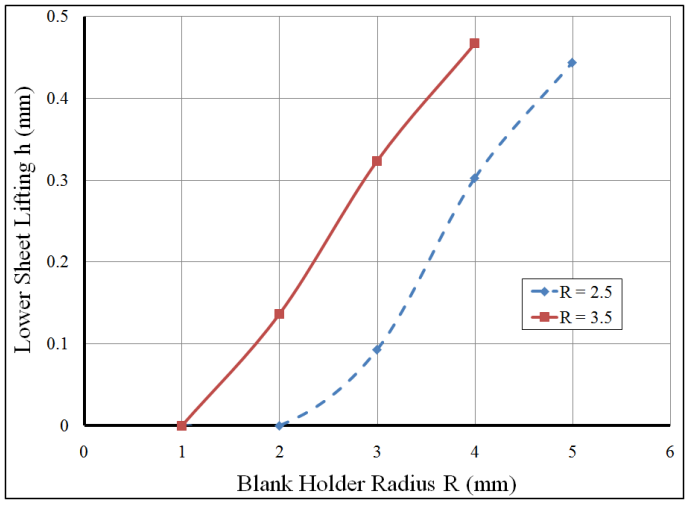

Figure 5.18. Effect of the rounded edge blank holder radius R on lifting h of the upper sheet.

The final shapes of the die-less clinched joint obtained by stepped edge blank holder of dimensions 5/0.4 from different clamping profiles are shown in Figure 5.19. In these simulations, three different clamping force profiles were employed as mentioned earlier in Section 2. As expected, the figure shows a decrease in the clamping force resulted in increased sliding between the two sheets, as observed from the right side of each figure. Also, lifting of the lower sheet increased as a result of decrease in the clamping force. Figure 5.20 indicates that a lower blank holder force results in better interlocking but increased lifting of the lower sheet. Moreover, the simulation and the experiment have shown that a very high punch force can lead to distorted shape of the die-less clinched joint whereas a small X-parameter, lower than 10%, can result in distortion of the bottom of the joint, as in Figure 5.21. That can be attributed to large thinning of the bottom that cannot withstand the elastic recovery that occurs after the release of the punch load.

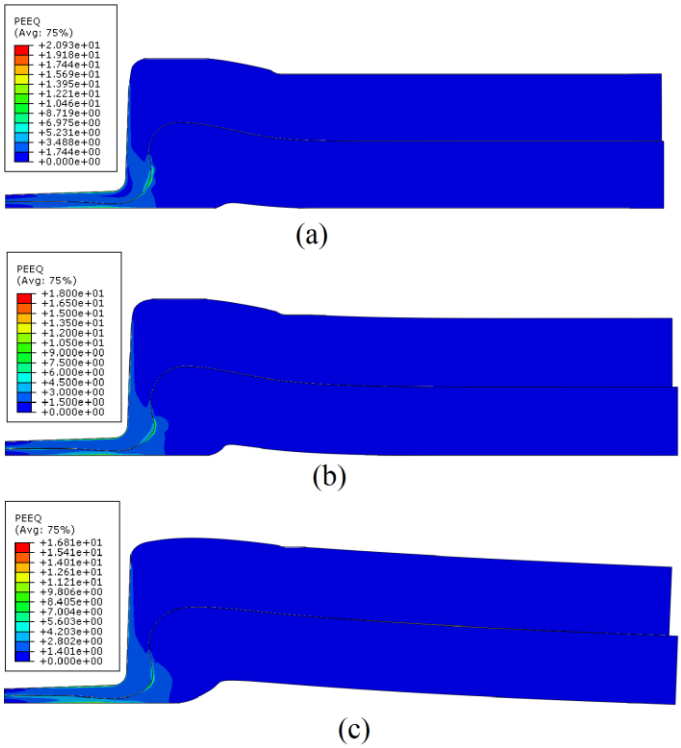

Figure 5.19. The final geometry of the die-less clinched joint obtained from FE model using; (a) experimental clamping profile, (b) theoretical clamping profile 1, and (c) theoretical clamping profile 2 (see earlier Figure 3).

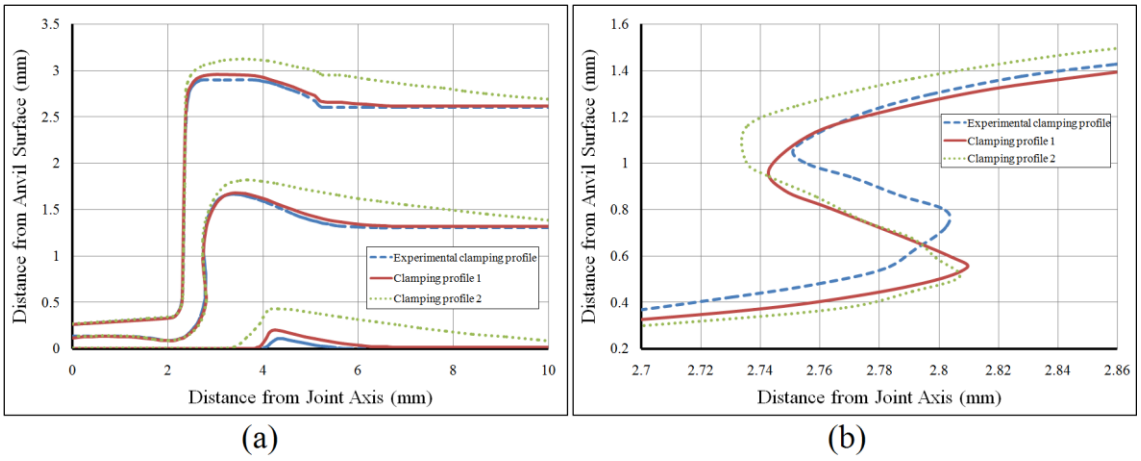

Figure 5.20. Effect of different clamping force profiles clamping on final shape of the die-less clinched joint for a stepped edge blank holder (5/0.4); (a) overall view of the joint, and (b) enlarged view of the S-shape.

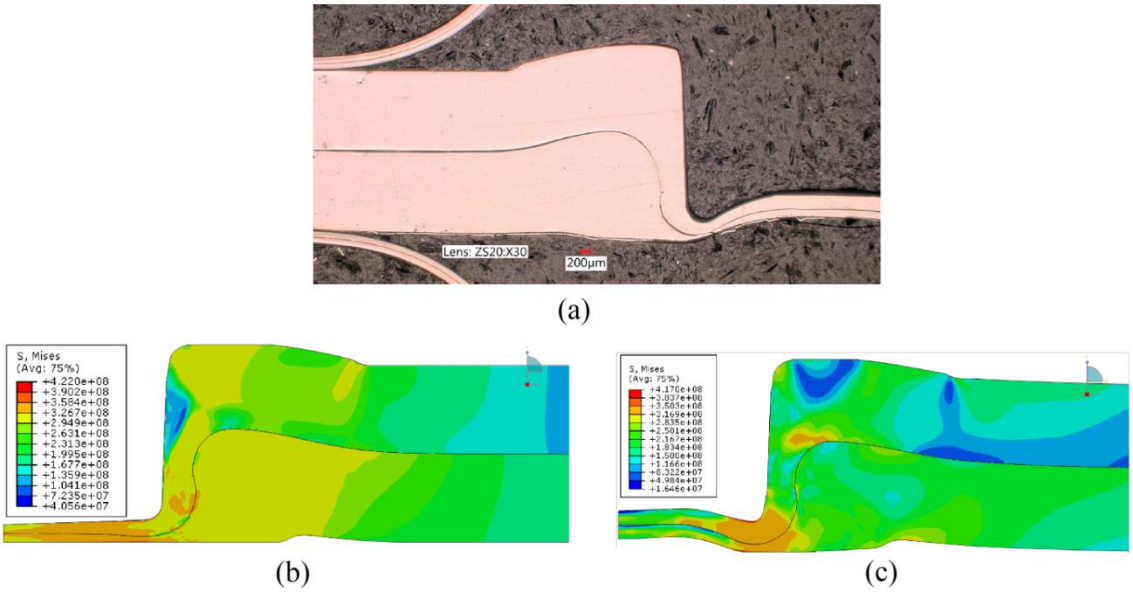

Figure 5.21. Final shape of die-less clinched joint for X-parameter = 95%; (a) experimental shape, (b) model shape before the release of punch load, and (c) model shape after the release of punch load.

5.4.4 Models of Post-clinch Joint Strength Tests

In-plane shear and peel tests were carried out on clinched joints to assess their shear and peel strengths. The details of the experimental set-up, specimen geometry and the results were presented recently in a separate paper by the authors [9]. In this section, the results of FE simulations of shear and peel tests are presented and compared with the experimental results.

5.4.4.1 In-plane Shear Strength Simulations

The final shape obtained from the 2D axisymmetric die-less clinching model simulation was used to build a 3D FE model of experimental in-plane shear test as shown in Figure 5.22. Due to symmetric geometry and loading conditions with respect to X-axis,

only one-half of the sample was modeled in order to save computational time. The clinched region of the in-plane sheet specimen geometry was meshed with edge elements of 0.1 mm size with a 10-node modified quadratic tetrahedron element (C3D10M), and, as earlier, an extended-Voce material model was used to describe the large strain plastic behavior of the joint. Two stress states were considered: the original stress-free state of the initial sheet (i.e., without taking into consideration the change in the material stress state due to formation of the joint), and another, a modified stress state corresponding to the average change in the stress state as a result of joint formation.

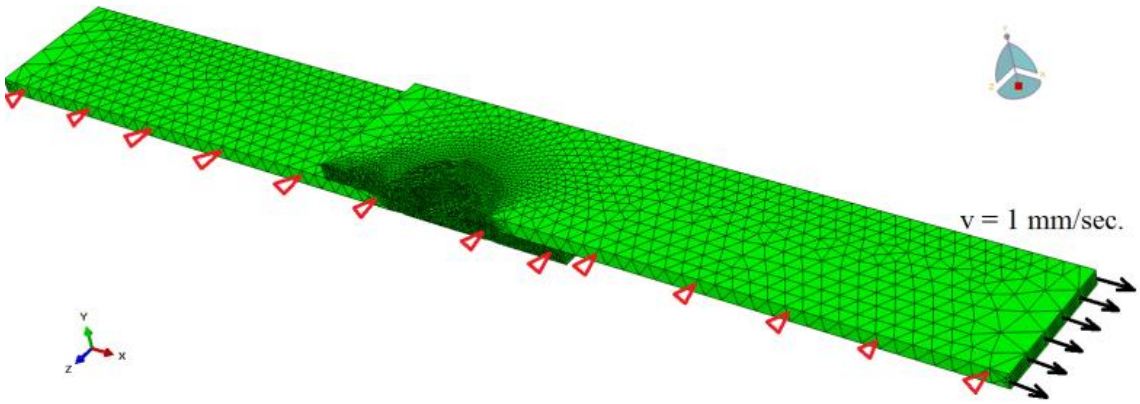

Figure 5.22. 3D FE model of the in-plane shear test with boundary and loading conditions.

Figure 5.23 shows the force-displacement curves for the two FE models for the two stress states and the corresponding experiments. As expected the modified stress state gave a force-displacement curve comparable to the experimental curve and considerably higher than the original stress state. The maximum force obtained from the modified stress state model (blue curve) of the joint was only about 3% higher than the experiments whereas the original stress state model results (red curve) exhibited a reduction in

maximum force of about 20%. Three loading regimes can be characterized along each curve. For explanation purpose, three points a, b, and c were chosen corresponding to the three stages in Figure 5.23. The origin at point 0 simply represents the start of the test. Mises stress distributions corresponding to points a, b and c from in-plane axial loading are shown in Figure 5.24. The initial stage of higher positive slope and stiffness in Figure 5.23 corresponds to elastic loading (Stage 1). The elastic-plastic transition and plastic loading of the joint occurs in Stage 2 (and at point a in Figure 5.23) when the punch-sided sheet tries to pull away from the die-sided sheet. A visible localized Mises stress region in the vicinity of the joint can be noted in Figure 5.24(a) while the interlock on the other side prevents the sheet pull out. As a result of the offset between the loading plane and neck, a moment is applied to the joint causing an upward lifting of the left side of the top sheet and a downward displacement of the right side of the bottom sheet. With increasing displacement, the joint stiffness decreases as a result of plastic deformation of the interlock. The stress distribution at the interlock becomes highly asymmetric with higher stress values towards the right loading arm of the test sample and in the upper sheet due to asymmetry of the contact conditions (see Figure 5.24(b)). The load continues to increase with increasing displacement but at a slower rate and reaches a maximum when a very large plastic deformation occurs, mainly on the inner surface of the punch-sided sheet. Finally, Stage 3 (and point c in Figure 5.23) is reached when the load starts to drop with further displacement until complete separation occurs, as shown in Figure 5.24(c).

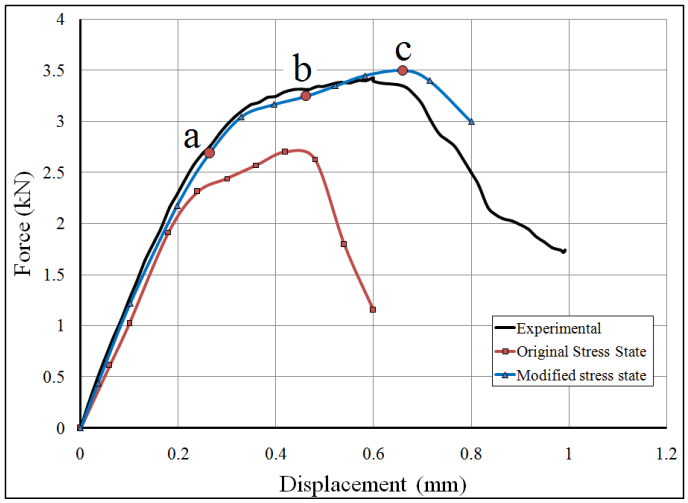

Figure 5.23. Force-displacement curves from two FE models for two different stress states, and corresponding in-plane shear experiments. Note that the joint was produced by using 5/0.3 stepped edge blank holder.

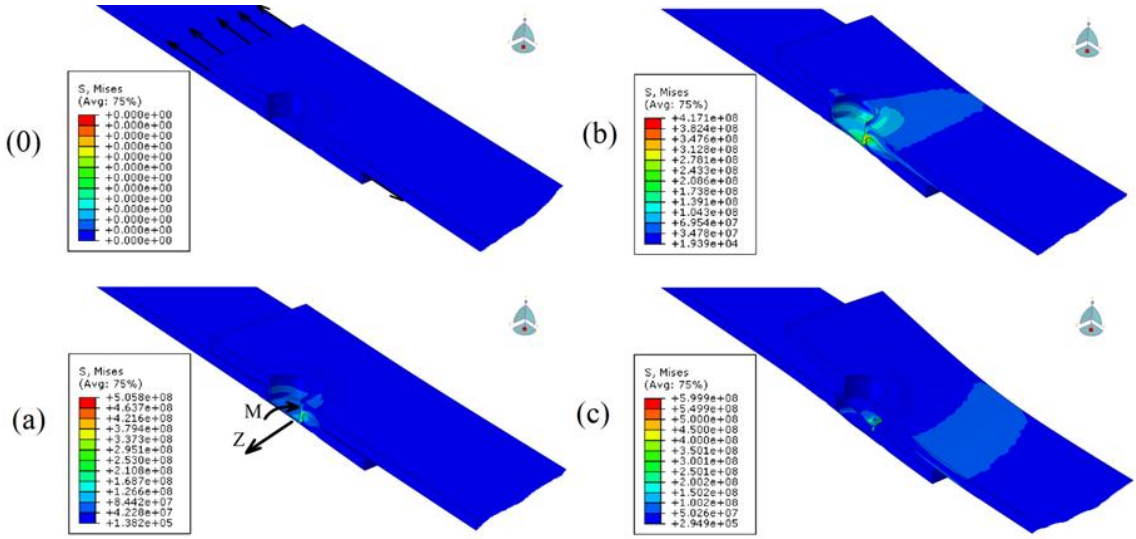

Figure 5.24. Mises stress distributions in an in-plane shear test specimen corresponding to initial stress-free state (point O) and 3 different deformed states corresponding to points a, b, and c along the force-displacement curve in Figure 23. Note that the joint was experimentally obtained using stepped edge blank holder, 5/0.3.

5.4.4.2 Peel Strength

In this sub-section results of T-peel tests of a clinched joint are compared with the FE simulations. A photograph of the T-peel test specimen loaded in axial direction is shown in Figure 5.25(a). A simplified 3D FE model, as in Figure 5.25(b), was developed for comparison with the experiment. In this model, for simplicity, the loading did not take into consideration the bending effect arising from the bent arm of the real test sample. The peel strength of the joint was calculated as the summation of all reaction forces on the nodes of the short side of the upper sheet. Also, the same two stress states were used in modeling of the shear test used to simulate the peel test.

Figure 5.26 shows a comparison of the force-displacement curves from experiments and FE simulations. As earlier in the case of in-plane shear tests, the model force-displacement response from modified stress state was comparable to the experimental results. In contrast, the model results based on original stress state resulted in a much lower value of peel strength. The results thus clearly establish the importance of taking into consideration the change in stress state due to joint formation for accurate simulations of post-clinch joint strength tests. The increased model displacement values at failure compared with experiment could perhaps arise from lack of consideration of the T-shape bending arm of the real sample in the FE model, as shown in Figure 5.27.

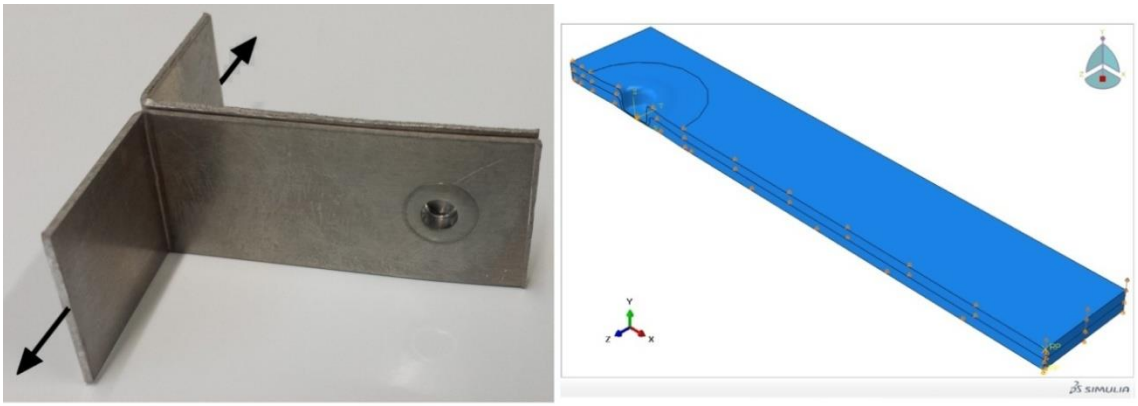

Figure 5.25. Peel test details, (a) experimental peel test specimen geometry and loading, and (b) 3D FE model of simplified peel test and loading.

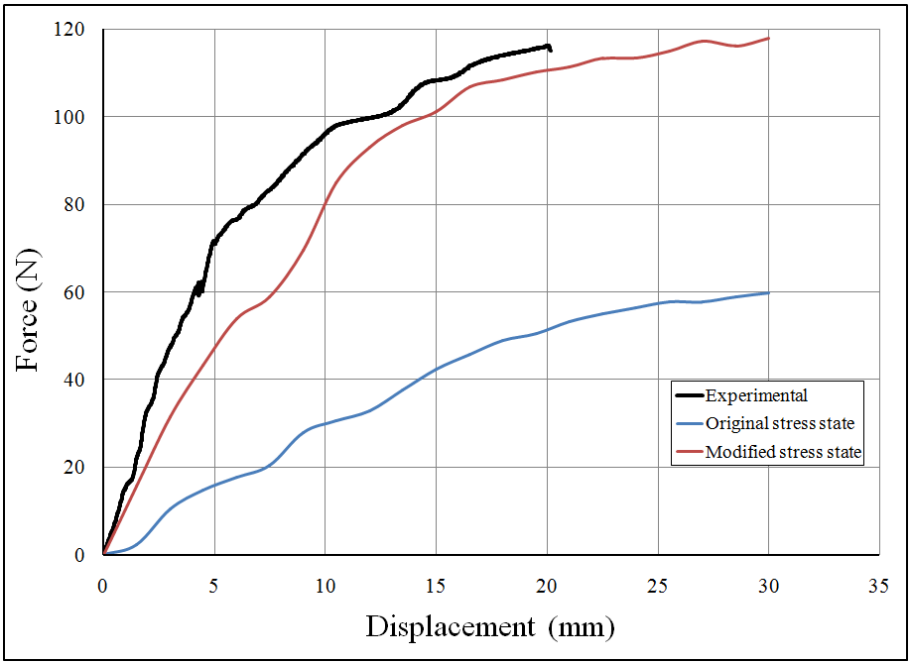

Figure 5.26. A comparison of experimental and model peel force-displacement curves.

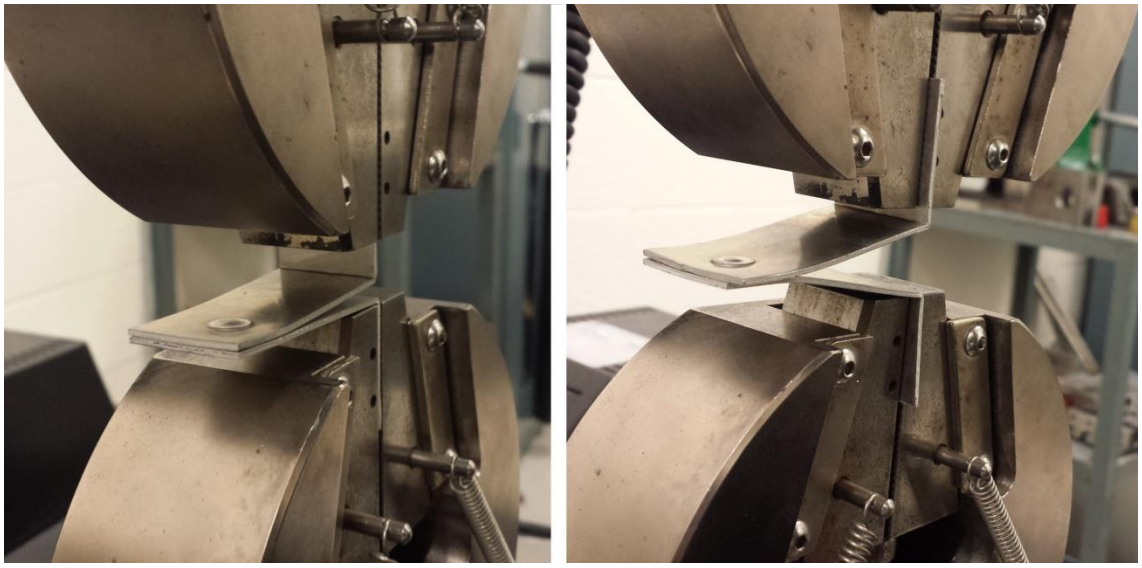

Figure 5.27. Experimental peel test specimen images at two different peel arm end displacements and the accompanied bending effect.

Figure 5.28 shows the Mises stress distribution from the FE model for 6 equally-distanced loading peel arm end displacement positions. It can be noted that there is a stress concentration (tension) in the interlock region on the same side of the long arm as well as a bending effect. With increasing displacement, the stress and plastic strain increase increases and ultimately complete separation of the joint occurs in the interlock region, as in Figure 5.28(f).

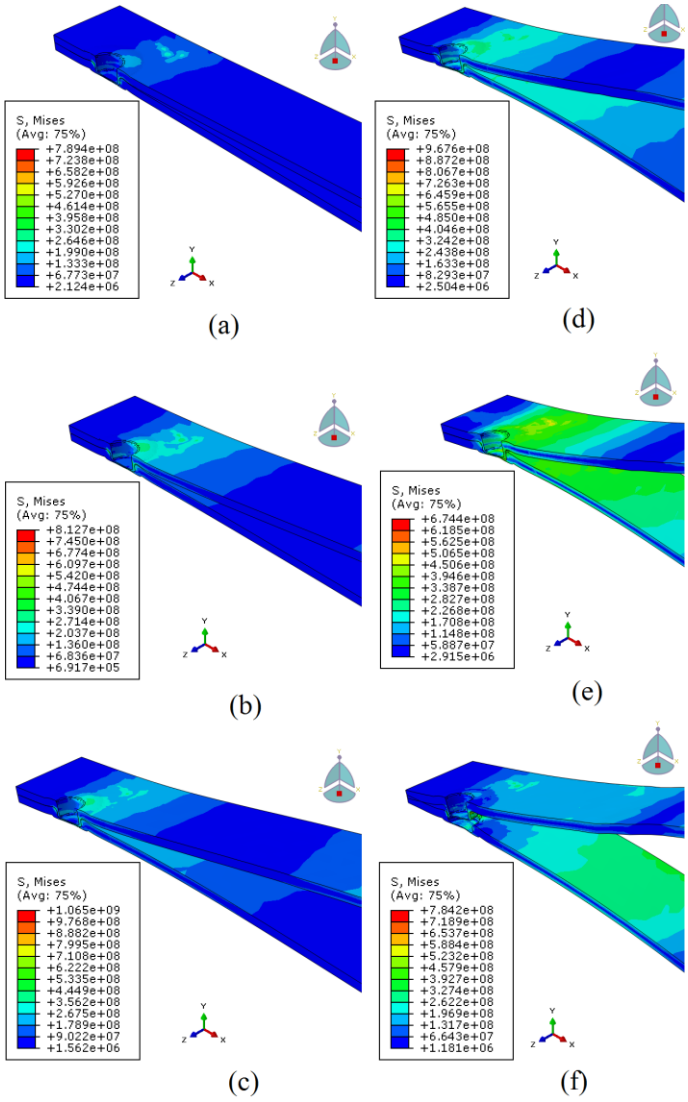

Figure 5.28. Mises stress distributions corresponding to 6 different peel end displacements.

5.5 Conclusions

Die-less clinch joining of AA7075 aluminum sheets and post-clinch joint strength were analyzed using the FE method and the results were compared with the experimental from previous work of the present authors. The effects of tool parameters such as blank holder shapes as well as process parameters such as clamping force on material flow

behavior, interlock depth, and neck thickness were investigated. The following specific conclusions can be drawn from the above study.

1- Four and three different stages of material flow during die-less clinching with stepped edge and rounded edge blank holder geometries were identified respectively from the punch force versus punch displacement curves. These stages were explained in terms of material flow in the radial and axial directions at each stage from FE model results.
2- The interlock forms from large material flow in the axial direction. It can be maximized by controlling the material flow in radial direction instead of the axial flow by decreasing the blank holder depth.
3- A reduction in groove depth from 1 mm to 0.4 mm resulted in an increase in the interlock depth by approximately 210 %, 190 % and 170 % for groove diameters of 7.5 mm, 6 mm and 5 mm respectively.
4- The fillet radius of the rounded edge blank holder has the same effect on the final shape of the die-less clinched joint as the groove diameter of the stepped edge blank holder. An increase in both of these parameters resulted in an increase the interlock depth.
5- The bottom thickness should be higher than 10% of the total sheet thickness to avoid distortion of the bottom of the die-less clinched joint.
6- In-plane shear strength of the joint can be accurately estimated from a 3D FE model of in-plane shear test provided an average stress state after joint formation is taken into consideration in the model simulation.

7- The in-plane shear and peel strength of the die-less clinched joint can be accurately predicted by the proposed FE models that simulate the lab-based in-plane shear and T-peel experiments. Slightly larger model peel arm displacement values compared to experimental measurements are possibly due to neglect of the experimental T-shape of the real sample in the model.

References

[1] T. Barnes, I. Pashby, Joining techniques for aluminium spaceframes used in automobiles: Part I solid and liquid phase welding, Journal of materials processing technology 99(1) (2000) 62-71.
[2] I.R.P. T.A. Barnes, Joining techniques for aluminium spaceframes used in automobiles Part II -adhesive bonding and mechanical fasteners, Journal of Materials Processing Technology 99 (2000) 72-79.
[3] F. Lambiase, A. Di Ilio, An experimental study on clinched joints realized with different dies, Thin-Walled Structures 85 (2014) 71-80.
[4] C. Borsellino, G. Di Bella, V. Ruisi, Study of new joining technique: flat clinching, Key Engineering Materials, Trans Tech Publ, 2007, pp. 685-692.
[5] J. Varis, Ensuring the integrity in clinching process, Journal of Materials Processing Technology 174(1) (2006) 277-285.
[6] F. Lambiase, A. Di Ilio, Finite element analysis of material flow in mechanical clinching with extensible dies, Journal of materials engineering and performance 22(6) (2013) 1629-1636.
[7] J. Varis, The suitability of clinching as a joining method for high-strength structural steel, Journal of Materials Processing Technology 132(1) (2003) 242-249.
[8] R. Neugebauer, M. Todtermuschke, R. Mauermann, F. Riedel, Overview on the state of development and the application potential of dieless mechanical joining processes, Archives of Civil and Mechanical Engineering 8(4) (2008) 51-60.
[9] M.K.S. Atia, M.K. Jain, Die-less Clinching Process and Joint Strength of AA7075 Aluminum Joints, Thin-Walled Structures 120 (2017) 421-431.
[10] T. Gerstmann, B. Awiszus, Recent developments in flat-clinching, Computational Materials Science 81 (2014) 39-44.
[11] F. Lambiase, A. Di Ilio, A. Paoletti, Joining aluminium alloys with reduced ductility by mechanical clinching, The International Journal of Advanced Manufacturing Technology 77(5-8) (2015) 1295-1304.
[12] J.P. Varis, J. Lepistö, A simple testing-based procedure and simulation of the clinching process using finite element analysis for establishing clinching parameters, Thin-Walled Structures 41(8) (2003) 691-709.
[13] S. Coppieters, P. Lava, R. Van Hecke, S. Cooreman, H. Sol, P. Van Houtte, D. Debruyne, Numerical and experimental study of the multi-axial quasi-static strength of clinched connections, International journal of material forming 6(4) (2013) 437-451.
[14] M. Eshtayeh, M. Hrairi, Recent and future development of the application of finite element analysis in clinching process, The International Journal of Advanced Manufacturing Technology 84(9-12) (2016) 2589-2608.

[15] S. Coppieters, S. Cooreman, P. Lava, H. Sol, P. Van Houtte, D. Debruyne, Reproducing the experimental pull-out and shear strength of clinched sheet metal connections using FEA, International journal of material forming 4(4) (2011) 429-440.
[16] S. Saberi, N. Enzinger, R. Vallant, H. Cerjak, J. Hinterdorfer, R. Rauch, Influence of plastic anisotropy on the mechanical behavior of clinched joint of different coated thin steel sheets, International journal of material forming 1 (2008) 273-276.
[17] X. He, L. Zhao, H. Yang, B. Xing, Y. Wang, C. Deng, F. Gu, A. Ball, Investigations of strength and energy absorption of clinched joints, Computational Materials Science 94 (2014) 58-65.
[18] X. He, F. Liu, B. Xing, H. Yang, Y. Wang, F. Gu, A. Ball, Numerical and experimental investigations of extensible die clinching, The International Journal of Advanced Manufacturing Technology 74(9-12) (2014) 1229-1236.
[19] T. Wen, H. Wang, C. Yang, L.T. Liu, On a reshaping method of clinched joints to reduce the protrusion height, The International Journal of Advanced Manufacturing Technology 71(9-12) (2014) 1709-1715.
[20] F. Lambiase, Influence of process parameters in mechanical clinching with extensible dies, The International Journal of Advanced Manufacturing Technology 66(9-12) (2013) 2123-2131.
[21] C.-J. Lee, J.-M. Lee, H.-Y. Ryu, K.-H. Lee, B.-M. Kim, D.-C. Ko, Design of hole-clinching process for joining of dissimilar materials–Al6061-T4 alloy with DP780 steel, hot-pressed 22MnB5 steel, and carbon fiber reinforced plastic, Journal of Materials Processing Technology 214(10) (2014) 2169-2178.
[22] B.J. Shi, Y.Q. Wang, S.L. Liu, H.Y. Tian, Design method of the parameters of tools for clinching technology, Advanced Materials Research, Trans Tech Publ, 2012, pp. 1491-1496.
[23] J. Mucha, The analysis of lock forming mechanism in the clinching joint, Materials & design 32(10) (2011) 4943-4954.
[24] X. He, Recent development in finite element analysis of clinched joints, The International Journal of Advanced Manufacturing Technology 48(5-8) (2010) 607-612.
[25] M.K.S. Atia, M.K. Jain, A Parametric Study of FE Modeling of Die-less Clinching of AA7075 Aluminum Sheets, Under review, International journal of material forming, 2017.
[26] L. Mattei, D. Daniel, G. Guiglionda, H. Klöcker, J. Driver, Strain localization and damage mechanisms during bending of AA6016 sheet, Materials Science and Engineering: A 559 (2013) 812-821.
[27] M.K.S. Atia, M.K. Jain, B. Selorme, Numerical modeling and experimental studies of extensible dies based clinching process for AA7075 aluminum sheet, Thin-Walled Structures Under review (2017).

Chapter 6

A Study of Hot Die-less Clinching Process for High Strength AA7075-T6 Sheets by Electrical Resistance Heating

---

Mostafa K. Sabra Atia, PhD student, is the first author and main contributor of the work who conceptualized the topic, interpreted the results and drafted the paper. Mukesh K. Jain, Professor, is the supervisor who substantially contributed to the work by checking the experimental results as well as polishing the language of the paper. This paper is submitted for publications in *Materials & Designs*.

A Study of Hot Die-less Clinching Process for High Strength AA7075-T6 Sheets by Electrical Resistance Heating

Mostafa K. Sabra Atia[a,b] and Mukesh K. Jain[a]

a Department of Mechanical Engineering, McMaster University, Hamilton, Ontario, Canada L8S 4L7

b Corresponding author: Tel.: +1 905-920-0398. E-mail address: atiam@mcmaster.ca (M. Atia).

Abstract

High strength 7xxx series aluminum sheet materials offer an opportunity for further light-weighting compared to other aluminum alloys. AA7075 aluminum alloy in particular has been in use in the aerospace industry for quite some time. However, mechanical joining of this alloy in peak-aged tempers, T6 temper, are generally not possible at room temperature. In this work, high strength AA7075-T6 aluminum sheets were joined by die-less clinching and rapid application of heat using an electrical resistance heating (ERH) system to enhance their ductility. ERH system provided a large current to the clinching region within a short period of less than 3 seconds. In addition, a new clinching tool design was developed that enabled current transmission from the blank holder to the anvil through the test sheets. Further, a parametric study of hot die-less clinching process was carried out by systematically varying the applied current (and thus the temperature of the clinch region), the period of current application, and the forming force to achieve outstanding joints with superior interlocking and post-clinch joint strength. Lastly, microstructure examination of the clinched joint region was conducted to analyze the material flow and gain an understanding of locking mechanisms at elevated temperatures in AA7075-T6 sheet. The results showed that the strength of the joint occurred not only from commonly observed geometrical and force locking mechanisms but also from a new material bonding (or locking) mechanism due to simultaneous application of large forming forces and heat.

Table 6.1. Nomenclature

T6	Artificial peak aged state which represents the hardest temper
N	Neck thickness of the joint
U	Interlock depth of the joint
Q	The amount of heat generated
t_1	Beginning times of the resistance heating operation
t_2	Ending times of the resistance heating operation
I(t)	The heating current as function of time t
R_B	The bulk resistance
R_C	The constriction resistance
T	Temperature
R_F	The film resistance
R(t)	The dynamic resistance of the sheet metals as function of time t
ρ	The resistivity
H	The hardness
A	The area of current path
L	The length of current path
ρ_t	The tunnel resistivity or the film resistance per unit area
ξ	The pressure factor
a	The contact spot number
F	The compressive force
ERH	Electrical resistance heating
T_{max}	Peak temperature
R(t)	The dynamic resistance of the sheet metals as function of time t
ρ	The resistivity

Keywords: Die-less clinching, resistance heating, AA7075-T6

6.1 Introduction

Conventional clinching is a common method of joining sheet material in which punch and die are used to locally deform sheet metals in order to form a geometrical interlock that creates steps on both sides of the jointed surfaces [1]. Die-less clinching, a more recent development, enables sheet clinching where only one of the surfaces exhibits a step. This often allows to design die-less clinched components with the step on the blind side of the component, making die-less clinching a more visually appealing process than the conventional clinching. However, die-less clinching requires significantly larger plastic strains than the conventional clinching which makes it especially difficult to apply

to peak-aged high strength aluminum alloys with much lower ductility compared to the lower strength aluminum (or softer temper) aluminum alloys. Thus, clinching of very desirable high strength aluminum alloys from 7xxx series for lightweight weight aerospace and automotive components remains a challenge.

Some recent attempts have been made to make conventional clinch joining more suitable for hard-to-clinch sheet materials. Thermal gun has been used to locally heat higher strength AA6082-T6 sheets to increase its ductility for conventionally clinched sheet metal by Lambiase et al. [2-4]. Similarly, He et al. [5] have utilized oxyacetylene torch to preheat the TA1 titanium sheets for attaining good conventional clinches. Neugebauer et al. [6] have utilized an IR source from underneath the anvil to locally heat magnesium sheets to form die-less clinched joints. While the above mentioned, and quite recent, hot clinching methods are quite useful advances in clinching technology, they are too slow for industrial use. Also, they have not been tested for higher strength 7xxx series aluminum alloys, and for more formidable die-less clinching process where the plastic strains tend to be much larger compared to conventional clinching.

In the present work, a new die-less hot clinching process has been developed and studied for joining AA7075-T6 sheet materials by application of high current of short duration using electrical resistance heating (ERH) to the sheets prior to clinching. The study includes an investigation of the effect the main forming parameters, namely, forming force, applied current and time period of application on the integrity and strength of the die-less clinched joint. The material flow and resulting interlock characteristics under different ERH cycles are also studied using optical and scanning electron

microscopy and micro-hardness measurements of the cut cross-sections of the joints. Lastly, the shear strength and associated failures modes of the joint are assessed by using a lap shear test.

6.2 Electrical Resistance Heating Characteristics

The generation of Joule heat in the ERH process can be described with the following expression [7]:

$$Q = \int_{t_1}^{t_2} I(t)^2 \; R(t) \; dt \qquad (6.1)$$

where, Q is the amount of heat generated, $I(t)$ and $R(t)$ are the applied current and dynamic resistance of the system consisting of the two sheet metals and the clinching tools where the current and resistance are functions of time t, and t_1 and t_2 represent the start and end times of the applied current.

Electric resistivity of sheet metal changes dynamically during electrical heating process. Dickinson et al. [8] have explained the variation in dynamic resistance based on competition between bulk and contact surface resistances. At first application of current, the heat generated is concentrated at the aluminum sheet surface due to the existence of a thin oxide film as well as contamination. Consequently, film breakdown occurs with increasing temperature and pressure, and the resistivity starts to sharply decrease, as shown schematically in Figure 6.1. However, the trend is reversed immediately with continued increase in temperature with current application time since the bulk electrical resistivity of most metals increases with increase in temperature. The resistivity starts to

increase and then saturates as the melting point of the material is reached. In hot clinching, however, the interest is primarily in the resistance trend prior to approaching the melting point as no melting of the sheet is involved.

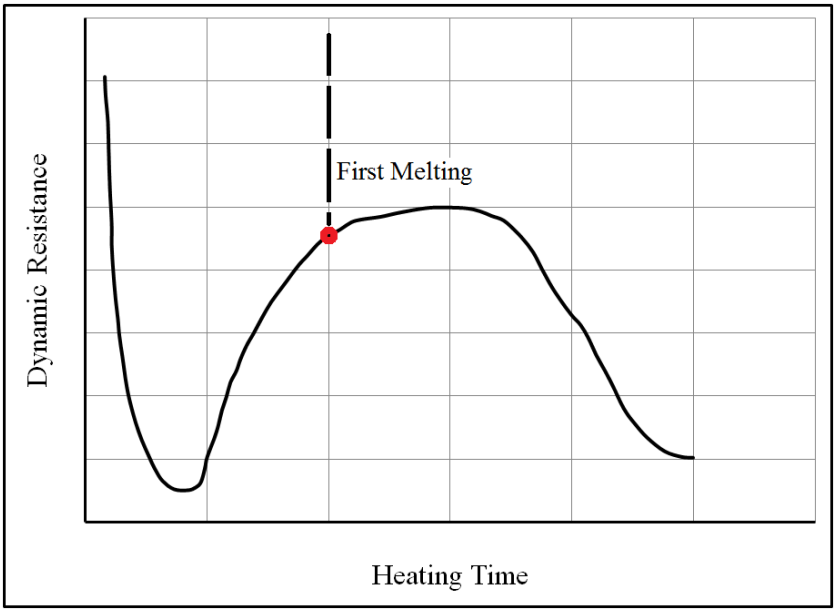

Figure 6.1. Variation of dynamic resistance with time during electrical resistance heating.

As mentioned earlier, the dynamic resistivity is a function of bulk and contact resistance. In fact, the effective resistivity, R, is a function of other resistances, and expressed in an additive form as [9]:

$$R = R_C + R_F + R_B \tag{6.2}$$

where R_C, R_F and R_B are referred to as constriction, film and bulk resistances respectively. The bulk resistance can be calculated from the following expression [9]:

$$R_B = \rho\left(\frac{l}{A}\right) \tag{6.3}$$

where ρ, l, and A are resistivity, length of current path over the sheet thickness, and area of current path respectively. If the sheet metal has a cleaned surface, the constriction and contact film resistances are equal and follow the following relation applies [10].

$$R_C = R_F = 0.89\rho\left(\frac{\xi H}{aF}\right)^{\frac{1}{2}} \qquad (6.4)$$

where H and F are hardness and compressive force respectively, and ξ is a pressure factor with values ranging from about $\xi = 0.2$ for a surface with considerable elastic action to $\xi = 1.0$ for a fully plastic contact. The symbol n in eqn. (4) is the contact spot number, where polished, well-rounded crossed cylinders tend towards $n = 1$, while large, overlapping, flat, electroplated surfaces have values of n between 10 and 20 [9]. It is to be noted that if the surface contains a dielectric film, the electrons are unable to pass the film. However, if the thickness of the film is comparable to the electron mean free path, the electrons can indeed pass through the film by tunnelling [9]. Therefore, the film resistance can be calculated from the following relation:

$$R_F = \frac{\rho_t \xi H}{F} \qquad (6.5)$$

where ρ_t is the tunnel resistivity or the film resistance per unit area. The tunnelling effect is sensitive to the film thickness but is independent of temperature [10]. The film can breakdown electrically by applying a voltage to the film or by mechanically applying a contact force [9].

In summary, the resistance heating is a complex process that depends upon aggregate bulk, constriction and film resistances. Each of the resistance components changes continuously during the heating cycle, i.e., the applied current can increase or

decrease the amount of heat available at any given time. It is shown that die-less clinching depends on the amount of plastic deformation required to form the joint which in turn depends on the amount of heat supplied by the applied current and the forming process parameters. In the present work, temperature was also measured for each individual current application cycle as described in Section 6.3.1.

6.3 Experimental procedure

6.3.1 Sheet material, machine set up and tooling

AA7075-T6 aluminum sheet of 1.27 mm nominal thickness were tested in uniaxial tension according ASTM standard E8/E8M to obtain its mechanical properties at room temperature to have an understanding of its initial strength. The tests were conducted on Instron universal testing machine at a cross-head speed of 1 mm/min using sub-size samples of dimension 120 mm length and 6 mm width (see Table 6.2).

Table 6.2. Mechanical properties of AA7075-T6 aluminum alloy at room temperature.

Material	Mechanical Properties				
	0.2% yield strength (MPa)	Ultimate strength, σ_{Ult} (MPa)	Max % Elongation	K (MPa)	n
AA7075-T6	620	695	12	976.9	0.1102

Artificially peak-aged T6 temper sheet of high strength and rather low elongation (see above Table 6.1) could not be die-less clinched at room temperature as discussed later in this paper. Therefore, an ERH heating step was applied immediately prior to clinching to enable the formation of the geometrical interlock using a recently developed integrated resistance heating and mechanical loading (IRHML) system in McMaster

University. A special die-less clinch tooling was designed and integrated to the above system as a part of the present research. The IRHML system consisted of two main sub-systems, a resistance heating system and a mechanical loading system. The resistance heating system was akin to what is used in spot welding where high currents are applied over a short duration. However, unlike spot welding, the heated sheets remained in the solid state. This was achieved using a medium frequency direct current (or MFDC) transformer, flexible copper shunts, two electrodes and a chiller as shown in Figure 6.2. The mechanical loading system consisted of a commercially available computer-controlled servo-hydraulic test machine from Instron.

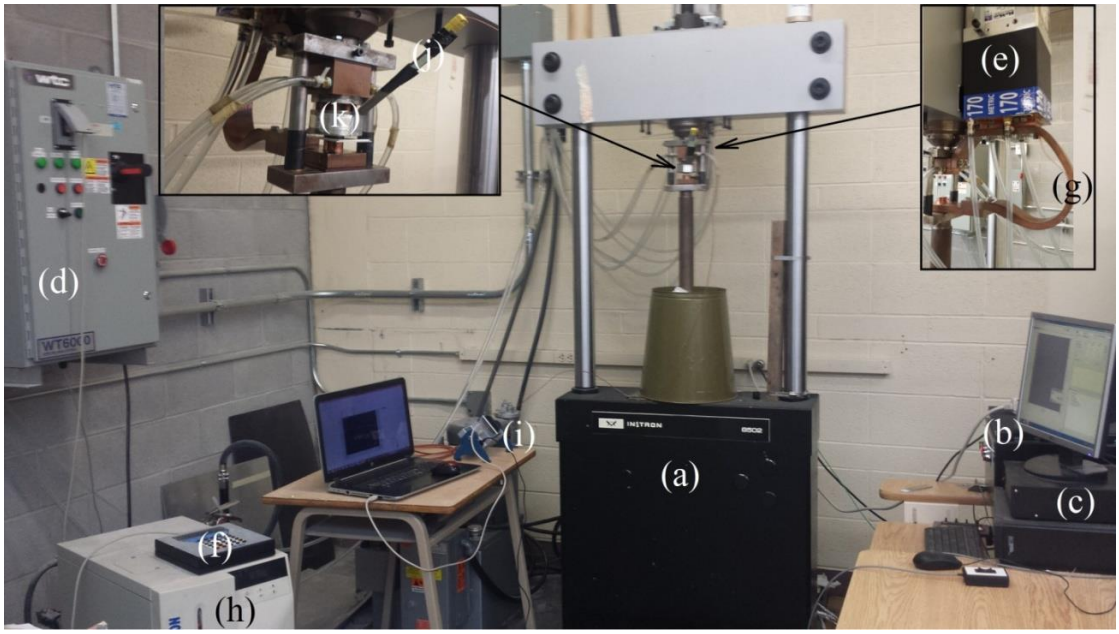

Figure 6.2. Integrated resistance heating and mechanical loading (IRHML)system, (a) Instron servo-hydraulic mechanical test frame, (b) mechanical loading controller, (c) data acquisition box, (d) welder, (e) mid-frequency DC transformer, (f) welder control box, (g) flexible copper shunts, (h) chiller, (i) data acquisition for temperature measurement system, and (j) K-type thermocouple.

Clinching tooling was especially designed to allow application of suitable current for resistance heating to the desired region of the AA7075-T6 sheet. The fabricated tool set consisted of blank holder, punch made of tungsten carbide and insolated by high strength Garolite G7, and a compression spring made from urethane-95 polymer in order to apply the clamping force (see Figure 6.3). Eight sliding electrodes were used to carry current from the blank holder to the anvil through the two aluminum sheets during the joining process. The blank holder had a groove diameter of 10 mm and a depth of 0.4 mm as discussed in previous work of the present authors [1], and the punch had a diameter of 4.6 mm and a draft angle of 2.5°.The temperature was measured using K-type thermocouple inserted through the punch. A data acquisition system from National Instruments (NI cDAQ-9174) was used to collect temperature values as a function of time.

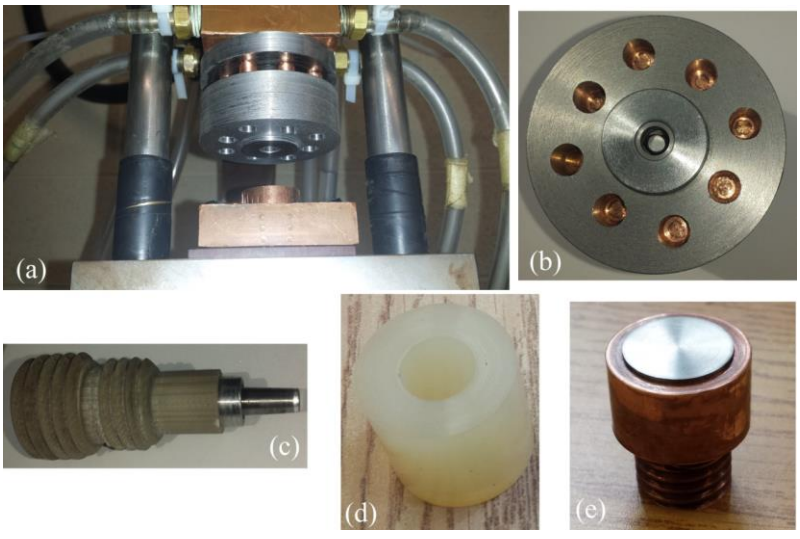

Figure 6.3. A set of photographs of die-less clinch tooling; (a) assembled tool set mounted on the test machine, (b) bottom view of the tooling showing the eight electrodes, (c) punch,(d) compression urethane spring, and (e) flat anvil.

6.3.2 Temperature measurement and current-temperature-time relationship

Due to difficulty to access the clinched region due to very high forming force in addition to the closed area, separate experiments were conducted by applying different levels of current for durations of 2 and 3 seconds and without applying forming force. A modified tool set was used for this purpose as shown in Figure 6.4.

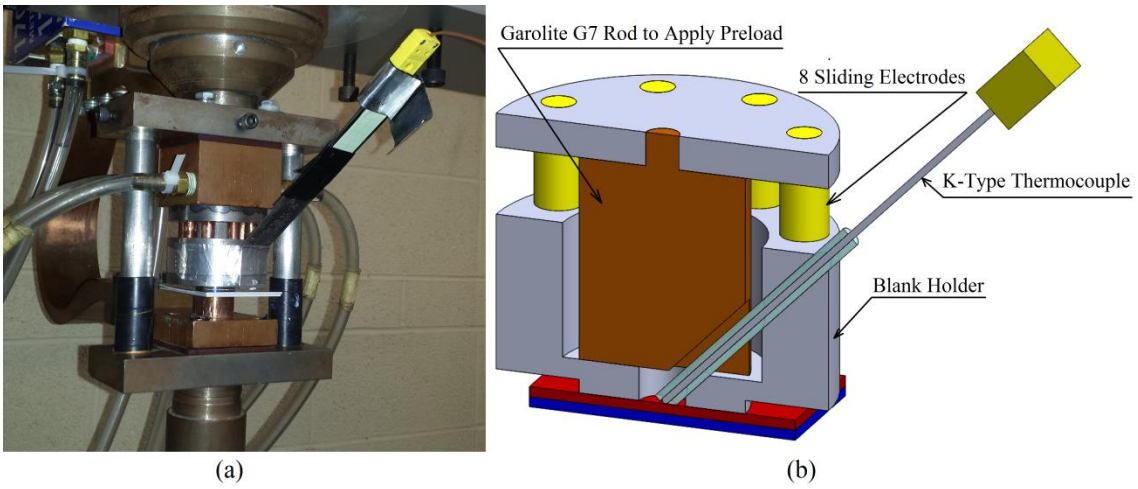

Figure 6.4. Modified tooling for temperature measurement, (a) tooling and thermocouple installation on the machine (b) a drawing of cut section though the tool set.

Figure 6.5 shows the temperature – time history from the thermocouple inserted into the punch cavity during the current application cycle as well as the off-current heat dissipation over about 120 second period. The sheet temperature rapidly increases with increasing applied current over the 2 or 3 second duration, as previously explained in Section 6.2. Moreover, the heat dissipates rapidly and especially in case of 15 kA current application in 3 seconds duration, and the temperature drops from 270°C to 100°C in about 15 seconds. It can be noted that the initial slope of temperature versus time curves

increases with the applied current. The current ramp cycles of 2 sec or 3 sec period result in a temperature increase in the ranges of 80°C - 175°C and 90°C - 270°C respectively. A prediction of change in the sheet temperature as a function applied current and time based on physical principles was not easily possible. Therefore, a regression equation based on experimentally measured peak temperature as a function of applied current and time period was obtained as follows:

$$T_{max} = \exp\left[2.923 + (0.12141I) + (0.2724t)\right] \qquad (6.6)$$

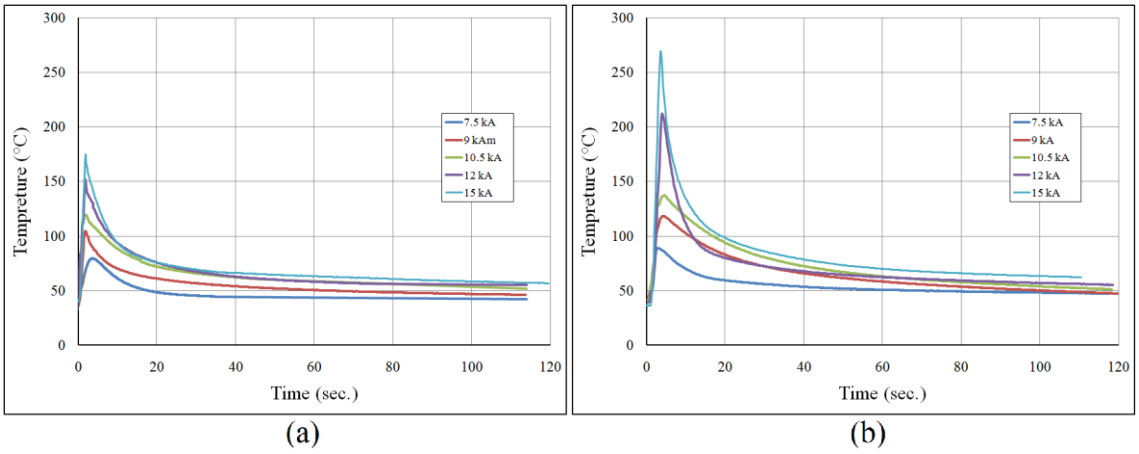

Figure 6.5. Curves show the temperature measurements for different heating cycles: (a) 2 Sec. resistance heating cycle and (b) 3 Sec. resistance heating cycle.

Figure 6.6 shows the measured maximum temperature T_{max} for different applied current values as solid lines. Also, included are dashed regression lines predicted by regression equation.

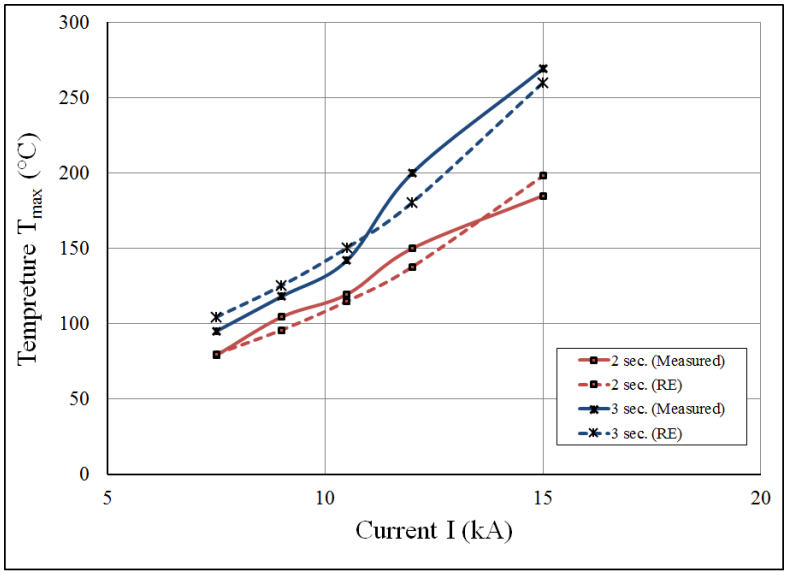

Figure 6.6. Measured and estimated maximum temperature versus applied current curves for two different time periods.

6.3.3 Hot die-less clinching process

The die-less clinching process can be divided into 5 stages as shown in Figure 6.7. Stage (i), depicted in Figure 6.7(i), involved installation of the two AA7075-T6 sheets between the punch and blank holder from the upper side and installation of flat anvil from the lower side. In stage (ii), the punch was moved downwards causing compression of the urethane spring which in turn applied a pre-clamping load of about 3 kN to the sheets. In stage (iii), currents of different magnitudes were applied as a linear ramp for 2 or 3 seconds. The current from the electrodes passed through the blank-holder causing local resistance heating of the two aluminum sheets. In stage (iv), the punch was moved downward at a speed of 30 mm/second until the desired maximum applied load was reached and the joint formation was completed. Finally, in stage (v), punch was moved upwards causing release of the clinched sheet pair. The loading and heating steps for a clinch cycle are shown schematically in Figure 6.8.

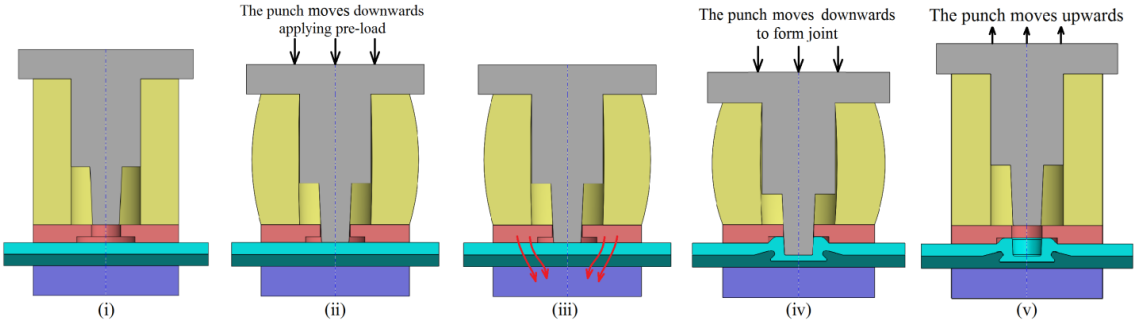

Figure 6.7. Schemes demonstrates the die-less clinch joining with application of electrical resistance heating.

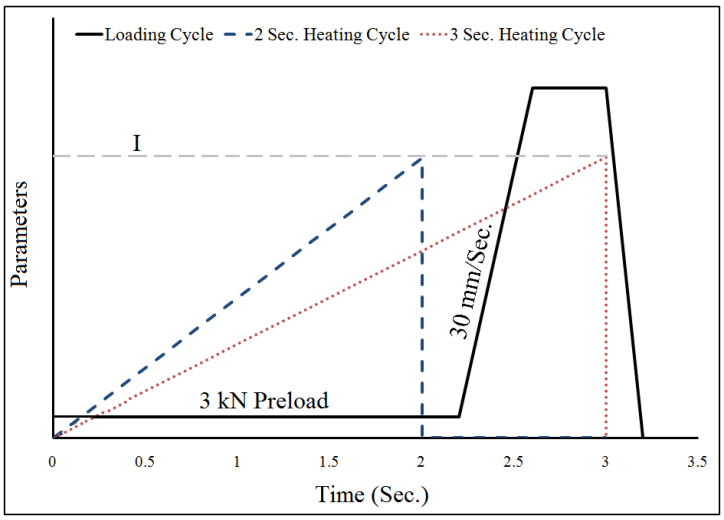

Figure 6.8. A schematic of punch forming force and applied current as a function of time.

In order to study the effect of different current application cycles on the flow of the material, various forming forces were applied to the two sheets. The clinched joints were subsequently cut transverse to the thickness at the center of the button and mounted using conventional optical metallographic methods of cold mounting in a polymeric resin. The mounts were then polished and etched to clearly reveal the geometry of the die-less clinches using a high magnification digital optical microscope (KEYENCE VHX-2000). A caustic etchant was used to reveal the microstructure of the clinched region. The

etchant consisted of a mixture of 10 gm sodium hydroxide (NaOH) diluted in 90 ml of distilled water and kept at 60°C in a water bath [1]. In order to obtain a good quality etch, the samples were subsequently immersed in Nitric acid of 50% concentration and washed in cold water. Finally, Vickers micro-hardness distribution was obtained to assess the local strengthening of the formed joint as a result of large plastic flow during die-less clinching. Optical microscopy (OM) and scanning electron microscopy (SEM) methods were utilized to study the microstructural characteristics of the clinched region.

6.3.4 Joint assessment using lap shear tests

Strength of the joints were obtained by single lap shear test using triplicate tests. For this purpose, rectangular strips of dimensions 25 mm width by 75 mm length were cut from AA7075-T6 aluminum sheet. Two strips were die-less clinched with an overlap of 25 mm to form one lap shear test sample. Mechanical characterization was carried out by using a computer-controlled universal MTS 100 kN servo-hydraulic testing system with a cross-head speed of 1mm/min until the two sheets were completely separated. The force and displacement data was continuously recorded during the test.

6.3.5 Design of experiments

The test matrix for design of experiments consisted of fixed parameters such as tool design parameters, the punch speed of 30 mm/sec, and a linear ramp for the applied current, whereas, the variable forming parameters were forming force in the range 40 kN - 70 kN, applied current in the range 7.5 kA - 15 kA, and heating times of either 2 or 3 seconds. The forming force was evaluated at four levels, current was evaluated at five levels, while the current duration was evaluated at two levels. Therefore, data from a test

matrix 40 tests in total was obtained in a full factorial orthogonal array as explained in Table 6.3. The measured data included temperature, interlock depth, neck thickness and joint shear strength.

Table 6.3. Levels of each factor in the full factorial design of experiments.

Factors		Levels					Unit
		1	2	3	4	5	
Heating Cycle	Current I	7.5	9	10.5	12	15	kA
	Time t	2	3	-	-	-	Sec.
Loading Cycle	Forming Force F	40	50	60	70	-	kN

6.4 Results and discussion

6.4.1 General Joint Characteristics

Figure 6.9 shows photographs of punch and anvil sides of a typical successful die-less hot clinched joint in AA7075-T6. Figure 6.10 shows a family of forming force versus punch stroke traces of hot die-less clinching joints for diffrent applied currents of 2 or 3 seconds duration. The traces are compared with the one at room temperature where no current was applied. It should be noted that the room tempreture clinching did not result in formation of interlock as discused in more detail later. Figure 6.11 shows a schematic drawing of a well-formed interlock. It can be noted that the main geometric parameters include the neck thickness N, the interlock depth U, and the bottom thickness X-parameter. By increasing the current, the forming curves tended to decrese in term of forming force. In fact, the combined effect of increassed applied current and current application period resulted in a significant decrease in the forming force. Similar to the

earlier die-less clinching work on AA7075-O sheet at room temperature by the present authors [1], the clinching process can be described in terms of 5 stages as shown schematically in Figure 6.12. In stage I, as the punch was moved from its stationary position, an increasing prssure was applied to the compression spring resulting in variable clamping of the sheet materials between the blank holder and flat anvil as shown in Figure 6.13. Stage II started when the punch came in contact with the sheets and exerted a force on the sheet. The initial punch penetration into the upper sheet was reflected in the slope of the punch force versus punch stroke curve. At this stage, the material flow occurred in axial direction (i.e., in the same direction as the punch) as well as in radial direction by friction. During stage III, there was significant increase in the flow of the material in the radial direction, and a high friction between two sheets and large rotation in the clinched region resulted in interlock formation. Stage IV started when the top surface of the punch-sided sheet came in contact with the top of the blank holder groove, and thus a large restriction in material flow occurred in the axial direction resulting in further development of the interlock. In stage V, the radial flow of the material increased significantly that resulted in much increase in geometric interlock. It is to be noted in Figure 6.10 that stage IV was a transiant stage between stage III and stage V. Furthermore, the difference between stages III and V in terms of the slope of punch force versus punch stroke curve becomes more obvious with increasing current and time due to increased material flow. Finally, due to retraction of the punch, the forming force started to decrease. The change in the unloading slope can be attributed to the elastic recovery or

springback where the punch continued to move while the urethane spring was still in compression.

Figure 6.9. Photographs of a successful hot clinched joint. The clinching conditions were 7.5 kA, 3 sec, and 60kN.

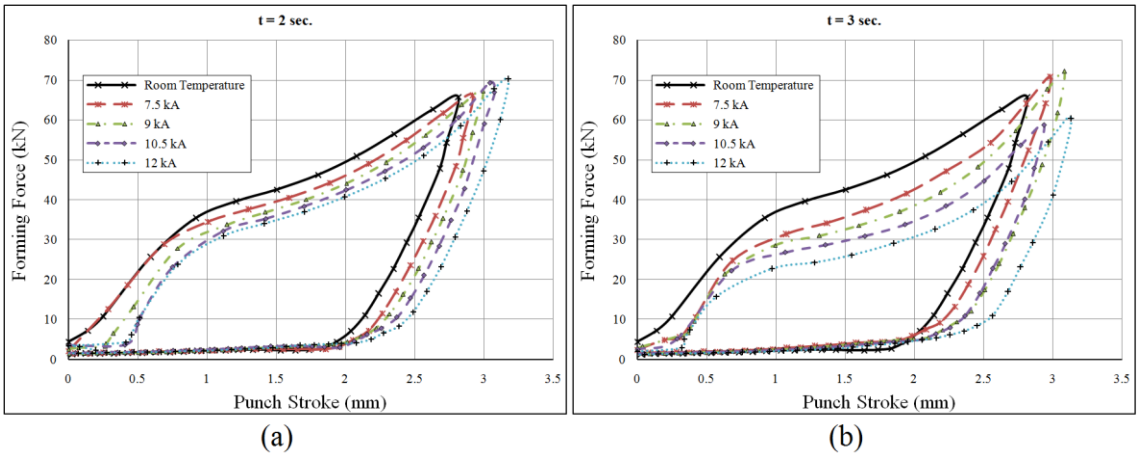

Figure 6.10. Punch force versus punch stroke curves for different applied current cycles.

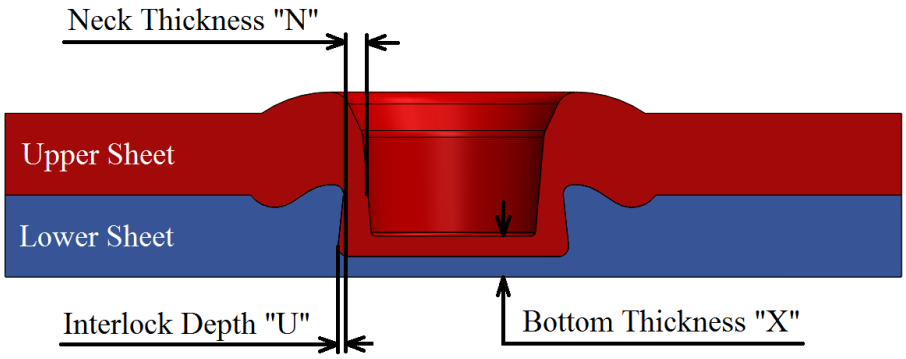

Figure 6.11. A schematic drawing of through-thickness cross-section of a die-less clinch showing main geometric parameters.

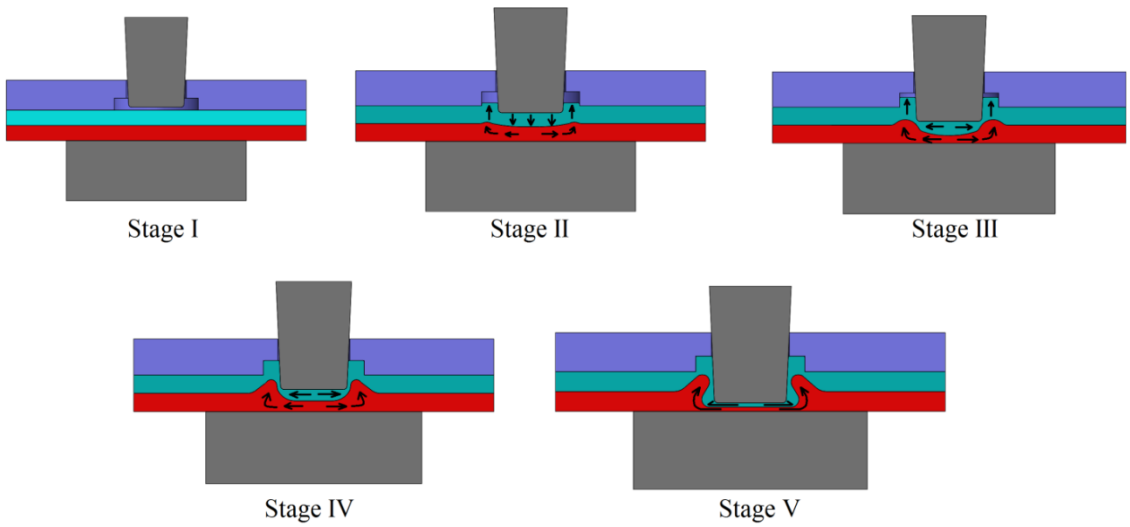

Figure 6.12. A schematic illustration of material flow during different stages of hot die-less clinching process from reference [1].

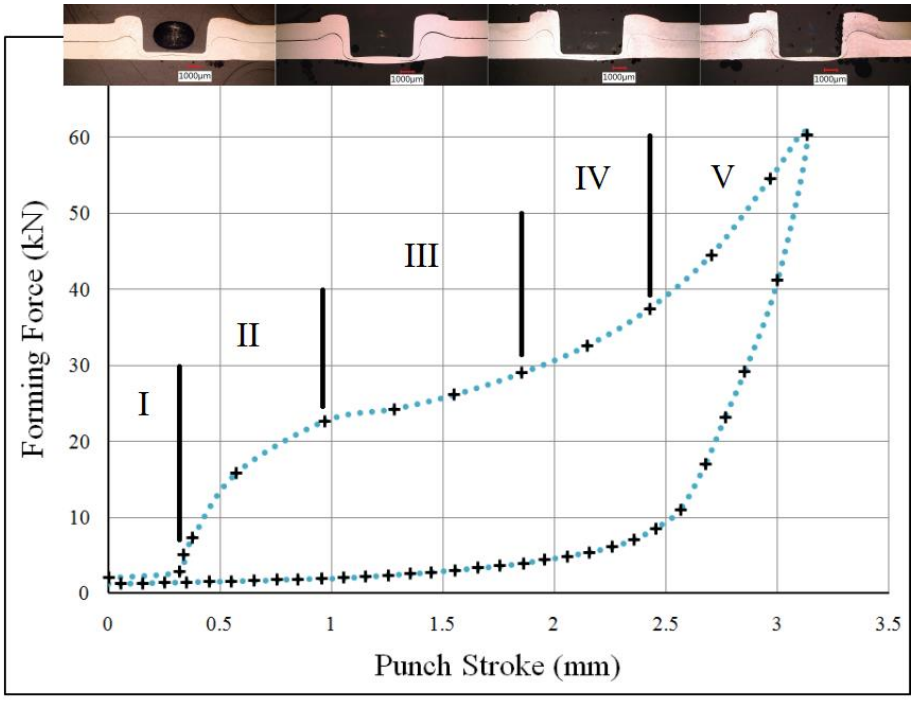

Figure 6.13. A typical forming curve and associated forming stages (I=12 kA and t=3 sec).

Figure 6.14(a-c) shows a set of optical images of through-thickness mounted cross-sections of the die-less clinched joints at different punch strokes. The photographs have been arranged in three separate columns and four rows for the ease of interpretation. Each column (from a to c) refers to a certain forming conditions, room temperature, and two applied current/time histories (12 kA for 2 sec and 12 kA for 3 sec) respectively, while each row corresponds to a specified forming force utilized in the test. It is to be noted that the room temperature forming did not lead to formation of interlock at any of the applied forming forces. In contrast, the use of localized electrical resistance heating resulted in the typical "S" shape of the wall interface indicative of the formation of interlock. A lower force was required to apply the same X-parameter as the temperature

of the sheet increased. Noticeably, at the highest forming force, the radial flow of the material increased significantly for the 3 sec period compared to 2 sec period which in turn led to a larger amount of interlock.

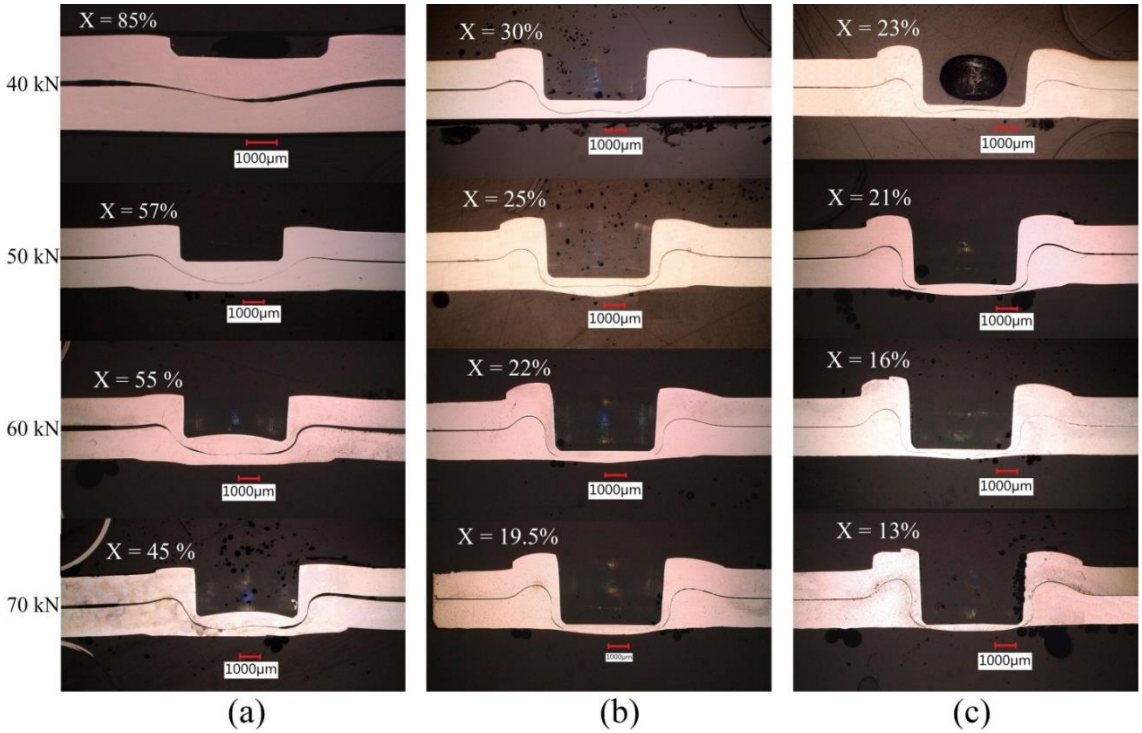

Figure 6.14. Optical images of cut cross-sections through die-less clinched joint for, (a) room temperature, (b) ERH at 12 kA for 2 Sec., and (c) ERH at 12 kA for 3 Sec.

6.4.2 Microstructure and locking mechanisms

Figure 6.15 shows optical micrographs for undeformed AA7075-T6 sheet, (a) without application of current (no heating), and (b) after subjecting to an applied current of 15 kA for 3 sec in 3 repeated cycles. The unheated sample exhibited pancake shaped grains in the grain size range 38 µm- 82 µm. In contrast, the heated sample showed an average grain size range of 34 µm - 94 µm. This result as well as the short heating time

indicated that no recrystallization occurred. For the short times involved, it is more likely that recovery occurred and the dislocation density was reduced and could be a source of enhancement in formability.

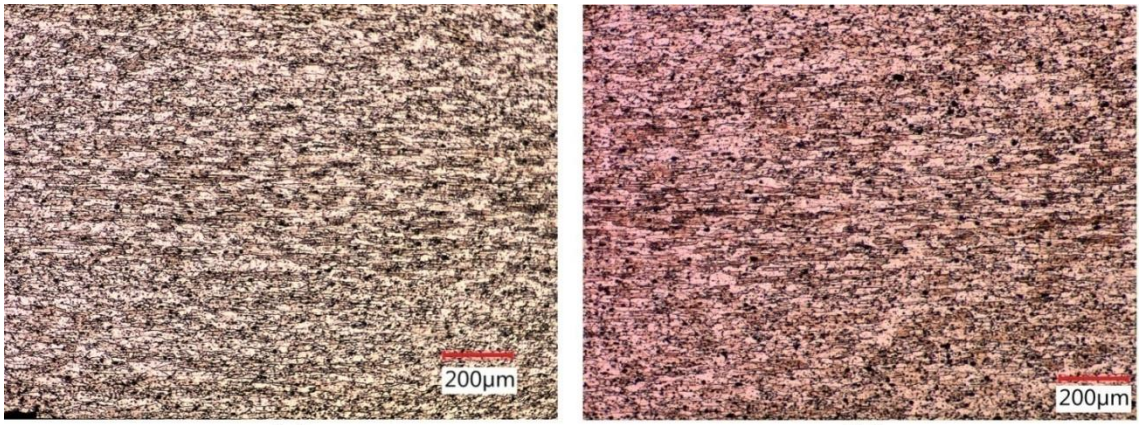

Figure 6.15. Optical micrographs show (a) the initial unheated AA7075-T6 sheet, and (b) after subjecting to 3 repeated cycles of an applied current of 15 kA for 3 sec.

Figure 6.16 presents a cross-section through die-less clinched joint. Along the interface between the two sheets, two locking zones can be identified; the bottom of the joint or zone A and the wall of the joint or zone B. Also, there are three possible locking mechanisms. The first mechanism is a force locking mechanism due to application of force and friction between two sheets. The second mechanism is a form locking mechanism due to the formed interlock geometry. Final mechanism is material locking. Cold welding is an example of material locking mechanism. The force as well as the form locking mechanisms are more likely to be present at zone B. The occurrence of material locking mechanism is more probable at zone A due exposure of this zone to high forming force for relatively long time accompanied with an increase in temperature that causes a

close contact between the combined materials. An indistinguishable boundary exists between the two sheets in zone A, as shown in the bottom row of Figure 6.14(b,c), which confirms that material locking mechanism operates in this area due to heating and relatively high applied force over small area. It is to be noted that the measurement of neck thickness N and interlock depth U could not be easily made in the hot clinched samples as shown in Figure 6.16(b). Therefore, to obtain this data, the upper sheet was mechanically rotated to break the material locking as shown in Figure 6.16(a).

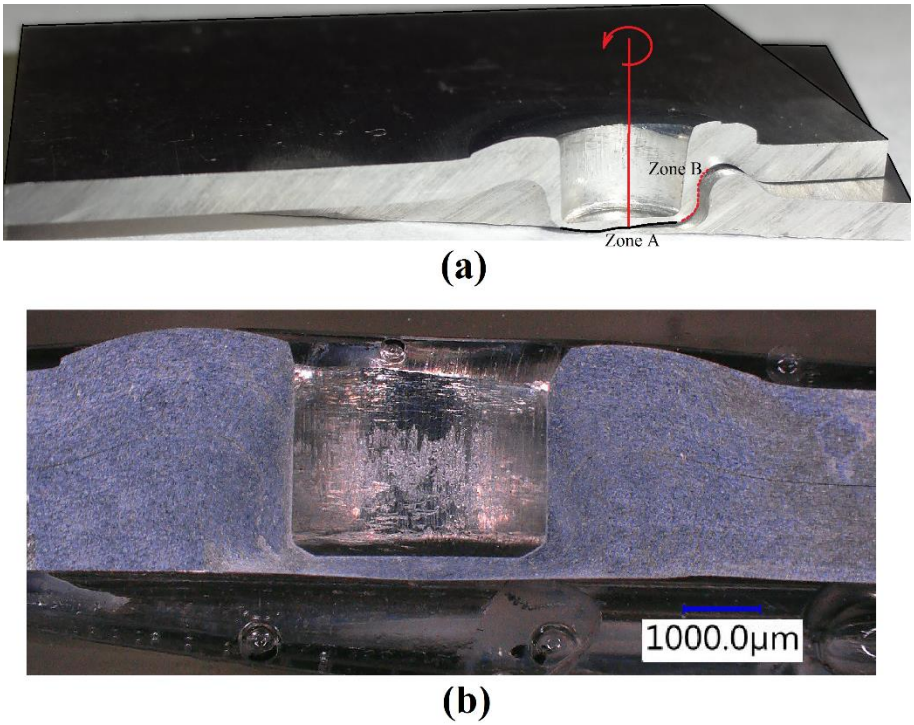

Figure 6.16. Cross-sections through die-less clinched joint showing; (a) the two zones of locking mechanisms (b) the unclear interface between the two sheets.

Figure 6.17(a) shows optical micrographs of a through-thickness cross-section of a fully formed joint. Figure 6.17(b-e) represents higher magnification optical images

from 4 different sub-regions of the image in Figure 6.17(a). In the upper right sub-region of Figure 6.17(b,c), the microstructure is changed from pancake grain structure at the top undeformed region to more equiaxial grains closer to the interface between two sheets. This grain shape change is likely due to the flow of the material in radial direction when the top surface of the upper sheet comes in contact with the top surface of the blank holder groove. The grains of the upper sheet are highly rotated and elongated in the neck region of Figure 6.17(d) due to deformation to form the wall of the joint but remain less rotated away from the interface. In contrast, the grain of the lower sheet are highly rotated near the interlock area and become equaixed grains in the nearby region. However, the lower region at the bottom of the joint of Figure 6.17(e) shows equiaxed grains at the top and bottom and a mixture of highly elongated and equiaxed grains at the interface. It is likely that strain-induced grain recrystallization occurred in this region during hot clinching.

Figure 6.18(a-d) shows the SEM micrographs from the bottom of a die-less clinched joint formed by applying 12 kA ramp for 3 sec duration, under the same conditions as in Figure 6.17. The material locking is clearer at the bottom of the joint and further confirms the possibility of diffusion bonding between the sheets in zone A due to a combination of heat and large compressive forces. The darker regions in the SEM images are likely associated with matrix-precipitate decohesion of the stringer-like grain boundary precipitates on highly elongated grain boundaries and subsequent linkage of such voids. There is also evidence of void formation from larger constituent particle break-up at large strains in other regions.

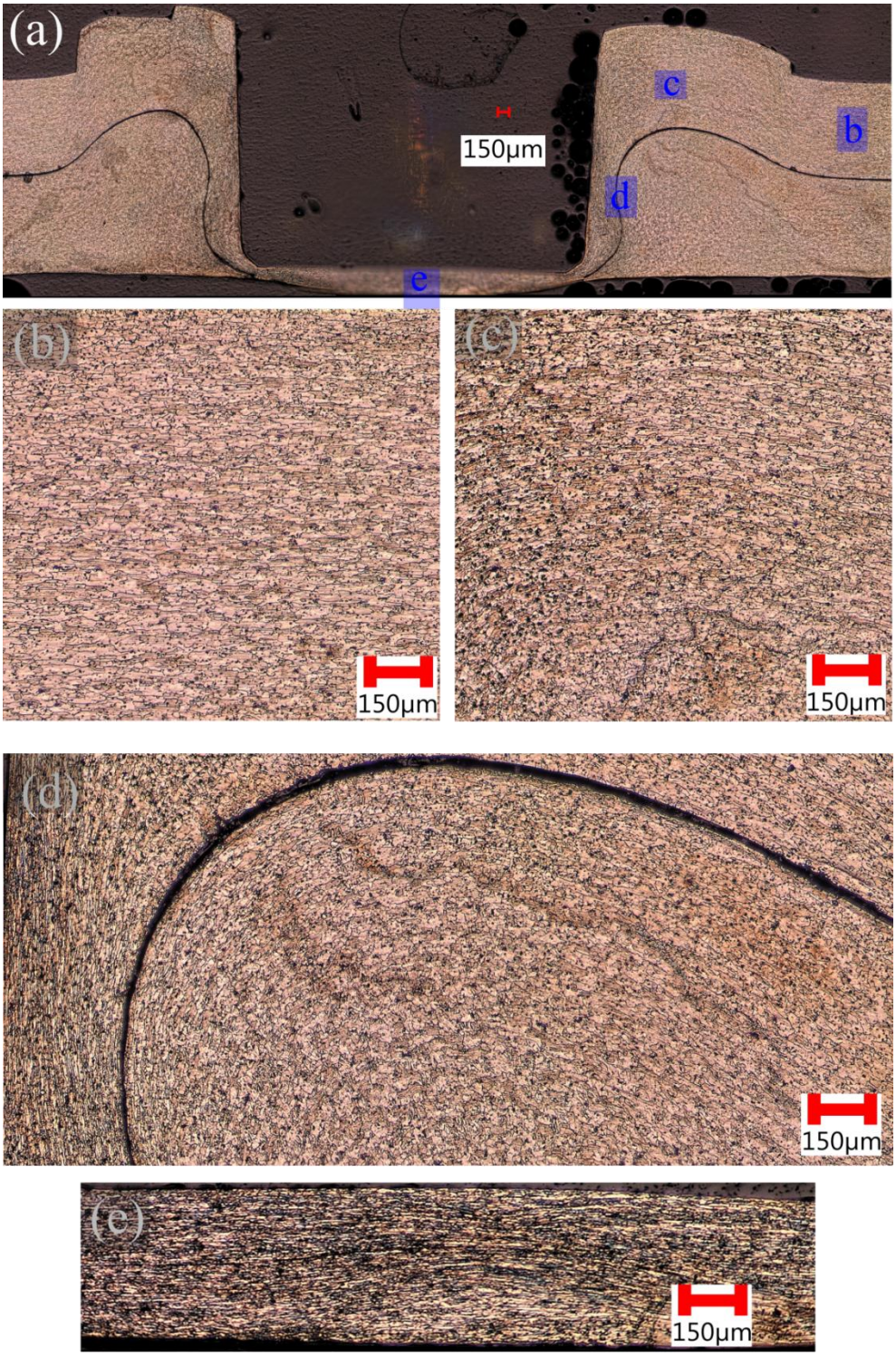

Figure 6.17. Optical micrographs from a die-less clinched joint formed by applying a current of 12 kA for 3 sec.

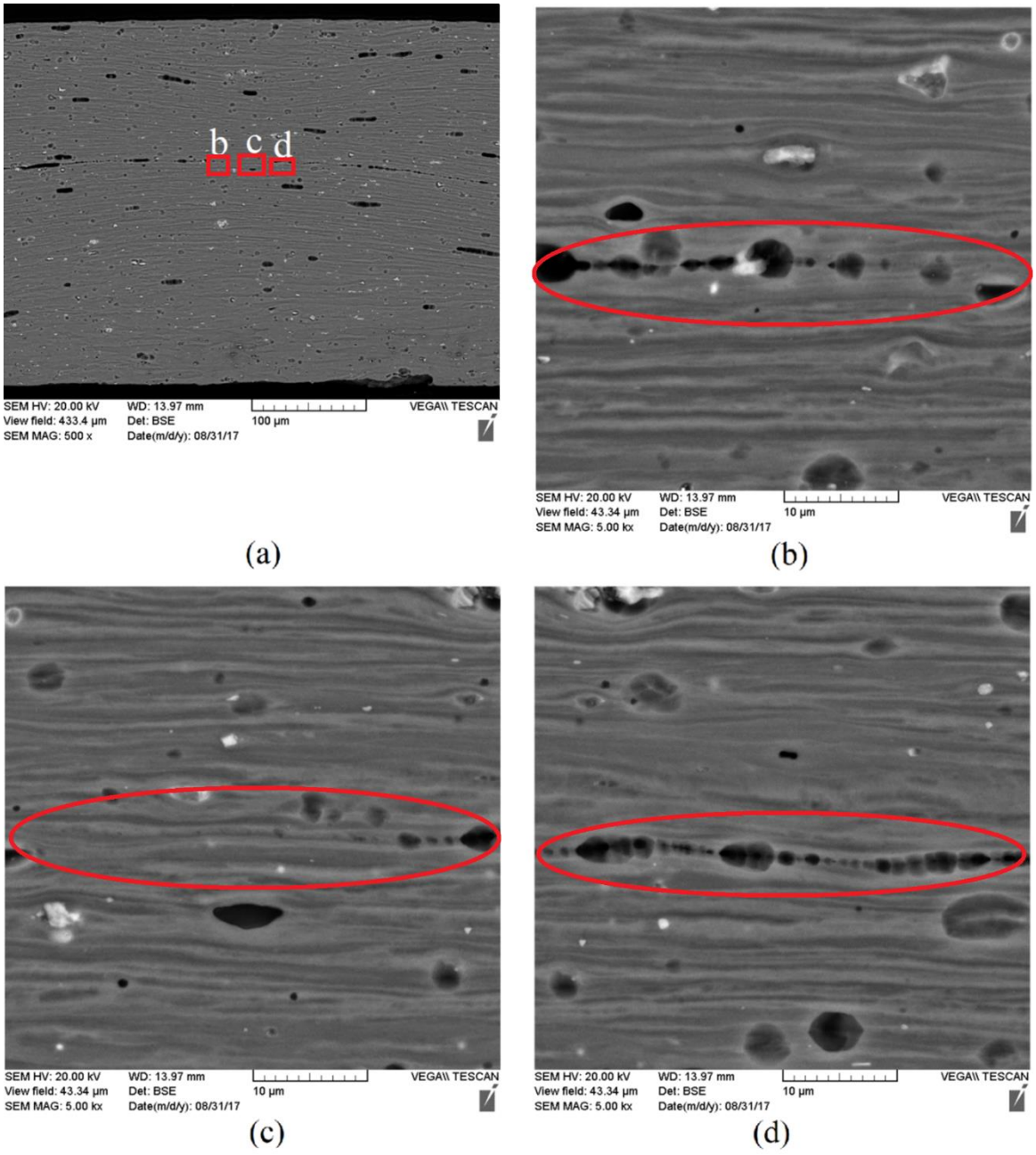

Figure 6.18. SEM micrographs showing the microstructure from the cross-section of a die-less clinched joint formed at12 kA ramp in 3 sec), (a) overall image from the bottom of the joint, and (b-d) additional larger magnification images from the sheet interface region (marked with a red ellipse) at the bottom of the joint.

6.4.3 Micro-hardness measurements

As-received AA7075-T6 sheets showed a relatively large micro-hardness values of 175 VH. However, the sample subjected to a heating cycle of 15 kA for 3 seconds exhibited a slight drop in the micro-hardness to 165 VH. Figure 6.19 demonstrates a map of Vickers hardness distribution through cross-section of a die-less clinched specimen from a forming force of 70 kN and a ramp heating cycle of 12 kA of 3 second duration. As expected, the micro-hardness in a given region increased with increasing plastic deformation (or plastic work). The sample exhibited the highest micro-hardness values in the punch corner radius region as well as at the neck region. The increase in micro-hardness of the highly deformed region is not as much as expected from the very large plastic deformation associated with die-less clinching. Overall, the low micro-hardness values appear to support the existence of a dislocation recovery process from rapid electrical resistance heating of the AA7075-T6 sheets prior to clinching.

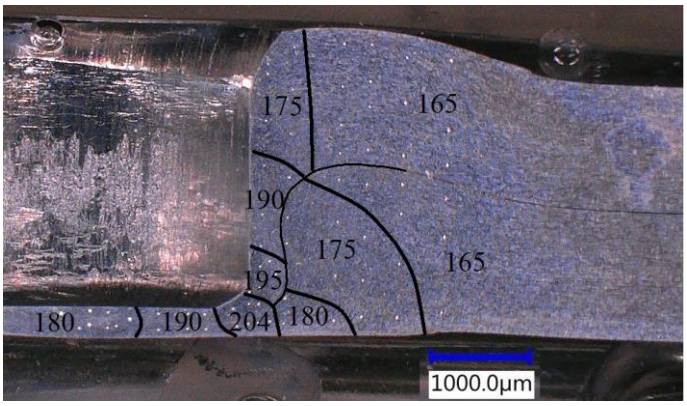

Figure 6.19. An optical image of a hot die-less clinch joint (formed by 60 kN, 15kA, and 3 sec. heating duration) showing superimposed Vickers micro-hardness contours.

6.4.4 Forming parameters and clinch characteristics

This section presents the effect of various clinch forming process parameters on geometrical characteristics of the die-less clinches. Figure 6.20 shows the effect of applied current and time on the bottom thickness of the joint (i.e., X-parameter) versus forming force curves. In general, there is a progressive decrease in the X vs. forming force curves with increasing current value and time. This is consistent with increased heat input and higher sheet temperatures at higher currents and longer duration, and therefore, improved formability of the sheet metals as mentioned earlier in Section 6.4.2. The flow of the material, and especially the radial flow at the top surface of the upper sheet, increases at higher temperatures causing a proportional increase in the interlock depth versus forming force curves as shown in Figure 6.21. Consequently, a slight reduction in the neck thickness N vs. forming force curves, occurs as shown in Figure 6.22. Any reduction in N value can cause premature failure of the joint at the neck during service. Therefore, an increasing applied current and its duration can also have a deleterious effect on clinch strength in some cases. In terms of increasing forming force, the geometric interlock was increased but the bottom and neck thickness values were decreased.

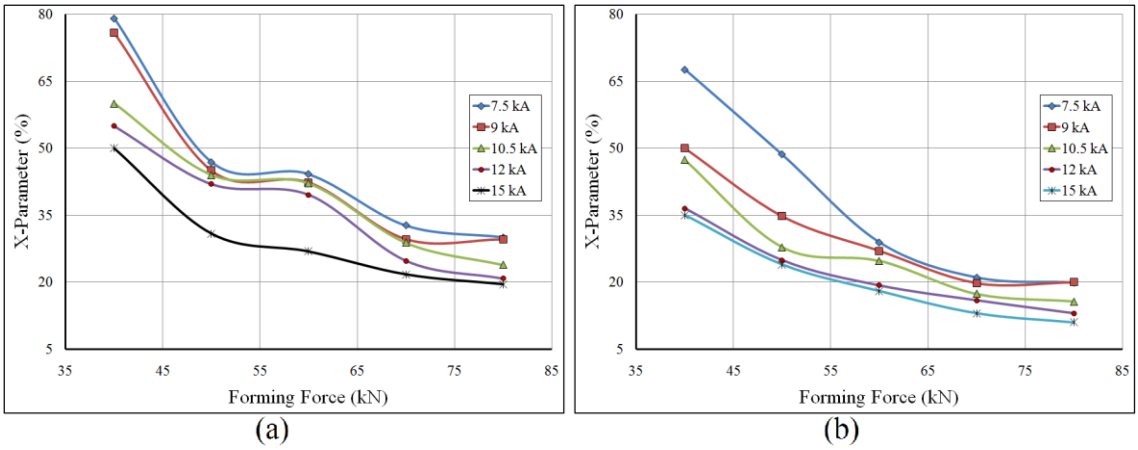

Figure 6.20. Effect of applied current on the bottom thickness of the joint (X parameter) for current durations of; (a) 2 sec., and (b) 3 sec.

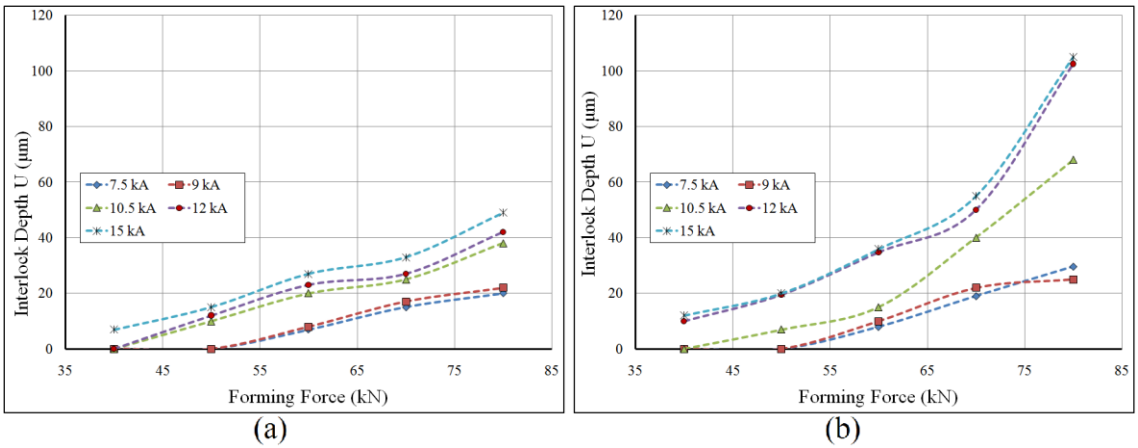

Figure 6.21. Effect of applied current value on interlock depth U for durations of; (a) 2 sec., and (b) 3 sec.

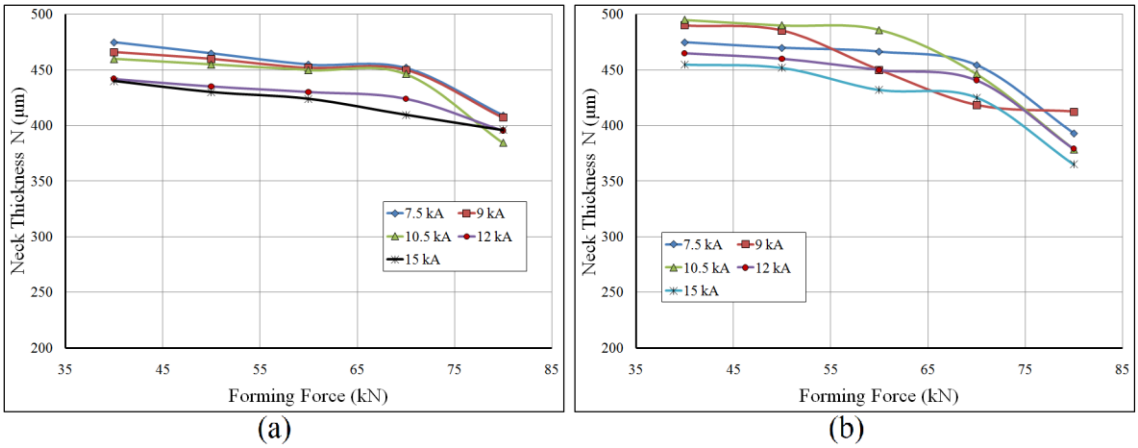

Figure 6.22. Effect of applied current on neck thickness N of the joint for current durations of; (a) 2 sec., and (b) 3 sec.

6.4.5 Joint strength and failure modes

The strength of the clinched joint is dependent on the cumulative force response of all locking mechanisms. A hot clinch joint exhibited geometric (form and force) and material locking, all or some, depending upon the process parameters. Table 6.4 summarizes the results from of the parametric study involving 5 different applied currents, 2 current durations, and 4 different forming forces in terms of joint strength and formed locking mechanisms. Note that a zero value for the joint strength refer to failure to form a successful joint. Figure 6.23 demonstrates the force – displacement traces obtained from single lap shear tests on various die-less clinched joints formed under different forming conditions. The traces show a rapid linear increase in force with increasing displacement followed by a drop in the force. This drop was due to failure of material locking mechanism at the bottom of the joint. However, the force continued to increase slowly with increased displacement due to the existence of the geometric interlock. The

punch-sided sheet tries to pull away from the anvil-sided sheet, and, as a result, the joint stiffness decreases. Eventually, a crack initiates that results in drop in the force-displacement curve. As the crack propagates, the force continues to decrease until a complete separation of the joint occurs. The strength of the joint increase with increasing the forming conditions (applied current, time, and forming force) due to increased material flow and material locking. However, for excessive applied current and forming force values, such as the case of 70 kN forming force with 15 kA heating current for 3 sec, significant reduction in the neck thickness occurred leading to a drop in the joint strength, as shown in Figure 6.23(b). Three failure modes were observed in single lap shear tests as shown in Figure 6.24; button failure, unbuttoning failure (after large plastic deformation) and a combination of unbuttoning failure by plastic deformation and fracture. Unbuttoning failure occurs mainly on joint with relatively small geometric interlock that allows easy slip over the internal surface of the anvil-sided sheet casing failure of the joint. Smaller geometrical interlock formed at lower punch stroke values (i.e., at lower forming force values). Joints formed under extremely large plastic deformation (i.e., at very high forming force values) were associated with significant reduction in the neck thickness N that led to a reduction in load carrying capacity of the joint and thus neck fracture (i.e., button failure mode). The optimum values of neck thickness and interlock depth resulted in the highest joint strength. The failure mode in this case was a combination of plastic deformation and fracture of the button such as for 70 kN forming force with applied current of 12 kA and current duration of 3 seconds.

Table 6.4. A summary of joint strength, geometrical and material locking mechanisms from single lap shear as well as cut samples for hot clinch joints obtained using different applied currents, current durations and forming forces.

I (kA)	F (kN)	2 sec. current duration				3 sec. current duration			
		S (kN)	Std. Dev.	Geom. Interlock	Material locking	S (kN)	Std. Dev.	Geom. Interlock	Material locking
7.5	40	0	0	No	No	0	0	No	No
	50	0	0	No	No	0	0	No	No
	60	0.85	0.06	Yes	No	1.1	0.28	Yes	No
	70	2	0.11	Yes	No	2.15	0.28	Yes	No
9	40	0	0	No	No	0	0	No	No
	50	0	0	No	No	0	0	No	No
	60	0.95	0.3	Yes	No	1	0.1	Yes	No
	70	2.45	0.05	Yes	No	2.80	0.18	Yes	Yes
10.5	40	0	0	No	No	0	0	No	No
	50	0	0	No	No	1	0.1	Yes	No
	60	1.1	0.03	Yes	No	1.98	0.05	Yes	Yes
	70	2.81	0.07	Yes	Yes	3.16	0.04	Yes	Yes
12	40	0	0	No	No	1.82	0.07	Yes	No
	50	0.98	0.1	Yes	No	2.6	0.08	Yes	Yes
	60	2.51	0.06	Yes	Yes	3.53	0.06	Yes	Yes
	70	3.17	0.04	Yes	Yes	3.8	0.04	Yes	Yes
15	40	0.97	0.06	Yes	No	2.14	0.02	Yes	Yes
	50	2.23	0.15	Yes	Yes	2.69	0.09	Yes	Yes
	60	2.67	0.061	Yes	Yes	3.57	0.06	Yes	Yes
	70	3.18	0.06	Yes	Yes	3.58	0.09	Yes	Yes

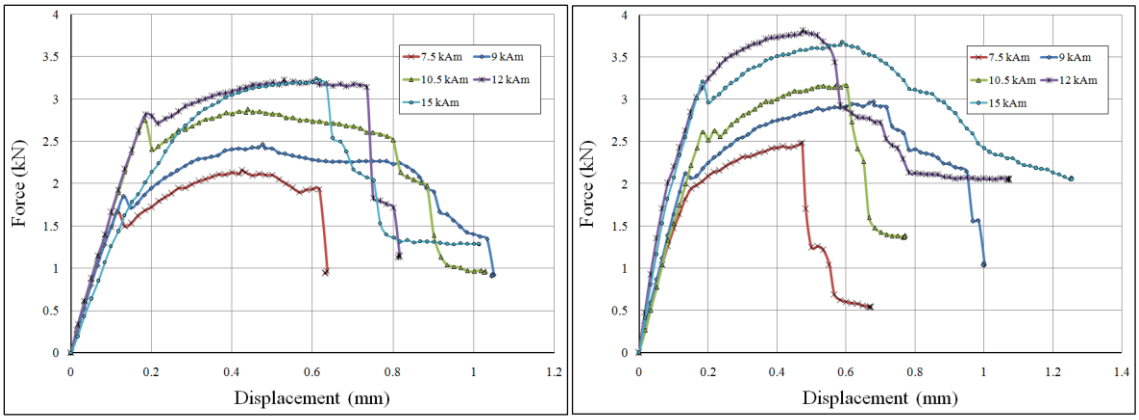

Figure 6.23. Force – displacement traces obtained from single lap shear tests on various die-less clinched joints formed with 70 kN force using different applied currents for durations of; (a) 2sec., and (b) 3 sec.

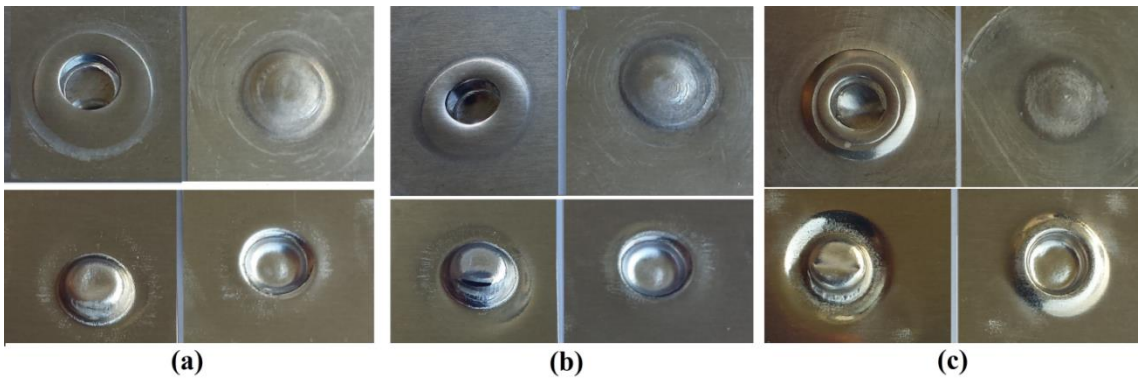

Figure 6.24. Various failure modes exhibited by different lap shear test specimens of die-less clinched joints, (a) unbuttoning failure, (b) combined unbuttoning and neck failure, and (c) button failure.

6.5 Summary and Conclusions

The paper presents a new approach for die-less clinching of high strength low-formability aluminum sheet materials using an electrical resistance heating system to locally heat the sheets prior to clinching. A new tooling design was developed to rapidly

heat by applying current over a short 2-3 second period to AA7075-T6 aluminum sheets prior to clinching. The study includes an investigation of the effect the main clinching parameters, namely, forming force, applied current and time of the electrical cycle on material flow and geometric interlock characteristics. The material flow under different electrical resistance heating cycles as well as the accompanying change in interlock characteristics has been investigated using optical and scanning electron microscopy and micro-hardness measurements of the cut cross-sections of the joints. Lastly, the shear strength and associated failures modes of the joint have been assessed by using in-plane single lap shear tests. The following conclusions have been drawn from the die-less clinching study:

1. Die-less clinching of AA7075 aluminum sheet in the peak-aged (T6 temper) condition has been successfully achieved using a rapid electrical resistance heating system. Electrical resistance heating can be used to significantly enhance clinch-formability of AA7075-T6 sheet that is hard to form at room temperature.
2. Three different locking mechanisms in die-less clinching of AA7075-T6 sheet have been identified, conventional form and force locking mechanisms in the neck region, as well as a new mechanism of material locking at the bottom region of the joint.
3. The failure modes in hot die-less clinching are affected mainly by the geometric interlock. However, the material locking affects the force-displacement behavior of the joint as it offers a resistance to the joint separation by increasing the required force to fail the joint. However, it also results in secondary yielding.

4. The strength of the hot die-less clinched joint increased by 16 %, 21%, 11%, 19%, and 14% respectively when formed by applying a forming force of 70 kN, a current of 7.5 kA, 9 kA, 10.5 kA, 12 kA, and 15 kA respectively over a period of 3 seconds compared with period of 2 seconds.

References

[1] M.K.S. Atia, M.K. Jain, Die-less Clinching Process and Joint Strength of AA7075 Aluminum Joints, Thin-Walled Structures Under Press (2017).
[2] F. Lambiase, A. Di Ilio, A. Paoletti, Joining aluminium alloys with reduced ductility by mechanical clinching, The International Journal of Advanced Manufacturing Technology 77(5-8) (2015) 1295-1304.
[3] F. Lambiase, Clinch joining of heat-treatable aluminum AA6082-T6 alloy under warm conditions, Journal of Materials Processing Technology 225 (2015) 421-432.
[4] F. Lambiase, A. Di Ilio, Damage analysis in mechanical clinching: experimental and numerical study, Journal of Materials Processing Technology 230 (2016) 109-120.
[5] X. He, Y. Zhang, B. Xing, F. Gu, A. Ball, Mechanical properties of extensible die clinched joints in titanium sheet materials, Materials & Design 71 (2015) 26-35.
[6] R. Neugebauer, C. Kraus, S. Dietrich, Advances in mechanical joining of magnesium, CIRP Annals-Manufacturing Technology 57(1) (2008) 283-286.
[7] K. Zhou, P. Yao, L. Cai, Constant current vs. constant power control in AC resistance spot welding, Journal of Materials Processing Technology 223 (2015) 299-304.
[8] D. Dickinson, J. Franklin, A. Stanya, Characterization of spot welding behavior by dynamic electrical parameter monitoring, Welding Journal 59(6) (1980) 170.
[9] W. Tan, Y. Zhou, H. Kerr, S. Lawson, A study of dynamic resistance during small scale resistance spot welding of thin Ni sheets, Journal of Physics D: Applied Physics 37(14) (2004) 1998.
[10] R. Holm, Electric Contacts: Theory and Application. 4th, New York: Springer-Verlag.

Chapter 7

Discussion

The research presented in this thesis consisted of experimental and numerical studies of joining of high-strength, precipitation-hardenable aluminum alloy AA7075 in different temper states by [i] conventional clinching and [ii] die-less clinching, both at room temperature, and [iii] die-less clinching at higher temperatures. The thesis was prepared in a 'sandwich' format and consistent of 5 separate journal papers in Chapters 2-6. In this chapter some of the common elements of all the experimental and simulation studies reported in Chapters 2-6 are discussed first. This is followed by a specific discussion pertaining to each of studies reported in Chapters 2-6.

7.1 Material anisotropy

In sheet forming, the material hardening behavior as well as the plastic anisotropy (typically represented by r values) of sheet metals play an important role in determining the amount of local plastic deformations. While extensive consideration was given to the work hardening behavior of AA7075 sheets in various tempers, and especially the applicability of suitable hardening laws from the literature, limited information about plastic anisotropy of the sheet was provided and discussed in the papers. Further, the deformation behavior of the sheet was assumed to be isotropic in all of the FE models of conventional and die-less clinching. It is to be noted that inclusion of plastic anisotropy was indeed considered at the beginning of the research but the experimental uniaxial stress-strain data that was obtained from samples tested in 3 different directions with respect to the rolling direction (i.e., RD, 45 and TD) did not support a strong argument for inclusion of anisotropy. Since there were several hundred FE simulations involved altogether, it was decided to choose an

axisymmetric model and an isotropic material to save on the computational time, but without impacting on the general nature of the results. For completeness, and in support of the choices made regarding plastic anisotropy in the modeling work, this data is present here as well as information gathered from the literature about the plastic anisotropy of AA7075 sheet.

Figures 7.1. 7.2, 7.3 and 7.4 show the stress-stain curves in the 3 directions for AA7075 sheet in the peak aged (T6 temper), partial annealed, fully annealed (O temper), and solution heat treated (W temper) states respectively. It can be noted that the change in the flow curve relatively small except in the case of W-temper where there is a considerable change in the failure strain as shown in Figure 7.4.

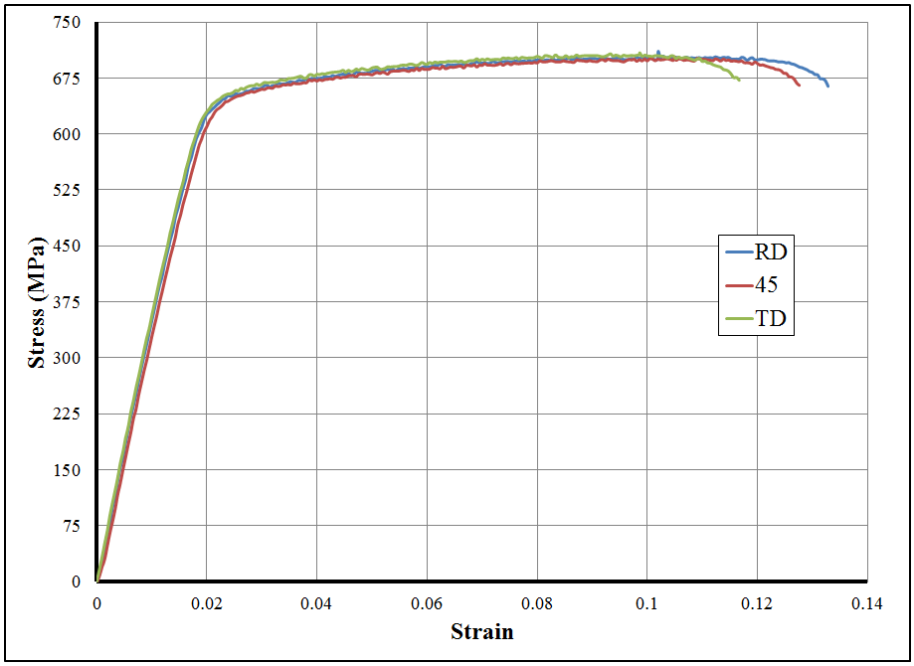

Figure 7.1. Uniaxial true stress-strain curves for AA7075-T6 sheet in different directions.

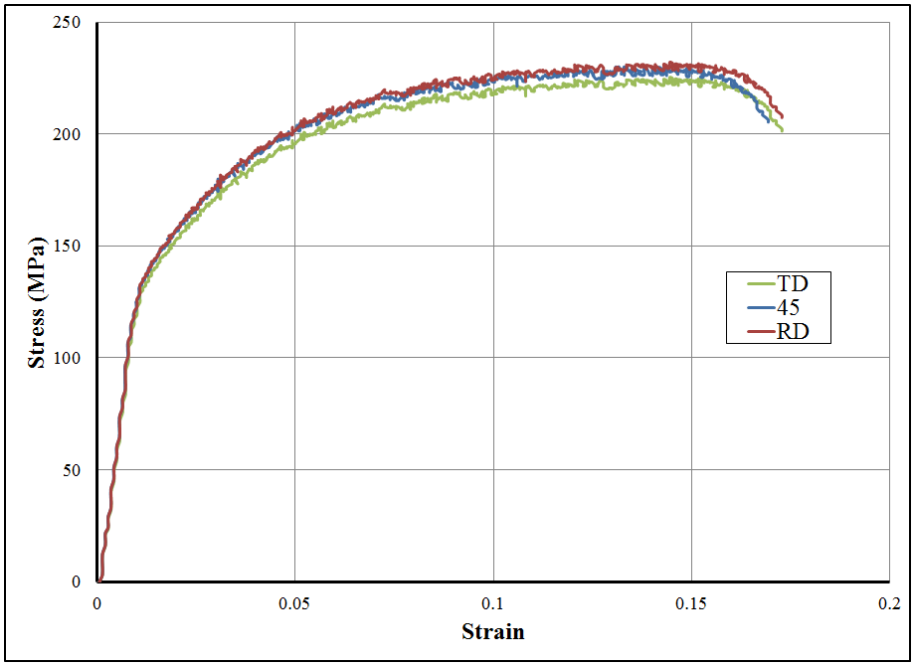

Figure 7.2. Uniaxial true stress-strain curves for partially annealed AA7075 sheet in different directions.

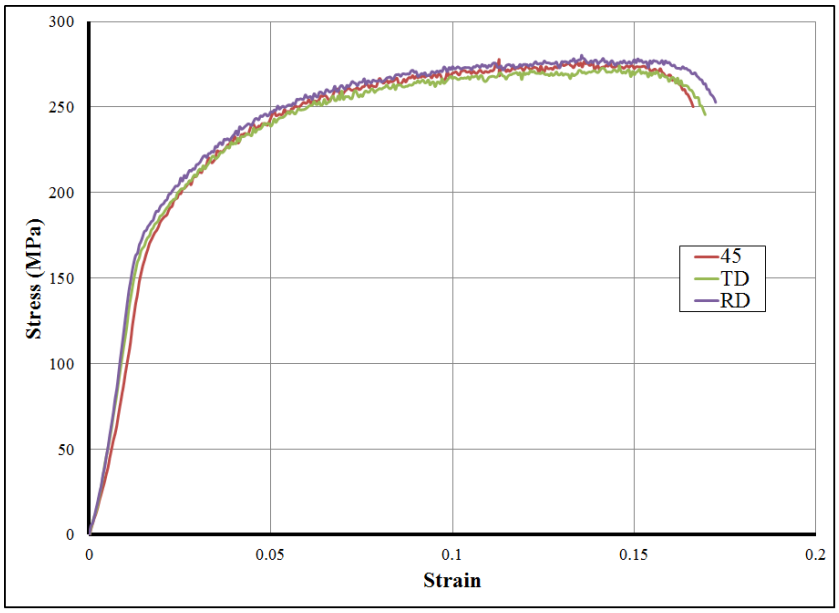

Figure 7.3. Uniaxial true stress-strain curves for fully annealed AA7075 sheet in different directions.

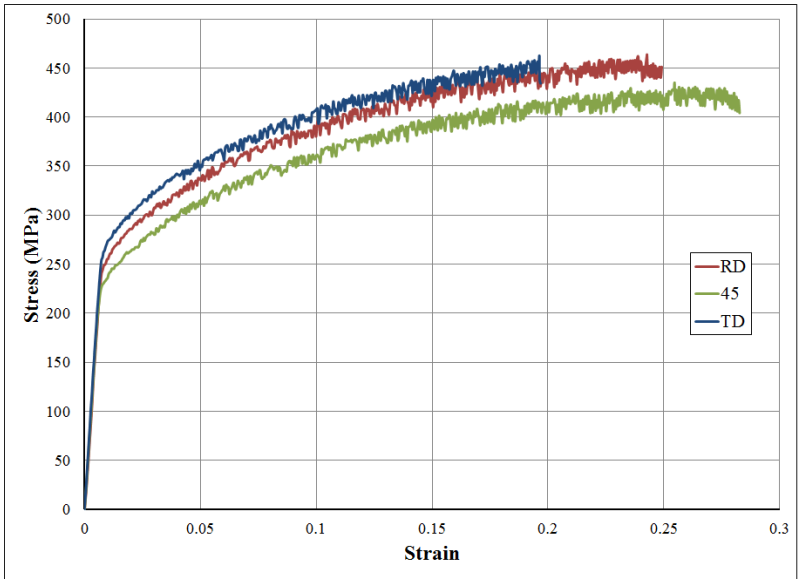

Figure 7.4. Curves show stress-strain curves for water-quenched AA7075-W sheet in different directions.

As per the review of the literature, Rahmaan et. al. have characterized the anisotropy behaviour of AA7075-T6 sheet in terms of different r values in shear as well as in tensile tests [1]. The results showed that AA7075-T6 sheet exhibited minimal anisotropy in the stress response (see Figure 7.5 below). The r-values in the RD, 45^0 and TD directions were 0.78, 0.95, and 1.34 respectively with a normal anisotropy ($\bar{r}$) of 1.005. Esmaeilpour et. al. [2] presented the normalized flow stress and r-value data for annealed AA7075-O sheet. Both the normalized flow stress and r-values varied marginally in the range 0.98-1 and 0.75 - 0.98, as shown in Figures 7.6 (a) and 7.6 (b) respectively. Both these papers suggested that isotropic assumption can be considered satisfactory, if not perfect, for FE simulation of conventional and die-less clinching.

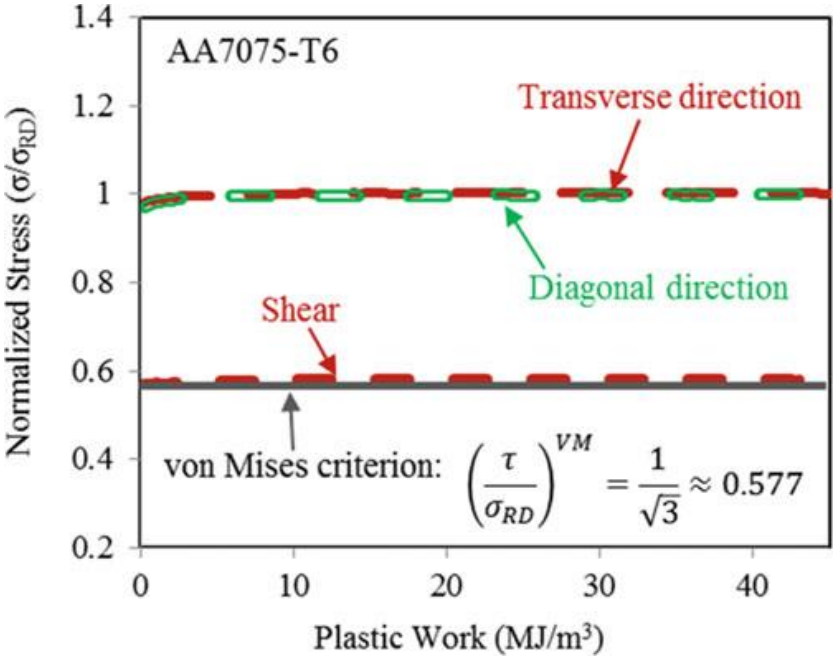

Figure 7.5. Normalized shear stress versus plastic work curves for AA7075-T6 sheet [1].

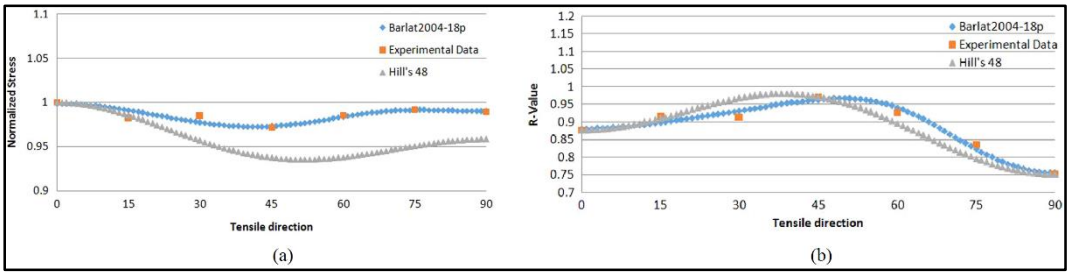

Figure 7.6. Uniaxial tensile test data for AA7075-O sheet as a function of test orientation; show (a) the normalized stress, and (b) r-values [2].

In addition to the above work largely supporting the present isotropic material assumption, some effort was made towards analyzing the role of plastic anisotropy on clinch forming force and material flow behavior from Axisymmetric models of conventional clinching of AA7075-O sheet based on the r-value data provided in Esmaeilpour et al. [2]. For this purpose, the directional r-value data was converted into a single value normal anisotropy parameter data and then Hill quadratic normal anisotropy

model was utilized in Abaqus-Explicit FE code. Figure 7.7 shows a comparison of the punch forming force versus punch stroke predicted by the FE model assuming isotropic and Hill quadratic normal anisotropic material (single r value) and the experimental measurements. It can be noted that there is a negligible difference between the two material models and both follow the experimental curve closely. Also, the final predicted shape of the clinched joint, as shown in Figure 7.8, revealed very similar shapes from the two yield criteria.

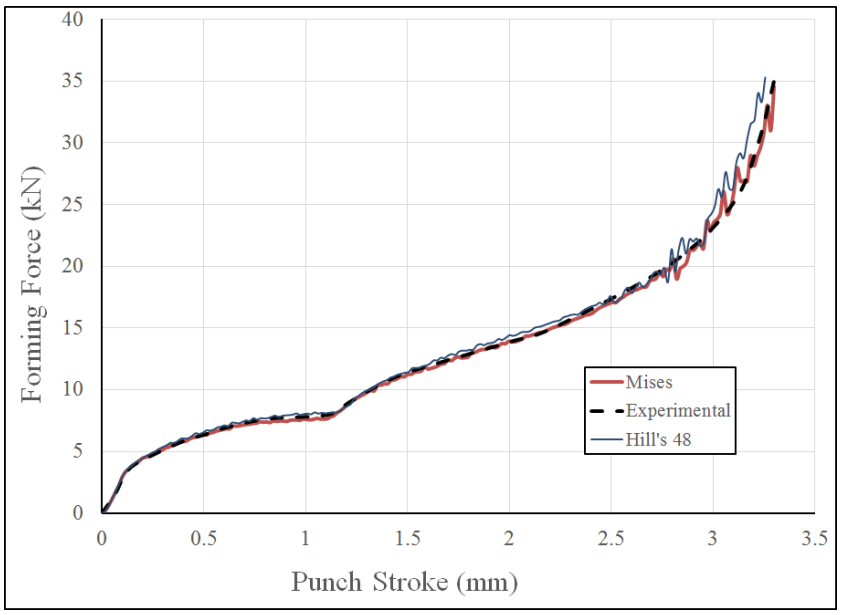

Figure 7.7. A comparison of the punch forming force versus punch stroke from conventional clinching simulations using isotropic Mises and normal anisotropic quadratic Hill yield criteria and experiments for AA7075-O sheet.

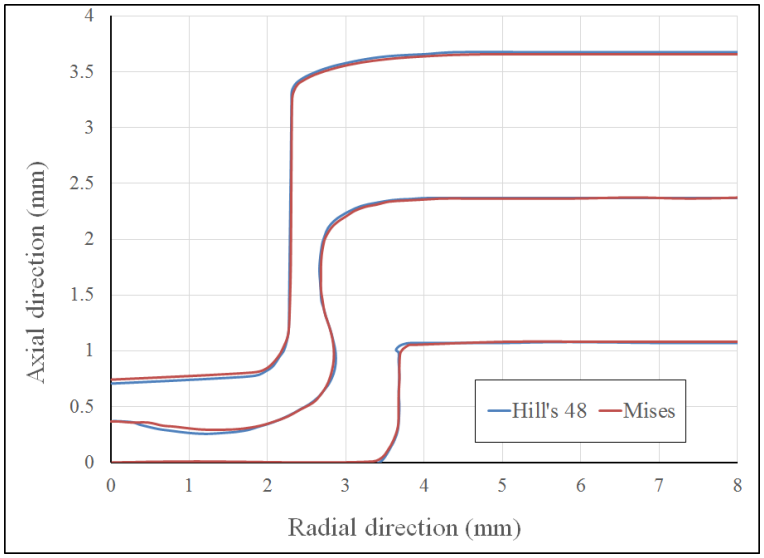

Figure 7.8. A comparison of geometrical clinched shapes from conventional clinching simulations using isotropic Mises and normal anisotropic quadratic Hill yield criteria for AA7075-O sheet.

Lastly, Figure 7.9(a,b) shows the equivalent plastic strain distribution from FE simulation of conventional clinching of AA7075-O sheet using isotropic and normal anisotropic Hill yield criteria. The Hill criterion did indeed result in slightly higher plastic strain values in the clinched region compared to the Mises criterion.

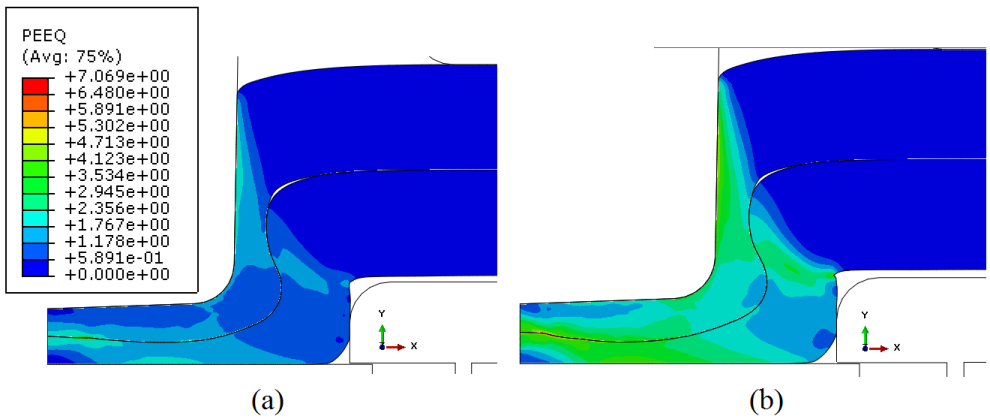

Figure 7.9. Equivalent plastic strain distributions in the clinched region from FE simulations of conventional clinching of AA7075-O sheet using (a) isotropic Mises criterion, and (b) normal anisotropic Hill criterion.

In conclusion, the isotropic assumption is reasonable for clinching of AA7075 sheet materials, in general. However, results from 3D models of clinching with planar anisotropic yield criterion of Hill (with 3 r-values) should be evaluated and compared with those from normal anisotropic Hill and isotropic Mises criteria in the future.

7.2 Material strain rate

Another assumption made in the FE simulations presented in Chapters 2-5 of this thesis involved selection of a rate-independent material hardening law for AA7075 sheet for simulations of conventional and die-less clinching at room temperature. The AA7075 sheet is relatively strain rate insensitive at room temperature and under quasi-static forming conditions [3]. This was verified in a limited manner by carrying out uniaxial tensile tests at 1 mm/min and 10 mm/min. There was not a large difference in the stress-strain curves at the above 2 test speeds. Also, recent results of Rahmaan et. al. [1], as shown in Figure 7.10, clearly reveal very little effect of strain rate on room temperature stress-strain behavior of AA7075-T6 sheet over a very wide range of strain rates. The same rate-independence can be assumed for other temper states of AA7075 sheet.

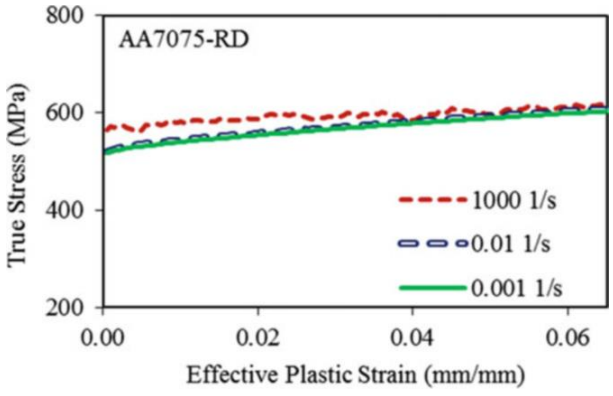

Figure 7.10. Average flow stress of AA7075-T6 sheet at room temperature and strain rates from 0.001 to 1000 s^{-1} [1].

7.3 Selection of plane of observation of the cut clinched specimens

The clinched specimens were cut through the sheet thickness on a plane that passed through the mid-diameter position of the clinch protrusion. This was done to analyze the experimental geometric shape and interlocking characteristics of the joint and compare it with the model results of the FE simulation. For such a comparison, all samples were cut in the long transverse (or LT) plane. No effort was made to assess the difference between the shapes resulting from a similar cut along the short transverse (or ST) plane. This approach was consistent with the assumption of material isotropy and the supporting data in sub-section 7.1. In retrospect, however, it may have been beneficial to at least compare geometrical shapes and interlocking characteristics resulting from cuts in LT and ST planes to re-confirm the validity of the isotropic assumption in the clinching simulations.

7.4 Consideration of springback

It is to be noted that the springback was analyzed in numerical studies reported in Chapter 4 only when dealing with die-less clinching. The samples were loaded to the desired forming force and then unloaded to analyze the changes in strain distribution and clinched geometrical parameters. However, the numerical results of conventional clinching in Chapter 2 and die-less clinching in Chapter 5 involved only the loading step to the desired forming force and all stress and strains reported in these chapters correspond to the end of the forming step only. No unloading was simulated.

7.5 Force-controlled versus displacement-controlled clinching experiments and simulations

It is to be noted that all of the experiments and corresponding FE simulations were carried out by applying specific applied forces. This was done with understanding that many of the clinching presses in industrial use operate under force-controlled conditions. In fact, for all conventional clinching, Norlok press (Model LL4000) was utilized for the present study and it did operate only under force-control conditions with force being measured with a load cell aligned to the direction of the punch movement. It is our understanding that the results and conclusions from this study are equally valid for tests conducted under displacement-control conditions. However, this should be explored in a separate study.

7.6 Significance of results and conclusions to the other formable sheet materials

It is believed that much of the new understanding of the effect of experimental and numerical process parameters on clinching characteristics of AA7075 sheets could be transferred to the other high strength aluminum or non-aluminum sheet materials. On the other hand, the effect of the material parameters on clinching characteristics of 7075 will need to be assessed carefully for its relevance to other sheet materials. For example, the use of mixed Swift-Voce hardening law with a weight function or the use of extended Voce law to represent material hardening behaviour must be assessed any new material for the clinch study. A similar comment can be made with regard to the need for assessment of the

effect of material anisotropy and strain rate on clinched characteristics of other materials when applying the results of this study.

7.7 Discussion on conventional clinching

Conventional clinching of AA7075-O sheets was studied experimentally as well as via FE simulations. The study included an investigation of the effect of the tool geometric parameters including different die depths as well as different forming forces and the results were used to validate the various FE models. Increasing die depth or forming force resulted in an increase of the material flow which in turn increased the interlock depth and decreased the neck thickness. However, further increase in both of them can result in weakening of the formed joint. The FE simulation covered many tool parameters such as the punch and die corner radii in addition to the clearance between punch and die. Clinch joining is a complex process and its simulation is greatly dependent on the material model. Use of a weight function between Swift and Voce constitutive models provided a better material hardening law up to large strains that resulted in better agreement between experimental and FE model results for AA7075-O aluminum sheet. The forming process could be divided into three forming stages, in addition to the initial stage of applying the blank holder force. During the first stage of forming (see Figure 2.11), a large reduction in the thickness of the die-sided sheet occurred and it remained constant with further punch movement. Also, the clearance between punch and die affected the reduction in the total thickness of the sheet metals. In contrast, punch and die corner radii affected the ratio of thickness reduction in punch and die-sided sheets respectively.

7.8 Discussion on die-less clinching

The room temperature die-less clinches were obtained using new tooling design (see Figure 3.5). The new design included punch, flat anvil, and blank holder with designed groove in order to control the material flow. Various blank holders of differed groove shapes were used in the study as shown in Figure 3.6. The most interesting blank holder shape was the one that had a groove with stepped edge. The main tool parameters of the stepped edge blank holder were the groove depth *t* and groove diameter *d*. Five different stages could be distinguished during die-less clinching process as shown in Figure 3.8. The material flow restriction in the axial direction in the fifth stage was found to be critical to increase in the interlock depth. The groove depth *t* has an influence effect on the material flow and directly affects the interlock formation (i.e., the *U* value). A very small groove depth could result in blocking of the material flow in the axial direction at early stages that resulted in failure of interlock formation. However, reasonable decrease of the groove depth *t* could enhance the interlocking by restricting the axial flow of the material at later stages and in turn increase the material to flow in radial direction. A blank holder of groove depth greater than 20% of sheet thickness is recommended for interlock formation with reasonable joint strength of 3.2 kN. In contrast, the groove diameter had a considerable influence on the neck reduction (i.e., the *N* value). Neck thickness *N* and interlock depth *U* together controlled the joint shear strength and associated failure mode as shown in Figure 3.18. Joint with small interlock *U* failed by plastic deformation of the interlock. On the other hand, formation of a joint with large interlock was associated with reduced neck thickness, which resulted in failure by neck fracture. Unlike lap shear strength, the peel

strength of the die-less clinched joint was largely affected by the interlock depth. The neck thickness, however, had a marginal effect on the peel strength.

7.9 Discussion on simulation of die-less clinching

In general, severe conditions of the clinch joining such as very small clinching area, the failure of camera monitoring, and the high speed of the process makes the experimental study of the clinching process quite difficult. FE modeling allows a simulation of not only for the clinch formation process but also of post-forming joint loading and deformation process. The cumulative errors of the FE simulation can be reduced by proper selection of numerical, material, and process parameters. It is shown that accuracy of simulation depends critically on the numerical parameters. However, computation time is another important factor which should be taken into consideration. The size of the element is a critical parameter for prediction of geometrical interlock shape as well as the computation time as in Figure 4.9 and Figure 4.10 respectively. Adaptive re-meshing technique is required to avoid excessive element distortion. However, the relocating algorithm as well as the frequency of re-meshing has almost no effect on the results (see Figure 4.11). Mass scaling factor is yet another key parameter to decrease the computational time. However, large mass scaling factor values can induce an inertial effect that can reduce the accuracy of predictions. A mass scaling factor of less than 150 is suggested for acceptable accuracy from the model. Also, the material model is a critical factor for the simulation and should be selected carefully because the die-less clinching process involves very large plastic strains. Further, assuming the tool set as a rigid body is a common assumption and can be

used in the simulation. Lastly, proper choice of friction coefficient is important factor for accurate prediction of geometrical interlock as well as spring-back.

7.10 Discussion on hot die-less clinching

The elevated temperature clinching operation has been studied by locally heating the sheet materials using a novel rapid electrical resistance heating (ERH) method. The blank holder and flat anvil were used as upper and lower electrodes respectively. A new tool set developed in the present research enabled the current to pass from the upper electrode to the lower electrode through two sheets as shown in Figure 6.3. The main studied process parameters were forming force, heating current, and current duration. The range of parameter values where good quality clinch could be achieved for AA7075-T6 aluminum sheet were established. The applied current and its duration were also correlated to peak temperature achieved in the clinch region via a new tool design where a thermocouple was inserted in the clinch region of the die to capture temperature data. A new material locking mechanism was also identified for hot clinching. This type of locking arises from large forming forces and increased temperature in the contact region between the two sheets at the bottom of the punch.

Refrences

[1]. T. Rahmaan, C. Butcher, M.J. Worswick, Constitutive response of AA7075-T6 aluminum alloy sheet in tensile and shear loading, Experimental and Applied Mechanics, Volume 4, Springer2017, pp. 115-122.

[2]. R. Esmaeilpour, H. Kim, T. Park, F. Pourboghrat, B. Mohammed, Comparison of 3D yield functions for finite element simulation of single point incremental forming (SPIF) of aluminum 7075, International Journal of Mechanical Sciences 133 (2017) 544-554.

[3]. E. El-Magd, M. Abouridouane, Characterization, modelling and simulation of deformation and fracture behaviour of the light-weight wrought alloys under high strain rate loading, International Journal of Impact Engineering 32(5) (2006) 741-758.

Chapter 8

Conclusions and Future Work

8 Conclusions and Future Work

8.1 Conclusions:

Joining of AA7075 aluminum sheets in different tempers has been studied experimentally as well as numerically by using two different forming techniques, conventional and die-less clinching. For each objective, the following conclusions can be drawn from the studies described in Chapters 2-6 of the thesis:

Objective 1: Study of room temperature clinch-ability of AA7075 aluminum alloy under different temper states and assessment of joint strength:

1. Clinch joining process depends greatly on the ability of the sheet metal to undergo large plastic deformation.
2. The new toolset design of the die-less clinching was effective to form a geometric interlock. The blank holder groove plays an important role in controlling the flow of the material and formation of interlock.
3. The main geometric parameters of the stepped edge blank holder include depth t and diameter d. The depth of the groove had considerable influence on the interlock formation, while its diameter had a stronger influence on the reduction in the neck thickness.
4. Shear strength of the die-less clinched joints depended largely on neck thickness and the interlock depth. In contrast, the joint peel strength depended solely on the neck thickness.

5. Die-less clinch-ability is strongly affected by the sheet material temper state where the ability of the material to flow in the direction opposite to the punch movement is critical to the clinching process. Annealed temper states resulted in better quality clinches in terms of interlock depth. Conversely, room temperature clinching of the 7075-T6 was considerably more difficult due to its higher strength and low ductility.
6. Die-less clinching of AA7075-W produced a much smaller interlock depth compared to the annealed state and resulted in poor joint strength. However, natural aging of this metastable state resulted in an improvement of the joint strength due to precipitation hardening.

Objective 2: Numerical modeling of material flow during room temperature die-less clinching of AA7075 sheet materials and post-clinch performance of the joints:

1. The material model is a critical factor of the simulation and should be selected carefully. Use of a 0.5 weight function between commonly used Swift and Voce constitutive models was found to yield good prediction of the final shape of conventionally clinched joints. However, weight function range of 0.2-0.9 did not show good agreement with experiments of die-less clinching. That is due to very large plastic deformation associated with die-less clinching compared with conventional clinching. Extended-Voce material model was effective in predicting the shape of the die-less clinched joint.

2. An adaptive re-meshing technique is required to avoid excessive element distortion in the simulation of die-less clinching.

3. A mass scaling factor is a key parameter to decrease the computational time of simulation of the die-less clinching process. However, large values can induce an inertial effect that can influence the accuracy of the results. A mass scaling factor of less than 150 is suggested for acceptable accuracy from the model.

4. FE simulation of the die-less clinching showed that the interlock forms from large material flow in the axial direction. It can be maximized by controlling the material flow at the later stage in radial direction instead of the axial flow by decreasing the blank holder depth.
5. The bottom thickness should be higher than 10% of the total sheet thickness to avoid distortion of the bottom of the die-less clinched joint.
6. In-plane shear strength, as well as peel strength of the joint, can be accurately estimated from a 3D FE model taking into consideration the average change in stress state after joint formation.

Objective 3: High temperature die-less clinching of AA7075 aluminum alloy by rapid local electrical resistance heating:

1. Die-less clinching of AA7075-T6 aluminum sheet is difficult to realize at room temperature. However, a rapid electrical resistance heating system was an effective tool to successfully obtain die-less joints.
2. Three different locking mechanisms in die-less clinching of AA7075-T6 sheet have been identified, conventional form and force locking mechanisms in the neck region, as well as a new material locking mechanism at the bottom region of the joint.

3. The failure modes in hot die-less clinching are affected mainly by the geometric interlock. However, the material locking affects the force-displacement behavior of the joint as it offers a resistance to the joint separation by increasing the required force to fail the joint. However, it also results in secondary yielding.

8.2 Future work

The following research topics are suggested as a future study:

1. FE model of clinching process could be further investigated by including the effect of the anisotropy of aluminum sheet for a better prediction of the interlock.
2. FE model of die-less clinching process could be further investigated by including the effect of stiffness (or rigidity) of the C-frame.
3. The proposed 3D FE model of joint loading and deformation process could be further developed to include a fracture criterion in it.
4. Lastly, experimental work involving the electrical resistance heating and subsequent die-less clinching should be extended to include FE simulations. The FE simulation will need to include electro-thermal and thermo-mechanical models to suitably characterize the electrical resistance heating process.

End